

Mapping Greenland ice sheet velocities at high temporal
resolution using satellite based imagery



Adriano Gomes de Lemos
School of Earth and Environment
University of Leeds

Submitted in accordance with the requirements for the degree of
Doctor of Philosophy

June 2019

Declaration

I confirm that the work submitted in this thesis is my own, except where work which has formed part of jointly-authored publications has been included. My contributions to jointly-authored papers and that of the other authors is explicitly indicated below. I confirm also that appropriate credit has been given within this thesis where reference has been made to the work of others.

The majority of the research included in the thesis, in Chapters 3 and 4, has been peer-reviewed and published. The remaining research in Chapter 5 has been prepared for submission to a peer-reviewed journal. This thesis is published using the University of Leeds alternative thesis format, which allows the research within it to be readily identified and accessed.

The thesis consists of a brief introductory chapter providing an overview of the main relationships between ice sheets and climate to set up the overall motivation for the research. This is followed by a chapter containing a collated and extended presentation of the methods that I have employed within the three main research chapters to track ice motion using repeat radar and optical satellite imagery. The third and fourth chapters are two first-author journal articles, and the fifth chapter is a draft paper that I intend to submit as a third journal article. The final chapter is a discussion of the main research outcomes, and provides an integration and synthesis of their main findings, plus a discussion of areas for future research.

The work in Chapter 3 of the thesis has appeared in publication as follows: Lemos, A.; Shepherd, A.; McMillan, M.; Hogg, A. E.; Hatton, E.; Joughin, I., 2018: Ice velocity of Jakobshavn Isbræ, Petermann Glacier, Nioghalvfjordsfjorden and Zachariæ Isstrøm, 2015-2017, from Sentinel 1-a/b SAR imagery. *The Cryosphere.*, 12, 2087–2097. <https://doi.org/10.5194/tc-2017-251>. I led the research project and wrote the paper, supervised by A. Shepherd, M. McMillan. I processed the data with the help of A.E. Hogg and E. Hatton, and I. Joughin provided the TerraSAR-X data products. All authors discussed the results and commented on the manuscript at all stages.

The work in Chapter 4 of the thesis has appeared in publication as follows: Lemos, A.; Shepherd, A.; McMillan, M.; Hogg, A. E., 2018: Seasonal Variations in the Flow of Land-Terminating Glaciers in Central-West Greenland Using Sentinel-1 Imagery. *Remote Sensing.*, 10, 1–12. <https://doi.org/10.3390/rs10121878>. I led the research project and wrote the paper, supervised by A. Shepherd, M. McMillan and A.E. Hogg. I processed the data with the help of A.E. Hogg. All authors discussed the results and commented on the manuscript at all stages.

The work in Chapter 5 of the thesis is prepared as a manuscript to be submitted as follows: Lemos, A.; Shepherd, A.; McMillan, M.; Hogg, E.H.; Selley, H.. The combined use of Sentinel-2 and Sentinel-1 imagery to track features in the Central-west sector of Greenland. I led the research project, and wrote the paper, under the supervision of A. Shepherd and M. McMillan. I processed the data with the help of A.E. Hogg and H. Selley. All authors discussed the results and commented on the manuscript at all stages.

This copy has been supplied on the understanding that it is copyright material and that no quotation from the thesis may be published without proper acknowledgement
Copyright © 2019 The University of Leeds and Adriano Lemos to be identified as Author of this work has been asserted by him in accordance with the Copyright, Designs and Patents Act 1988.

Acknowledgements

This work was funded by a Coordenação de Aperfeiçoamento de Pessoal de Nível Superior (CAPES) PhD studentship, hosted in the Centre for Polar Observation and Modelling (CPOM) at the University of Leeds.

First of all, I am thankful to my supervisors, Andy Shepherd and Malcolm McMillan, for their support, advice and encouragement over the last few years. The work in this thesis has been greatly improved by their contribution.

I would like to thank all my office mates for all the support: Kate, Anna, Hannes, Rach, Tom, Inès, and Heather. Thanks to the friendship along these years: Thiago e Rodrigo, que me apresentaram Leeds; Mariana, Erica, Samara, Gesner, Larissa, Sheyla, Luis, Will, parceiros em todos os momentos; Christian, Virgínia, Samuel, Peter, Cristiano, Thiago, Baiano, Abel, Piaui, Marcos, Jorge e Claudio por todo suporte remoto; The non-Brazilians also: Andreas, Rebecca, Vesa, Peter, Marie, Manolis, Michael, Owen and Humbug, Montserrat and Jaume.

Agradecer meus primos, Vivian, Vinicius e Victor, e meus tios, Celio e Valeria. Enio, Rosane, Lucas, Romulo, Rose, Victor, Nathalya, Aparecida, Waldir, Hugo e Luana, pessoas especiais que fazem parte de minha vida há anos.

Gostaria de agradecer meus pais, Adriano e Eliana, e meus irmãos, Barbara e Renan, por todo suporte, mesmo que de longe. Vocês fazem muita falta! Também ao meu avo, que nos deixou no meio da jornada. Por fim, gostaria de agradecer minha parceira, Marina. Obrigado por todo seu suporte e compreensão durante todo esse período, sem você tudo seria mais difícil. É muito bom ter você e o Gurizinho junto de mim.

Abstract

In this thesis, I develop and demonstrate a system for monitoring fluctuations in the speed of Greenland ice sheet outlet glaciers with high temporal frequency from imagery acquired by a range of satellite missions. This work is motivated by an ambition to utilise a new era of operational satellites to better understand how environmental changes are affecting the flow and mass of Greenland's outlet glaciers. First, I exploited the systematic and frequent acquisition schedule of the Sentinel-1 satellite constellation to track weekly variations in the speed of four fast-flowing, marine-terminating glaciers - Jakobshavn Isbræ, Petermann Glacier, Zachariæ Isstrøm and Nioghalvfjærdsfjorden - between 2015–2017. By combining the Sentinel-1 data with an eight-year time-series derived from TerraSAR-X, I produced a decadal record of variations in glacier flow. On a technical level, I was able to demonstrate the value of Sentinel-1's 6-day revisit time for glaciology, because it leads to an increase in the degree of correlation between consecutive images and also to improved tracking of movement near to the glacier calving fronts. On a scientific level, I was able to demonstrate that a strong correlation exists between iceberg calving events and glacier speedup, and to show for the first time that Jakobshavn Isbræ has begun to slow down. Next, I assessed the capability of the Sentinel-1 constellation to detect and chart seasonal changes in the speed of five slow-flowing glaciers situated in a 14,000 km^2 land-terminating sector of central-west Greenland. These new measurements offer significantly improved spatial and temporal resolution when compared to previous missions, in all seasons. I was able to show that there are marked differences in the degree of seasonal speedup of the five glaciers – with summertime increases in ice flow ranging from 21 to 49 % - reinforcing the need for comprehensive monitoring and the challenges of making regional extrapolations. Thanks to the high temporal frequency

afforded by Sentinel-1, I was also able to document for the first time the detailed spatial pattern of speedup persistence, and to show that short-lived peaks of melting match transient spikes in glacier velocity. Finally, I explored the added value and complementarity of the Sentinel-2 multi-spectral instrument (MSI) for tracking ice motion. I was able to combine measurements acquired by Sentinel-1 and Sentinel-2 to detect short-term changes in iceberg drift, iceberg calving, ice motion, and supraglacial lake area at Jakobshavn Isbræ. I also showed that measurements of glacier flow determined from both satellites are in good agreement, and that the spatial coverage they afford is greatest in opposing seasons, illustrating the promise of Sentinel-2 for glaciology.

Abbreviations

79-G	Nioghalvfjerdingsfjorden
AW	Atlantic water
AWS	automatic weather station
CCI	Climate Change Initiative
DEM	digital elevation model
ESA	European Space Agency
EW	Extra-Wide swath
GL	grounding-line
GMSL	global mean sea level
GPS	global positioning system
GrIS	Greenland Ice Sheet
IF	ice front
IG	Isorlersuup Glacier
InSAR	Interferometric Synthetic Aperture Radar technique
IS	Isunnguata Sermia
IW	Irminger water
IW	Interferometric Wide swath
JI	Jakobshavn Isbræ
L1C	Level-1C
MSI	multi-spectral instrument
NAC	North Atlantic Current
NCC	normalized cross-correlation
ØG	Ørkendalen Glacier
PDDs	Positive degree days
PG	Petermann Glacier
PROMICE	Programme for Monitoring of the Greenland Ice Sheet
RG	Russell Glacier
S1	Sentinel-1
S2	Sentinel-2
SAR	synthetic aperture radar
SLC	single look complex
SM	Strip Map
SMB	surface mass balance
TOPS	Terrain Observation by Progressive Scan
TSX	TerraSAR-X

WV	Wave mode
ZI	Zachariæ Isstrøm

Contents

List of Figures	x
List of Tables	xvi
1 Introduction and Background	1
1.1 Ice sheet and Climate	1
1.2 Glaciological factors influencing ice motion	4
1.2.1 Atmospheric influence	4
1.2.2 Oceanographic influence	6
1.3 Observations of Greenland ice motion during the satellite era	7
1.4 Aim	13
1.5 Objectives	13
1.6 Thesis Structure	14
2 Tracking Ice motion in Greenland	26
2.1 Introduction to tracking ice motion	26
2.2 SAR intensity tracking	29
2.3 Optical feature tracking	36
3 Ice velocity of Jakobshavn Isbræ, Petermann Glacier, Nioghalvfjerdingsfjorden and Zachariæ Isstrøm, 2015-2017, from Sentinel 1-a/b SAR imagery	49
3.1 Introduction	50
3.2 Study Areas	51
3.3 Data and Methodology	54
3.4 Results and Discussions	61

3.5	Conclusions	69
3.6	Supplementary Material	69
4	Seasonal Variations in the Flow of Land-Terminating Glaciers in Central-West Greenland Using Sentinel-1 Imagery	83
4.1	Introduction	84
4.2	Study Area	86
4.3	Data and Methods	88
4.4	Results and Discussions	89
4.5	Conclusions	99
5	The combined use of Sentinel-2 and Sentinel-1 imagery to track features in the Central-west sector of Greenland	109
5.1	Introduction	110
5.2	Study Area	111
5.3	Data and Methods	112
5.4	Results	115
5.5	Discussions	131
5.6	Conclusions	133
6	Discussions, Conclusions, and Future work	143
6.1	Summary of main results	143
6.2	Synthesis of the main conclusions	148
6.3	Recommendations for future work	151
A	Appendix 1	157
A.1	Paper published in the journal The Cryosphere	157
A.2	Paper published in the journal Remote Sensing	175

List of Figures

1.1	(a) Greenland ice sheet integrated meltwater runoff, as simulated by regional climate models (Trusel et al., 2018). (b) Greenland mass balance and its components surface mass balance (SMB) and discharge (D) (van den Broeke et al., 2009).	3
1.2	Elements of the hydrological system of a land-terminating glacier in Greenland. The dashed line represents the equilibrium line, the limit between the accumulation and ablation regions, and the vertical profile the superficial (V_s) and basal (V_{bs}) velocities. Extracted from Zwally et al. (2002).	5
1.3	Schematic illustration presenting the North Atlantic Current (NAC) influencing marine-terminate glaciers in Greenland. Adapted from Joughin et al. (2012a).	7
1.4	Ice velocity mosaic generated from multi-missions dataset acquired between 1992 and 2016 in Greenland. Extracted from Mouginot et al. (2017).	10
1.5	Seasonal velocity variation of the western sector of Greenland of August 2006 relative to the September 2004 to December 2006 mean speed. Extracted from Joughin et al. (2008a).	12
2.1	Illustration of the revisit frequency of Sentinel-1a and b, combining ascending and descending acquisitions, expressed in days per revisit. Extracted from European Space Agency (ESA) website.	30
2.2	Illustration of different imaging modes of Sentinel-1. Extracted from Geudtner et al. (2014).	31
2.3	Intensity tracking processing chain using IW SLC Sentinel-1 images. . .	35

2.4	Density of acquisitions from Sentinel-2a/b between 03-Dec-2016 to 03-Dec-2017. Extracted from Petr Ševčík EOX IT Services GmbH (2018).	38
2.5	Feature tracking processing chain using L1C Sentinel-2 images.	40
3.1	Time-averaged ice velocity magnitude maps for the period Oct/2014–Feb/2017 (a) Jakobshavn Isbræ (JI; 69°N, 50°W), (b) Petermann Glacier (PG; 81°N, 62°W), (c) Nioghalvfjærdsfjorden (79G; 79°N, 20°W) and Zachariæ Isstrøm (ZI; 78°N, 20°W) glaciers, derived from Sentinel-1 SAR images. Velocities are shown on a logarithm scale and overlaid on a SAR backscatter intensity image and thin grey lines represent elevation. The along-flow profiles are indicated by solid green lines scaled in kilometres, the solid black lines show the across-flow transects, the red triangles represent the locations at which velocity time series are extracted and the thick solid and dashed black lines represent the ice front locations (IF) and the grounding lines (GL), respectively. The inset figures show the location of each glacier	54
3.2	Average velocities (2014–2017) extracted from along- and across-flow profiles of Jakobshavn Isbræ, Petermann Glacier, Nioghalvfjærdsfjorden and Zachariæ Isstrøm. Figures a–d present along-flow profiles of ice velocity (solid black lines), surface elevation from the GIMP DEM (Howat et al., 2014); dashed blue lines and bed elevation from the IceBridge Bed-Machine Greenland V2 product (Morlighem et al., 2015); dashed yellow lines. The location of each profile is shown in Figure 3.1 (green lines). The grey shaded area represents the floating regions, and the light grey dashed line the ice front positions. The blue, black and red markers represent the locations of the across-flow profiles. Figures e–h show the across-flow velocity profiles (solid white lines in Figure 3.1), centred on the main profile (solid green line).	56
3.3	Time-averaged (2014–2017) uncertainty in ice velocity at each site expressed in percentage, based on the signal to noise ratio (SNR) for (a) JI, (b) PG, and (c) 79G and ZI.	59

3.4 Comparison between co-located and contemporaneous Sentinel 1-a/b (6 to 12 days average) and TerraSAR-X (11 days average) Jakobshavn Isbræ velocity measurements at Jif, J1 and J2 locations (blue, black and red dots respectively), together with root mean square (rms) and correlation coefficients (R^2). 60

3.5 Temporal evolution of Jakobshavn Isbræ (a) ice front position extracted from Joughin et al. (2014), ESA Greenland Ice Sheet Climate Change Initiative (CCI) project (European Space Agency (ESA), 2017), and Sentinel-1a/b SAR images represented in blue, black and magenta dots respectively, where higher values correspond to ice front retreat. Changes in ice velocity through time is also shown (b, c), extracted at the locations indicated in Figure 3.1. The velocity data derived from TerraSAR-X (11 days - Joughin et al. (2016)) are shown as grey squares, and the data from Sentinel 1-a/b (6 to 12 days) as coloured triangles. 63

3.6 Comparison between Jakobshavn Isbræ ice velocity and calving front position anomalies at the Jif site, 0.8 km upstream of the calving front, between 2009 and early 2017. Positive values correspond to ice front retreat and speed up respectively. The red and black lines represent the linear regression through the 2009-2011 and 2012-2017 periods, respectively, together with the correlation coefficients (R^2). 65

3.7 Temporal evolution of ice velocity at the locations indicated in Figure 1 over (a) Petermann Glacier, (b) Nioghalvfjerdingsfjorden and (c) Zachariæ Isstrøm. The data derived from TerraSAR-X (11 days - Joughin et al., 2016) and Sentinel 1-a/b (6 to 12 days) are represented as grey squares and coloured triangles, respectively. 67

4.1	Average ice velocity in (a) summer (May–Jul), (b) winter (Aug–Apr), and (c) the difference between summer and winter, derived from Sentinel-1 (S1) synthetic aperture radar (SAR) imagery. The uncertainties in the maps associated with the summer, winter, and difference between the summer and winter ice speeds are also shown (d–f, respectively). Velocities and the uncertainties are overlaid on a SAR backscatter intensity image. Also shown are elevation contours (thin grey lines), profiles along (solid black lines) and across (dotted black lines) the centre of five glaciers. The location of the KAN_L weather station is also mapped (red dot, a).	87
4.2	Mean summer and winter ice velocity (a–e) and geometry (f–j) along central profiles of five glaciers in west-central Greenland (see Figure 4.1 for glacier locations) in 2016 and 2017. Surface and bed elevations are from the Greenland Ice Mapping Project digital elevation model (GIMP-DEM) (Howat et al., 2014) and IceBridge BedMachine Greenland, Version 3 (Morlighem et al., 2017), respectively.	92
4.3	Ice velocity (Top), with uncertainty ranges represented by the light shading, and geometry (Bottom) along an across-flow profile of the study area (see Figure 4.1 for location) in 2016 to 2017.	94
4.4	Seasonal changes in ice flow at two different elevations bands on each glacier. Actual measurements are represented by the dots, spline fits as continuous lines, and speedup periods the intervals between the consecutive coloured dotted lines.	95
4.5	Persistence of ice speedup (a), the start (b) and end date (c) of the summer season.	96
4.6	Averaged speed of three glaciers (G1, IG, and RG) with similar geometry and data sampling at two elevations bands during 2017. Also shown are daily temperature and positive degree days (PDDs) recorded at the nearby KAN_L automatic weather station (670 m.a.s.l.) and distributed by the Programme for Monitoring of the Greenland Ice Sheet.	98

5.1	Optical true-color composite Sentinel-2 L1C (a) and SAR Sentinel-1 (b) same-day image comparison. The solid green contour represents cloud mask provided by ESA, and the coloured squares are insets of Figures 5.2–5.5.	116
5.2	Zoom of cloud coverage (a-b) and cloud free areas (c-d) subsets extracted from Figure 5.1a inside the red and blue squares. The images are acquired in different days of the year as indicated in their upper left corner.	118
5.3	Tracked icebergs in the Ilulissat Fjord using true-colour composite Sentinel-2 (a-b) and SAR Sentinel-1 (c-d) images. The subsets were extracted in the yellow square from Figure 5.1b. The gridline is spaced by 750 m x 750 m. Solid green and red lines represent digitized features from the scenes a,c and b,d respectively.	120
5.4	Calving front locations using true-colour composite Sentinel-2 (a-b) and SAR Sentinel-1 (c-d) images. The subsets were extracted in the cyan square from Figure 5.1b. The gridline is spaced by 750 m x 750 m. Solid green and red lines represent digitized features from the scenes a,c and b,d respectively.	121
5.5	Supraglacial lakes observed in true-colour composite Sentinel-2 (a-b) and SAR Sentinel-1 (c-d) imagery (see magenta square in Figure 5.1b for location). The gridline is spaced by 750 m x 750 m. Solid green and red lines represent digitized features from the scenes a,c and b,d respectively.	123
5.6	Seasonal variations in the speed of Jakobshavn Isbræ and the surrounding ice sheet estimated using Sentinel-1 (a–d) and Sentinel-2 (e–g) imagery.	125
5.7	Ice velocity variation at the main trunk of Jakobshavn Isbræ in a logarithm colour scale. We present Sentinel-1 in winter, and Sentinel-2 (upper) and Sentinel-1 (lower) images in spring, summer and autumn. The solid black lines along and across the glacier represent the profile and ground line location, respectively, used in Figure 5.8.	128
5.8	Velocity profiles extracted over the main trunk of Jakobshavn Isbræ. Black and red lines represent Sentinel-1 and Sentinel-2 profiles, respectively. The profile and ground line location are represented as solid black lines along and across the glacier, respectively, in Figure 5.7.	129

5.9	Differences in the velocities from Sentinel-2 and Sentinel-1 data in common areas of the ice sheet covered by velocity tracking for each season. .	130
6.1	Copy of Figure 3.5. Temporal evolution of Jakobshavn Isbræ (a) ice front position extracted from Joughin et al. (2014), ESA Greenland Ice Sheet Climate Change Initiative (CCI) project (European Space Agency (ESA), 2017), and Sentinel-1a/b SAR images represented in blue, black and magenta dots respectively, where higher values correspond to ice front retreat. Changes in ice velocity through time is also shown (b, c), extracted at the locations indicated in Figure 3.1. The velocity data derived from TerraSAR-X (11 days - Joughin et al. (2016)) are shown as grey squares, and the data from Sentinel 1-a/b (6 to 12 days) as coloured triangles.	145
6.2	Copy of Figure 4.5. Persistence of ice speedup (a), the start (b) and end date (c) of the summer season.	146
6.3	Copy of Figure 5.5. Supraglacial lakes observed in true-colour composite Sentinel-2 (a-b) and SAR Sentinel-1 (c-d) imagery (see magenta square in Figure 3.1b for location). The gridline is spaced by 750 m x 750 m. Solid green and red lines represent digitized features from the scenes a,c and b,d respectively.	148
6.4	Copy of (a) Figure 3.6 and (b) Figure 4.6. In (a): Comparison between Jakobshavn Isbræ ice velocity and calving front position anomalies at the Jif site, 0.8 km upstream of the calving front, between 2009 and early 2017. Positive values correspond to ice front retreat and speed up respectively. The red and black lines represent the linear regression through the 2009-2011 and 2012-2017 periods, respectively, together with the correlation coefficients (R ²). In (b): Averaged speed of three glaciers (G1, IG, and RG) with similar geometry and data sampling at two elevations bands during 2017. Also shown are daily temperature and positive degree days (PDDs) recorded at the nearby KAN L automatic weather station (670 m.a.s.l.) and distributed by the Programme for Monitoring of the Greenland Ice Sheet.	150

List of Tables

2.1	Spatial resolution, central wavelength and bandwidth of the different bands acquired by Sentinel-2. Adapted from ESA, 2015.	37
3.1	Speedup Persistence and seasonal percentage increase in speed relative to winter and annual background for each glacier for the Sentinel-1 dataset. Speedup persistence has an uncertainty of ± 12 days due to the image acquisition interval of Sentinel-1a.	62
4.1	Seasonal velocity, speedup, speedup persistence, ice thickness and surface slope of the five glaciers averaged in two elevations bands (P1, between 650 and 750 m.a.s.l.; P2, over 820 m.a.s.l.).	90
5.1	List of Sentinel-2 and Sentinel-1 used in this study	113
5.2	Changes in the area of supraglacial lakes records in Sentinel-1 and Sentinel-2 imagery (see Figure 5.5 for lake locations).	124
5.3	Common areas of the ice sheet covered by velocity tracking for each season.	126
5.4	Seasonal average speed separated by elevation bands estimated by near-coincident Sentinel-1 and Sentinel-2 imagery.	127

Chapter 1

Introduction and Background

In this chapter, I will start with an overview of the relationship between ice sheets and climate, reviewing the contribution of the two main ice sheets, Greenland and Antarctica, to mean sea level rise over the past decades. I will then summarize how changes in atmospheric and ocean temperatures affect ice motion, before focusing specifically on Greenland and the observed changes in ice motion over the past 25 years. I end the chapter by outlining the aims, objectives and structure of my thesis.

1.1 Ice sheet and Climate

In last two decades the Greenland and Antarctic Ice Sheets have lost ice at increasing rates (Shepherd et al., 2018; McMillan et al., 2016; Rignot et al., 2019). The losses and gains in ice sheet mass are determined by the total mass balance, which is determined as the net effect of the surface mass balance and ice discharge exported from the ice sheet (van den Broeke et al., 2009). Surface mass balance is defined as the sum of the surface accumulation, mass gain from solid and liquid precipitation and water vapour deposition, and ablation, mass loss via surface runoff and sublimation (Vernon et al., 2013). Between 1993–2010, studies based on a combination of observations and modelling showed that the global mean sea level (GMSL) increased at a rate of 3.2 mm yr^{-1} (Church et al., 2013). During this same period, ice loss from the Greenland and Antarctic ice sheets contributed an average of 0.33 mm yr^{-1} and 0.27 mm yr^{-1} , respectively, to global sea-level rise (Church et al., 2013). This estimate of the contribution of Greenland to sea level rise was based upon satellite observations

of ice sheet mass loss, which showed that between 1992 and 2011 the Greenland Ice Sheet lost mass at an average rate of 142 ± 49 Gt yr^{-1} (e.g. Shepherd et al. (2012)). Subsequently, mass loss was estimated to have increased to 269 ± 51 Gt yr^{-1} between 2011 and 2014 (McMillan et al., 2016). In Antarctica, the average rate of mass loss between 1992 and 2017 was estimated to be 109 ± 56 Gt yr^{-1} (Shepherd et al., 2018). For both ice sheets, ice mass loss was a response to warmer ocean and air temperatures to which they have been exposed (Rignot and Kanagaratnam, 2006; Joughin et al., 2012b). Rates of ice loss from Greenland have been higher in during the last two decades than at any time in the past 350 years (Trusel et al., 2018), due to increased surface melting and ice discharge (Figure 1.1 - Shepherd et al. (2012); McMillan et al. (2016)). Between 1991–2015, Greenland lost 60 % of its mass due to surface melting and runoff (Enderlin et al., 2014; van den Broeke et al., 2016). The complexity of a glacier’s response to environmental change challenges efforts to model their future evolution (Joughin et al., 2012a; Bondzio et al., 2017) and, therefore, frequent and systematic monitoring is essential to understand the processes governing their dynamic stability and contribution so future mean sea level rise (Joughin et al., 2010; Shepherd et al., 2012).

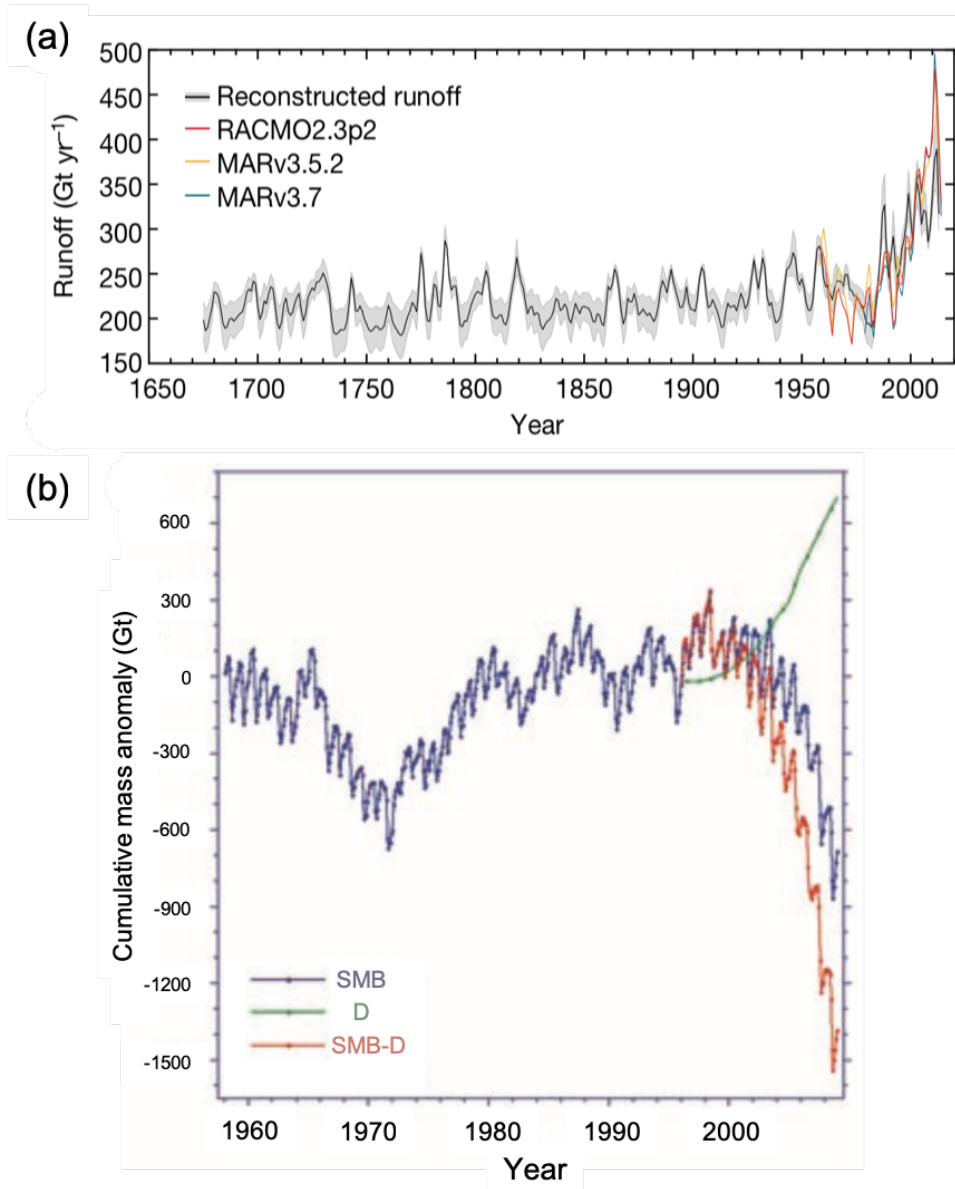


Figure 1.1: (a) Greenland ice sheet integrated meltwater runoff, as simulated by regional climate models (Trusel et al., 2018). (b) Greenland mass balance and its components surface mass balance (SMB) and discharge (D) (van den Broeke et al., 2009).

1.2 Glaciological factors influencing ice motion

Changes in glacier flow provide a key indicator of the role that the air-ice-ocean interaction plays in ice-sheet stability. In Greenland, the speedup of marine- and land-terminating glaciers has been associated with rises in the regional air and ocean temperatures (Holland et al., 2008; Hanna et al., 2012). Inland, meltwater that forms at the ice surface can either accumulate in topographic depressions, forming supraglacial lakes (Leeson et al., 2013) that often drain (McMillan et al., 2007), or it can flow directly into the ice sheet through moulins or crevasses (Chu, 2014). Once it has entered the ice sheet, meltwater can feed the englacial drainage system and, after reaching the ice-bedrock interface, can enhance ice flow via basal lubrication in marine- and land-terminating glaciers (Hoffman et al., 2011; Chu, 2014). Near to the ocean margin, marine-terminating glacier flow is also highly-influenced by seasonal changes in the position of their calving front, which periodically alters lateral and basal resistive stresses at the terminus (Joughin et al., 2014; Moon et al., 2014, 2015). Calving front retreat can also occur over longer timescales through episodic calving of ice-bergs, and their melting contributes up to 50 % of the total fresh-water ice sheet mass loss (Enderlin et al., 2014).

1.2.1 Atmospheric influence

In Greenland, the majority (60 %) of recent ice loss (1991–2015) has been due to surface melting and runoff (van den Broeke et al., 2016), which have risen as summers have warmed (Hanna et al., 2012, 2014). In addition to the direct impact on loss of ice due to runoff, increased surface melting has also been linked to increases in the speed of ice flow through basal lubrication predominantly in land-terminating glaciers, but also occurring in marine-terminating glaciers (Figure 1.2 - (Zwally et al., 2002; Hoffman et al., 2011; Chu, 2014; Moon et al., 2014; Joughin et al., 2014)). Rising air temperatures lead to increased surface melting, which can in turn lead to an increase in the amount of water feeding into the subglacial drainage system (Chu, 2014) after supraglacial lakes drain or moulins open (Hoffman et al., 2011; Chu, 2014). As a consequence of this excess meltwater, subglacial water pressure rises, which reduces the effective pressure between the ice-bedrock interface and leads to enhanced basal sliding (Harper et al., 2005; Nienow et al., 2005; Andrews et al., 2015). During the melting season,

1.2 Glaciological factors influencing ice motion

frictional heating caused by water flow enlarges the conduits of the subglacial hydrologic system, allowing a greater volume of water to be accommodated (Bartholomew et al., 2010; Cowton et al., 2013). As a consequence, from mid-season to the end of the melt season, the drainage system transmission capacity exceeds the meltwater input, draining water efficiently through low-pressure channels (Schoof, 2010; Cowton et al., 2013), slowing down the glaciers up to winter velocities (e.g. Zwally et al. (2002); Bartholomew et al. (2010)). Furthermore, due to the efficiency to drain meltwater easily, previous study demonstrated that despite the high correlation between seasonal variation of surface melting enhancing basal sliding, the speedup persistence is three times longer during colder than warmer summers in the western sector of Greenland (Sundal et al., 2011). Moreover, over the same region, Tedstone et al. (2015) showed that despite an increase of 50 % in the meltwater production between 1985–1994 and 2007–14, the land-terminating glaciers slowed down 12 % over the same period.

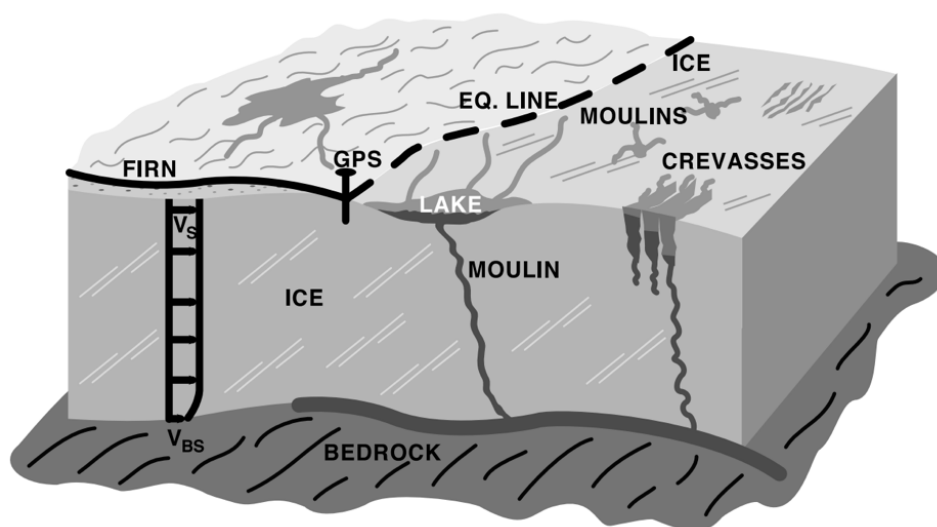


Figure 1.2: Elements of the hydrological system of a land-terminating glacier in Greenland. The dashed line represents the equilibrium line, the limit between the accumulation and ablation regions, and the vertical profile the superficial (V_s) and basal (V_{bs}) velocities. Extracted from Zwally et al. (2002).

1.2.2 Oceanographic influence

In the previous section I described how basal lubrication is the predominant mechanism to enhance land-terminating, and marine-terminating, glaciers through ice surface melting. Over marine-terminating glaciers, however, observation and modelling studies have been demonstrating that calving events have more influence on the glaciers' speedup (Howat et al., 2005; Nick et al., 2009). Because marine-terminating glaciers are exposed to the adjacent ocean dynamics and circulation, their velocity can be directly influenced by melting at the ice-ocean interface. The intrusion of warm water into the fjord can lead to glacier terminus thinning and retreat, which reduces resistive stresses, and consequently drives velocity fluctuations (Joughin et al., 2008a,b, 2012b, 2014; Bondzio et al., 2017). Resistive stresses are exerted between the ice-bed, in tide-water glaciers, and between the lateral- and side-wall of the fjord, if an ice shelf exists (Cuffey and Paterson, 2010; Joughin et al., 2012a). Furthermore, warmer sub-surface ocean waters affect the sea-ice thickness and ice mélange adjacent to glaciers terminus, which also influence the calving regime by exerting mechanical resistive stresses (Joughin et al., 2008b; Cassotto et al., 2015). Figure 1.3 shows a schematic illustration of the processes influencing the flow of a marine-terminating glacier in Greenland. Warmer waters are represented by the North Atlantic Current (NAC), presented here as the mixture of the Irminger water (IW), acting on the western and southeastern regions, and Atlantic water (AW) elsewhere (Joughin et al., 2012a).

During the satellite era, the largest changes in marine glacier response have been observed at Jakobshavn Isbræ. Previous studies of Jakobshavn Isbræ, western Greenland, showed that during the late 1990s, the ice tongue experienced successive break up events and the glacier began to speedup, exhibiting annual increases in speed of 7 % per year from 2004 and 2007 (Joughin et al., 2008a, 2012a, 2014). Until 2012 and 2013, the speed up continued, reaching maximum velocities in excess of 17 km yr^{-1} (Joughin et al., 2012b, 2014). Jakobshavn Isbræ is susceptible to changes in the adjacent ocean and Holland et al. (2008) have shown that warm water originating in the Irminger Sea likely enhanced basal melting and weakened the floating ice tongue, triggering its break up in 1997. Furthermore, Gladish et al. (2015) showed that subsequent changes which, occurred between 2001–2014, were mainly triggered by changes in Ilulissat Ice-

1.3 Observations of Greenland ice motion during the satellite era

fjord water temperatures adjacent to the glacier. Ocean forcing is the main driver, but it has been suggested (van de Wal et al., 2015) that the speedup over this period in the southwest of Greenland might have been enhanced by anomalously high melting across the ice sheet surface (Tedesco et al., 2013).

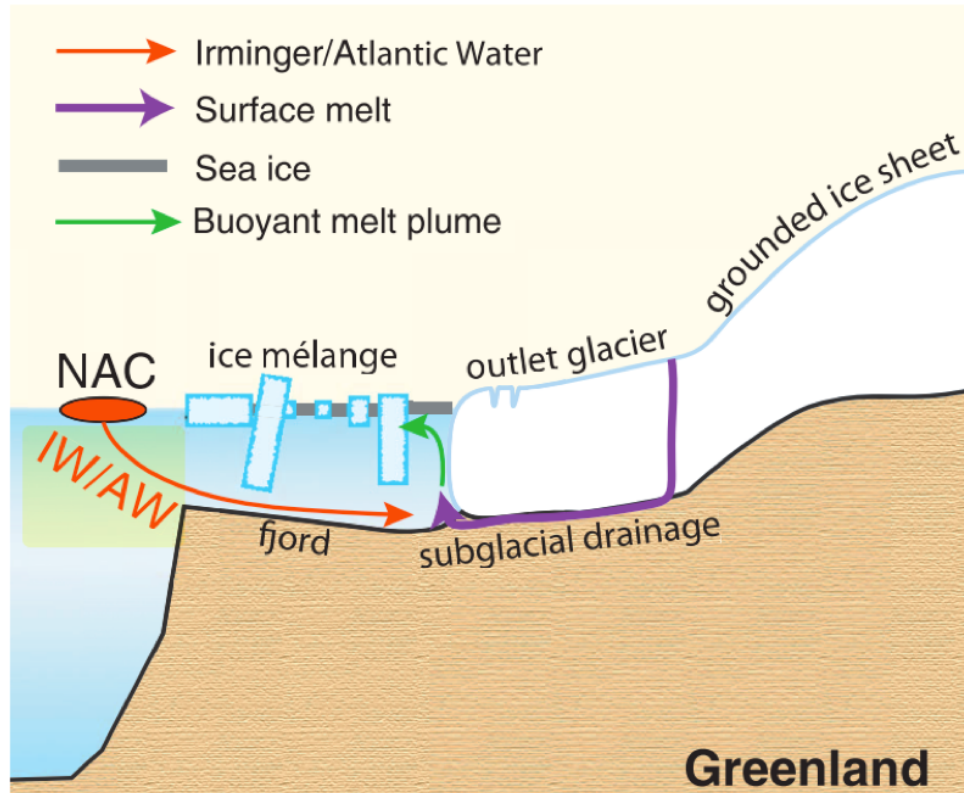


Figure 1.3: Schematic illustration presenting the North Atlantic Current (NAC) influencing marine-terminate glaciers in Greenland. Adapted from Joughin et al. (2012a).

1.3 Observations of Greenland ice motion during the satellite era

Ice velocity variability in Greenland has been observed over a range of timescales, varying from daily (e.g. Das et al. (2008); Shepherd et al. (2009); Bartholomew et al. (2012)), seasonal (Joughin et al., 2008a, 2012b, 2014; Bartholomew et al., 2010, 2011) to interannual variations (Sundal et al., 2011; Joughin et al., 2008b, 2012b, 2014). Our

1.3 Observations of Greenland ice motion during the satellite era

understanding of the timescales and mechanisms underpinning the processes that control fluctuations in the Greenland ice sheet flow has been dramatically improved by the availability of frequent and systematic satellite observations (Moon et al., 2012; Joughin et al., 2014; Nagler et al., 2015; Hill et al., 2018; Joughin et al., 2018). These observations are important indicators of how the cryosphere has been affected by climate change during recent decades than at any time in the past 350 years (Trusel et al., 2018), as a result of higher surface melting and ice discharge (Shepherd et al., 2012; McMillan et al., 2016). Glacier velocities, in particular, have been routinely tracked in repeat optical (Rosenau et al., 2015; Fahnestock et al., 2016; Gardner et al., 2018) and synthetic aperture radar (SAR) imagery (Goldstein et al., 1993; Lucchitta et al., 1995; Joughin et al., 2010; Rignot et al., 2011; Nagler et al., 2015). Although both techniques can yield high-quality measurements of ice sheet flow, they are also affected by changing environmental conditions. In the case of optical imagery, clouds frequently interfere, and in the case of SAR imagery, surface melting can be especially problematic. A combination of the two methods is therefore likely the best approach for continuous and consistent monitoring. The systematic acquisition cycle of Sentinel-1a/b is able to provide averaged velocity measurements every 6 days and, in conjunction with Sentinel-2a/b, providing measurements every 3 days over the polar regions, offers the potential to monitor average ice flow every 2 days, which is unprecedented during the satellite era. Going forward, the novel combination of operational satellite missions at the continental scale is essential for the systematic identification of short-term changes of numerous glaciological features, and for understanding the processes that drive ice velocity change.

The central-east and southeast coast of Greenland is mostly composed of marine-terminating glaciers, presenting rapid ice loss through accelerated flow (Enderlin et al., 2014), known as dynamic thinning, followed by increase in speed between 2000–2010 (Joughin et al., 2010; Moon et al., 2012). Helheim glacier (66.4°N, 38°W) is the fastest flowing glacier in this sector, with ice speed reaching $\sim 11000 \text{ m yr}^{-1}$ (Howat et al., 2005). The northeast sector largely flows at slow rates of $\sim 200 \text{ m yr}^{-1}$, with the exception of Nioghalvfjærdsfjorden and Zachariæ Isstrøm glaciers (Joughin et al., 2010) (Figure 1.4). These two glaciers together drain more than 10 % of the Greenland Ice Sheet (Rignot and Mouginot, 2012). Their maximum velocities are found near the

1.3 Observations of Greenland ice motion during the satellite era

grounding line, and the average velocity reaches $\sim 1400 \text{ m yr}^{-1}$ and $\sim 2600 \text{ m yr}^{-1}$ in Nioghalvfjerdingsfjorden and Zachariæ Isstrøm, respectively, the first had a slight acceleration of 12 % whilst the later tripled its ice speed from 2007 to 2015 (Mouginot et al., 2015; Hill et al., 2018). In the Northwest (Figure 1.4), Petermann Glacier is the fastest glacier in the sector, and has an average velocity of $\sim 1100 \text{ m yr}^{-1}$ at its grounding line which remains relatively stable since the 1990s (Rignot, 1996; Rignot and Steffen, 2008; Hill et al., 2018) and a multi-annual trend (2006–2010) in flow speed of 30 m yr^{-2} (Nick et al., 2012).

The western margin of Greenland is regarded as the major source of recent mass losses from the ice sheet, and was responsible, between 2011–2014, for 41 % of the total mass imbalance (McMillan et al., 2016). Jakobshavn Isbræ, for instance, is the fastest glacier in Greenland (Enderlin et al., 2014; Joughin et al., 2014), draining ~ 6.5 % of the ice sheet (Joughin et al., 2004). Since the 1950s it has been experiencing several retreat events of the ice tongue before the complete disintegration in 2003 (Joughin et al., 2008b), and observations show that, in response, the glacier has been thinning continuously since the early 2000's (Sørensen et al., 2018). Between 2004–2011, Jakobshavn Isbræ sped-up by 4.4 % (Joughin et al., 2012b), and these fluctuations in the calving front position have been identified as the main trigger for seasonal and inter-annual changes in its speed, as it leads to reduced basal and lateral resistive stresses (Joughin et al., 2012b, 2014, 2018). The south west sector of Greenland is, in its majority, formed by land-terminating glaciers, and presented, through global position system and satellite measurements, a decrease in the inter-annual velocity by 10 % between 1990–2007 (van de Wal et al., 2008), and 12 % from 1985–1994 compared to 2007–2014 periods (Tedstone et al., 2015), respectively. In contrast, Narsap Sermia, a marine-terminating glacier in the same sector, sped-up by 60 % between 2005–2010 (Moon et al., 2012).

1.3 Observations of Greenland ice motion during the satellite era

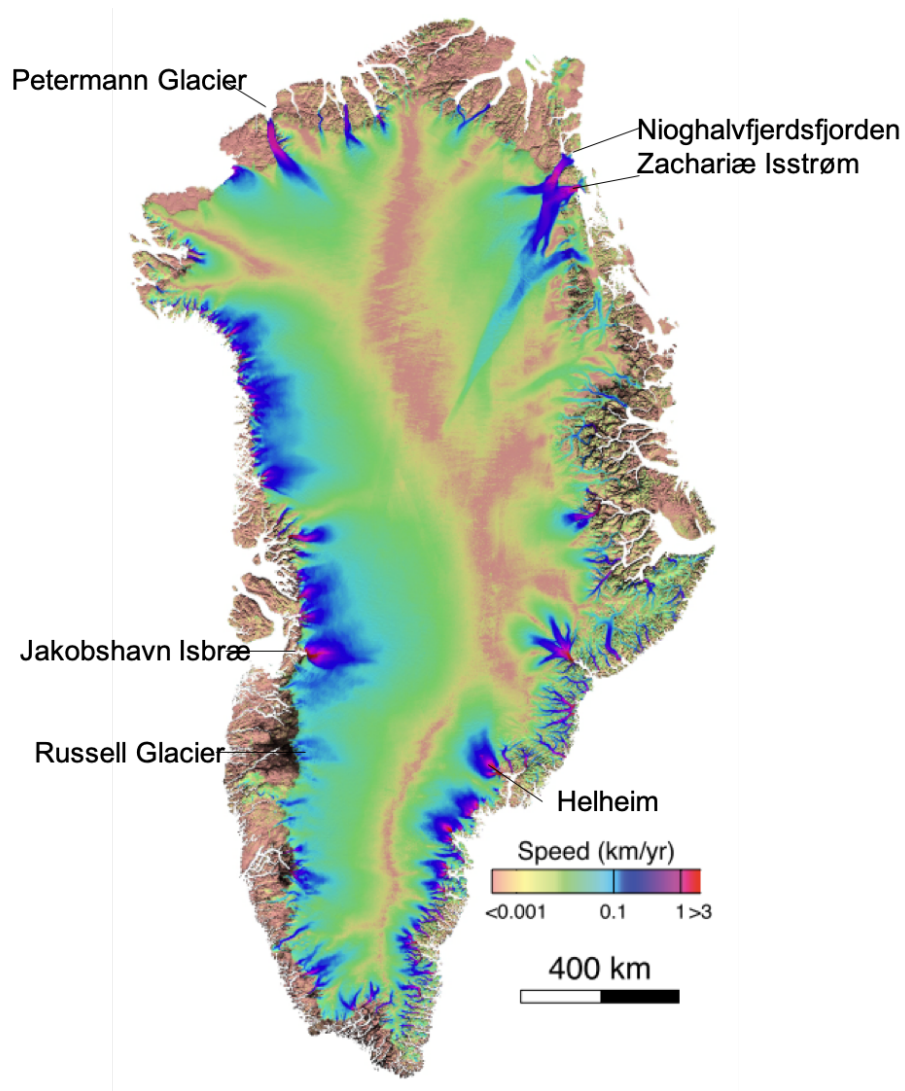


Figure 1.4: Ice velocity mosaic generated from multi-missions dataset acquired between 1992 and 2016 in Greenland. Extracted from Mouginot et al. (2017).

Seasonal changes in ice flow around Greenland have been observed at both fast-moving marine-terminating and slow-moving land-terminating glaciers (Figure 1.5 - Rignot and Kanagaratnam (2006); Joughin et al. (2008a); Shepherd et al. (2009); Palmer et al. (2011); Sundal et al. (2011); Joughin et al. (2013); Moon et al. (2014)). In the North-western sector, Petermann Glacier, one of the remaining glaciers in Greenland with a floating ice tongue, has been observed to increase its speed by 25 % in

1.3 Observations of Greenland ice motion during the satellite era

summer, relative to the winter velocity (Nick et al., 2012). Despite being a marine-terminating glacier, the seasonal cycle which has been observed at both Petermann and other marine-terminating glaciers in this region, is predominantly controlled by changes in basal traction, induced by the penetration of surface melt water to the bed (Nick et al., 2012; Moon et al., 2014, 2015). In the western sector of the ice sheet, the marine-terminating Jakobshavn Isbræ also undergoes a clear seasonal modulation in speed. The amplitude of Jakobshavn’s seasonal acceleration varies from year-to-year. For example, in 2013 the seasonal increase in velocity was 30 % to 50 % greater than previous summers due to the retreat of the ice front into deeper water, which enhanced ice frontal melting and increased ice speed and thickness of the terminus (Joughin et al., 2014). Seasonal velocity variations are not just limited to fast-flowing marine-terminating glaciers. For example in the south-western region of the ice sheet, the Russel Glacier sector has received a relatively high amount attention due to the propensity of its glaciers to exhibit seasonal speedup and its ease of access for field-based research. In-situ GPS observations have shown that seasonal velocity variations are strongly linked to changes in surface melting (Shepherd et al., 2009; Bartholomew et al., 2010, 2011, 2012; Chandler et al., 2013; Sole et al., 2013; van de Wal et al., 2015). Satellite measurements have provided a large-scale perspective of changes in ice flow (Joughin et al., 2008a; Palmer et al., 2011; Sundal et al., 2011; Fitzpatrick et al., 2013) and in the seasonal evolution of supraglacial lakes (Leeson et al., 2012; Howat et al., 2013; Leeson et al., 2013, 2015). Together, these measurements, in conjunction with numerical ice flow modelling, have led to an improved understanding of the link between regional hydrology, supra-glacial lake drainage and sub-annual changes in ice flow (Clason et al., 2015; Koziol and Arnold, 2018).

1.3 Observations of Greenland ice motion during the satellite era

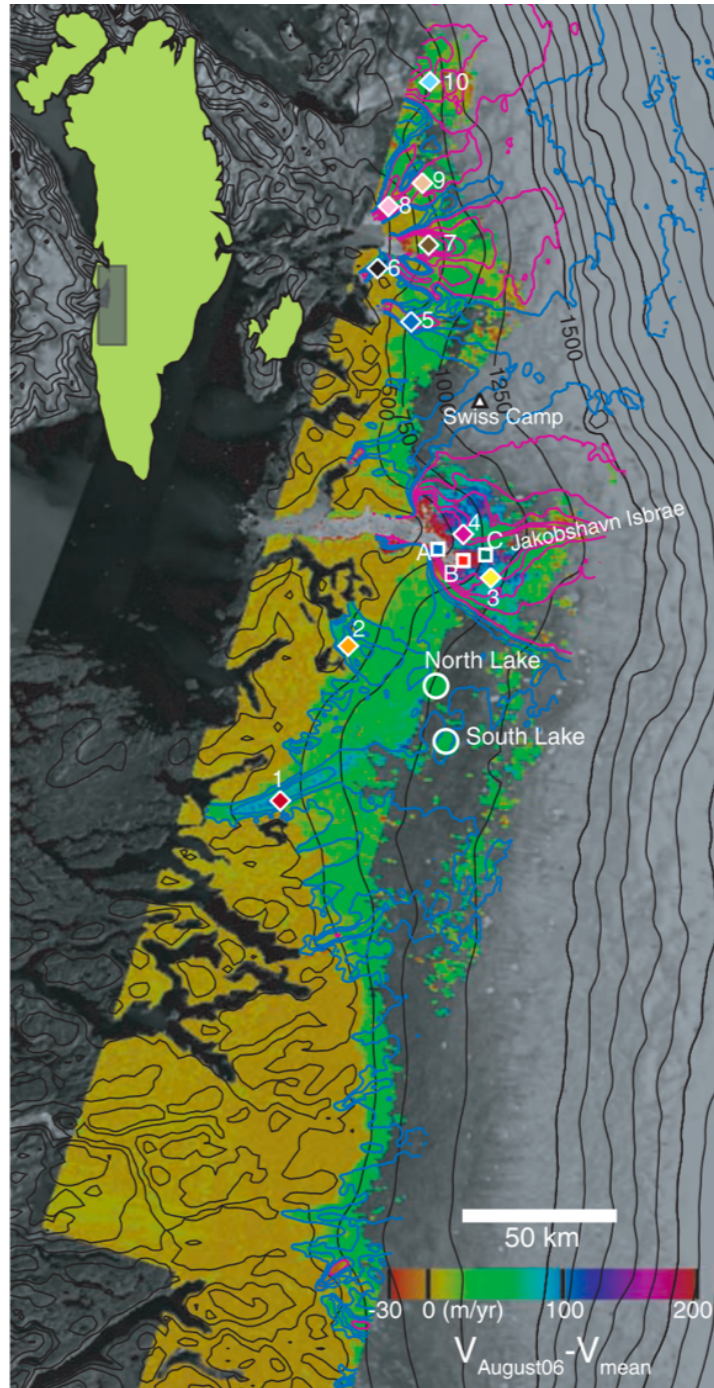


Figure 1.5: Seasonal velocity variation of the western sector of Greenland of August 2006 relative to the September 2004 to December 2006 mean speed. Extracted from Joughin et al. (2008a).

The observed acceleration of many glaciers in Greenland over the last decade is understood to have been driven by rises in air and adjacent ocean temperatures, which have enhanced the surface melting and terminus retreat (Holland et al., 2008; Moon et al., 2014, 2015). The associated increases in basal sliding and calving of their ice fronts in turn has produced enhanced discharge, leading to dynamical imbalance and additional ice loss (Joughin et al., 2010, 2014). Glacier speed is, however, highly variable in space and time (Howat et al., 2010; Moon et al., 2012; Enderlin et al., 2014), due to the geometry of individual glaciers (Felikson et al., 2017), and the high spatial variability in the forcing mechanisms (Jensen et al., 2016; Carr et al., 2017). This complexity in glacier response challenges efforts to model their future evolution (Joughin et al., 2012b; Bondzio et al., 2017) and, therefore, frequent and systematic monitoring is essential to understand the processes governing their dynamic stability. Only through advancing our understanding of the velocity response of Greenland’s glaciers over a range of timescales will we be able to confidently estimate their future contribution to future mean sea level rise (Joughin et al., 2010; Price et al., 2011; Shepherd et al., 2012).

1.4 Aim

The aim of my thesis is to develop high frequency monitoring of Greenland glacier dynamics using new multi-mission satellite datasets acquired by the Sentinel-1 and Sentinel-2 constellations, in order to assess how ice velocity variability relates to local environmental change across a range of timescales.

1.5 Objectives

In order to address the aim of this thesis, I defined the following objectives:

1. Assess the ability of the new operational satellite mission, Sentinel-1, to systematically and continuously track Greenland glacier motion;
2. Systematically map the ice speed of several of the key marine- and land-terminating glaciers in Greenland throughout the year and with high temporal frequency, from two to twelve days intervals;

3. Establish the different factors affecting seasonal and inter-annual velocity variations at land- and marine-terminating glaciers in Greenland;
4. Increase the temporal and spatial coverage of ice velocity measurements by using estimates from multi-mission satellites.

1.6 Thesis Structure

Following this introductory chapter, in Chapter 2, I provide an overview of the methods and datasets used in my thesis to achieve these objectives. This is followed by 3 chapters that describe the main results from my thesis. In Chapter 3, I analyse seasonal and inter-annual changes in the velocity of four key marine-terminating glaciers across Greenland. In Chapter 4, I generate and analyse seasonal changes in the velocity of five land-terminating glaciers in the Central-west sector of Greenland. In Chapter 5, I analyse combined measurements from both synthetic aperture radar, from the Sentinel-1 satellites, and optical, from Sentinel-2 constellation, to evaluate their complementarity for tracking ice features and motion at Jakobshavn Isbræ, Greenland. The final chapter provides a synthesis of the findings of this thesis, placing my results within a wider context, and discussing and outlining the potential avenues for future research.

References

- L. C. Andrews, G. A. Catania, M. J. Hoffman, J. D. Gulley, M. P. Lüthi, C. Ryser, R. L. Hawley, and T. A. Neumann. Direct observations of evolving subglacial drainage beneath the Greenland Ice Sheet. *Nature*, 514(7520):80–83, 2015. ISSN 14764687. doi: 10.1038/nature13796. 4
- I. D. Bartholomew, P. Nienow, D. Mair, A. Hubbard, M. a. King, and A. Sole. Seasonal evolution of subglacial drainage and acceleration in a Greenland outlet glacier. *Nature Geoscience*, 3(6):408–411, 2010. ISSN 1752-0894. doi: 10.1038/ngeo863. URL <http://www.nature.com/doifinder/10.1038/ngeo863>. 5, 7, 11
- I. D. Bartholomew, P. Nienow, A. Sole, D. Mair, T. Cowton, M. King, and S. Palmer. Seasonal variations in Greenland Ice Sheet motion: Inland extent and behaviour at higher elevations. *Earth and Planetary Science Letters*, 307(3-4):271–278, 2011.

REFERENCES

- ISSN 0012-821X. doi: 16/j.epsl.2011.04.014. URL <http://www.sciencedirect.com/science/article/pii/S0012821X11002305>. 7, 11
- I. D. Bartholomew, P. Nienow, A. Sole, D. Mair, T. Cowton, and M. a. King. Short-term variability in Greenland Ice Sheet motion forced by time-varying meltwater drainage: Implications for the relationship between subglacial drainage system behavior and ice velocity. *Journal of Geophysical Research: Earth Surface*, 117:1–17, 2012. ISSN 21699011. doi: 10.1029/2011JF002220,2012. 7, 11
- J. H. Bondzio, M. Morlighem, H. Seroussi, T. Kleiner, M. Rückamp, J. Mouginot, T. Moon, E. Y. Larour, and A. Humbert. The mechanisms behind Jakobshavn Isbrae’s acceleration and mass loss: a 3D thermomechanical model study. *Geophysical Research Letters*, 44:6252–6260, 2017. ISSN 00948276. doi: 10.1002/2017GL073309. URL <http://doi.wiley.com/10.1002/2017GL073309>. 2, 6, 13
- J. R. Carr, C. R. Stokes, and A. Vieli. Threefold increase in marine-terminating outlet glacier retreat rates across the Atlantic Arctic: 1992–2010. *Annals of Glaciology*, 58(74):72–91, 2017. ISSN 02603055. doi: 10.1017/aog.2017.3. 13
- R. Cassotto, M. Fahnstock, J. M. Amundson, M. Truffer, and I. Joughin. Seasonal and interannual variations in ice melange and its impact on terminus stability, Jakobshavn Isbræ, Greenland. *Journal of Glaciology*, 61(225):76–88, 2015. ISSN 00221430. doi: 10.3189/2015JoG13J235. 6
- D. M. Chandler, J. L. Wadham, G. P. Lis, T. Cowton, A. Sole, I. D. Bartholomew, J. Telling, P. Nienow, E. B. Bagshaw, D. Mair, S. Vinen, and A. Hubbard. Evolution of the subglacial drainage system beneath the Greenland Ice Sheet revealed by tracers. *Nature Geoscience*, 6(3):195–198, 2013. ISSN 1752-0894. doi: 10.1038/ngeo1737. URL <http://www.nature.com/doifinder/10.1038/ngeo1737>. 11
- V. W. Chu. *Greenland ice sheet hydrology: A review*, volume 38. 2014. ISBN 0309133313507. doi: 10.1177/0309133313507075. URL <http://ppg.sagepub.com/cgi/doi/10.1177/0309133313507075>. 4
- J. Church, P. Clark, A. Cazenave, J. Gregory, S. Jevrejeva, A. Levermann, M. Merrifield, G. Milne, R. Nerem, P. Nunn, A. Payne, W. Pfeffer, D. Stammer, and A. Unnikrishnan. 2013: Sea Level Change. In: *Climate Change 2013: The Physical Science*

REFERENCES

- Basis. Contribution of Working Group I to the Fifth Assessment Report of the Intergovernmental Panel on Climate Change* [Stocker, T.F., D. Qin, G.-K. Plattner, M. Tignor, S.K. Allen, J. . 2013. ISBN 9781107661820. 1
- C. C. Clason, D. W. F. Mair, P. W. Nienow, I. D. Bartholomew, a. Sole, S. Palmer, and W. Schwanghart. Modelling the transfer of supraglacial meltwater to the bed of Leverett Glacier, Southwest Greenland. *The Cryosphere*, 9(1):123–138, 2015. ISSN 1994-0424. doi: 10.5194/tc-9-123-2015. URL <http://www.the-cryosphere.net/9/123/2015/>. 11
- T. Cowton, P. Nienow, A. Sole, J. Wadham, G. Lis, I. D. Bartholomew, D. Mair, and D. Chandler. Evolution of drainage system morphology at a land-terminating Greenlandic outlet glacier. *Journal of Geophysical Research: Earth Surface*, 118(1): 29–41, 2013. ISSN 21699011. doi: 10.1029/2012JF002540. 5
- K. M. Cuffey and W. Paterson. *The Physics of Glaciers*. 4th ed. edition, 2010. ISBN 9780123694614. 6
- S. B. Das, I. Joughin, M. D. Behn, I. M. Howat, M. A. King, D. Lizarralde, and M. P. Bhatia. Fracture Propagation to the Base of the Greenland Ice Sheet During Supraglacial Lake Drainage. *Science*, 320(May):778–782, 2008. 7
- E. M. Enderlin, I. M. Howat, S. Jeong, M.-J. Noh, J. H. van Angelen, and M. R. van den Broeke. An improved mass budget for the Greenland ice sheet. *Geophys. Res. Lett.*, 41:1–7, 2014. doi: 10.1002/2013GL059010. Received. 2, 4, 8, 9, 13
- M. Fahnestock, T. Scambos, T. Moon, A. Gardner, T. Haran, and M. Klinger. Rapid large-area mapping of ice flow using Landsat 8. *Remote Sensing of Environment*, 185:84–94, 2016. ISSN 00344257. doi: 10.1016/j.rse.2015.11.023. URL <http://dx.doi.org/10.1016/j.rse.2015.11.023>. 8
- D. Felikson, T. C. Bartholomew, G. A. Catania, N. J. Korsgaard, K. H. Kjær, M. Morlighem, B. Noël, M. Van Den Broeke, L. A. Stearns, E. L. Shroyer, D. A. Sutherland, and J. D. Nash. Inland thinning on the Greenland ice sheet controlled by outlet glacier geometry. *Nature Geoscience*, 10(5):366–369, 2017. ISSN 17520908. doi: 10.1038/ngeo2934. 13

- A. A. Fitzpatrick, A. Hubbard, I. Joughin, D. J. Quincey, D. Van As, A. P. Mikkelsen, S. H. Doyle, B. Hasholt, and G. A. Jones. Ice flow dynamics and surface meltwater flux at a land-terminating sector of the Greenland ice sheet. *Journal of Glaciology*, 59(216):687–696, 2013. ISSN 00221430. doi: 10.3189/2013JoG12J143. 11
- A. S. Gardner, G. Moholdt, T. Scambos, M. Fahnestock, S. Ligtenberg, and M. V. D. Broeke. Increased West Antarctic ice discharge and East Antarctic stability over the last seven years. *The Cryosphere*, 12:521–547, 2018. doi: <https://doi.org/10.5194/tc-12-521-2018>. 8
- C. Gladish, D. Holland, A. Rosing-Asvid, J. W. Behrens, and J. Boje. Oceanic Boundary Conditions for Jakobshavn Glacier. Part II: Provenance and Sources of Variability of Disko Bay and Ilulissat Icefjord Waters, 1990–2011. *Journal of Physical Oceanography*, 45(2003):33–63, 2015. ISSN 0022-3670. doi: 10.1175/JPO-D-14-0045.1. 6
- R. M. Goldstein, H. Engelhardt, B. Kamb, and R. M. Frolich. Satellite Radar Interferometry for Monitoring Ice Sheet Motion: Application to an Antarctic Ice Stream. *Science*, 262(3 December):1525–1530, 1993. 8
- E. Hanna, S. H. Mernild, J. Cappelen, and K. Steffen. Recent warming in Greenland in a long-term instrumental (1881-2012) climatic context: I. Evaluation of surface air temperature records. *Environmental Research Letters*, 7(4), 2012. ISSN 17489326. doi: 10.1088/1748-9326/7/4/045404. 4
- E. Hanna, X. Fettweis, S. H. Mernild, J. Cappelen, M. H. Ribergaard, C. a. Shuman, K. Steffen, L. Wood, and T. L. Mote. Atmospheric and oceanic climate forcing of the exceptional Greenland ice sheet surface melt in summer 2012. *International Journal of Climatology*, 34(4):1022–1037, 2014. ISSN 08998418. doi: 10.1002/joc.3743. 4
- J. T. Harper, N. F. Humphrey, W. T. Pfeffer, T. Fudge, and S. O’Neel. Evolution of subglacial water pressure along a glacier’s length. *Annals of Glaciology*, 40(1981): 31–36, 2005. ISSN 02603055. doi: 10.3189/172756405781813573. 4
- E. A. Hill, J. R. Carr, C. R. Stokes, and G. H. Gudmundsson. Dynamic changes in outlet glaciers in northern Greenland from 1948 to 2015. *The Cryosphere*, 12: 3243–3263, 2018. ISSN 1994-0440. doi: 10.5194/tc-2018-17. URL <https://www.the-cryosphere-discuss.net/tc-2018-17/>. 8, 9

REFERENCES

- M. J. Hoffman, G. A. Catania, T. A. Neumann, L. C. Andrews, and J. A. Rumrill. Links between acceleration, melting, and supraglacial lake drainage of the western Greenland Ice Sheet. *Journal of Geophysical Research: Earth Surface*, 116(4):1–16, 2011. ISSN 21699011. doi: 10.1029/2010JF001934. 4
- D. M. Holland, R. H. Thomas, B. D. Young, M. H. Ribergaard, and B. Lyberth. Acceleration of Jakobshavn Isbræ triggered by warm subsurface ocean waters. *Nature Geoscience*, 1:1–6, 2008. doi: 10.1038/ngeo316. 4, 6, 13
- I. M. Howat, I. Joughin, S. Tulaczyk, and S. Gogineni. Rapid retreat and acceleration of Helheim Glacier, east Greenland. *Geophysical Research Letters*, 32(22):1–4, 2005. ISSN 00948276. doi: 10.1029/2005GL024737. 6, 8
- I. M. Howat, J. E. Box, Y. Ahn, A. Herrington, and E. M. McFadden. Seasonal variability in the dynamics of marine-terminating outlet glaciers in Greenland. *Journal of Glaciology*, 56(198):601–613, 2010. ISSN 00221430. doi: 10.3189/002214310793146232. 13
- I. M. Howat, S. de la Peña, J. H. van Angelen, J. T. M. Lenaerts, and M. R. van den Broeke. Brief Communication: "Expansion of meltwater lakes on the Greenland Ice Sheet". *The Cryosphere*, 7(1):201–204, 2013. ISSN 1994-0424. doi: 10.5194/tc-7-201-2013. URL <http://www.the-cryosphere.net/7/201/2013/>. 11
- T. S. Jensen, J. E. Box, and C. S. Hvidberg. A sensitivity study of annual area change for Greenland ice sheet marine terminating outlet glaciers: 1999–2013. *Journal of Glaciology*, 62:1–10, 2016. ISSN 0022-1430. doi: 10.1017/jog.2016.12. URL http://www.journals.cambridge.org/abstract/{_}S0022143016000125. 13
- I. Joughin, W. Abdalati, and M. Fahnestock. Large fluctuations in speed on Greenland's Jakobshavn Isbrae glacier. *Nature*, 432(7017):608–10, dec 2004. ISSN 1476-4687. doi: 10.1038/nature03130. URL <http://www.ncbi.nlm.nih.gov/pubmed/15577906>. 9
- I. Joughin, S. B. Das, M. A. King, B. E. Smith, I. M. Howat, and T. Moon. Seasonal Speedup Along the Western Flank of the Greenland Ice Sheet. *Science*, 320(April): 781–784, 2008a. doi: 10.1126/science.1153288. x, 6, 7, 10, 11, 12

REFERENCES

- I. Joughin, I. M. Howat, M. Fahnestock, B. Smith, W. Krabill, R. B. Alley, H. Stern, and M. Truffer. Continued evolution of Jakobshavn Isbrae following its rapid speedup. *Journal of Geophysical Research: Earth Surface*, 113(4):1–14, 2008b. ISSN 21699011. doi: 10.1029/2008JF001023. 6, 7, 9
- I. Joughin, B. E. Smith, I. M. Howat, T. Scambos, and T. Moon. Greenland flow variability from ice-sheet-wide velocity mapping. *Journal of Glaciology*, 56(197):415–430, aug 2010. ISSN 00221430. doi: 10.3189/002214310792447734. URL <http://openurl.ingenta.com/content/xref?genre=article&issn=0022-1430&volume=56&issue=197&spage=415>. 2, 8, 13
- I. Joughin, R. B. Alley, and D. M. Holland. Ice-Sheet Response to Oceanic Forcing. *Science*, 338(6111):1172–6, 2012a. ISSN 1095-9203. doi: 10.1126/science.1226481. URL <http://www.ncbi.nlm.nih.gov/pubmed/23197526>. x, 2, 6, 7
- I. Joughin, B. E. Smith, I. M. Howat, D. Floricioiu, R. B. Alley, M. Truffer, and M. Fahnestock. Seasonal to decadal scale variations in the surface velocity of Jakobshavn Isbrae, Greenland: Observation and model-based analysis. *Journal of Geophysical Research: Earth Surface*, 117(2):1–20, 2012b. ISSN 21699011. doi: 10.1029/2011JF002110. 2, 6, 7, 9, 13
- I. Joughin, S. B. Das, G. E. Flowers, M. D. Behn, R. B. Alley, M. A. King, B. E. Smith, J. L. Bamber, M. R. Van Den Broeke, and J. H. Van Angelen. Influence of ice-sheet geometry and supraglacial lakes on seasonal ice-flow variability. *Cryosphere*, 7(4):1185–1192, 2013. ISSN 19940416. doi: 10.5194/tc-7-1185-2013. 10
- I. Joughin, B. E. Smith, D. E. Shean, and D. Floricioiu. Brief communication: Further summer speedup of Jakobshavn Isbræ. *The Cryosphere*, 8(1):209–214, 2014. ISSN 19940416. doi: 10.5194/tc-8-209-2014. 4, 6, 7, 8, 9, 11, 13
- I. Joughin, B. E. Smith, and I. Howat. Greenland Ice Mapping Project: Ice Flow Velocity Variation at sub-monthly to decadal time scales. *The Cryosphere*, 12:2211–2227, 2018. doi: <https://doi.org/10.5194/tc-12-2211-2018>. 8, 9
- C. P. Koziol and N. Arnold. Modelling seasonal meltwater forcing of the velocity of land-terminating margins of the Greenland Ice Sheet. *The Cryosphere*, 12(3):971–991, 2018. ISSN 19940424. doi: 10.5194/tc-12-971-2018. 11

REFERENCES

- A. Leeson, A. Shepherd, S. Palmer, A. Sundal, and X. Fettweis. Simulating the growth of supraglacial lakes at the western margin of the Greenland ice sheet. *Cryosphere*, 6(5):1077–1086, 2012. ISSN 19940416. doi: 10.5194/tc-6-1077-2012. 11
- A. Leeson, A. Shepherd, K. Briggs, and X. Fettweis. Supraglacial lakes on Greenland migrate inland under warming climate. *Nature Climate Change*, 16(January):51–55, 2015. ISSN 1758-678X. doi: 10.1038/NCLIMATE2463. 11
- A. A. Leeson, A. Shepherd, A. V. Sundal, A. M. Johansson, N. Selmes, K. Briggs, A. E. Hogg, and X. Fettweis. A comparison of supraglacial lake observations derived from MODIS imagery at the western margin of the Greenland ice sheet. *Journal of Glaciology*, 59(218):1179–1188, 2013. ISSN 00221430. doi: 10.3189/2013JoG13J064. 4, 11
- B. K. Lucchitta, C. E. Rosanova, and K. F. Mullins. Velocities of Pine Island Glacier, West Antarctica, from ERS-1 SAR images. *Annals of Glaciology*, 21:277–283, 1995. ISSN 02603055. doi: 10.1017/S0260305500015949. 8
- M. McMillan, P. Nienow, A. Shepherd, T. Benham, and A. Sole. Seasonal evolution of supra-glacial lakes on the Greenland Ice Sheet. *Earth and Planetary Science Letters*, 262:484–492, 2007. ISSN 0012821X. doi: 10.1016/j.epsl.2007.08.002. 4
- M. McMillan, A. Leeson, A. Shepherd, K. Briggs, T. W. K. Armitage, A. Hogg, P. K. Munneke, M. van den Broeke, B. Noël, W. J. van de Berg, S. Ligtenberg, M. Horwath, A. Groh, A. Muir, and L. Gilbert. A high resolution record of Greenland mass balance. *Geophysical Research Letters*, 43:1–9, 2016. doi: 10.1002/GRL.54619. 1, 2, 8, 9
- T. Moon, I. Joughin, B. Smith, and I. Howat. 21st-century evolution of Greenland outlet glacier velocities. *Science*, 336(6081):576–8, may 2012. ISSN 1095-9203. doi: 10.1126/science.1219985. URL <http://www.ncbi.nlm.nih.gov/pubmed/22556249>. 8, 9, 13
- T. Moon, I. Joughin, B. Smith, M. R. Broeke, W. J. Berg, B. Noël, and M. Usher. Distinct patterns of seasonal Greenland glacier velocity. *Geophysical Research Letters*, 41:7209–7216, 2014. doi: 10.1002/2014GL061836. 4, 10, 11, 13

- T. Moon, I. Joughin, and B. Smith. Seasonal to multiyear variability of glacier surface velocity, terminus position, and sea ice/ice mélange in northern Greenland. *Journal of Geophysical Research: Earth Surface*, 120:818–833, 2015. doi: 10.1002/2015JF003494. Received. 4, 11, 13
- J. Mouginot, E. Rignot, B. Scheuchl, I. Fenty, A. Khazendar, M. Morlighem, A. Buzzi, and J. Paden. Fast retreat of Zachariæ Isstrøm , northeast Greenland. *Science Express*, 10.1126(November), 2015. doi: 10.1126/science.aac7111. 9
- J. Mouginot, E. Rignot, B. Scheuchl, and R. Millan. Comprehensive Annual Ice Sheet Velocity Mapping Using Landsat-8, Sentinel-1, and RADARSAT-2 Data. *Remote Sensing*, 9(364):1–20, 2017. ISSN 0018-9235. doi: 10.3390/rs9040364. URL <http://www.mdpi.com/2072-4292/9/4/364/htm>. x, 10
- T. Nagler, H. Rott, M. Hetzenecker, J. Wuite, and P. Potin. The Sentinel-1 Mission: New Opportunities for Ice Sheet Observations. *Remote Sensing*, 7(7):9371–9389, 2015. ISSN 2072-4292. doi: 10.3390/rs70709371. URL <http://www.mdpi.com/2072-4292/7/7/9371/>. 8
- F. Nick, a. Luckman, a. Vieli, C. Van Der Veen, D. Van As, R. Van De Wal, F. Pattyn, a.L. Hubbard, and D. Floricioiu. The response of Petermann Glacier, Greenland, to large calving events, and its future stability in the context of atmospheric and oceanic warming. *Journal of Glaciology*, 58(208):229–239, 2012. ISSN 00221430. doi: 10.3189/2012JoG11J242. URL <http://www.igsoc.org/journal/58/208/j11J242.html>. 9, 11
- F. M. Nick, A. Vieli, I. M. Howat, and I. Joughin. Large-scale changes in Greenland outlet glacier dynamics triggered at the terminus. *Nature Geoscience*, 2(2):110–114, 2009. ISSN 1752-0894. doi: 10.1038/ngeo394. URL <http://dx.doi.org/10.1038/ngeo394>. 6
- P. W. Nienow, A. L. Hubbard, B. P. Hubbard, D. M. Chandler, D. W. F. Mair, M. J. Sharp, and I. C. Willis. Hydrological controls on diurnal ice flow variability in valley glaciers. *Journal of Geophysical Research: Earth Surface*, 110(4):1–11, 2005. ISSN 21699011. doi: 10.1029/2003JF000112. 4

REFERENCES

- S. Palmer, A. Shepherd, P. Nienow, and I. Joughin. Seasonal speedup of the Greenland Ice Sheet linked to routing of surface water. *Earth and Planetary Science Letters*, 302(3-4):423–428, 2011. ISSN 0012821X. doi: 10.1016/j.epsl.2010.12.037. URL <http://dx.doi.org/10.1016/j.epsl.2010.12.037>. 10, 11
- S. F. Price, A. J. Payne, I. M. Howat, and B. E. Smith. Committed sea-level rise for the next century from Greenland ice sheet dynamics during the past decade. *Proceedings of the National Academy of Sciences*, 108(22):8978–8983, 2011. ISSN 0027-8424. doi: 10.1073/pnas.1017313108. URL <http://www.pnas.org/cgi/doi/10.1073/pnas.1017313108>. 13
- E. Rignot. Tidal motion, ice velocity and melt rate of Petermann Gletscher, Greenland, measured from radar interferometry. *Journal of Glaciology*, 42(142):476–485, 1996. ISSN 00221430. 9
- E. Rignot and P. Kanagaratnam. Changes in the Velocity Structure of the Greenland Ice Sheet. *Science*, 311(February):986–990, 2006. doi: 10.1126/science.1121381. 2, 10
- E. Rignot and J. Mouginot. Ice flow in Greenland for the International Polar Year 2008-2009. *Geophysical Research Letters*, 39(11):1–7, 2012. ISSN 00948276. doi: 10.1029/2012GL051634. 8
- E. Rignot and K. Steffen. Channelized bottom melting and stability of floating ice shelves. *Geophysical Research Letters*, 35(2):1–5, 2008. ISSN 00948276. doi: 10.1029/2007GL031765. 9
- E. Rignot, I. Velicogna, M. R. Van Den Broeke, A. Monaghan, and J. T. M. Lenaerts. Acceleration of the contribution of the Greenland and Antarctic ice sheets to sea level rise. *Geophysical Research Letters*, 38(5):1–5, 2011. ISSN 00948276. doi: 10.1029/2011GL046583. 8
- E. Rignot, J. Mouginot, B. Scheuchl, M. R. van den Broeke, M. J. van Wessem, and M. Morlighem. Four decades of Antarctic Ice Sheet mass balance from 1979-2017. *Proceedings of the National Academy of Sciences*, pages 1–9, 2019. ISSN 0027-8424. doi: 10.1073/pnas.1812883116. 1

REFERENCES

- R. Rosenau, M. Scheinert, and R. Dietrich. A processing system to monitor Greenland outlet glacier velocity variations at decadal and seasonal time scales utilizing the Landsat imagery. *Remote Sensing of Environment*, 169:1–19, 2015. ISSN 00344257. doi: 10.1016/j.rse.2015.07.012. URL <http://dx.doi.org/10.1016/j.rse.2015.07.012>. 8
- C. Schoof. Ice-sheet acceleration driven by melt supply variability. *Nature*, 468(7325):803–806, 2010. ISSN 0028-0836. doi: 10.1038/nature09618. URL <http://dx.doi.org/10.1038/nature09618>. 5
- A. Shepherd, A. Hubbard, P. Nienow, M. King, M. McMillan, and I. Joughin. Greenland ice sheet motion coupled with daily melting in late summer. *Geophysical Research Letters*, 36(L01501):1–4, 2009. ISSN 0094-8276. doi: 10.1029/2008GL035758. URL <http://doi.wiley.com/10.1029/2008GL035758>. 7, 10, 11
- A. Shepherd, E. R. Ivins, G. A., V. R. Barletta, M. J. Bentley, S. Bettadpur, K. H. Briggs, D. H. Bromwich, R. Forsberg, N. Galin, M. Horwath, S. Jacobs, I. Joughin, M. A. King, J. T. M. Lenaerts, J. Li, S. R. M. Ligtenberg, A. Luckman, S. B. Luthcke, M. McMillan, R. Meister, G. Milne, J. Mouginot, A. Muir, J. P. Nicolas, J. Paden, A. J. Payne, H. Pritchard, E. Rignot, H. Rott, L. S. Sørensen, T. A. Scambos, B. Scheuchl, E. J. O. Schrama, B. Smith, A. V. Sundal, J. H. van Angelen, W. J. van de Berg, M. R. van den Broeke, D. G. Vaughan, I. Velicogna, J. Wahr, P. L. Whitehouse, D. J. Wingham, D. Yi, D. Young, and H. J. Zwally. A Reconciled Estimate of Ice-Sheet Mass Balance. *Science*, 338(November):1183–1189, 2012. doi: 10.1126/science.1228102. 2, 8, 13
- A. Shepherd, H. A. Fricker, and S. L. Farrell. Trends and connections across the Antarctic cryosphere. *Nature*, 558:223–232, 2018. 1, 2
- A. Sole, P. W. Nienow, I. D. Bartholomew, D. W. F. Mair, T. R. Cowton, A. J. Tedstone, and M. a. King. Winter motion mediates dynamic response of the Greenland Ice Sheet to warmer summers. *Geophysical Research Letters*, 40(15):3940–3944, 2013. ISSN 00948276. doi: 10.1002/grl.50764. 11
- L. S. Sørensen, S. B. Simonsen, R. Forsberg, K. Khvorostovsky, R. Meister, and M. E. Engdahl. 25 years of elevation changes of the Greenland Ice Sheet from ERS, Envisat,

REFERENCES

- and CryoSat-2 radar altimetry. *Earth and Planetary Science Letters*, 495:234–241, 2018. ISSN 0012821X. doi: 10.1016/j.epsl.2018.05.015. URL <https://doi.org/10.1016/j.epsl.2018.05.015>. 9
- A. V. Sundal, A. Shepherd, P. Nienow, E. Hanna, S. Palmer, and P. Huybrechts. Melt-induced speed-up of Greenland ice sheet offset by efficient subglacial drainage. *Nature*, 469(7331):521–4, jan 2011. ISSN 1476-4687. doi: 10.1038/nature09740. URL <http://www.ncbi.nlm.nih.gov/pubmed/21270891>. 5, 7, 10, 11
- M. Tedesco, X. Fettweis, T. Mote, J. Wahr, P. Alexander, J. E. Box, and B. Wouters. Evidence and analysis of 2012 Greenland records from spaceborne observations, a regional climate model and reanalysis data. *The Cryosphere*, 7(2):615–630, 2013. ISSN 1994-0424. doi: 10.5194/tc-7-615-2013. URL <http://www.the-cryosphere.net/7/615/2013/>. 7
- A. J. Tedstone, P. W. Nienow, N. Gourmelen, A. Dehecq, D. Goldberg, and E. Hanna. Decadal slowdown of a land-terminating sector of the Greenland Ice Sheet despite warming. *Nature*, 526(7575):692–695, 2015. ISSN 0028-0836. doi: 10.1038/nature15722. URL <http://www.nature.com/doi/10.1038/nature15722>. 5, 9
- L. D. Trusel, S. B. Das, M. B. Osman, M. J. Evans, B. E. Smith, X. Fettweis, J. R. McConnell, B. P. Y. Noël, and M. R. van den Broeke. Nonlinear rise in Greenland runoff in response to post-industrial Arctic warming. *Nature*, 564(7734):104–108, 2018. ISSN 0028-0836. doi: 10.1038/s41586-018-0752-4. URL <http://www.nature.com/articles/s41586-018-0752-4>. x, 2, 3, 8
- R. S. van de Wal, C. J. Smeets, W. Boot, M. Stoffelen, R. Van Kampen, S. H. Doyle, F. Wilhelms, M. R. Van Den Broeke, C. H. Reijmer, J. Oerlemans, and A. Hubbard. Self-regulation of ice flow varies across the ablation area in south-west Greenland. *The Cryosphere*, 9:603–611, 2015. ISSN 19940424. doi: 10.5194/tc-9-603-2015. 7, 11
- R. S. W. van de Wal, W. Boot, M. R. van den Broeke, C. J. P. P. Smeets, C. H. Reijmer, J. J. A. Donker, and J. Oerlemans. Large and Rapid Melt-Induced Velocity Changes in the Ablation Zone of the Greenland Ice Sheet. *Science*, 321:111–113, 2008. doi: 10.1126/science.1158540. 9

REFERENCES

- M. van den Broeke, J. L. Bamber, J. Ettema, E. Rignot, E. Schrama, W. J. van de Berg, E. van Meijgaard, I. Velicogna, and B. Wouters. Partitioning recent Greenland mass loss. *Science*, 326(November):984–986, 2009. ISSN 0036-8075. doi: 10.1126/science.1178176. x, 1, 3
- M. van den Broeke, E. Enderlin, I. Howat, P. Kuipers Munneke, B. Noël, W. J. van de Berg, E. van Meijgaard, and B. Wouters. On the recent contribution of the Greenland ice sheet to sea level change. *The Cryosphere*, 10:1933–1946, 2016. ISSN 1994-0440. doi: 10.5194/tc-2016-123. URL <http://www.the-cryosphere-discuss.net/tc-2016-123/>. 2, 4
- C. L. Vernon, J. L. Bamber, J. E. Box, M. R. van den Broeke, X. Fettweis, E. Hanna, and P. Huybrechts. Surface mass balance model intercomparison for the Greenland ice sheet. *The Cryosphere*, 7(2):599–614, 2013. ISSN 1994-0424. doi: 10.5194/tc-7-599-2013. URL <https://www.the-cryosphere.net/7/599/2013/>. 1
- H. J. Zwally, W. Abdalati, T. Herring, K. Larson, J. Saba, and K. Steffen. Surface Melt – Induced Acceleration of Greenland Ice-Sheet Flow. *Science*, 297(July):218–223, 2002. doi: 10.1126/science.1072708. x, 4, 5

Chapter 2

Tracking Ice motion in Greenland

In this Chapter, I begin by describing the different methods for tracking ice motion, including remote sensing and in situ techniques. Then, I focus on the techniques and satellite platforms used to make measurements in the microwave part of the spectrum, namely satellites Sentinel-1a and b, that I used within Chapters 3 and 4 of the thesis. Then, I describe the multi spectral images of Sentinel-2a and b satellites used in Chapter 5, followed by the feature tracking technique using optical images, finishing with a discussion of the relative advantages and limitations of both techniques.

2.1 Introduction to tracking ice motion

Ice motion measurements are essential for monitoring ice sheet dynamics and ice discharge, and for assessing an ice sheet's mass budget (Joughin et al., 1995). Different techniques have been employed to estimate glaciers' velocities, using both in situ and remote monitoring platforms. Thanks to the systematic acquisitions at high spatial and temporal resolution, images from spaceborne sensors are, currently, widely used to identify and monitor glaciological features. Optical imagery, which operates in the visible and near-infrared electro magnetic spectrum, has been used to observe the Earth's surface since the launch of the Landsat constellation in 1972 (Wulder et al., 2012). Using these optical instruments, velocity changes have been systematically monitored (Rosenau et al., 2015; Fahnestock et al., 2016). These records are now important indicators of how the cryosphere has been affected by variations in the surrounding climate system. Early in the satellite era velocity tracking tended to be manual and small

2.1 Introduction to tracking ice motion

scale (Goldstein et al., 1993; Lucchitta et al., 1995), but more recently this process has become more automated and routinely tracked in repeat optical (Rosenau et al., 2015; Fahnestock et al., 2016; Gardner et al., 2018) and synthetic aperture radar (SAR) imagery (Joughin et al., 2010; Rignot et al., 2011b; Nagler et al., 2015), which operates in the microwave region of the electro magnetic spectrum, between 1 and 12 GHz . Although both SAR and optical instruments can yield high-quality measurements of ice sheet flow, they are also affected by changing environmental conditions. In the case of optical imagery, clouds frequently interfere, partially or completely masking the ice surface. In the case of SAR imagery, surface melting can be especially problematic as it changes the backscattering properties of the ice sheet. A combination of the two methods is therefore likely to be the best approach for continuous and consistent monitoring.

In situ measurements of ice motion

During the early glaciological studies of the 1960s, field campaigns were organized with the objective of forming a better understanding of the internal stresses and strains of glaciers flow under gravity. For instance, in order to measure surface motion, a network of stakes had to be installed and monitored daily, and in some occasions hourly, and the distance displaced was measured with a reference point and a theodolite (e.g. Iken and Bindschadler (1986); Kamb and Engelhardt (1987)). As technology advanced, for example to exploit Global Position Systems (GPS), glaciologists further benefited from these new forms of in situ measurements (e.g. Zwally et al. (2002); Shepherd et al. (2009); Joughin et al. (2010)). Substantial advances were achieved, such as the near coincidence of the ice acceleration with the duration of surface melting, followed by deceleration after the melting ceases, which indicates that glacial sliding is enhanced by rapid migration of surface meltwater to the ice-bedrock interface (Zwally et al., 2002; Shepherd et al., 2009). Nonetheless, field data tends to be limited in space and time and so it is difficult to derive comprehensive, ice sheet wide observational datasets from field data alone. The high cost and the difficulty of field campaigns has led to alternative methods of analysis, and specifically those which utilize satellite data.

Satellite measurements of ice motion

At present, the only way to systematically monitor ice velocity at a continental scale is through satellite imagery. Glacier velocities were first measured using Landsat satellite data acquired during the 1980s through digital optical image comparison (Lucchitta and Ferguson, 1986). Currently, optical images are still largely used for mapping glacier velocity at large scale (e.g. Dehecq et al. (2015); Fahnestock et al. (2016); Armstrong et al. (2017)). However, due to the dependency of optical data upon daylight conditions, cloud-free skies and the limited acquisitions across the polar regions, the use of Synthetic Aperture Radar (SAR) images has become common since the launch of ERS-1 in 1991. In the following decades, these data have been used to monitor dynamic processes occurring across remote areas such as the Greenland and Antarctic ice sheets, using the techniques of Interferometric Synthetic Aperture Radar (InSAR) and SAR feature tracking (Joughin et al., 2010; Rignot and Mouginot, 2012; Nagler et al., 2015; Mouginot et al., 2017).

The Interferometric Synthetic Aperture Radar technique has been used since the 1970's (e.g. Graham (1974)), when data from airborne campaigns were first used to generate topographic maps. After the launch of the first European Remote Sensing (ERS-1) satellite in 1991 by the European Space Agency (ESA), Goldstein et al. (1993) was the first to apply the InSAR technique for the purpose of remote glaciological study. They applied the InSAR technique to SAR imagery of the Rutford Ice Stream, Antarctica, to measure ice flow and grounding line position. A synthetic aperture radar is a coherent imaging system, containing information relating both to the amplitude (magnitude) and phase of the radar echo received during acquisition. Pulses of electromagnetic radiation are transmitted by the antenna of the SAR system, and the backscattered energy received depends on the surface morphology and roughness, dielectric properties and absorption of the target, and its range from the satellite. The interferometric technique uses phase difference information from at least two complex SAR images acquired over the same region but from a different position, time, or both (Bamler and Hartl, 1998), in order to determine topography and surface motion information (Joughin et al., 1996). In so-called satellite repeat-pass interferometry, where acquisitions are typically separated in space and time, the phase difference contains both

topography and displacement information. If the surface topography is known, for example from an external Digital Elevation Model, then the topographic phase component can be simulated and removed, in order to isolate the surface motion information.

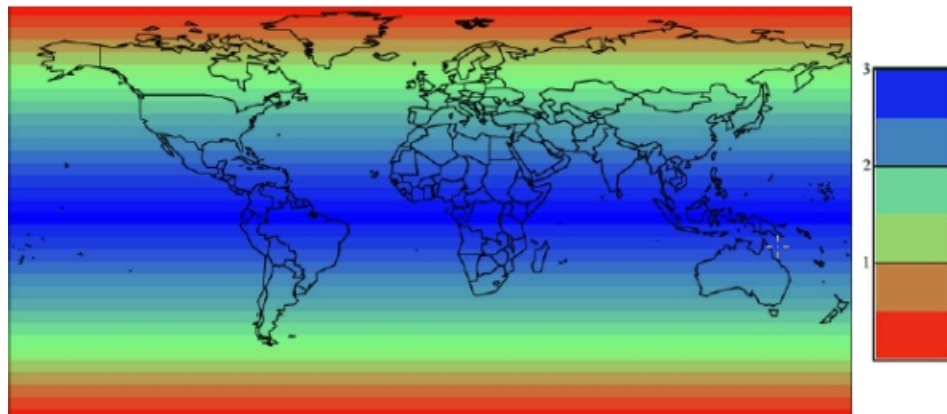
Despite the use of interferometry to measure glacier velocity (Pritchard et al., 2005; Joughin et al., 2004; Howat et al., 2005; Rignot and Kanagaratnam, 2006; Joughin et al., 2008, 2010), the technique is restricted to short (typically 1-3 days) temporal baselines, which reduces its use on a wider scale (Paul et al., 2015). InSAR is a coherent processing technique and, contrary to optical and intensity tracking techniques, the phase information in the SAR image must be sufficiently stable to enable its use (Joughin et al., 2010). Decorrelation (phase instability) occurs due to locally steeper terrain slope, changes in the backscattering properties of the surface being imaged, or the spatial or temporal baseline increasing (Massom and Lubin, 2006; Joughin et al., 2010). Temporal decorrelation is a particular issue in the cryosphere field, due to the rearrangement of snow grains near the surface during compaction, areas of high accumulation and melting, and movement due to flow and snow drifting (Joughin et al., 2010). While InSAR has been widely used in the glaciological field, it can be limited by coherence levels and spatial coverage. For these reasons, the technique of SAR intensity tracking has become widely used in cryospheric study. In essence, this technique matches nearly identical features, such as crevasses, between sequential images (Strozzi et al., 2002). In this thesis, the intensity tracking technique has been primarily used and is described in further detail in section 2.2.

2.2 SAR intensity tracking

Sentinel-1 platform

Sentinel-1 mission is a constellation formed by Sentinel-1a, launched in April 2014, and Sentinel-1b in April 2016. Each satellite has a repeat cycle of 12 days and 180 degrees orbital phasing difference, resulting in a revisit time of 6 days over the same area after the Sentinel-1b launch (Figure 2.1). The Sentinel SAR instruments operate at c-band in the radar region of the electromagnetic spectrum, with a centre frequency of 5.405 GHz, corresponding to a wavelength of 5.55 cm. Their scanning modes are Strip Map (SM), Extra-Wide swath (EW), Wave mode (WV), and the Interferometric Wide swath

(IW), which are represented in the Figure 2.2. To map ice velocity, I used the IW mode due to its swath coverage of 250km and spatial resolution of 5 m in ground range and 20 m in azimuth. Moreover, The IW mode acquires data divided into 3 sub-swaths, using the Terrain Observation by Progressive Scan (TOPS) mode imaging technique, providing larger swath width at ground resolution with enhanced image performance, as all targets are acquired by the entire azimuth antenna pattern (Geudtner et al., 2014). Each IW sub-swath consists of a series of bursts, which have to be re-sampled to a common pixel spacing in range and azimuth with burst synchronisation and phase preservation (Torres et al., 2012).



- ✓ Two satellites in a 12 day orbit
- ✓ Repeat frequency: 6 days (important for coherence)
- ✓ Revisit frequency: (asc/desc & overlap): 3 days at the equator, <1 day at high latitudes (Europe ~ 2 days)

Figure 2.1: Illustration of the revisit frequency of Sentinel-1a and b, combining ascending and descending acquisitions, expressed in days per revisit. Extracted from European Space Agency (ESA) website.

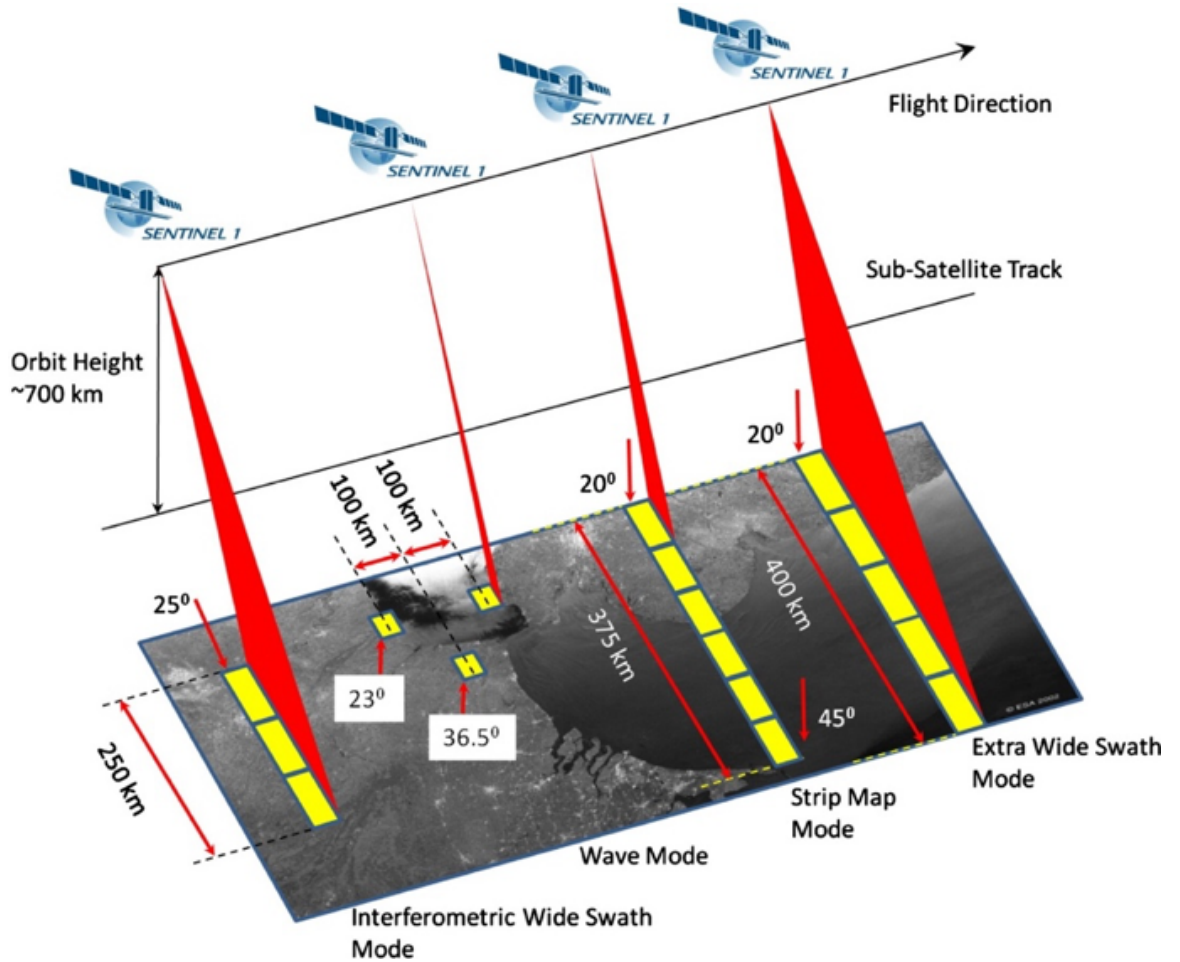


Figure 2.2: Illustration of different imaging modes of Sentinel-1. Extracted from Geudtner et al. (2014).

Summary of the satellite and ancillary data used

To map ice velocity for the studies described in Chapters 3 and 4, I used single look complex (SLC) synthetic aperture radar images acquired in the interferometric wide swath mode from the Sentinel-1a and Sentinel-1b satellites. The Level-1 data from Sentinel-1 is available in single look complex imagery and ground range detected imagery (GRD). The ground range detected products are focused SAR data that have been detected, multi-looked and projected to ground range using an Earth ellipsoid model, and the resulting product has approximately square spatial resolution and square pixel spacing

with reduced speckle due to the multi-look processing. Here, I use single look complex images in order to exploit the original backscatter statistics for speckle filtering and classification, and to perform terrain-corrected geocoding using high resolution digital elevation models. Moreover, for the intensity tracking processing, when coherence is retained, the speckle pattern of the two images is correlated, and intensity tracking with small image patches can be performed more accurately (Strozzi et al., 2002). The dataset used in Chapter 3 was acquired over the period spanning from October 2014 to February 2017 and from October 2016 to February 2017, for Sentinel-1a and Sentinel-1b, respectively, providing a total of 187 ice velocity maps. During co-registration and the geocoding step, explained in the next section, I used the precise orbits provided by the European Space Agency (Sentinels_POD_Team, 2013), and the Greenland Ice Mapping Project (GIMP) digital elevation model (DEM) posted on a 90 m grid (Howat et al., 2014), respectively. To map the bedrock, I used the bed elevation from the Ice-Bridge BedMachine Greenland V2 product (Morlighem et al., 2015). Furthermore, to evaluate my ice velocity measurements, I used independent estimates derived from TerraSAR-X (TSX) SAR imagery through the speckle tracking technique (Joughin, 2002), which has a repeat period acquisition of 11 days and spatial resolution up to 3 m, from January 2009 to January 2017 (Joughin et al., 2016). The ice front positions were extracted from Joughin et al. (2014), and ESA Greenland Ice Sheet Climate Change Initiative (CCI) project (2017). In Chapter 4, the SLC IW Sentinel-1 images were acquired between January 2016 and December 2017, generating 96 individual ice velocity maps. I then computed positive degree days (PDDs) as a measure of the surface melting using air temperatures recorded at the nearby KAN_L automatic weather station and distributed by the Programme for Monitoring of the Greenland Ice Sheet (PROMICE, <https://www.promice.dk/WeatherStations.html>).

Methodology applied

Synthetic aperture radar intensity tracking is a robust technique and has been widely applied throughout Greenland and Antarctica to estimate ice motion (Strozzi et al., 2002; Luckman et al., 2003; Pritchard et al., 2005; Luckman et al., 2007; Sundal et al., 2011; McMillan et al., 2014; Nagler et al., 2015; Hogg et al., 2017). In contrast to InSAR, the intensity tracking technique is able to estimate offsets in both slant-range (the line-of-sight of the satellite) and azimuth (along the orbit of the satellite) directions,

through a cross-correlation algorithm of image real-valued (amplitude) SAR intensity images patches (Strozzi et al., 2002; Pritchard et al., 2005). The temporal baseline interval used for SAR intensity tracking procedure is roughly between days to few weeks and thereby more extensive than the period required for InSAR. This opens up a greater volume of data suitable for scientific investigation (Paul et al., 2013). Longer temporal baseline intervals typically produce lower coherence between a pair of images (decorrelation), caused by, e.g. meteorological conditions (ice and snow surface melting, snowfall, and wind).

I use the SAR intensity tracking technique (Strozzi et al., 2002), in GAMMA-SAR software (GAMMA REMOTE SENSING, 2015), to estimate surface ice velocities due to glacier flow, assuming that the ice flow occurs parallel to the surface slope. The intensity tracking algorithm generates slant-range and azimuth displacements (2D components) and, in order to obtain a 3-D displacement map, both components are combined with a digital elevation model (DEM) assuming the ice flow is parallel to the surface slope. This method uses a cross-correlation algorithm applied to image patches (Strozzi et al., 2002; Pritchard et al., 2005; Paul et al., 2015) to estimate offsets between similar features, such as crevasses and radar speckle patterns, in two co-registered SAR images (Figure 2.3). Images are co-registered using the precise orbit information, available 20 days after the image acquisition, establishing a co-registration accuracy of 5 cm $1-\sigma$ (Sentinels.POD_Team, 2013). The elimination of the orbital offsets isolates displacement due to the glacier movement (Strozzi et al., 2002). To estimate ice flow, I then used windows sizes of 350 pixels in ground range (~ 1.7 km) and 75 pixels in azimuth (~ 1.5 km) for each glacier, to produce series of velocity maps with spatial resolution of 388m in ground range and 320m in azimuth. The window and step size used was based on sensitivity testing of a range of values, where a trade-off between the spatial resolution, spatial coverage and measurement accuracy of the output result was considered. For an individual pair, the quality of the resulting velocity field depends on the nature of the ice flow, the change in snow surface properties between the processed images, the associated correlation of the speckle pattern, and the scale of the local features observed.

In the processing chain used in this thesis, image matches with low certainty, defined as returning a normalized cross-correlation (NCC) of less than 5 % of its maximum peak,

were rejected and the results are then converted into displacement in ground range coordinates using the Greenland Ice Mapping Project digital elevation model posted on a 90m grid (Howat et al., 2014). Along- and across-track displacement components were then combined to determine the displacement magnitude, which is then converted to an estimate of annual velocity using the temporal baseline of each image pair. Final velocity products were posted on 100m by 100m grids. Post-processing of ice velocity data allows the opportunity to reduce noise and remove outliers (Paul et al., 2015), so I apply a low-pass filter (moving mean) twice to the data, using a kernel of 1 km by 1 km, and reject values where the deviation between the unfiltered and filtered velocity magnitude exceeds 30 %, which causes large deviation from the original measurement and, therefore, it is unreliable. I apply a labelling algorithm, based on the image histogram, to identify and classify regions with similar values, and use this to exclude isolated pixels which exhibit a spatially non-coherent pattern of velocity. This same approach is also used to remove areas where the classified region was smaller than 1/1000th of the processed image size (Figure 2.3).

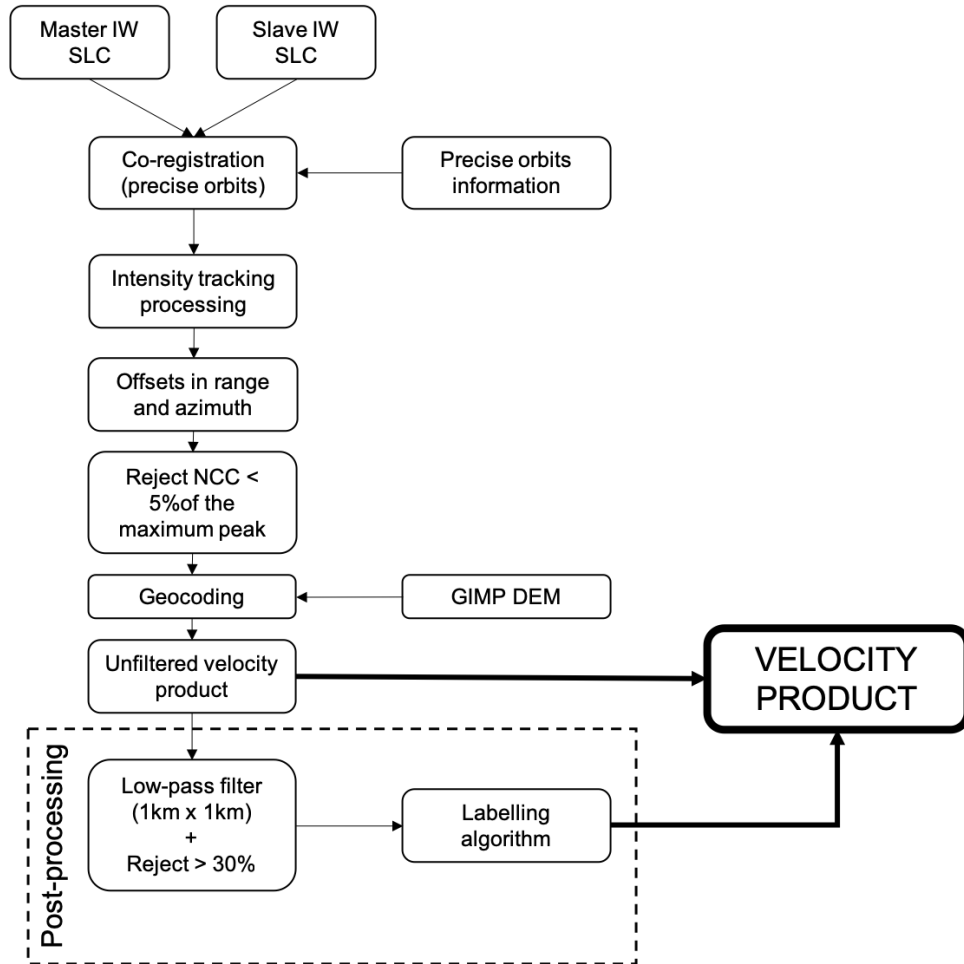


Figure 2.3: Intensity tracking processing chain using IW SLC Sentinel-1 images.

Error source and budget for the SAR measurements

Errors in velocity estimates arise primarily through inexact co-registration of the SAR images, uncertainties in the digital elevation model used in the terrain correction, and fluctuations in ionospheric activity and tropospheric water vapour (Nagler et al., 2015; Hogg et al., 2017). Synthetic aperture radar sensors are sensitive to snow and ice conditions on the glacier surface, especially due to the presence of liquid water, reducing the quality of the results (Paul et al., 2017). Here, I present three different methods to estimate errors associated to the ice velocity measurements. It is possible to have an estimative of the matching accuracy by measuring the mean local offsets in range

and azimuth on flat and stable areas, such as bedrock and ice-free ground regions (Pritchard et al., 2005; Paul et al., 2017). Another method is by stacking the velocity measurements and observe the consistency of velocity time series, providing statistical estimates, such as the temporal mean and standard deviation (Rignot et al., 2011a; Rignot and Mouginot, 2012). To estimate the accuracy of my Sentinel-1 average velocity data I computed pixel-by-pixel errors based on the signal-to-noise ratio (SNR) of the cross-correlation function (Hogg et al., 2017). The SNR is the ratio between the cross-correlation function peak (C_p) and the average correlation level (C_l) on the tracking window used to estimate the velocities (de Lange et al., 2007). In general, due to the non-uniform flow, lack of stable features, and geometry distortions, glaciers exhibit higher errors across their faster flowing and steeper areas, and along their shear margins. In addition, where localized rates of surface elevation change are high, the surface slope may have evolved away from that of the DEM used during the processing. For instance, in Chapter 3, I assess the sensitivity of my velocity estimates to this effect at the Jakobshavn Isbræ site, where glacier thinning is most pronounced. I used airborne estimates of elevation change from IceBridge and pre-Icebridge data acquired from the NASA Airborne Topographic Mapper (ATM) (Studinger, 2014) to update the DEM. I found that in an extreme case, the large thinning rates ($\sim 12 \text{ m yr}^{-1}$) may introduce an additional uncertainty of $\sim 3 \%$, which may bias the velocity estimates in the region, albeit it is limited to the first 10 km upstream of the grounding line. Moreover, over floating ice tongues, uncompensated vertical tidal displacement may also introduce additional uncertainty of 2-4 % into velocity estimates.

2.3 Optical feature tracking

Sentinel-2 platform

Sentinel-2 is an optical imaging component of the European Commission’s (EC) Copernicus Earth Observation satellite program, built and launched in partnership with the European Space Agency. The first of the satellites, Sentinel-2a, was launched in June 2015, followed by, Sentinel-2b, which was launched in March 2017. The main sensor on each Sentinel-2 satellite is the Multi-Spectral Instrument (MSI), which acquires images within 13 different spectral bands and with a spatial resolution that varies from 10 to 60 m (Table 2.1 – European Space Agency (ESA) (2015)). Sentinel-2 Level-1C (L1C)

2.3 Optical feature tracking

images are recorded as top-of-atmosphere reflectance, with ground footprints of 109 by 109 km. The L1C images products are orthorectified using the PlanetDEM digital elevation model (DEM), posted in a 90 x 90 m grid (European Space Agency (ESA), 2015). Both satellites follow sun-synchronous orbits, ensuring a consistent angle of sunlight on the Earth's surface. Although each satellite has a 10-day orbital repeat period, when combined they provide repeat sampling every 5 days because their orbits are offset. The actual frequency of repeat acquisitions however depends on the capacity of the entire system, which is defined in an image acquisition plan. At higher latitudes where the imaging swaths from neighbouring orbits overlap, the revisit time offered by the constellation is even shorter than 5 days (Figure 2.4 - Kääb et al. (2016)).

Table 2.1: Spatial resolution, central wavelength and bandwidth of the different bands acquired by Sentinel-2. Adapted from ESA, 2015.

Band Number	Spatial resolution (m)	Sentinel-2a		Sentinel-2b	
		Central wavelength (nm)	Bandwidth (nm)	Central wavelength (nm)	Bandwidth (nm)
1	60	442.7	21	442.2	21
2	10	492.4	66	492.1	66
3	10	559.8	36	559	36
4	10	664.6	31	664.9	31
5	20	704.1	15	703.8	16
6	20	740.5	15	739.1	15
7	20	782.8	20	779.7	20
8	10	832.8	106	832.9	106
8a	20	864.7	21	864	22
9	60	945.1	20	943.2	21
10	60	1373.5	31	1376.9	30
11	20	1613.7	91	1610.4	94
12	20	2202.4	175	2185.7	185

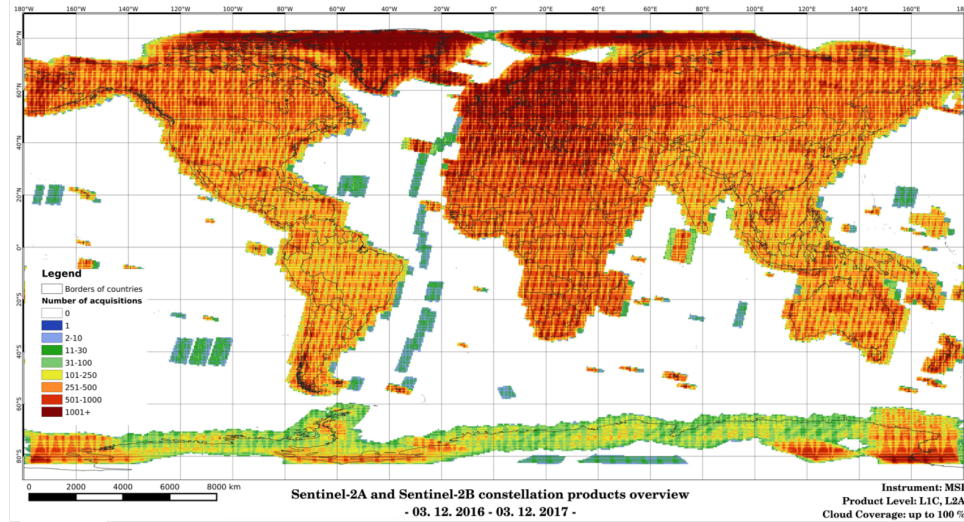


Figure 2.4: Density of acquisitions from Sentinel-2a/b between 03-Dec-2016 to 03-Dec-2017. Extracted from Petr Ševčík EOX IT Services GmbH (2018).

Methodology applied

The derivation of ice velocity measurements using optical datasets was first demonstrated in the 1980s (e.g. Lucchitta and Ferguson (1986)). At that time, the method was based on photogrammetric techniques and visual comparison between two co-registered images. When applied to glacier surfaces, this technique of optical image feature tracking relies on the detection of coherent visible features such as crevasses and calving fronts in temporally-separated images, in order to determine ice motion (Lucchitta and Ferguson, 1986; Scambos et al., 1992). Initially, this was done by visual comparison using in a smaller scale, and this limited the scope and precision of the resulting estimates of ice motion (Bindschadler and Scambos, 1991; Scambos et al., 1992). Nowadays, the feature-tracking technique commonly applies the cross-correlation method to automatically detect the motion of small areas (chips). This is essentially the same as the method used for SAR intensity tracking, albeit requiring optically visible features and good visual contrast between the images used (Rosenau et al., 2015; Fahnestock et al., 2016). There exist different methods for image matching, such as the normalized cross-correlation applied in the spatial domain, the one applied in the frequency domain through Fast Fourier Transform, and other four methods applied in the phase domain

Heid and Kääb (2012). In this thesis, I estimate ice motion using a normalised cross-correlation feature tracking algorithm (GAMMA REMOTE SENSING, 2015) applied to Sentinel-2 L1C near-infrared Band 8 images with 10 m spatial (Table 2.1), following the methodology applied in Kääb et al. (2016) and described in Heid and Kääb (2012). First, the images are co-registered using a cross-correlation algorithm applied after masking out areas of known fast ice flow (Figure 2.5). The co-registration of two images from a repeat orbit reduces the final offset field containing geo-location noise and biases due to shifts and jitter Kääb et al. (2016). I then track movement using patches of 75 x 75 pixels, corresponding to areas of 750 m by 750 m on the ground. From these data I estimate ice velocity by assuming that the ice flows parallel to the surface slope. Finally, I apply a median filter using a kernel of 100 m by 100 m to remove outliers (Figure 2.5).

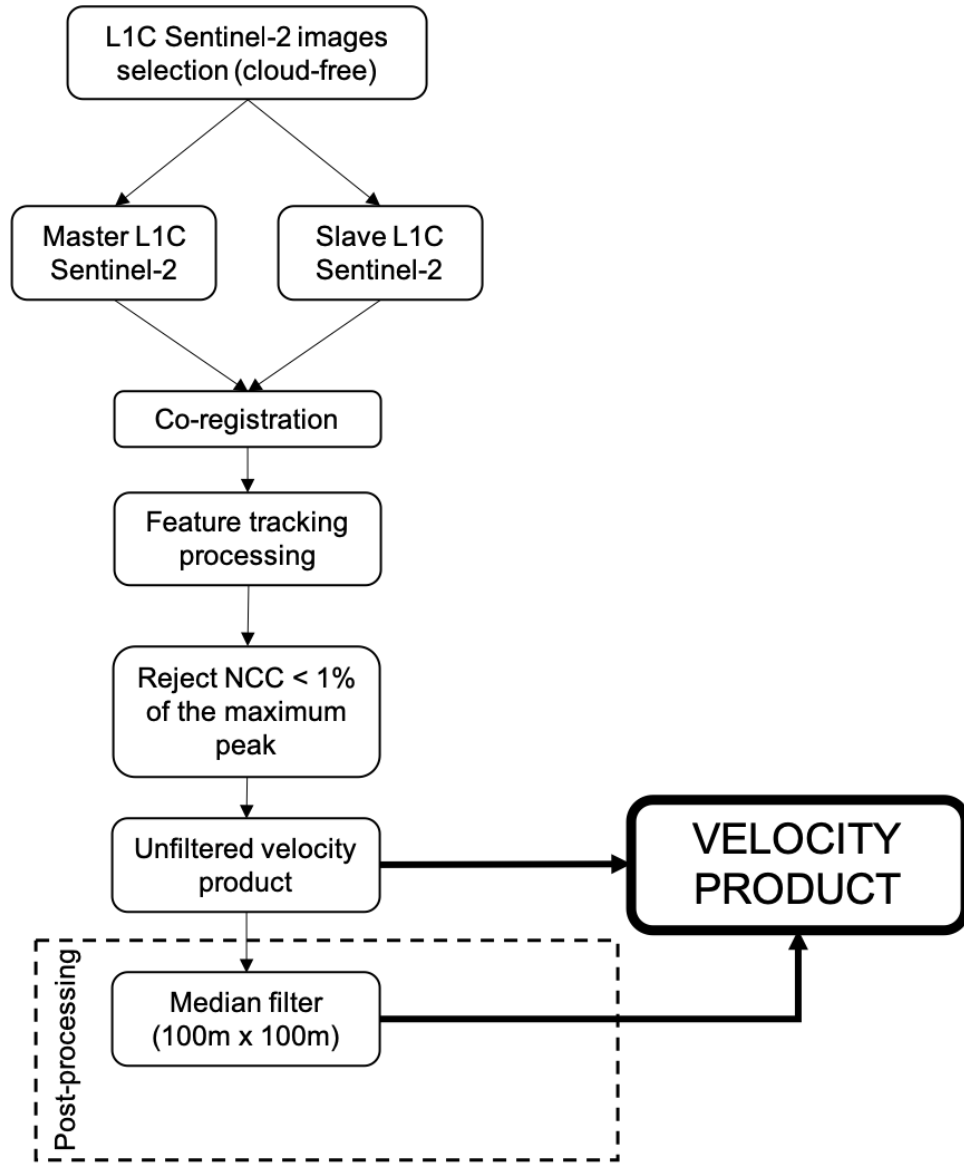


Figure 2.5: Feature tracking processing chain using L1C Sentinel-2 images.

Error source and budget for optical

The major limitation when tracking ice motion using optical images is the need for day-light acquisitions, which restricts their use during night-time or in winter. Furthermore, glaciers are often located in relatively steep, or mountainous, regions, and the presence of clouds and shadows created by the terrain topography also limit the performance

of optical feature tracking (Kääb et al., 2016; Paul et al., 2016, 2017). Clouds, and their shadows, for example, are often found to obscure portions of Sentinel-2 scenes, which can limit the image coverage, and can introduce errors due to false matches in the tracking caused by false matches. Although an automatic cloud mask is included in all Sentinel-2 L1C imagery, based on a ratio of the reflectance recorded in different bands (European Space Agency (ESA), 2015), the algorithm is not designed for glaciated terrain and performs poorly in some cases. This is not surprising, as snow covered regions are known to be a challenge for cloud detection algorithms (Paul et al., 2016; Frantz et al., 2018). Systematic errors associated to the satellite jitter, which affects the geometric accuracy of high-resolution images, can be statistically modelled and corrected (Paul et al., 2017). Displacements over stable ground can provide an estimative of the digital elevation model errors that propagate into the orthorectified images, and are difficult to be removed or removed (Paul et al., 2017). Furthermore, the major error source in ice velocity estimation using optical images is the inexact co-registration linked to the digital elevation model used to orthorectify the images (Jeong and Howat, 2015). Therefore, in order to minimize mismatches due to orthorectification, it is recommended to use only image pairs that are acquired on the same satellite path (Kääb et al., 2016). I estimate individual velocity error maps based on the signal to noise ratio (SNR) of the cross-correlation algorithm, being the ratio of the cross-correlation function peak (C_p) and the average correlation level (C_l) within the used patch (de Lange et al., 2007), thereby maintaining a consistent metric to that used in the SAR intensity tracking velocity estimates.

References

- W. H. Armstrong, R. S. Anderson, and M. A. Fahnestock. Spatial Patterns of Summer Speedup on South Central Alaska Glaciers. *Geophysical Research Letters*, 44(18): 9379–9388, 2017. ISSN 19448007. doi: 10.1002/2017GL074370. 28
- R. Bamler and P. Hartl. Synthetic aperture radar interferometry. *Inverse Problems*, 14:1–54, 1998. ISSN 0266-5611. doi: 10.1088/0266-5611/14/4/001. 28
- R. A. Bindschadler and T. A. Scambos. Satellite-Image-Derived Velocity Antarctic Ice Stream. *Science*, 252:242–246, 1991. 38

- R. de Lange, A. Luckman, and T. Murray. Improvement of satellite radar feature tracking for ice velocity derivation by spatial frequency filtering. *IEEE Transactions on Geoscience and Remote Sensing*, 45(7):2309–2318, 2007. ISSN 01962892. doi: 10.1109/TGRS.2007.896615. 36, 41
- A. Dehecq, N. Gourmelen, and E. Trouve. Deriving large-scale glacier velocities from a complete satellite archive: Application to the Pamir-Karakoram-Himalaya. *Remote Sensing of Environment*, 162:55–66, 2015. ISSN 00344257. doi: 10.1016/j.rse.2015.01.031. URL <http://dx.doi.org/10.1016/j.rse.2015.01.031>. 28
- European Space Agency (ESA). <https://sentinel.esa.int/web/sentinel/user-guides/sentinel-1-sar/revisit-and-coverage>. Visited in June 2019. x, 30
- European Space Agency (ESA). Sentinel-2 User Handbook. (1):1–64, 2015. 36, 37, 41
- M. Fahnstock, T. Scambos, T. Moon, A. Gardner, T. Haran, and M. Klinger. Rapid large-area mapping of ice flow using Landsat 8. *Remote Sensing of Environment*, 185:84–94, 2016. ISSN 00344257. doi: 10.1016/j.rse.2015.11.023. URL <http://dx.doi.org/10.1016/j.rse.2015.11.023>. 26, 27, 28, 38
- D. Frantz, E. Haß, A. Uhl, J. Stoffels, and J. Hill. Improvement of the Fmask algorithm for Sentinel-2 images: Separating clouds from bright surfaces based on parallax effects. *Remote Sensing of Environment*, 215(March):471–481, 2018. ISSN 00344257. doi: 10.1016/j.rse.2018.04.046. 41
- GAMMA REMOTE SENSING. Interferometric SAR Processor - ISP. Volume 1.9. Technical Report December, 2015. 33, 39
- A. S. Gardner, G. Moholdt, T. Scambos, M. Fahnstock, S. Ligtenberg, and M. V. D. Broeke. Increased West Antarctic ice discharge and East Antarctic stability over the last seven years. *The Cryosphere*, 12:521–547, 2018. doi: <https://doi.org/10.5194/tc-12-521-2018>. 27
- D. Geudtner, R. Torres, P. Snoeij, M. Davidson, and B. Rommen. Sentinel-1 System Capabilities and Applications. In *IEEE IGARSS*, pages 1457–1460, 2014. ISBN 9781479957750. x, 30, 31

REFERENCES

- R. M. Goldstein, H. Engelhardt, B. Kamb, and R. M. Frolich. Satellite Radar Interferometry for Monitoring Ice Sheet Motion: Application to an Antarctic Ice Stream. *Science*, 262(3 December):1525–1530, 1993. 27, 28
- L. C. Graham. Synthetic interferometer radar for topographic mapping. *Proceedings of the IEEE*, 62(6):763–768, 1974. doi: 10.1109/PROC.1974.9516. 28
- T. Heid and A. Kääb. Evaluation of existing image matching methods for deriving glacier surface displacements globally from optical satellite imagery. *Remote Sensing of Environment*, 118:339–355, 2012. ISSN 00344257. doi: 10.1016/j.rse.2011.11.024. URL <http://dx.doi.org/10.1016/j.rse.2011.11.024>. 39
- A. E. Hogg, A. Shepherd, S. L. Cornford, K. Briggs, N. Gourmelen, J. Graham, I. Joughin, J. Mouginot, T. Nagler, A. J. Payne, E. Rignot, and J. Wuite. Increased ice flow in Western Palmer Land linked to ocean melting. *Geophys. Res. Lett.*, 44: 1–9, 2017. doi: 10.1002/2016GL072110. 32, 35, 36
- I. M. Howat, I. Joughin, S. Tulaczyk, and S. Gogineni. Rapid retreat and acceleration of Helheim Glacier, east Greenland. *Geophysical Research Letters*, 32(22):1–4, 2005. ISSN 00948276. doi: 10.1029/2005GL024737. 29
- I. M. Howat, a. Negrete, and B. E. Smith. The Greenland Ice Mapping Project (GIMP) land classification and surface elevation data sets. *The Cryosphere*, 8(4):1509–1518, 2014. ISSN 1994-0424. doi: 10.5194/tc-8-1509-2014. URL <http://www.the-cryosphere.net/8/1509/2014/tc-8-1509-2014.html>. 32, 34
- A. Iken and R. A. Bindschadler. Combined measurements of Subglacial Water Pressure and Surface Velocity of Findelengletscher, Switzerland: Conclusions about Drainage System and Sliding Mechanism. *Journal of Glaciology*, 32(110):101–119, 1986. ISSN 0022-1430. doi: 10.3189/S0022143000006936. URL https://www.cambridge.org/core/product/identifier/S0022143000006936/type/journal_{_}article. 27
- S. Jeong and I. M. Howat. Performance of Landsat 8 Operational Land Imager for mapping ice sheet velocity. *Remote Sensing of Environment*, 170(8):90–101, 2015. ISSN 00344257. doi: 10.1016/j.rse.2015.08.023. URL <http://dx.doi.org/10.1016/j.rse.2015.08.023>. 41

-
- I. Joughin. Ice-sheet velocity mapping: a combined interferometric and speckle-tracking approach. *Annals of Glaciology*, 34(1):195–201, jan 2002. ISSN 02603055. doi: 10.3189/172756402781817978. URL <http://openurl.ingenta.com/content/xref?genre=article&issn=0260-3055&volume=34&issue=1&spage=195>. 32
- I. Joughin, D. P. Winebrenner, and M. A. Fahnestock. Observations of ice-sheet motion in Greenland using satellite radar interferometry. *Geophysical Research Letters*, 22(5):571–574, 1995. ISSN 0094-8276. doi: 10.1029/95GL00264. 26
- I. Joughin, R. Kwok, and M. A. Fahnestock. Estimation of ice-sheet motion using satellite radar interferometry: method and error analysis with application to Humboldt Glacier, Greenland. *Journal of Glaciology*, 42(142):564–575, 1996. 28
- I. Joughin, W. Abdalati, and M. Fahnestock. Large fluctuations in speed on Greenland’s Jakobshavn Isbrae glacier. *Nature*, 432(7017):608–10, dec 2004. ISSN 1476-4687. doi: 10.1038/nature03130. URL <http://www.ncbi.nlm.nih.gov/pubmed/15577906>. 29
- I. Joughin, S. B. Das, M. A. King, B. E. Smith, I. M. Howat, and T. Moon. Seasonal Speedup Along the Western Flank of the Greenland Ice Sheet. *Science*, 320(April):781–784, 2008. doi: 10.1126/science.1153288. 29
- I. Joughin, B. E. Smith, and W. Abdalati. Glaciological advances made with interferometric synthetic aperture radar. *Journal of Glaciology*, 56(200):1026–1042, 2010. 27, 28, 29
- I. Joughin, B. Smith, I. Howat, and T. Scambos. MEaSURES Multi-year Greenland Ice Sheet Velocity Mosaic, Version 1. [Indicate subset used]. *Boulder, Colorado USA. NASA National Snow and Ice Data Center Distributed Active Archive Center*, 2016. URL <http://dx.doi.org/10.5067/QUA5Q9SVMSJG>. 32
- A. Kääb, S. H. Winsvold, B. Altena, C. Nuth, T. Nagler, and J. Wuite. Glacier remote sensing using sentinel-2. part I: Radiometric and geometric performance, and application to ice velocity. *Remote Sensing*, 8(7):1–24, 2016. ISSN 20724292. doi: 10.3390/rs8070598. 37, 39, 41
- B. Kamb and H. Engelhardt. Waves of accelerated motion in a glacier approaching surge: The mini-surges of Variegated Glacier, Alaska, U.S.A. *J. Glaciol.*, 33(113):27–46, 1987. ISSN 0022-1430. 27

REFERENCES

- B. K. Lucchitta and H. M. Ferguson. Antarctica: measuring glacier velocity from satellite images. *Science (New York, N.Y.)*, 234(4780):1105–1108, 1986. ISSN 0036-8075. doi: 10.1126/science.234.4780.1105. 28, 38
- B. K. Lucchitta, C. E. Rosanova, and K. F. Mullins. Velocities of Pine Island Glacier, West Antarctica, from ERS-1 SAR images. *Annals of Glaciology*, 21:277–283, 1995. ISSN 02603055. doi: 10.1017/S0260305500015949. 27
- A. Luckman, T. Murray, H. Jiskoot, and H. Pritchard. ERS SAR feature-tracking measurement of outlet glacier velocities on a regional scale in East Greenland. *Annals of Glaciology*, 36:129–134, 2003. 32
- A. Luckman, D. Quincey, and S. Bevan. The potential of satellite radar interferometry and feature tracking for monitoring flow rates of Himalayan glaciers. *Remote Sensing of Environment*, 111(2-3):172–181, nov 2007. ISSN 00344257. doi: 10.1016/j.rse.2007.05.019. URL <http://linkinghub.elsevier.com/retrieve/pii/S0034425707002842>. 32
- R. Massom and D. Lubin. Synthetic aperture radar interferometry and related techniques. In *Polar Remote Sensing. Volume II: Ice Sheets*, chapter 2. Springer Berlin Heidelberg, 2006. 29
- M. McMillan, A. Shepherd, N. Gourmelen, A. Dehecq, A. Leeson, A. Ridout, T. Flament, A. Hogg, L. Gilbert, T. Benham, M. D. Broeke, J. A. Dowdeswell, X. Fettweis, B. Noël, and T. Strozzi. Rapid dynamic activation of a marine-based Arctic ice cap. *Geophysical Research Letters*, 41:8902–8909, 2014. doi: 10.1002/2014GL062255. 32
- M. Morlighem, E. Rignot, J. Mouginot, H. Seroussi, and E. Larour. IceBridge Bed-Machine Greenland, Version 2. Boulder, Colorado USA. NASA National Snow and Ice Data Center Distributed Active Archive Center. [09/08/2017]. 2015. doi: 10.5067/AD7B0HQNSJ29. 32
- J. Mouginot, E. Rignot, B. Scheuchl, and R. Millan. Comprehensive Annual Ice Sheet Velocity Mapping Using Landsat-8, Sentinel-1, and RADARSAT-2 Data. *Remote Sensing*, 9(364):1–20, 2017. ISSN 0018-9235. doi: 10.3390/rs9040364. URL <http://www.mdpi.com/2072-4292/9/4/364/htm>. 28

- T. Nagler, H. Rott, M. Hetzenecker, J. Wuite, and P. Potin. The Sentinel-1 Mission: New Opportunities for Ice Sheet Observations. *Remote Sensing*, 7(7):9371–9389, 2015. ISSN 2072-4292. doi: 10.3390/rs70709371. URL <http://www.mdpi.com/2072-4292/7/7/9371/>. 27, 28, 32, 35
- F. Paul, N. E. Barrand, S. Baumann, E. Berthier, T. Bolch, K. Casey, H. Frey, S. P. Joshi, V. Konovalov, R. Le Bris, N. Mölg, G. Nosenko, C. Nuth, A. Pope, A. Racoviteanu, P. Rastner, B. Raup, K. Scharrer, S. Steffen, and S. Winsvold. On the accuracy of glacier outlines derived from remote-sensing data. *Annals of Glaciology*, 54(63):171–182, 2013. ISSN 02603055. doi: 10.3189/2013AoG63A296. 33
- F. Paul, T. Bolch, A. Kääb, T. Nagler, C. Nuth, K. Scharrer, A. Shepherd, T. Strozzi, F. Ticconi, R. Bhambri, E. Berthier, S. Bevan, N. Gourmelen, T. Heid, S. Jeong, M. Kunz, T. R. Lauknes, A. Luckman, J. Merryman, G. Moholdt, A. Muir, J. Neelmeijer, M. Rankl, J. VanLooy, and T. Van Niel. The glaciers climate change initiative: Methods for creating glacier area, elevation change and velocity products. *Remote Sensing of Environment*, 162:408–426, 2015. ISSN 00344257. doi: 10.1016/j.rse.2013.07.043. URL <http://dx.doi.org/10.1016/j.rse.2013.07.043>. 29, 33, 34
- F. Paul, S. Winsvold, A. Kääb, T. Nagler, and G. Schwaizer. Glacier Remote Sensing Using Sentinel-2. Part II: Mapping Glacier Extents and Surface Facies, and Comparison to Landsat 8. *Remote Sensing*, 8(7):575, 2016. ISSN 2072-4292. doi: 10.3390/rs8070575. URL <http://www.mdpi.com/2072-4292/8/7/575>. 41
- F. Paul, T. Bolch, K. Briggs, A. Kääb, M. McMillan, R. McNabb, T. Nagler, C. Nuth, P. Rastner, T. Strozzi, and J. Wuite. Error sources and guidelines for quality assessment of glacier area, elevation change, and velocity products derived from satellite data in the Glaciers_cci project. *Remote Sensing of Environment*, 203 (November):256–275, 2017. ISSN 00344257. doi: 10.1016/j.rse.2017.08.038. URL <https://doi.org/10.1016/j.rse.2017.08.038>. 35, 36, 41
- H. Pritchard, T. Murray, A. Luckman, T. Strozzi, and S. Barr. Glacier surge dynamics of Sortebrae, east Greenland, from synthetic aperture radar feature tracking. *Journal of Geophysical Research*, 110(F03005):1–13, 2005. ISSN 0148-0227. doi: 10.1029/

REFERENCES

- 2004JF000233. URL <http://doi.wiley.com/10.1029/2004JF000233>. 29, 32, 33, 36
- E. Rignot and P. Kanagaratnam. Changes in the Velocity Structure of the Greenland Ice Sheet. *Science*, 311(February):986–990, 2006. doi: 10.1126/science.1121381. 29
- E. Rignot and J. Mouginot. Ice flow in Greenland for the International Polar Year 2008-2009. *Geophysical Research Letters*, 39(11):1–7, 2012. ISSN 00948276. doi: 10.1029/2012GL051634. 28, 36
- E. Rignot, J. Mouginot, and B. Scheuchl. Ice Flow of the Antarctic Ice Sheet. *Science*, 333(September):1427–1431, 2011a. 36
- E. Rignot, I. Velicogna, M. R. Van Den Broeke, A. Monaghan, and J. T. M. Lenaerts. Acceleration of the contribution of the Greenland and Antarctic ice sheets to sea level rise. *Geophysical Research Letters*, 38(5):1–5, 2011b. ISSN 00948276. doi: 10.1029/2011GL046583. 27
- R. Rosenau, M. Scheinert, and R. Dietrich. A processing system to monitor Greenland outlet glacier velocity variations at decadal and seasonal time scales utilizing the Landsat imagery. *Remote Sensing of Environment*, 169:1–19, 2015. ISSN 00344257. doi: 10.1016/j.rse.2015.07.012. URL <http://dx.doi.org/10.1016/j.rse.2015.07.012>. 26, 27, 38
- T. a. Scambos, M. J. Dutkiewicz, J. C. Wilson, and R. a. Bindshadler. Application of image cross-correlation to the measurement of glacier velocity using satellite image data. *Remote Sensing of Environment*, 42(3):177–186, 1992. ISSN 00344257. doi: 10.1016/0034-4257(92)90101-O. URL <http://linkinghub.elsevier.com/retrieve/pii/0034425792901010>. 38
- Sentinels_POD_Team. Sentinels POD Service File Format Specifications, European Space Agency, Paris, France. 2013. 32, 33
- A. Shepherd, A. Hubbard, P. Nienow, M. King, M. McMillan, and I. Joughin. Greenland ice sheet motion coupled with daily melting in late summer. *Geophysical Research Letters*, 36(L01501):1–4, 2009. ISSN 0094-8276. doi: 10.1029/2008GL035758. URL <http://doi.wiley.com/10.1029/2008GL035758>. 27

- T. Strozzi, A. Luckman, T. Murray, U. Wegmuller, and C. L. Werner. Glacier motion estimation using SAR offset-tracking procedures. *IEEE Transactions on Geoscience and Remote Sensing*, 40(11):2384–2391, nov 2002. ISSN 0196-2892. doi: 10.1109/TGRS.2002.805079. URL <http://ieeexplore.ieee.org/lpdocs/epic03/wrapper.htm?arnumber=1166597>. 29, 32, 33
- M. Studinger. IceBridge ATM L4 Surface Elevation Rate of Change, Version 1, Greenland subset. Boulder, Colorado USA, NASA National Snow and Ice Data Center Distributed Active Archive Center, <https://doi.org/10.5067/BCW6CI3TXOCY>. 2014. 36
- A. V. Sundal, A. Shepherd, P. Nienow, E. Hanna, S. Palmer, and P. Huybrechts. Melt-induced speed-up of Greenland ice sheet offset by efficient subglacial drainage. *Nature*, 469(7331):521–4, jan 2011. ISSN 1476-4687. doi: 10.1038/nature09740. URL <http://www.ncbi.nlm.nih.gov/pubmed/21270891>. 32
- R. Torres, P. Snoeij, D. Geudtner, D. Bibby, M. Davidson, E. Attema, P. Potin, B. Rommen, N. Floury, M. Brown, I. N. Traver, P. Deghaye, B. Duesmann, B. Rosich, N. Miranda, C. Bruno, M. L’Abbate, R. Croci, A. Pietropaolo, M. Huchler, and F. Rostan. GMES Sentinel-1 mission. *Remote Sensing of Environment*, 120:9–24, may 2012. ISSN 00344257. doi: 10.1016/j.rse.2011.05.028. URL <http://linkinghub.elsevier.com/retrieve/pii/S0034425712000600>. 30
- M. A. Wulder, J. G. Masek, W. B. Cohen, T. R. Loveland, and C. E. Woodcock. Opening the archive: How free data has enabled the science and monitoring promise of Landsat. *Remote Sensing of Environment*, 122:2–10, 2012. ISSN 00344257. doi: 10.1016/j.rse.2012.01.010. URL <http://dx.doi.org/10.1016/j.rse.2012.01.010>. 26
- H. J. Zwally, W. Abdalati, T. Herring, K. Larson, J. Saba, and K. Steffen. Surface Melt – Induced Acceleration of Greenland Ice-Sheet Flow. *Science*, 297(July):218–223, 2002. doi: 10.1126/science.1072708. 27

Chapter 3

Ice velocity of Jakobshavn Isbræ, Petermann Glacier, Nioghalvfjerdsfjorden and Zachariæ Isstrøm, 2015-2017, from Sentinel 1-a/b SAR imagery

Authors: Adriano Lemos, Andrew Shepherd, Malcolm McMillan, Anna E. Hogg, Emma Hatton and Ian Joughin

Abstract

Systematically monitoring Greenland's outlet glaciers is central to understanding the timescales over which their flow and sea level contributions evolve. In this study we use data from the new Sentinel-1a/b satellite constellation to generate 187 velocity maps, covering 4 key outlet glaciers in Greenland; Jakobshavn Isbræ, Petermann Glacier, Nioghalvfjerdsfjorden and Zachariæ Isstrøm. These data provide a new high temporal resolution record (6 days averaged solutions) of each glacier's evolution since 2014, and resolve recent seasonal speedup periods and inter-annual changes in Greenland outlet

glacier speed with an estimated certainty of 10 %. We find that since 2012, Jakobshavn Isbræ has been decelerating, and now flows approximately 1250 m yr^{-1} (10 %) slower than 5 years previously, thus reversing an increasing trend in ice velocity that has persisted during the last decade. Despite this, we show that seasonal variability in ice velocity remains significant; up to 750 m yr^{-1} (14 %) at a distance of 12 km inland of the terminus. We also use our new dataset to estimate the duration of speedup periods (80-95 days), and to demonstrate a strong relationship between ice front position and ice flow at Jakobshavn Isbræ, with increases in speed of $\sim 1800 \text{ m yr}^{-1}$ in response to 1 km of retreat. Elsewhere, we record significant seasonal changes in flow of up to 25 % (2015) and 18 % (2016) at Petermann Glacier and Zachariæ Isstrøm, respectively. This study provides a first demonstration of the capacity of a new era of operational radar satellites to provide frequent, and timely, monitoring of ice sheet flow, and to better resolve the timescales over which glacier dynamics evolve.

3.1 Introduction

Between 1992 and 2011, the Greenland Ice Sheet lost mass at an average rate of $142 \pm 49 \text{ Gt yr}^{-1}$ (Shepherd et al., 2012), increasing to $269 \pm 51 \text{ Gt yr}^{-1}$ between 2011 and 2014 (McMillan et al., 2016). Ice sheet mass balance is determined from the surface mass balance and ice discharge exported from the ice sheet (van den Broeke et al., 2009). In 2005, dynamic imbalance was responsible for roughly two-thirds of Greenland’s total mass balance, making an important contribution to freshwater input into the ocean and 0.34 mm yr^{-1} to the global sea level rise at that time (Rignot and Kanagaratnam, 2006). Despite the anomalous atmospheric warming events, especially in 2012 (Tedesco et al., 2013), presenting a more spatially extensive and longer lasting surface melt during this period, marine-terminating outlet glaciers in Greenland still contributed with roughly 30 % (2000–2012) of total mass loss (Enderlin et al., 2014). The observed acceleration of many marine-based glaciers in the western and northern regions of Greenland over the last decade may have been driven by rises in air and adjacent ocean temperatures, which enhanced the surface melting and terminus retreat (Holland et al., 2008; Moon et al., 2014, 2015). The associated increases in basal sliding and calving of their ice fronts in turn produce enhanced discharge, leading to dynamical imbalance and additional ice loss (Joughin et al., 2010, 2014). Acceleration of marine-terminating glaciers

is, however, highly variable in space and time (Howat et al., 2010; Moon et al., 2012; Enderlin et al., 2014), due to the geometry of individual glaciers (Felikson et al., 2017), and the high spatial variability in the forcing mechanisms (Jensen et al., 2016; Carr et al., 2017). This complexity in glacier response challenges efforts to model their future evolution (Joughin et al., 2012; Bondzio et al., 2017) and, therefore, frequent and systematic monitoring is essential to understand the processes governing their dynamic stability and contribution so future mean sea level rise (Joughin et al., 2010; Shepherd et al., 2012).

Ice motion measurements are essential for monitoring ice sheet dynamics and ice discharge, and for assessing an ice sheet’s mass budget (Joughin et al., 1995). At present, the only way to monitor ice velocity at a continental scale is through satellite imagery. Glacier velocities were first measured using Landsat satellite data acquired during the 1970s through digital optical image comparison (Lucchitta and Ferguson, 1986). Currently, optical images are still largely used for mapping glaciers velocity at large scale (e.g. Dehecq et al. (2015); Fahnestock et al. (2016); Armstrong et al. (2017)). However, due to the dependency upon daylight conditions and the limited acquisitions across the polar Regions, the use of Synthetic Aperture Radar (SAR) images has become common since the launch of ERS-1 in 1991. In the following decades, these data have been used to monitor dynamic processes occurring across remote areas such as the Greenland and Antarctic ice sheets (Joughin et al., 2010; Rignot and Mouginot, 2012; Nagler et al., 2015; Mouginot et al., 2017). More recently, after the launch by the European Space Agency (ESA) of the Sentinel 1-a and 1-b satellites, in April 2014 and April 2016 respectively, many key ice margin areas are systematically monitored every 6 to 12 days. This novel dataset provides the opportunity to systematically monitor the dynamical process driving glacier ice velocity over periodic and short temporal scales. Here we use the Sentinel SAR archive to investigate the temporal variation in ice flow since October 2014 at four large outlet glaciers of the Greenland ice sheet.

3.2 Study Areas

In this study, we map ice velocity of the Jakobshavn Isbræ (JI), Petermann Glacier (PG), Nioghalvfjærdsfjorden (79-G) and Zachariæ Isstrøm (ZI), which are four of the

largest marine-based ice streams in Greenland. Combined they contain ice equivalent to 1.8 m of global sea-level rise (Mouginot et al., 2015; Jensen et al., 2016), and drain $\sim 21.5\%$ of Greenland’s ice (Rignot and Kanagaratnam, 2006; Rignot and Mouginot, 2012; Münchow et al., 2014).

Jakobshavn Isbræ terminates in the Ilulissat Icefjord in western Greenland (Figure 3.1a), and is the fastest glacier draining the ice sheet (Enderlin et al., 2014; Joughin et al., 2014). During the late 1990s, the ice tongue experienced successive break up events and the glacier began to speedup, exhibiting annual increases in speed of 7 % per year from 2004 and 2007 (Joughin et al., 2008b, 2012, 2014). Until 2012 and 2013, the speed up has continued, reaching maximum velocities in excess of 17 km yr^{-1} (Joughin et al., 2012, 2014). It has been suggested (van de Wal et al., 2015) that the speedup over this period in the southwest of Greenland might be enhanced by anomalously high melting across the ice sheet surface (Tedesco et al., 2013). Jakobshavn Isbræ is susceptible to changes in the adjacent ocean and Holland et al. (2008) have shown that warm water originating in the Irminger Sea likely enhanced basal melting and weakened the floating ice tongue, triggering its break up in 1997. Furthermore, Gladish et al. (2015) showed that subsequent changes occurred between 2001–2014 which were mainly triggered by changes in Ilulissat Icefjord water temperatures adjacent to the glacier. At present, JI is a tidewater glacier and has a bimodal behaviour, retreating by $\sim 3 \text{ km}$ during summer and advancing by a similar amount during winter seasons (Cassotto et al., 2015). Moreover, as showed by Jensen et al. (2016) through analysis of optical images from 1999 to 2013, it has not exhibited an unusually large change in area ($-10.3 \text{ km}^2 \text{ yr}^{-1}$).

Petermann Glacier flows into the Hall Basin in the Nares Strait in Northwest Greenland (Figure 3.1b), and has a perennial floating ice tongue of 1280 km^2 in area (Hogg et al., 2016). PG is grounded on bedrock $\sim 300 \text{ m}$ below sea level and, therefore, is also influenced by the adjacent ocean (Münchow et al., 2014; Hogg et al., 2016). The retreat of the ice stream calving front led to an area decrease of 352 km^2 from 1959 to 2008, 270 km^2 in 2010 and 130 km^2 in 2012 (Johannessen et al., 2013). It is considered a dynamically stable marine-terminating glacier despite several grounding line advancing and retreating events between 1992 and 2011, with a terminus retreat rate of 25.2 m

yr^{-1} (Hogg et al., 2016). PG has an average velocity of ~ 1100 m yr^{-1} at its grounding line since the 1990s (Rignot, 1996; Rignot and Steffen, 2008) and a multi-annual trend (2006–2010) in flow speed of 30 m yr^{-2} (Nick et al., 2012). The ice shelf is thicker than 100 m and it is 15 km wide, with low resistive stresses along flow due to the limited attachment to the fjord walls, diminishing the velocity response after calving events (Nick et al., 2012).

Nioghalvfjerdingsfjorden and Zachariæ Isstrøm are situated in the northeast of Greenland (Figure 3.1c and Figure 3.1d respectively). The two glaciers together drain more than 10% of the Greenland Ice Sheet (Rignot and Mouginot, 2012), and their maximum velocities are found near the grounding line. They have exhibited different behaviour in recent years, although located in the same region. 79-G underwent a modest velocity increase of ~ 150 m yr^{-1} between 2001 and 2011 at the grounding line (Khan et al., 2014). In contrast, during the same period, ZI exhibited a much larger increase in speed greater than 600 m yr^{-1} (Khan et al., 2014). The ice thinning rates above the grounding line varies from 5.1 m yr^{-1} in ZI (2010–2014) to 1.4 m yr^{-1} in 79-G (2012–2014) (Mouginot et al., 2015). Between 1999 and 2013, ZI has undergone an average area change of -26.0 km^2 yr^{-1} , due to break off of the ice tongue and is now a tidewater glacier (Khan et al., 2014; Jensen et al., 2016). In contrast, 79-G had a much lower average area change during the same period of -4.7 km^2 yr^{-1} and still retains a small ice shelf (Jensen et al., 2016), although recent ice shelf thinning (Mouginot et al., 2015) may increase vulnerability to break up in the future.

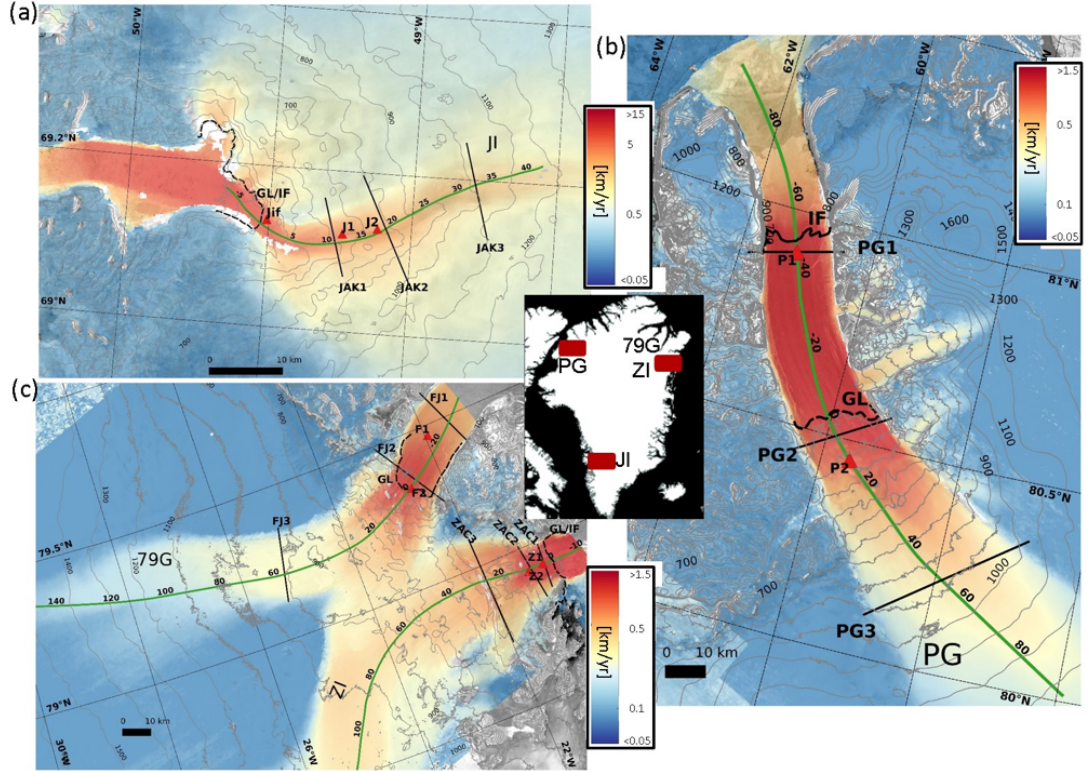


Figure 3.1: Time-averaged ice velocity magnitude maps for the period Oct/2014–Feb/2017 (a) Jakobshavn Isbræ (JI; 69°N , 50°W), (b) Petermann Glacier (PG; 81°N , 62°W), (c) Nioghalvfjordsfjorden (79G; 79°N , 20°W) and Zachariæ Isstrøm (ZI; 78°N , 20°W) glaciers, derived from Sentinel-1 SAR images. Velocities are shown on a logarithm scale and overlaid on a SAR backscatter intensity image and thin grey lines represent elevation. The along-flow profiles are indicated by solid green lines scaled in kilometres, the solid black lines show the across-flow transects, the red triangles represent the locations at which velocity time series are extracted and the thick solid and dashed black lines represent the ice front locations (IF) and the grounding lines (GL), respectively. The inset figures show the location of each glacier

3.3 Data and Methodology

To map ice velocity, we used Single Look Complex (SLC) Synthetic Aperture Radar images acquired in the Interferometric Wide swath (IW) mode from the Sentinel-1a and Sentinel-1b satellites. Data used in this study were acquired in the period span-

ning from October 2014 to February 2017 and from October 2016 to February 2017, for Sentinel-1a and Sentinel-1b respectively (Figure S3.2 and Table S3.1). Each satellite has a repeat cycle of 12 days and 180 degrees orbital phasing difference, resulting in a revisit time of 6 days over the same area after the Sentinel-1b launch. The Sentinel SAR instruments operate at C-Band, with a centre frequency of 5.405 GHz, corresponding to a wavelength of 5.55 cm. The IW mode has a 250 km swath and spatial resolution of 5 m in ground range and 20 m in azimuth. It has burst synchronization for interferometry and acquires data in 3 sub-swaths, each containing a series of bursts, which are acquired using the Terrain Observation with Progressive Scans SAR (TOPSAR) imaging technique (Yague-Martinez et al., 2016). We followed the workflow described below to derive 187 ice velocity maps from pairs of Sentinel-1a/b SAR images over Jakobshavn Isbræ, Petermann Glacier, Nioghalvfjerdingsfjorden and Zachariæ Isstrøm, using the GAMMA-SAR software (GAMMA REMOTE SENSING, 2015).

We used the SAR intensity tracking technique (Strozzi et al., 2002) to estimate surface ice velocities due to glacier flow, assuming that the ice flow occurs parallel to the surface. This method uses a cross correlation algorithm applied to image patches (Strozzi et al., 2002; Pritchard et al., 2005; Paul et al., 2015) to estimate offsets between similar features, such as crevasses and radar speckle patterns, in two co-registered SAR images (Table S3.1). Images were co-registered using the precise orbit information, available 20 days after the image acquisition, establishing a co-registration accuracy of 5 cm 3D 1-sigma (Sentinels_POD_Team, 2013). The elimination of the orbital offsets isolates displacement due to the glacier movement (Strozzi et al., 2002). To estimate ice flow, we then used windows sizes of 350 pixels in ground range (~ 1.7 km) and 75 pixels in azimuth (~ 1.5 km) for each glacier, to produce a series of velocity maps with spatial resolution of 388 m in ground range and 320 m in azimuth.

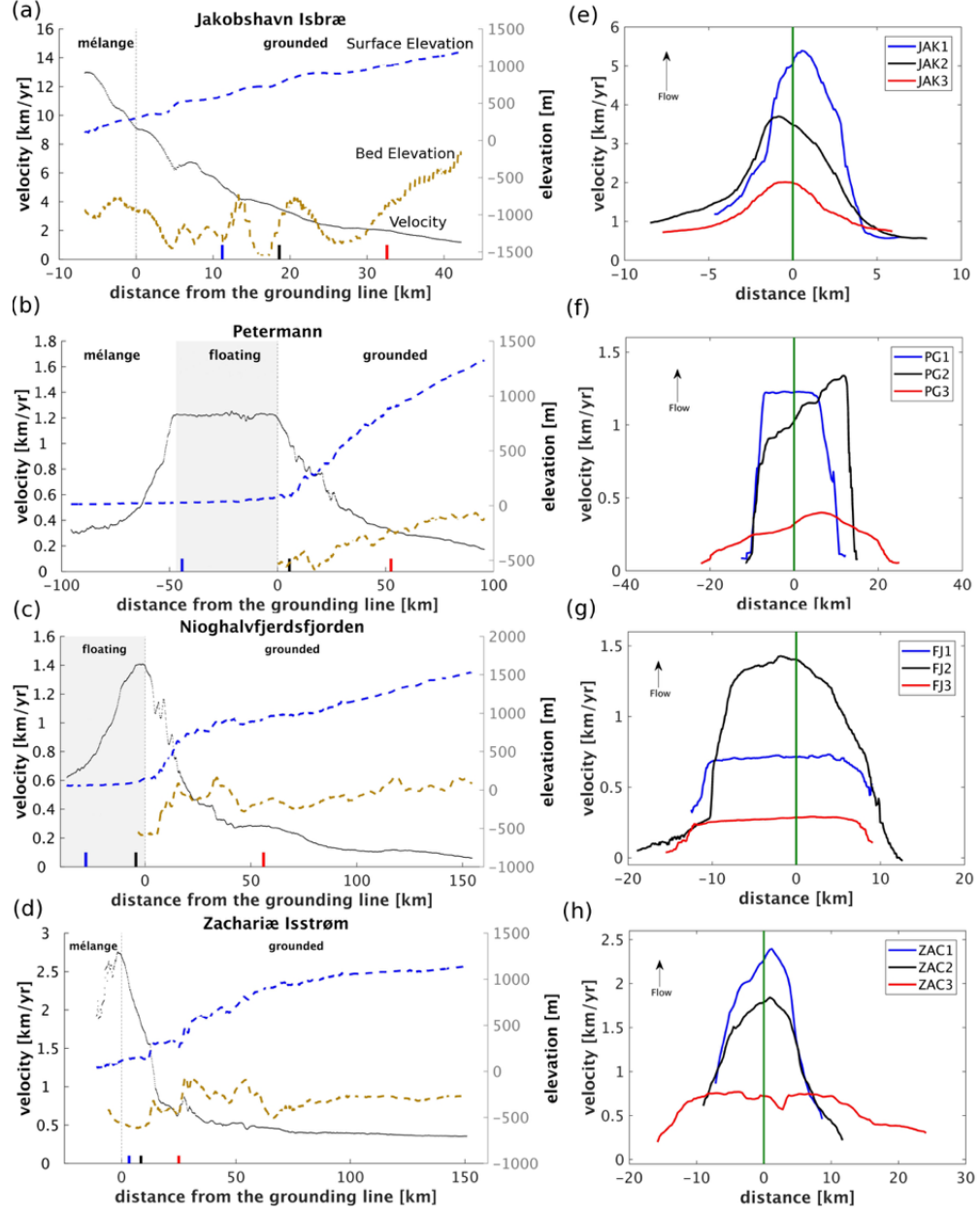


Figure 3.2: Average velocities (2014–2017) extracted from along- and across-flow profiles of Jakobshavn Isbræ, Petermann Glacier, Nioghalvfjærdsfjorden and Zachariæ Isstrøm. Figures a–d present along-flow profiles of ice velocity (solid black lines), surface elevation from the GIMP DEM (Howat et al., 2014); dashed blue lines and bed elevation from the IceBridge BedMachine Greenland V2 product (Morlighem et al., 2015); dashed yellow lines. The location of each profile is shown in Figure 3.1 (green lines). The grey shaded area represents the floating regions, and the light grey dashed line the ice front positions. The blue, black and red markers represent the locations of the across-flow profiles. Figures e–h show the across-flow velocity profiles (solid white lines in Figure 3.1), centred on the main profile (solid green line).

Image matches with low certainty, defined as returning a normalised cross-correlation of less than 5 % of its maximum peak, were rejected and the results were then converted into displacement in ground range coordinates using the Greenland Ice Mapping Project (GIMP) digital elevation model (DEM) posted on a 90 m grid (Howat et al., 2014). Along- and across- track displacement components were combined to determine the displacement magnitude, which was then converted to an estimate of annual velocity using the temporal baseline of each image pair. Final velocity products were posted on 100 m by 100 m grids. Post-processing of ice velocity data reduces noise and removes outliers (Paul et al., 2015), so we applied a low-pass filter (moving mean) twice to the data, using a kernel of 1 km by 1 km, and we reject values where the deviation between the unfiltered and filtered velocity magnitude exceeds 30 %. We apply a labelling algorithm, based on the image histogram, to identify and classify regions with similar values, excluding isolated pixels with a non-coherent area of velocity values, or where the area of the classified region was smaller than 1/1000th of the processed image size.

Errors in our velocity estimates arise primarily through inexact co-registration of the SAR images, uncertainties in the digital elevation model used in the terrain correction, and fluctuations in ionospheric activity and tropospheric water vapour (Nagler et al., 2015; Hogg et al., 2017). To estimate the accuracy of our Sentinel-1 average velocity data (Figure 3.1 and Figure 3.3) we computed pixel-by-pixel errors based on the signal to noise ratio (SNR) of the cross correlation function (Hogg et al., 2017). The SNR is the ratio between the cross-correlation function peak (C_p) and the average correlation level (C_l) on the tracking window used to estimate the velocities (de Lange et al., 2007). We then averaged these estimates across all images in our temporal stack to determine the percentage errors associated with our mean velocity maps (Figure 3.3). Although in isolated areas the error exceeds 30 %, the mean error across the whole imaged area were approximately 10 % for JI, 7 % for PG, and 8 % for 79G and ZI. Due to the non-uniform flow, lack of stable features and remaining geometry distortions, the four glaciers exhibit higher errors across their faster flowing and steeper areas, and along the shear margins. Where localised rates of surface elevation change are high, the surface slope may have evolved away from that of the GIMP DEM used in our processing. To assess the sensitivity of our velocity estimates to this effect, we selected the JI site where thinning is most pronounced, and used airborne estimates of elevation change

from IceBridge and Pre-Icebridge data acquired from the NASA Airborne Topographic Mapper (ATM) (Studinger, 2014) to update the DEM. We find that in this extreme case, the large thinning rates ($\sim 12 \text{ m yr}^{-1}$) may introduce an additional uncertainty of 200-300 m yr^{-1} which may bias the velocity estimates in this region, albeit limited to the first 10 km upstream of the grounding line (Table S3.2). Over floating ice tongues, uncompensated vertical tidal displacement may also introduce additional uncertainty into our velocity fields. The sensitivity of our results to this effect was assessed based upon a net 50 cm tidal displacement over 6-12 day repeat period and a centre swath incidence angle of 35 degrees. We estimate that such a tidal signal would introduce $\sim 20\text{--}40 \text{ m yr}^{-1}$ additional uncertainty into the ground range component of our velocity fields. In the context of this study, this uncertainty does not affect the results at JI or ZI, and it is limited only to the floating sections of PG and 79G.

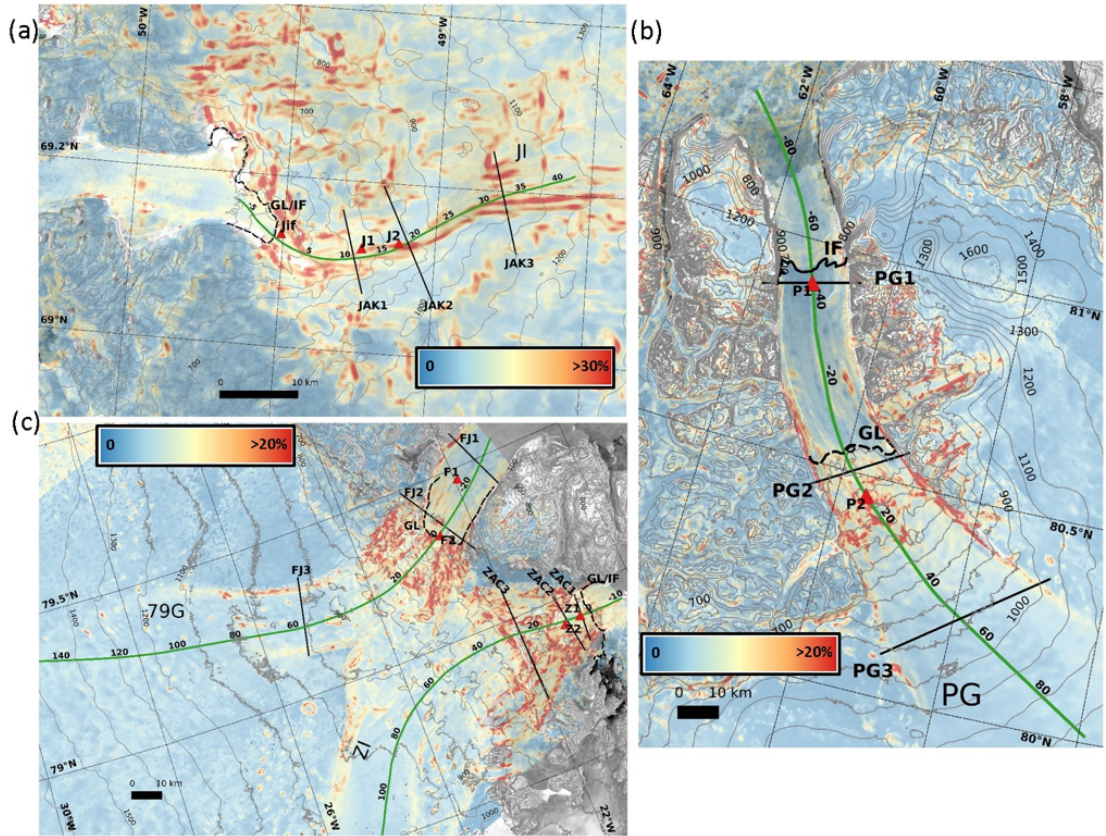


Figure 3.3: Time-averaged (2014–2017) uncertainty in ice velocity at each site expressed in percentage, based on the signal to noise ratio (SNR) for (a) JI, (b) PG, and (c) 79G and ZI.

To provide an independent evaluation of our ice velocity dataset, we finally compared them (Table S3.1) to independent estimates derived from TerraSAR-X (TSX) SAR imagery through the speckle tracking technique (Joughin, 2002), which has a repeat period acquisition of 11 days and spatial resolution up to 3 m (Joughin et al., 2016). The TSX data consist of 444 image pairs covering Jakobshavn Isbræ over the period January 2009 to January 2017, 18 pairs at Petermann Glacier over the period November 2010 to December 2016, and 17 pairs at Nioghalvfjordsfjorden over the period March 2011 to December 2016. In general, the temporal evolution of the S1-a/b measurements matches very closely with the TSX estimates. At JI, we are able to compare S1 and TSX datasets at three different locations to assess their consistency

(Figure 3.4). Even though the flow speed at these sites is high, which typically proves more challenging for feature tracking techniques, we find good agreement between the two datasets, especially at the J1 and J2 sites, with mean differences of 40 m yr^{-1} and 76 m yr^{-1} respectively. However, nearer to the calving front (site Jif), the S1-a/b measurements tend to give significantly higher velocities than TSX with a mean difference of 489 m yr^{-1} (5 % of the mean velocity) between the two datasets.

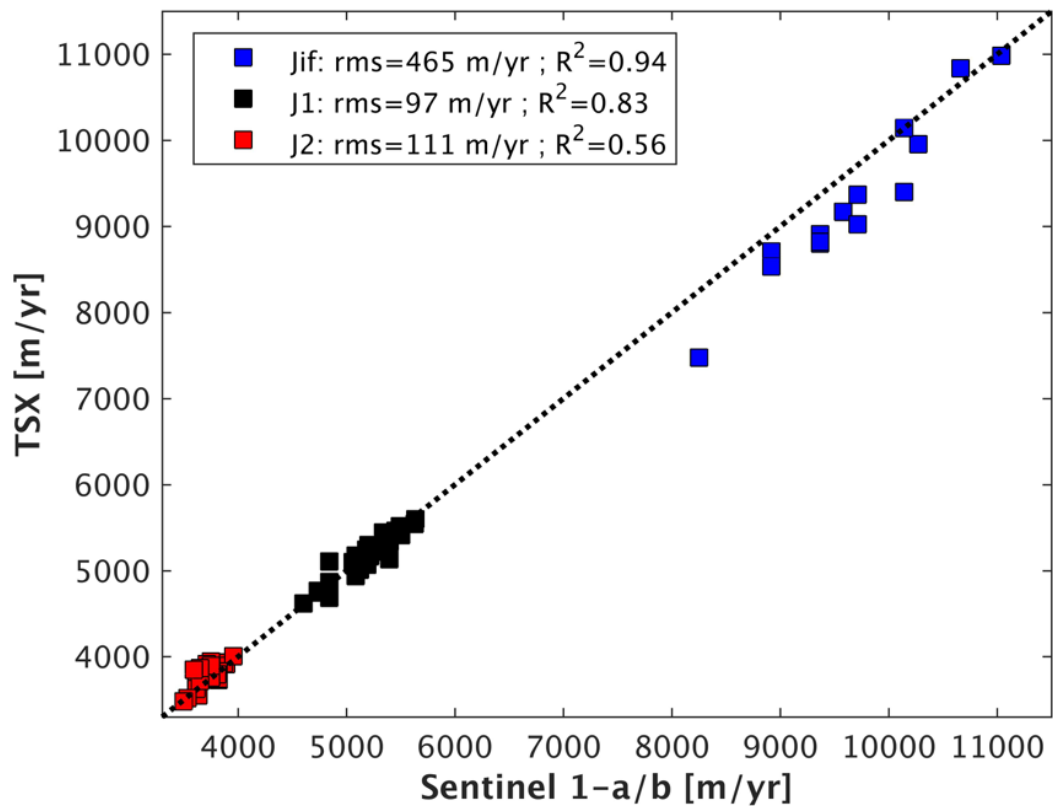


Figure 3.4: Comparison between co-located and contemporaneous Sentinel 1-a/b (6 to 12 days average) and TerraSAR-X (11 days average) Jakobshavn Isbræ velocity measurements at Jif, J1 and J2 locations (blue, black and red dots respectively), together with root mean square (rms) and correlation coefficients (R^2).

3.4 Results and Discussions

We used our complete Sentinel-1a/b dataset (Table S3.1) to generate contemporary, time-averaged velocity fields at each of our study sites (Figure 3.1). To investigate spatial and temporal variations in ice velocity, we then extracted profiles in the along- and across-flow directions, together with time series at fixed glacier locations (Figure 3.1). Our velocity profiles in Jakobshavn Isbræ, Petermann Glacier, Nioghalvfjerdingsfjorden and Zachariæ Isstrøm reached maximum mean speeds, along the stacked dataset (averaged over period 2014–2017), of approximately 9 km yr^{-1} , 1.2 km yr^{-1} , 1.4 km yr^{-1} , 2.7 km yr^{-1} , respectively. The location of the velocity maxima varied between glaciers, as a result of their differing geometries. For JI and ZI, neither of which have a significant floating tongue, we find a progressive increase in ice velocity towards the calving front (Figures 3.2a and 3.2d). For PG, the maximum velocity is reached at the grounding line and remains steady along the ~ 46 km of ice tongue (Figure 3.2b). In contrast, although 79G also reaches its maximum velocity close to the grounding line, its speed then diminishes by ~ 50 % (Figure 3.2c) near the ice front location where the ice flow divides into two main portions before it reaches several islands and ice rises (Figure S3.1b). Furthermore, it is interesting to note that, despite being located in the same region, the adjacent glacier ZI flows ~ 60 % faster in comparison. JI, PG and ZI glaciers show velocity increases progressively downstream across the transverse profiles. The four glaciers, JI, PG, 79G and ZI respectively reduce their maximum velocity to half at distances of 12 km, 22 km, 18 km, and 12 km inland of their grounding lines, highlighting the importance of resolving glacier velocities within their near terminus regions.

3.4 Results and Discussions

Table 3.1: Speedup Persistence and seasonal percentage increase in speed relative to winter and annual background for each glacier for the Sentinel-1 dataset. Speedup persistence has an uncertainty of ± 12 days due to the image acquisition interval of Sentinel-1a.

Speedup Persistence	Speedup Persistence	Summer speedup (%)	Vannual/Vwinter(%)
JI (J1)	95 days (2015)	14%	6%
	80 days (2016)	9%	4%
PG (P1)	25 days (2015)	25%	0%
	55 days (2016)	17%	6%
79G (F2)	45 days (2016)	10%	1%
ZI (Z1)	45 days (2016)	18%	3%

Next, we used the Sentinel-1a/b and TerraSAR-X velocities to assess the seasonal and longer-term variations in Jakobshavn Isbræ ice velocity over the period 2009–2017. Our Sentinel-1a/b velocity estimates at JI resolve clear seasonal velocity fluctuations, superimposed upon longer term decadal scale variability, which continues observations made by previous satellite instruments (Joughin et al., 2012, 2014). At site J1 we find an average seasonal change in speed of 750 m yr^{-1} , or 14 % between 2014 and 2015 and a speedup persistence of 80-95 days, being twice longer than for the other three glaciers (Table 3.1). Inland, the amplitude of seasonal variability diminishes, to an average of 300 m yr^{-1} (8 %) at J2. Our near-continuous, decadal-scale record clearly shows that the amplitude of the seasonal signal has evolved through time. At J1, for example, the average seasonal variability in ice speed was 400 m yr^{-1} during 2009–2011, increasing by more than a factor of 3, to 1400 m yr^{-1} between 2012 and 2013 and then diminishing to 750 m yr^{-1} between 2015–2017.

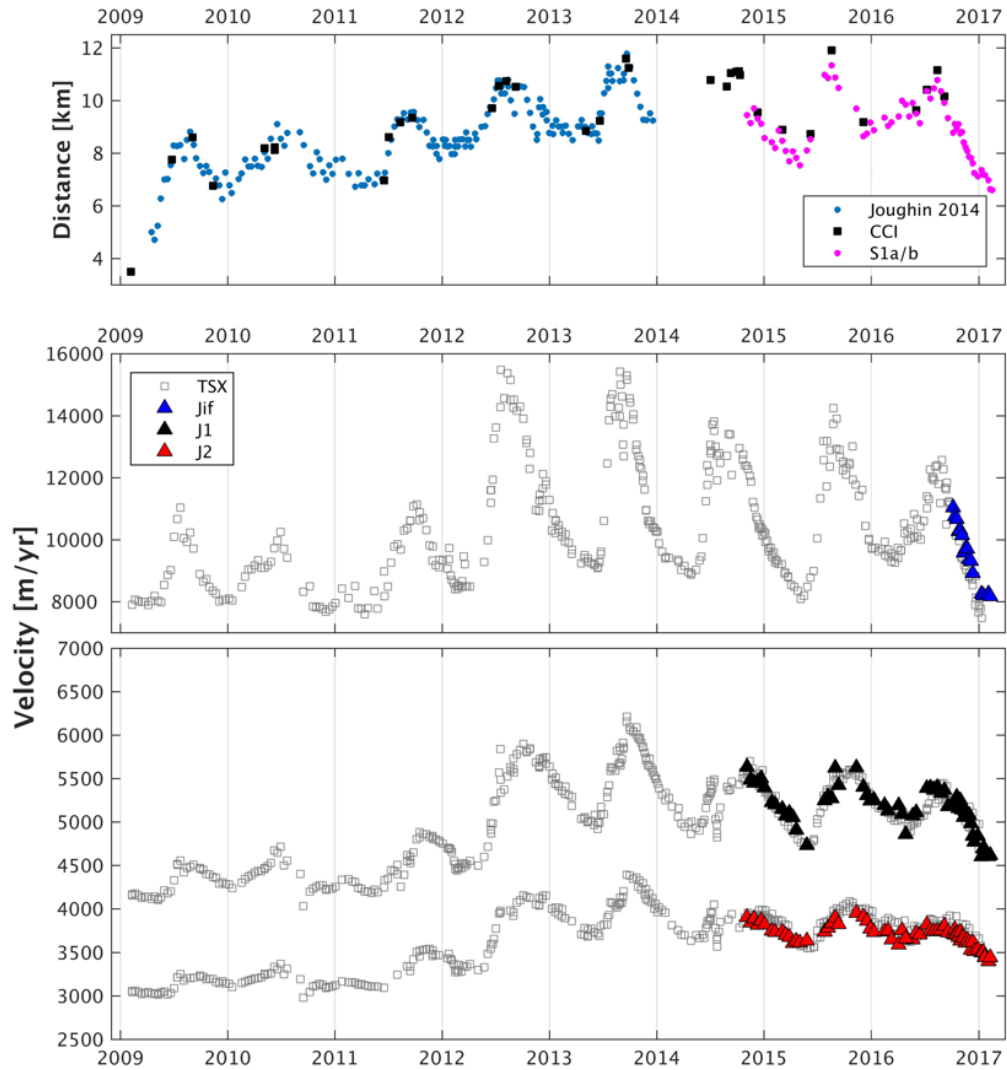


Figure 3.5: Temporal evolution of Jakobshavn Isbræ (a) ice front position extracted from Joughin et al. (2014), ESA Greenland Ice Sheet Climate Change Initiative (CCI) project (European Space Agency (ESA), 2017), and Sentinel-1a/b SAR images represented in blue, black and magenta dots respectively, where higher values correspond to ice front retreat. Changes in ice velocity through time is also shown (b, c), extracted at the locations indicated in Figure 3.1. The velocity data derived from TerraSAR-X (11 days - Joughin et al. (2016)) are shown as grey squares, and the data from Sentinel 1-a/b (6 to 12 days) as coloured triangles.

Turning to the longer term evolution of JI (Figure 3.5; time series location shown in Figure 3.1), fitting a linear trend to the data suggests an annual acceleration since 2009 of $\sim 218 \text{ m yr}^{-1}$ at Jif, diminishing inland to $\sim 128 \text{ m yr}^{-2}$ at J1, and $\sim 102 \text{ m yr}^{-2}$ at J2. Although this provides a simple characterisation of the longer-term evolution in ice speed, it is clear from our time series that computing a linear trend does not capture the full decadal scale variability in ice velocity. In particular, we note that much of the acceleration occurred between 2011 and 2013 (Figures 3.5b and 3.5c), and since then there has been a notable absence of multi-annual acceleration as earlier records suggest (Joughin et al., 2014). Computing trends in ice velocity since 2012 near the glacier terminus (Jif), for example, shows a modest decline in speed of 321 m yr^{-2} over the 5-year period (Figure 3.5b). The calving front position migration has been suggested as the trigger to the stresses regimes variations and consequently the main driver to the JI velocity fluctuations (Joughin et al., 2008b,a, 2012, 2014; Bondzio et al., 2017). After successive and gradually increased rate of the ice front retreat until 2012 (Figure 3.5a), the JI grounding line is now located on a higher bed location (Joughin et al., 2012; An et al., 2017). This may be acting to stabilise the grounding line, and in turn contribute to the glacier deceleration, although the main cause remains to be determined and further investigations is necessary. We used our observations of calving front position to assess the correlation between ice speed and calving front location, relative to their respective long term means (Figure 3.6). Based on the linear regression (Figure 3.6), our dataset indicates correlation coefficients (R^2) of 0.62 (2009–2011) and 0.79 (2012–2017), and velocity changes by 1100 and 1600 m yr^{-1} per kilometre of calving front retreat, respectively.

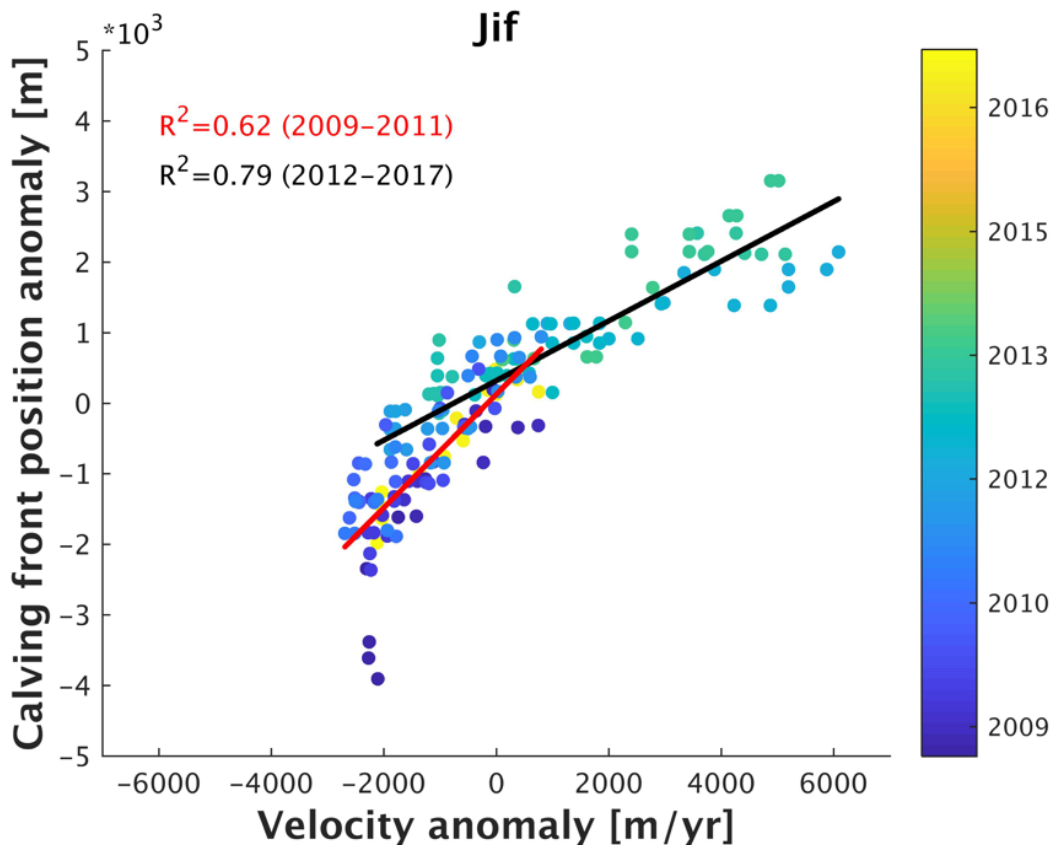


Figure 3.6: Comparison between Jakobshavn Isbræ ice velocity and calving front position anomalies at the Jif site, 0.8 km upstream of the calving front, between 2009 and early 2017. Positive values correspond to ice front retreat and speed up respectively. The red and black lines represent the linear regression through the 2009-2011 and 2012-2017 periods, respectively, together with the correlation coefficients (R^2).

At Petermann Glacier we extracted two velocity time series at P1, located ~ 45 km downstream of the grounding line and close to the calving front of the ice tongue; and P2, ~ 10 km upstream of the grounding line. These locations were chosen to examine any differences in velocity evolution over the grounded and floating portions of the glacier. Our P1 time series starts in early 2015 because it is not covered by the TerraSAR-X dataset (Figure 3.7a). We observe that, in general, ice at P1 flows ~ 400 m yr^{-1} faster than P2. Fitting a linear trend to the longer P2 dataset indicates no significant trend in ice velocity since 2011, although the precision of this trend is

hampered by the sparse data coverage during the early part of this period. Continued monitoring by Sentinel-1 will improve our confidence in resolving any decadal scale variability. The improvement in temporal sampling provided by Sentinel-1 at this site is clear (Figure 3.7a), allows us to resolve the seasonal cycle in velocity since 2015 and helps to delimit the duration of the speedup period. At P1, we detect a seasonal change in speed of $\sim 300 \text{ m yr}^{-1}$, equivalent to a 25 % increase relative to its winter velocity (Table 3.1). Despite the high seasonal change, the relation between P1's annual mean and winter velocity is 0 %, likely due to the short speedup period (25 days - Table 3.1). This provides further evidence of a seasonal velocity cycle which has been observed at both Petermann and other glaciers in this region, and is understood to be predominantly controlled by changes in basal traction, induced by penetration of surface melt water to the bed (Nick et al., 2012; Moon et al., 2014, 2015). This is further supported by our analysis of changes in calving front position (Figure S3.1a) which shows that, in contrast to JI, seasonal acceleration does not coincide with ice front retreat. Specifically, we found that during the summers of 2015 and 2016, the calving front of PG advanced $\sim 1 \text{ km}$ during the speedup (Figure S3.1a). These observations are consistent with previous modelling results, which did not find evidence of acceleration driven by large calving events in 2010 and 2012 (Nick et al., 2012; Münchow et al., 2014), suggesting that the ice shelf exerts low backstress on the glacier. More recently, we note that since September 2016 PG has developed a new crack near the ice front, which has continued to grow in length up to the present day.

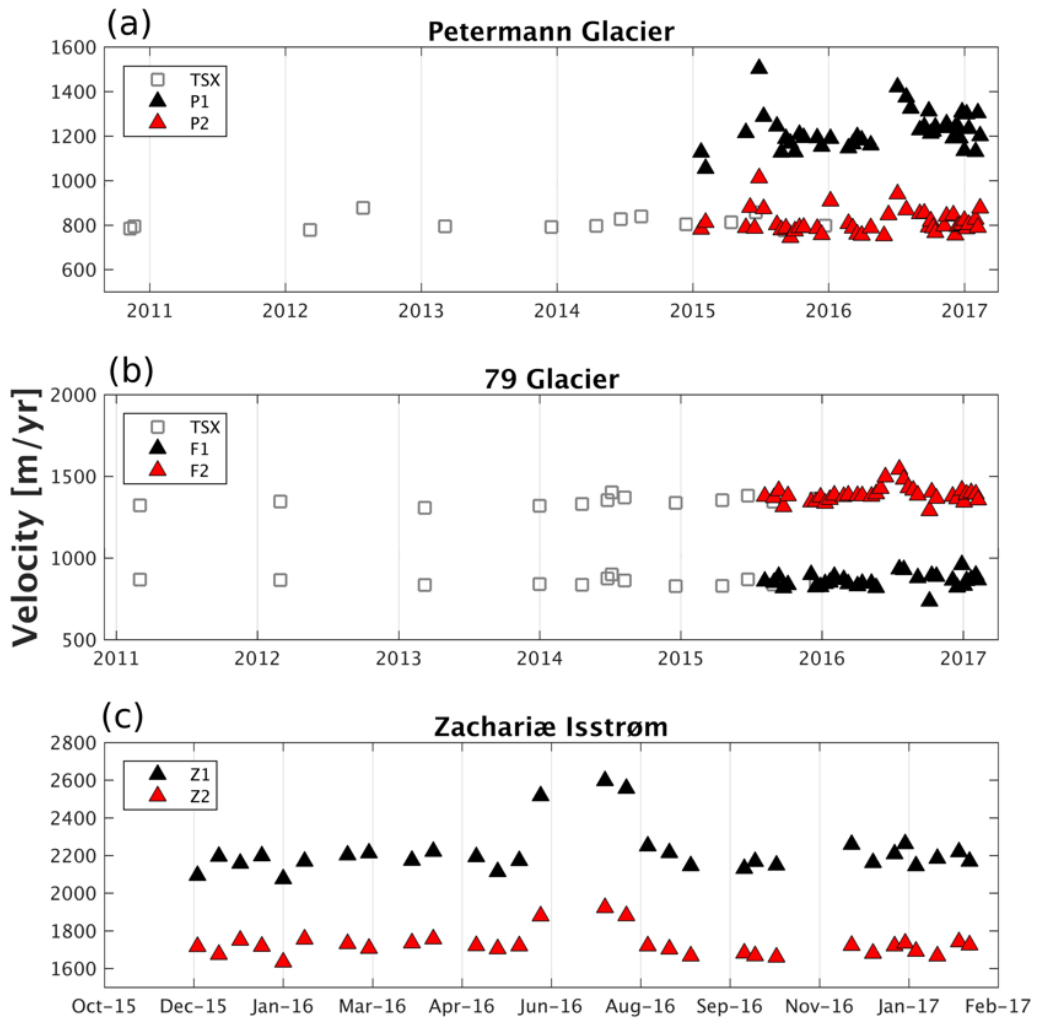


Figure 3.7: Temporal evolution of ice velocity at the locations indicated in Figure 1 over (a) Petermann Glacier, (b) Nioghalvfjerdssjorden and (c) Zachariæ Isstrøm. The data derived from TerraSAR-X (11 days - Joughin et al., 2016) and Sentinel 1-a/b (6 to 12 days) are represented as grey squares and coloured triangles, respectively.

At 79-G, we again extracted velocity time series over the ice shelf (F1, ~ 20 km downstream of the grounding line) and at the grounding line (F2). In contrast to PG and due to the steeper surface gradient upstream of the grounding line (Figure 3.2c),

ice flow is slower on the floating tongue than at the grounding line location (Figure 3.7b). We observe a seasonal speed up of $\sim 10\%$ at F2 during summer 2016 (Table 3.1), although evidence of the same acceleration on the ice shelf is not clear given the magnitude of the signal and the precision of our data. Fitting a linear trend to our data returns an annual change in velocity of 15 m yr^{-2} since 2011, although assessing the significance of this result is difficult given the limited data sampling early in the period. Turning to Zachariæ Isstrøm, we extract time series at two locations slightly upstream of the grounding line in order to observe different temporal responses between them (Figure 3.7c). At this glacier, no observations are available within the TSX dataset and so our time series is limited to the period December 2015 to January 2017. Nonetheless, like its neighbour ZI, we again find evidence of a summer speed up during 2016, equating to around 400 m yr^{-1} , or 18% (Table 3.1). Given the short period of observations we do not attempt to derive a longer-term trend in ice velocity at this site.

We compared our estimates to the results of previous studies to assess the level of stability relative to past work. At Petermann, we have observed increases in ice velocity of $\sim 10\%$ at P1 and $\sim 8\%$ at P2 between the 2015/2016 and 2016/2017 winters, matching in percentage with the observations made by Münchow et al. (2016) between 2013/14 and 2015/16. Furthermore, the Sentinel-1a/b dataset indicates a multi-annual acceleration of $\sim 32\text{ m/yr}^2$ between 2015-2017 at P1, which is similar to the $\sim 30\text{ m/yr}^2$ reported by Nick et al. (2012) based upon observational measurements over a longer period, from 2006 to 2010. The same authors also show seasonal variations of $\sim 20\text{--}25\%$ over the same location, similar to the $\sim 22\%$ shown by the Sentinel-1 dataset. At 79-G, Mougnot et al. (2015) showed a speedup of 8% from 1976 to 2014 with the main changes occurring after 2006, similar to our estimates which also suggest a slight multi-year trend of $\sim 16\text{ m yr}^{-2}$ ($\sim 8\%$) for F2 between 2015 and 2017. Zachariæ Isstrøm shows seasonal variation up to 15% between 2015 and 2017 in the Sentinel-1 dataset, agreeing with seasonal variation up to 20% estimated by Mougnot et al. (2017) using Landsat-8 optical images during 2014-2016. Overall, our Sentinel 1 results shows a close agreement with previous studies using different techniques and demonstrated to be a powerful tool for monitoring the cryosphere.

3.5 Conclusions

We have presented a new, high temporal resolution record of ice velocity evolution for four important, and with high discharge, marine based glaciers in Greenland, updated to the present day (October 2014 to February 2017). Using SAR data acquired by the Sentinel-1a/b constellation, with its 250 km wide swath and frequent revisit time, we have produced 187 velocity maps, which, in combination with 479 maps from the TerraSAR-X satellite, provide detailed spatial and temporal coverage of these key sites. Importantly, the systematic acquisition cycle of Sentinel-1a/b, which now provides averaged measurements of all of these sites every 6 days allows for detailed monitoring of both seasonal and multi-annual velocity fluctuations, and allow us to demonstrate the speedup persistence in a higher resolution. The short revisit time of 6 days, made possible since the launch of Sentinel-1b in April 2016, particularly benefits the retrieval of velocity signals across fast flowing regions close to the ice front, due to a reduction in the decorrelation occurring between image pairs. Using this new dataset, we confirm evidence of intra-annual variations in ice velocity and clear seasonal cycles occurring over the past few years at JI, PG, 79G and ZI. Of the sites studied here, JI exhibits the largest velocity variations, as demonstrated in other studies, which we show are strongly correlated with the evolution of the position of its calving front. Notably, however, in the last 5 years the longer-term ice speed has started to decrease (321 m yr^{-2}). This study demonstrates the utility of a new era of operational SAR imaging satellites for building systematic records of ice sheet outlet glacier velocity and its good agreement with TerraSAR-X products, which indicates Sentinel-1 can confidently extend the times series that began with other sensors. Looking to the future, these datasets are key for the timely identification of emerging signals of dynamic imbalance, and for understanding the processes driving ice velocity change.

3.6 Supplementary Material

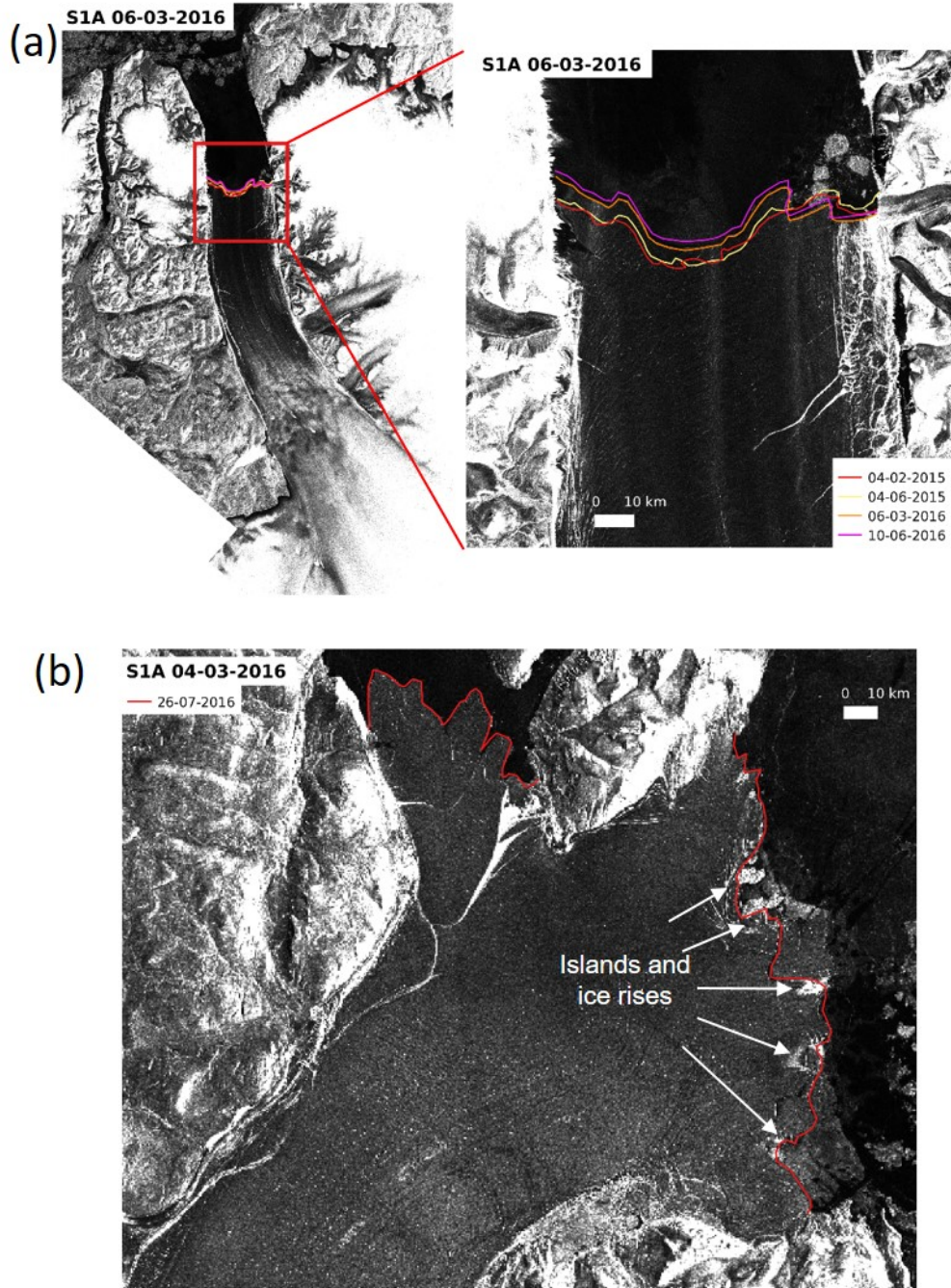


Figure S3.1: Ice front location extracted from Sentinel-1 images on (a) Petermann Glacier and (b) Nioghalvfjerdsfjorden.

3.6 Supplementary Material

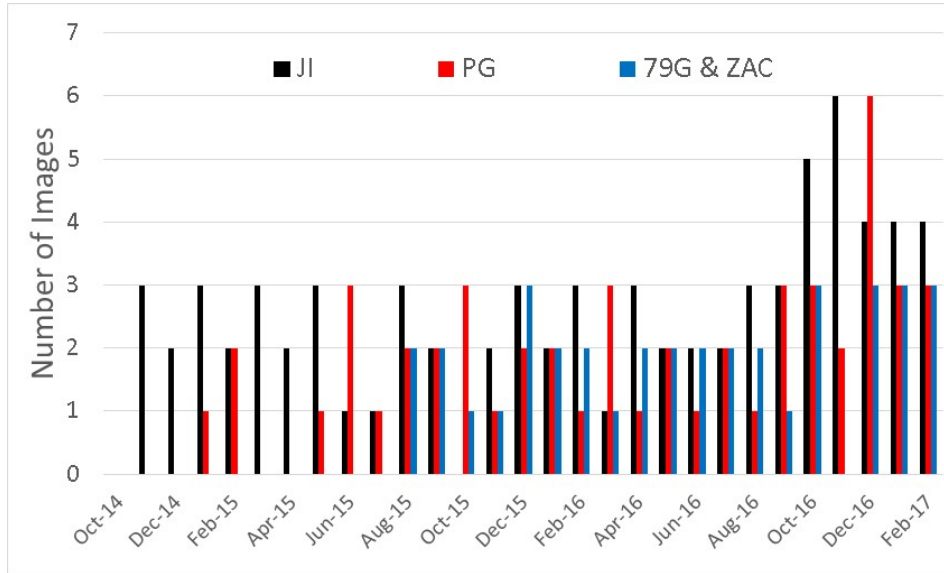


Figure S3.2: Number of images used separated per month.

Table S3.1: List of Sentinel-1 images used.

Glacier	Scene 1				Scene 2			
	Satellite	day	month	year	Satellite	day	month	year
JI	S1A	4	Nov	14	S1A	16	Nov	14
	S1A	16	Nov	14	S1A	28	Nov	14
	S1A	28	Nov	14	S1A	10	Dec	14
	S1A	10	Dec	14	S1A	22	Dec	14
	S1A	22	Dec	14	S1A	3	Jan	15
	S1A	3	Jan	15	S1A	15	Jan	15
	S1A	27	Jan	15	S1A	8	Feb	15
	S1A	8	Feb	15	S1A	20	Feb	15
	S1A	20	Feb	15	S1A	4	Mar	15
	S1A	4	Mar	15	S1A	16	Mar	15
	S1A	16	Mar	15	S1A	28	Mar	15
	S1A	28	Mar	15	S1A	9	Apr	15
	S1A	9	Apr	15	S1A	21	Apr	15
	S1A	21	Apr	15	S1A	3	May	15
	S1A	3	May	15	S1A	15	May	15
	S1A	27	May	15	S1A	8	Jun	15
	S1A	8	Jun	15	S1A	26	Jul	15
	S1A	26	Jul	15	S1A	7	Aug	15
	S1A	7	Aug	15	S1A	19	Aug	15
	S1A	19	Aug	15	S1A	31	Aug	15
	S1A	31	Aug	15	S1A	12	Sep	15
	S1A	12	Sep	15	S1A	24	Sep	15
	S1A	11	Nov	15	S1A	23	Nov	15
	S1A	5	Dec	15	S1A	17	Dec	15

3.6 Supplementary Material

	S1A	17	Dec	15	S1A	29	Dec	15
	S1A	29	Dec	15	S1A	10	Jan	16
	S1A	10	Jan	16	S1A	22	Jan	16
	S1A	22	Jan	16	S1A	3	Feb	16
	S1A	3	Feb	16	S1A	27	Feb	16
	S1A	15	Feb	16	S1A	27	Feb	16
	S1A	27	Feb	16	S1A	10	Mar	16
	S1A	10	Mar	16	S1A	3	Apr	16
	S1A	3	Apr	16	S1A	15	Apr	16
	S1A	15	Apr	16	S1A	27	Apr	16
	S1A	27	Apr	16	S1A	9	May	16
	S1A	27	Apr	16	S1A	21	May	16
	S1A	9	May	16	S1A	21	May	16
	S1A	21	May	16	S1A	2	Jun	16
	S1A	2	Jun	16	S1A	14	Jun	16
	S1A	14	Jun	16	S1A	8	Jul	16
	S1A	14	Jun	16	S1A	1	Aug	16
	S1A	20	Jul	16	S1A	1	Aug	16
	S1A	1	Aug	16	S1A	13	Aug	16
	S1A	13	Aug	16	S1A	25	Aug	16
	S1A	25	Aug	16	S1A	6	Sep	16
	S1A	6	Sep	16	S1A	18	Sep	16
	S1A	18	Sep	16	S1A	30	Sep	16
	S1A	30	Sep	16	S1B	6	Oct	16
	S1B	6	Oct	16	S1A	12	Oct	16
	S1A	12	Oct	16	S1B	18	Oct	16
	S1B	18	Oct	16	S1A	24	Oct	16
	S1A	12	Oct	16	S1B	30	Oct	16
	S1A	24	Oct	16	S1B	30	Oct	16
	S1B	30	Oct	16	S1A	5	Nov	16
	S1B	30	Oct	16	S1B	23	Nov	16
	S1A	5	Nov	16	S1B	11	Nov	16
	S1B	11	Nov	16	S1A	17	Nov	16
	S1A	17	Nov	16	S1B	23	Nov	16
	S1B	23	Nov	16	S1A	29	Nov	16
	S1A	29	Nov	16	S1B	5	Dec	16
	S1B	5	Dec	16	S1A	11	Dec	16
	S1A	11	Dec	16	S1B	17	Dec	16
	S1B	17	Dec	16	S1A	23	Dec	16
	S1B	10	Jan	17	S1A	16	Jan	17
	S1A	16	Jan	17	S1B	22	Jan	17
	S1B	22	Jan	17	S1A	28	Jan	17
	S1A	28	Jan	17	S1B	3	Feb	17
	S1B	3	Feb	17	S1A	9	Feb	17
	S1A	9	Feb	17	S1B	15	Feb	17
	S1B	15	Feb	17	S1A	21	Feb	17
	S1A	23	Jan	15	S1A	4	Feb	15
	S1A	4	Feb	15	S1A	16	Feb	15
	S1A	23	May	15	S1A	4	Jun	15
	S1A	4	Jun	15	S1A	16	Jun	15
	S1A	16	Jun	15	S1A	28	Jun	15
	S1A	28	Jun	15	S1A	10	Jul	15
	S1A	10	Jul	15	S1A	15	Aug	15
	S1A	15	Aug	15	S1A	27	Aug	15
PG								

3.6 Supplementary Material

S1A	27	Aug	15	S1A	8	Sep	15
S1A	8	Sep	15	S1A	20	Sep	15
S1A	20	Sep	15	S1A	2	Oct	15
S1A	2	Oct	15	S1A	14	Oct	15
S1A	14	Oct	15	S1A	26	Oct	15
S1A	26	Oct	15	S1A	7	Nov	15
S1A	1	Dec	15	S1A	13	Dec	15
S1A	13	Dec	15	S1A	6	Jan	16
S1A	6	Jan	16	S1A	18	Jan	16
S1A	23	Feb	16	S1A	6	Mar	16
S1A	6	Mar	16	S1A	18	Mar	16
S1A	18	Mar	16	S1A	30	Mar	16
S1A	30	Mar	16	S1A	23	Apr	16
S1A	23	Apr	16	S1A	5	May	16
S1A	29	May	16	S1A	10	Jun	16
S1A	10	Jun	16	S1A	4	Jul	16
S1A	4	Jul	16	S1A	28	Jul	16
S1A	28	Jul	16	S1A	9	Aug	16
S1A	9	Aug	16	S1A	2	Sep	16
S1A	2	Sep	16	S1A	14	Sep	16
S1A	14	Sep	16	S1A	26	Sep	16
S1A	26	Sep	16	S1B	2	Oct	16
S1B	2	Oct	16	S1A	8	Oct	16
S1A	8	Oct	16	S1B	14	Oct	16
S1B	14	Oct	16	S1B	7	Nov	16
S1B	7	Nov	16	S1A	13	Nov	16
S1A	13	Nov	16	S1B	1	Dec	16
S1B	1	Dec	16	S1A	7	Dec	16
S1A	7	Dec	16	S1B	13	Dec	16
S1B	13	Dec	16	S1A	19	Dec	16
S1A	19	Dec	16	S1B	25	Dec	16
S1B	25	Dec	16	S1A	31	Dec	16
S1A	31	Dec	16	S1B	6	Jan	17
S1B	6	Jan	17	S1A	12	Jan	17
S1A	12	Jan	17	S1B	30	Jan	17
S1B	30	Jan	17	S1A	5	Feb	17
S1A	5	Feb	17	S1B	11	Feb	17
S1B	11	Feb	17	S1A	17	Feb	17
S1A	6	Aug	15	S1A	30	Aug	15
S1A	30	Aug	15	S1A	11	Sep	15
S1A	11	Sep	15	S1A	23	Sep	15
S1A	23	Sep	15	S1A	5	Oct	15
S1A	5	Oct	15	S1A	10	Nov	15
S1A	4	Dec	15	S1A	16	Dec	15
S1A	16	Dec	15	S1A	28	Dec	15
S1A	28	Dec	15	S1A	9	Jan	16
S1A	9	Jan	16	S1A	21	Jan	16
S1A	21	Jan	16	S1A	2	Feb	16
S1A	2	Feb	16	S1A	26	Feb	16
S1A	26	Feb	16	S1A	9	Mar	16
S1A	9	Mar	16	S1A	2	Apr	16
S1A	2	Apr	16	S1A	14	Apr	16
S1A	14	Apr	16	S1A	8	May	16
S1A	8	May	16	S1A	20	May	16

79-G and
ZI

3.6 Supplementary Material

S1A	20	May	16	S1A	1	Jun	16
S1A	1	Jun	16	S1A	13	Jun	16
S1A	13	Jun	16	S1A	19	Jul	16
S1A	19	Jul	16	S1A	31	Jul	16
S1A	31	Jul	16	S1A	12	Aug	16
S1A	12	Aug	16	S1A	24	Aug	16
S1A	24	Aug	16	S1A	5	Sep	16
S1A	5	Sep	16	S1B	5	Oct	16
S1B	5	Oct	16	S1A	11	Oct	16
S1A	11	Oct	16	S1A	23	Oct	16
S1A	23	Oct	16	S1B	4	Dec	16
S1B	4	Dec	16	S1B	16	Dec	16
S1B	16	Dec	16	S1B	28	Dec	16
S1B	28	Dec	16	S1A	3	Jan	17
S1A	3	Jan	17	S1B	9	Jan	17
S1B	9	Jan	17	S1B	21	Jan	17
S1B	21	Jan	17	S1B	2	Feb	17
S1B	2	Feb	17	S1A	8	Feb	17
S1A	8	Feb	17	S1B	14	Feb	17

- Table S3.2: Velocity magnitude differences of JI using surface elevation rate of change information derived from IceBridge and Pre-Icebridge data acquired from the NASA Airborne Topographic Mapper (ATM) [Studinger, 2014] for terrain correction, and velocity magnitude without using thinning correction.

Difference [m/yr]	Distance along the profile from the grounding line [km]								
	0 - 5	5 - 10	10 - 15	15 - 20	20 - 25	25 - 30	30 - 35	35 - 40	40 - 45
Mean	-65.7	-18.1	-12.4	-2.9	3.0	-3.8	0.9	1.9	1.9
Max	55.8	58.6	33.2	9.9	37.6	36.9	13.1	16.0	20.2
Min	-277.3	-160.4	-75.3	-17.2	-32.8	-39.3	-11.8	-6.0	-6.6

References

- L. An, E. Rignot, S. Elieff, M. Morlighem, R. Millan, J. Mouginot, D. M. Holland, D. Holland, and J. Paden. Bed elevation of Jakobshavn Isbræ, West Greenland, from high-resolution airborne gravity and other data. *Geophysical Research Letters*, 44:3728–3736, 2017. ISSN 00948276. doi: 10.1002/2017GL073245. URL <http://doi.wiley.com/10.1002/2017GL073245>. 64
- W. H. Armstrong, R. S. Anderson, and M. A. Fahnestock. Spatial Patterns of Summer Speedup on South Central Alaska Glaciers. *Geophysical Research Letters*, 44(18): 9379–9388, 2017. ISSN 19448007. doi: 10.1002/2017GL074370. 51
- J. H. Bondzio, M. Morlighem, H. Seroussi, T. Kleiner, M. Rückamp, J. Mouginot, T. Moon, E. Y. Larour, and A. Humbert. The mechanisms behind Jakobshavn Isbrae’s acceleration and mass loss: a 3D thermomechanical model study. *Geophysical Research Letters*, 44:6252–6260, 2017. ISSN 00948276. doi: 10.1002/2017GL073309. URL <http://doi.wiley.com/10.1002/2017GL073309>. 51, 64
- J. R. Carr, C. R. Stokes, and A. Vieli. Threefold increase in marine-terminating outlet glacier retreat rates across the Atlantic Arctic: 1992–2010. *Annals of Glaciology*, 58(74):72–91, 2017. ISSN 02603055. doi: 10.1017/aog.2017.3. 51
- R. Cassotto, M. Fahnestock, J. M. Amundson, M. Truffer, and I. Joughin. Seasonal and interannual variations in ice melange and its impact on terminus stability, Jakobshavn Isbræ, Greenland. *Journal of Glaciology*, 61(225):76–88, 2015. ISSN 00221430. doi: 10.3189/2015JoG13J235. 52
- R. de Lange, A. Luckman, and T. Murray. Improvement of satellite radar feature tracking for ice velocity derivation by spatial frequency filtering. *IEEE Transactions on Geoscience and Remote Sensing*, 45(7):2309–2318, 2007. ISSN 01962892. doi: 10.1109/TGRS.2007.896615. 57
- A. Dehecq, N. Gourmelen, and E. Trouve. Deriving large-scale glacier velocities from a complete satellite archive: Application to the Pamir-Karakoram-Himalaya. *Remote Sensing of Environment*, 162:55–66, 2015. ISSN 00344257. doi: 10.1016/j.rse.2015.01.031. URL <http://dx.doi.org/10.1016/j.rse.2015.01.031>. 51

REFERENCES

- E. M. Enderlin, I. M. Howat, S. Jeong, M.-J. Noh, J. H. van Angelen, and M. R. van den Broeke. An improved mass budget for the Greenland ice sheet. *Geophys. Res. Lett.*, 41:1–7, 2014. doi: 10.1002/2013GL059010. Received. 50, 51, 52
- European Space Agency (ESA). Greenland Ice Sheet Climate Change Initiative (CCI) project: Greenland calving front locations v.3.0, available at: http://products.esa-icesheets-cci.org/products/details/greenland_calving_front_locations_v3_0.zip/ (last access: 11 June 2018). 2017. xii, 63
- M. Fahnestock, T. Scambos, T. Moon, A. Gardner, T. Haran, and M. Klinger. Rapid large-area mapping of ice flow using Landsat 8. *Remote Sensing of Environment*, 185:84–94, 2016. ISSN 00344257. doi: 10.1016/j.rse.2015.11.023. URL <http://dx.doi.org/10.1016/j.rse.2015.11.023>. 51
- D. Felikson, T. C. Bartholomaeus, G. A. Catania, N. J. Korsgaard, K. H. Kjær, M. Morlighem, B. Noël, M. Van Den Broeke, L. A. Stearns, E. L. Shroyer, D. A. Sutherland, and J. D. Nash. Inland thinning on the Greenland ice sheet controlled by outlet glacier geometry. *Nature Geoscience*, 10(5):366–369, 2017. ISSN 17520908. doi: 10.1038/ngeo2934. 51
- GAMMA REMOTE SENSING. Interferometric SAR Processor - ISP. Volume 1.9. Technical Report December, 2015. 55
- C. Gladish, D. Holland, A. Rosing-Asvid, J. W. Behrens, and J. Boje. Oceanic Boundary Conditions for Jakobshavn Glacier. Part II: Provenance and Sources of Variability of Disko Bay and Ilulissat Icefjord Waters, 1990–2011. *Journal of Physical Oceanography*, 45(2003):33–63, 2015. ISSN 0022-3670. doi: 10.1175/JPO-D-14-0045.1. 52
- A. E. Hogg, A. Shepherd, N. Gourmelen, and M. Engdahl. Grounding line migration from 1992 to 2011 on Petermann Glacier, North-West Greenland. *Journal of Glaciology*, 62:1–11, 2016. doi: 10.1017/jog.2016.83. 52, 53
- A. E. Hogg, A. Shepherd, S. L. Cornford, K. Briggs, N. Gourmelen, J. Graham, I. Joughin, J. Mouginot, T. Nagler, A. J. Payne, E. Rignot, and J. Wuite. Increased ice flow in Western Palmer Land linked to ocean melting. *Geophys. Res. Lett.*, 44:1–9, 2017. doi: 10.1002/2016GL072110. 57

REFERENCES

- D. M. Holland, R. H. Thomas, B. D. Young, M. H. Ribergaard, and B. Lyberth. Acceleration of Jakobshavn Isbræ triggered by warm subsurface ocean waters. *Nature Geoscience*, 1:1–6, 2008. doi: 10.1038/ngeo316. 50, 52
- I. M. Howat, J. E. Box, Y. Ahn, A. Herrington, and E. M. McFadden. Seasonal variability in the dynamics of marine-terminating outlet glaciers in Greenland. *Journal of Glaciology*, 56(198):601–613, 2010. ISSN 00221430. doi: 10.3189/002214310793146232. 51
- I. M. Howat, a. Negrete, and B. E. Smith. The Greenland Ice Mapping Project (GIMP) land classification and surface elevation data sets. *The Cryosphere*, 8(4):1509–1518, 2014. ISSN 1994-0424. doi: 10.5194/tc-8-1509-2014. URL <http://www.the-cryosphere.net/8/1509/2014/tc-8-1509-2014.html>. xi, 56, 57
- T. S. Jensen, J. E. Box, and C. S. Hvidberg. A sensitivity study of annual area change for Greenland ice sheet marine terminating outlet glaciers: 1999–2013. *Journal of Glaciology*, 62:1–10, 2016. ISSN 0022-1430. doi: 10.1017/jog.2016.12. URL http://www.journals.cambridge.org/abstract/_S0022143016000125. 51, 52, 53
- O. M. Johannessen, M. Babiker, and M. W. Miles. Unprecedented Retreat in a 50-Year Observational Record for Petermann. *Atmospheric and Oceanic Science Letters*, 6(5):259–265, 2013. doi: 10.3878/j.issn.1674-2834.13.0021.1. 52
- I. Joughin. Ice-sheet velocity mapping: a combined interferometric and speckle-tracking approach. *Annals of Glaciology*, 34(1):195–201, jan 2002. ISSN 02603055. doi: 10.3189/172756402781817978. URL <http://openurl.ingenta.com/content/xref?genre=article&issn=0260-3055&volume=34&issue=1&spage=195>. 59
- I. Joughin, D. P. Winebrenner, and M. A. Fahnestock. Observations of ice-sheet motion in Greenland using satellite radar interferometry. *Geophysical Research Letters*, 22(5):571–574, 1995. ISSN 0094-8276. doi: 10.1029/95GL00264. 51
- I. Joughin, S. B. Das, M. A. King, B. E. Smith, I. M. Howat, and T. Moon. Seasonal Speedup Along the Western Flank of the Greenland Ice Sheet. *Science*, 320(April):781–784, 2008a. doi: 10.1126/science.1153288. 64

REFERENCES

- I. Joughin, I. M. Howat, M. Fahnestock, B. Smith, W. Krabill, R. B. Alley, H. Stern, and M. Truffer. Continued evolution of Jakobshavn Isbrae following its rapid speedup. *Journal of Geophysical Research: Earth Surface*, 113(4):1–14, 2008b. ISSN 21699011. doi: 10.1029/2008JF001023. 52, 64
- I. Joughin, B. E. Smith, I. M. Howat, T. Scambos, and T. Moon. Greenland flow variability from ice-sheet-wide velocity mapping. *Journal of Glaciology*, 56(197):415–430, aug 2010. ISSN 00221430. doi: 10.3189/002214310792447734. URL <http://openurl.ingenta.com/content/xref?genre=article&issn=0022-1430&volume=56&issue=197&spage=415>. 50, 51
- I. Joughin, B. E. Smith, I. M. Howat, D. Floricioiu, R. B. Alley, M. Truffer, and M. Fahnestock. Seasonal to decadal scale variations in the surface velocity of Jakobshavn Isbrae, Greenland: Observation and model-based analysis. *Journal of Geophysical Research: Earth Surface*, 117(2):1–20, 2012. ISSN 21699011. doi: 10.1029/2011JF002110. 51, 52, 62, 64
- I. Joughin, B. E. Smith, D. E. Shean, and D. Floricioiu. Brief communication: Further summer speedup of Jakobshavn Isbræ. *The Cryosphere*, 8(1):209–214, 2014. ISSN 19940416. doi: 10.5194/tc-8-209-2014. xii, 50, 52, 62, 63, 64
- I. Joughin, B. Smith, I. Howat, and T. Scambos. MEaSUREs Multi-year Greenland Ice Sheet Velocity Mosaic, Version 1. [Indicate subset used]. *Boulder, Colorado USA. NASA National Snow and Ice Data Center Distributed Active Archive Center*, 2016. URL <http://dx.doi.org/10.5067/QUA5Q9SVMSJG>. xii, 59, 63
- S. a. Khan, K. H. Kjaer, M. Bevis, J. L. Bamber, J. Wahr, K. K. Kjeldsen, A. a. Bjork, N. J. Korsgaard, L. a. Stearns, M. R. van den Broeke, L. Liu, N. K. Larsen, and I. S. Muresan. Sustained mass loss of the northeast Greenland ice sheet triggered by regional warming. *Nature Climate Change*, 4(April):292–299, 2014. ISSN 1758-678X. doi: 10.1038/nclimate2161. URL <http://dx.doi.org/10.1038/nclimate2161>{%}5Cn10.1038/nclimate2161{%}5Cn<http://www.nature.com/nclimate/journal/v4/n4/abs/nclimate2161.html>{#}supplementary-information. 53

REFERENCES

- B. K. Lucchitta and H. M. Ferguson. Antarctica: measuring glacier velocity from satellite images. *Science (New York, N.Y.)*, 234(4780):1105–1108, 1986. ISSN 0036-8075. doi: 10.1126/science.234.4780.1105. 51
- M. McMillan, A. Leeson, A. Shepherd, K. Briggs, T. W. K. Armitage, A. Hogg, P. K. Munneke, M. van den Broeke, B. Noël, W. J. van de Berg, S. Ligtenberg, M. Horwath, A. Groh, A. Muir, and L. Gilbert. A high resolution record of Greenland mass balance. *Geophysical Research Letters*, 43:1–9, 2016. doi: 10.1002/GRL.54619. 50
- T. Moon, I. Joughin, B. Smith, and I. Howat. 21st-century evolution of Greenland outlet glacier velocities. *Science*, 336(6081):576–8, may 2012. ISSN 1095-9203. doi: 10.1126/science.1219985. URL <http://www.ncbi.nlm.nih.gov/pubmed/22556249>. 51
- T. Moon, I. Joughin, B. Smith, M. R. Broeke, W. J. Berg, B. Noël, and M. Usher. Distinct patterns of seasonal Greenland glacier velocity. *Geophysical Research Letters*, 41:7209–7216, 2014. doi: 10.1002/2014GL061836. 50, 66
- T. Moon, I. Joughin, and B. Smith. Seasonal to multiyear variability of glacier surface velocity, terminus position, and sea ice/ice mélange in northern Greenland. *Journal of Geophysical Research: Earth Surface*, 120:818–833, 2015. doi: 10.1002/2015JF003494.Received. 50, 66
- M. Morlighem, E. Rignot, J. Mouginot, H. Seroussi, and E. Larour. IceBridge Bed-Machine Greenland, Version 2. Boulder, Colorado USA. NASA National Snow and Ice Data Center Distributed Active Archive Center. [09/08/2017]. 2015. doi: 10.5067/AD7B0HQNSJ29. xi, 56
- J. Mouginot, E. Rignot, B. Scheuchl, I. Fenty, A. Khazendar, M. Morlighem, A. Buzzi, and J. Paden. Fast retreat of Zachariæ Isstrøm , northeast Greenland. *Science Express*, 10.1126(November), 2015. doi: 10.1126/science.aac7111. 52, 53, 68
- J. Mouginot, E. Rignot, B. Scheuchl, and R. Millan. Comprehensive Annual Ice Sheet Velocity Mapping Using Landsat-8, Sentinel-1, and RADARSAT-2 Data. *Remote Sensing*, 9(364):1–20, 2017. ISSN 0018-9235. doi: 10.3390/rs9040364. URL <http://www.mdpi.com/2072-4292/9/4/364/htm>. 51, 68

REFERENCES

- A. Münchow, L. Padman, and H. A. Fricker. Interannual changes of the floating ice shelf of Petermann Gletscher, North Greenland, from 2000 to 2012. *Journal of Glaciology*, 60(221):489–499, 2014. ISSN 00221430. doi: 10.3189/2014JoG13J135. 52, 66
- A. Münchow, L. Padman, P. Washam, and K. W. Nicholls. The ice shelf of Petermann Gletscher, North Greenland, and its connection to the Arctic and Atlantic Oceans. *Oceanography*, 29(4):84–95, 2016. doi: 10.5670/oceanog.2016.101. 68
- T. Nagler, H. Rott, M. Hetzenecker, J. Wuite, and P. Potin. The Sentinel-1 Mission: New Opportunities for Ice Sheet Observations. *Remote Sensing*, 7(7):9371–9389, 2015. ISSN 2072-4292. doi: 10.3390/rs70709371. URL <http://www.mdpi.com/2072-4292/7/7/9371/>. 51, 57
- F. Nick, a. Luckman, a. Vieli, C. Van Der Veen, D. Van As, R. Van De Wal, F. Pattyn, a.L. Hubbard, and D. Floricioiu. The response of Petermann Glacier, Greenland, to large calving events, and its future stability in the context of atmospheric and oceanic warming. *Journal of Glaciology*, 58(208):229–239, 2012. ISSN 00221430. doi: 10.3189/2012JoG11J242. URL <http://www.igsoc.org/journal/58/208/j11J242.html>. 53, 66, 68
- F. Paul, T. Bolch, A. Käab, T. Nagler, C. Nuth, K. Scharrer, A. Shepherd, T. Strozzi, F. Ticconi, R. Bhambri, E. Berthier, S. Bevan, N. Gourmelen, T. Heid, S. Jeong, M. Kunz, T. R. Lauknes, A. Luckman, J. Merryman, G. Moholdt, A. Muir, J. Neelmeijer, M. Rankl, J. VanLooy, and T. Van Niel. The glaciers climate change initiative: Methods for creating glacier area, elevation change and velocity products. *Remote Sensing of Environment*, 162:408–426, 2015. ISSN 00344257. doi: 10.1016/j.rse.2013.07.043. URL <http://dx.doi.org/10.1016/j.rse.2013.07.043>. 55, 57
- H. Pritchard, T. Murray, A. Luckman, T. Strozzi, and S. Barr. Glacier surge dynamics of Sortebrae, east Greenland, from synthetic aperture radar feature tracking. *Journal of Geophysical Research*, 110(F03005):1–13, 2005. ISSN 0148-0227. doi: 10.1029/2004JF000233. URL <http://doi.wiley.com/10.1029/2004JF000233>. 55

REFERENCES

- E. Rignot. Tidal motion, ice velocity and melt rate of Petermann Gletscher, Greenland, measured from radar interferometry. *Journal of Glaciology*, 42(142):476–485, 1996. ISSN 00221430. 53
- E. Rignot and P. Kanagaratnam. Changes in the Velocity Structure of the Greenland Ice Sheet. *Science*, 311(February):986–990, 2006. doi: 10.1126/science.1121381. 50, 52
- E. Rignot and J. Mouginot. Ice flow in Greenland for the International Polar Year 2008-2009. *Geophysical Research Letters*, 39(11):1–7, 2012. ISSN 00948276. doi: 10.1029/2012GL051634. 51, 52, 53
- E. Rignot and K. Steffen. Channelized bottom melting and stability of floating ice shelves. *Geophysical Research Letters*, 35(2):1–5, 2008. ISSN 00948276. doi: 10.1029/2007GL031765. 53
- Sentinels_POD_Team. Sentinels POD Service File Format Specifications, European Space Agency, Paris, France. 2013. 55
- A. Shepherd, E. R. Ivins, G. A., V. R. Barletta, M. J. Bentley, S. Bettadpur, K. H. Briggs, D. H. Bromwich, R. Forsberg, N. Galin, M. Horwath, S. Jacobs, I. Joughin, M. A. King, J. T. M. Lenaerts, J. Li, S. R. M. Ligtenberg, A. Luckman, S. B. Luthcke, M. McMillan, R. Meister, G. Milne, J. Mouginot, A. Muir, J. P. Nicolas, J. Paden, A. J. Payne, H. Pritchard, E. Rignot, H. Rott, L. S. Sørensen, T. A. Scambos, B. Scheuchl, E. J. O. Schrama, B. Smith, A. V. Sundal, J. H. van Angelen, W. J. van de Berg, M. R. van den Broeke, D. G. Vaughan, I. Velicogna, J. Wahr, P. L. Whitehouse, D. J. Wingham, D. Yi, D. Young, and H. J. Zwally. A Reconciled Estimate of Ice-Sheet Mass Balance. *Science*, 338(November):1183–1189, 2012. doi: 10.1126/science.1228102. 50, 51
- T. Strozzi, A. Luckman, T. Murray, U. Wegmuller, and C. L. Werner. Glacier motion estimation using SAR offset-tracking procedures. *IEEE Transactions on Geoscience and Remote Sensing*, 40(11):2384–2391, nov 2002. ISSN 0196-2892. doi: 10.1109/TGRS.2002.805079. URL <http://ieeexplore.ieee.org/lpdocs/epic03/wrapper.htm?arnumber=1166597>. 55

-
- M. Studinger. IceBridge ATM L4 Surface Elevation Rate of Change, Version 1, Greenland subset. Boulder, Colorado USA, NASA National Snow and Ice Data Center Distributed Active Archive Center, <https://doi.org/10.5067/BCW6CI3TXOCY>. 2014. 58
- M. Tedesco, X. Fettweis, T. Mote, J. Wahr, P. Alexander, J. E. Box, and B. Wouters. Evidence and analysis of 2012 Greenland records from spaceborne observations, a regional climate model and reanalysis data. *The Cryosphere*, 7(2):615–630, 2013. ISSN 1994-0424. doi: 10.5194/tc-7-615-2013. URL <http://www.the-cryosphere.net/7/615/2013/>. 50, 52
- R. S. van de Wal, C. J. Smeets, W. Boot, M. Stoffelen, R. Van Kampen, S. H. Doyle, F. Wilhelms, M. R. Van Den Broeke, C. H. Reijmer, J. Oerlemans, and A. Hubbard. Self-regulation of ice flow varies across the ablation area in south-west Greenland. *The Cryosphere*, 9:603–611, 2015. ISSN 19940424. doi: 10.5194/tc-9-603-2015. 52
- M. van den Broeke, J. L. Bamber, J. Ettema, E. Rignot, E. Schrama, W. J. van de Berg, E. van Meijgaard, I. Velicogna, and B. Wouters. Partitioning recent Greenland mass loss. *Science*, 326(November):984–986, 2009. ISSN 0036-8075. doi: 10.1126/science.1178176. 50
- N. Yague-Martinez, P. Prats-Iraola, F. R. Gonzalez, R. Brcic, R. Shau, D. Geudtner, M. Eineder, and R. Bamler. Interferometric Processing of Sentinel-1 TOPS data. *IEEE Transactions on Geoscience and Remote Sensing*, 54(4):2220–2234, 2016. ISSN 01962892. doi: 10.1109/TGRS.2015.2497902. 55

Chapter 4

Seasonal Variations in the Flow of Land-Terminating Glaciers in Central-West Greenland Using Sentinel-1 Imagery

Authors: **Adriano Lemos, Andrew Shepherd, Malcolm McMillan and Anna E. Hogg**

Abstract

Land-terminating sectors of the Greenland ice sheet flow faster in summer after surface meltwater reaches the subglacial drainage system. Speedup occurs when the subglacial drainage system becomes saturated, leading to a reduction in the effective pressure which promotes sliding of the overlying ice. Here, we use observations acquired by the Sentinel-1a and b synthetic aperture radar to track changes in the speed of land-terminating glaciers across a 14,000 km^2 sector of west-central Greenland on a weekly basis in 2016 and 2017. The fine spatial and temporal sampling of the satellite data allows us to map the speed of summer and winter across the entire sector and to resolve the weekly evolution of ice flow across the downstream portions of five glaciers.

Near to the ice sheet margin (at 650 m.a.s.l.), glacier speedup begins around day 130, persisting for around 90 days, and then peaks around day 150. At four of the five glaciers included in our survey the peak speedup is similar in both years, in Russell Glacier there is marked interannual variability of 32% between 2016 and 2017. We present, for the first time, seasonal and altitudinal variation in speedup persistence. Our study demonstrates the value of Sentinel-1's systematic and frequent acquisition plan for studying seasonal changes in ice sheet flow.

4.1 Introduction

In recent decades the Greenland Ice Sheet has lost ice at an increasing rate, rising by 89% between 2011–2014 relative to 1992–2011 (Shepherd et al., 2012; McMillan et al., 2016). The majority (60%) of this ice loss has been due to surface melting and runoff (Enderlin et al., 2014; van den Broeke et al., 2016), which have risen as summers have warmed (Hanna et al., 2012, 2014). Between 2011 and 2014, 41% of all ice loss from Greenland ($269 \pm 51 \text{ GT yr}^{-1}$; (McMillan et al., 2016)) was from the south-western sector alone, where changes in the degree of surface melting have been pronounced (Crozier et al., 2018).

In addition to the direct impact on runoff, increased surface melting has also been linked to increases in the speed of ice flow through basal lubrication (Zwally et al., 2002; Hoffman et al., 2011; Chu, 2014). Rising air temperatures lead to increased surface melting, which can in turn lead to an increase in the amount of water feeding into the subglacial drainage system (Chu, 2014) after supraglacial lakes drain or moulins open (Hoffman et al., 2011; Chu, 2014). As a consequence of this excess meltwater, subglacial water pressure rises, which reduces the effective pressure between the ice-bedrock interface and leads to enhanced basal sliding (Harper et al., 2005; Nienow et al., 2005; Andrews et al., 2015). During the melting season, frictional heating caused by water flow enlarges the conduits of the subglacial hydrologic system, allowing a greater volume of water to be accommodated (Bartholomew et al., 2010; Cowton et al., 2013). As a consequence, from mid-season to the end of the melt season, the drainage system transmission capacity exceeds the meltwater input, draining water efficiently through low-pressure channels (Schoof, 2010; Cowton et al., 2013).

Seasonal changes in ice flow have been observed in both fast-moving and slow-moving glaciers (Rignot and Kanagaratnam, 2006; Joughin et al., 2008; Shepherd et al., 2009; Palmer et al., 2011; Sundal et al., 2011; Joughin et al., 2013; Moon et al., 2014). In south-west Greenland, the summertime speedup of land-terminating glaciers is widespread and is widely interpreted as being driven by seasonal changes in the degree of basal lubrication (Zwally et al., 2002; Sole et al., 2011; Sundal et al., 2011). At low elevations (under 1000 m), seasonal changes in the movement of Greenland’s glaciers are thought to be dominated by short-term events, typically lasting between 1 day to 1 week during the summer (Bartholomew et al., 2012; van de Wal et al., 2015), with ice speeds increasing by 100 to 150% relative to winter (Sundal et al., 2011; Fitzpatrick et al., 2013). Resolving such changes has been a challenge, because observations of ice sheet flow have historically been made using episodically acquired satellite imagery (Crozier et al., 2018; Harper et al., 2005; Nienow et al., 2005) and GPS sensors installed at point locations on the ice sheet (Shepherd et al., 2009; Bartholomew et al., 2010, 2012). Systematically monitoring seasonal variations in ice flow is therefore an important task as it will improve our understanding of the present and likely future response of the Greenland Ice Sheet to a changing climate.

Since the 1970s, the speed of glacier flow in the polar regions has been measured with repeat optical satellite imagery (Lucchitta and Ferguson, 1986). However, despite their ongoing use (Dehecq et al., 2015; Fahnestock et al., 2016; Armstrong et al., 2017; Gardner et al., 2018), optical images are daylight dependent which limits their utility outside of the summer season. Unfortunately, satellite imagery may also be obscured by clouds. Synthetic aperture radar (SAR) images do not suffer from either limitation and have also been extensively used to measure ice speed since the launch of the European Remote Sensing Satellite 1 (ERS-1) in 1991 (Goldstein et al., 1993; Joughin et al., 1995; Lucchitta et al., 1995; Joughin et al., 2010; Rignot et al., 2011). A persistent obstacle to the use of both optical and SAR satellite imagery for tracking ice motion has been the episodic nature of acquisitions. Since the launch of the Sentinel-1a (S1a) and Sentinel-1b (S1b) SAR constellation in April 2014 and April 2016, respectively, it has become possible to systematically measure changes in ice speed every 6 days (Nagler et al., 2015; Joughin et al., 2018; Lemos et al., 2018). Here, we use a sequence

of Sentinel-1a and 1b SAR images to track seasonal changes in ice sheet flow across a land-terminating sector of the Greenland Ice Sheet between 2014 and 2017.

4.2 Study Area

Our study focusses on a 14,000 km^2 sector of central-west Greenland between 66.6°N – 67.4°N (Figure 4.1). The study area includes five glaciers; Isorlersuup Glacier (IG), Ørkendalen Glacier (ØG), Russell Glacier (RG) and Isunnguata Sermia (IS), and an unnamed outlet glacier which we refer to as Glacier 1 (G1). The area has received a relatively high amount attention due to the propensity of its glaciers to exhibit seasonal speedup. In-situ GPS observations have shown that seasonal velocity variations are strongly linked to changes in surface melting (Shepherd et al., 2009; Bartholomew et al., 2010, 2011, 2012; Chandler et al., 2013; Sole et al., 2013; van de Wal et al., 2015). Satellite measurements have provided a large-scale perspective of changes in ice flow (Joughin et al., 2008; Palmer et al., 2011; Sundal et al., 2011; Fitzpatrick et al., 2013) and in the extent of supraglacial lakes (Leeson et al., 2012; Howat et al., 2013; Leeson et al., 2013, 2015). Together, these measurements, in conjunction with numerical ice flow modelling have led to an improved understanding of the link between regional hydrology and changes in ice flow, for example the role of supra-glacial lake drainage (Clason et al., 2015; Koziol and Arnold, 2018).

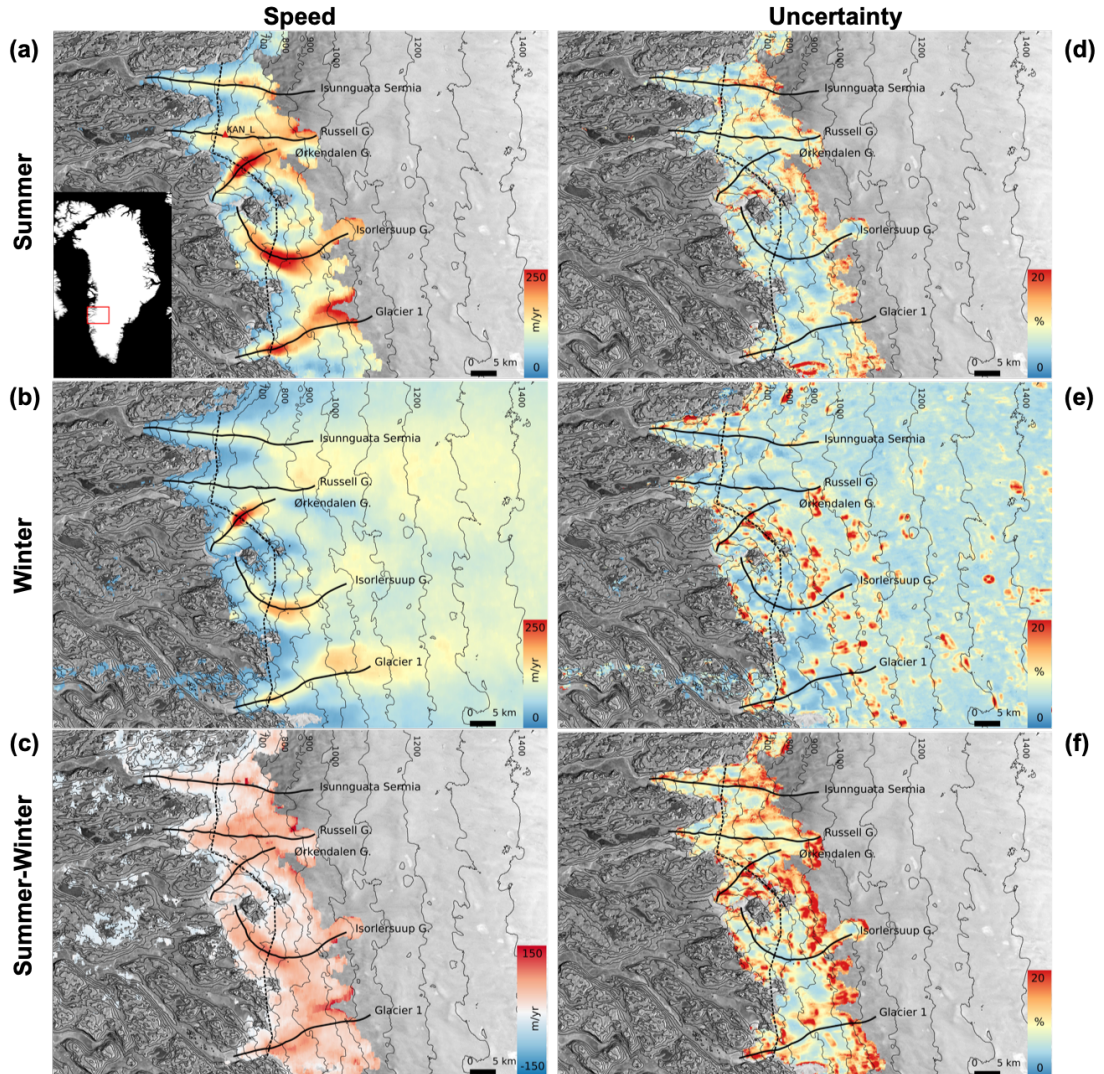


Figure 4.1: Average ice velocity in (a) summer (May–Jul), (b) winter (Aug–Apr), and (c) the difference between summer and winter, derived from Sentinel-1 (S1) synthetic aperture radar (SAR) imagery. The uncertainties in the maps associated with the summer, winter, and difference between the summer and winter ice speeds are also shown (d–f, respectively). Velocities and the uncertainties are overlaid on a SAR backscatter intensity image. Also shown are elevation contours (thin grey lines), profiles along (solid black lines) and across (dotted black lines) the centre of five glaciers. The location of the KAN_L weather station is also mapped (red dot, a).

4.3 Data and Methods

Previous studies have demonstrated the capability of Sentinel-1 (S1) for mapping ice sheet flow (Nagler et al., 2015; Joughin et al., 2018; Lemos et al., 2018). Here, we use single-look complex (SLC) synthetic aperture radar (SAR) images acquired in the interferometric wide swath (IW) mode to investigate the detailed patterns of seasonal glacier velocity change. The images used were acquired between January 2016 and December 2017, with a revisit time of 6 or 12 days due to the repeat cycle of 12 days and the 180 degree orbital phase difference between the two satellites. We used the GAMMA-SAR software (GAMMA REMOTE SENSING, 2015) to generate 96 individual ice velocity maps from different pairs of Sentinel-1a (S1a) and Sentinel-1b (S1b) SAR images.

Ice velocities were computed using a feature tracking technique applied to SAR backscatter intensity images (Strozzi et al., 2002), assuming that the ice flow occurs parallel to the surface and at a constant rate during the image acquisition period. This is a well-established technique, measuring the displacement of similar SAR image features (e.g., crevasses and speckle patterns) based on a cross correlation algorithm applied to image segments (windows) in two co-registered SAR images (Strozzi et al., 2002; Pritchard et al., 2005; Paul et al., 2015; Lemos et al., 2018). The window and step size used was based on sensitivity testing of a range of values, where a trade-off between the spatial resolution, spatial coverage and measurement accuracy of the output result were considered. For an individual pair, the end results depend on the change in snow surface properties between the processed images, the correlation of the speckle pattern, and the scale of the local features observed. For the present study, ice motion was estimated using window sizes of 350 x 75 pixels in ground range and azimuth, respectively, corresponding to dimensions of approximately 1.7 and 1.5 km. We used the Greenland Ice Mapping Project (GIMP) digital elevation model (DEM) (Howat et al., 2014) to geocode the displacements, and the final velocity measurements were posted on to a regular 100 m grid. The post-processing to remove poor quality data followed the methodology of Lemos et al. (2018). We applied a low-pass filter twice, using a kernel of 1 km by 1 km, rejecting values where the deviation between the unfiltered and filtered speed magnitude exceeded 30%. Finally, we apply a labelling algorithm based on

the image histogram, identifying regions with similar values and rejecting non-coherent velocity magnitudes and isolated measurements with an area smaller than 1/1000th of the processed image size.

Errors in ice velocity measurements derived from repeat satellite imagery can be caused by inaccurate image co-registration, mis-modelled terrain correction (Nagler et al., 2015; Hogg et al., 2017) and atmospheric interference, including changes in ionospheric properties and in tropospheric water vapour (Liao et al., 2018). To estimate velocity errors, we scale each individual velocity map by the time-averaged signal to noise ratio (SNR) of the cross-correlation function (Lemos et al., 2018). The SNR is determined as the ratio between the cross-correlation function peak (Cp) and the average correlation level (Cl) on the tracking window used to estimate the velocities (de Lange et al., 2007). Typically, the estimated velocity error is $\sim 10\%$ across the majority of the study area, rising to 20% in regions lacking stable features (Figure 4.1d–f).

4.4 Results and Discussions

First, we generated average summer and winter regional velocity maps (Figure 4.1a,b, respectively) in each calendar year using images that fell within the average periods of the start and end days of speedup in the sector (Table 4.1). The velocity coverage is better in winter than summer, especially over the slow-moving inland ice, due to the absence of melting. During winter, the scattering properties of the snowpack are relatively stable and this allows radar speckle to be tracked over the otherwise featureless terrain (Strozzi et al., 2002; Paul et al., 2015). In contrast, the retrieval of summer velocities is limited to within ~ 30 km of the ice sheet margin where there is a sufficient amount of persistent physical features to be able to track motion. Nevertheless, because of the relatively large number of individual velocity maps, we were able to resolve the seasonal pattern of speedup with unprecedented detail and show, for example, that speedup is clearly concentrated towards the centre of each glacier (Figure 4.1).

The maximum recorded winter speed ranges from 121 ± 5 m yr^{-1} at IS to 296 ± 22 m yr^{-1} at OG, and the maximum recorded summer speed ranges from 196 ± 18

Table 4.1: Seasonal velocity, speedup, speedup persistence, ice thickness and surface slope of the five glaciers averaged in two elevations bands (P1, between 650 and 750 m.a.s.l.; P2, over 820 m.a.s.l.).

Location	Summer speed ($\text{m} \text{yr}^{-1}$)	Winter speed ($\text{m} \text{yr}^{-1}$)	Speedup relative to winter (%)	Summer velocity peak ($\text{m} \text{yr}^{-1}$)	Annual mean velocity ($\text{m} \text{yr}^{-1}$)	Speedup start day	Speedup end day	Speedup Persistence (days)	Mean thickness (m)	Mean slope (%)
Glacier 1	P1 187 ± 13	125 ± 9	49%	214 ± 13	133 ± 10	136	196	60	470	2.2%
	P2 154 ± 18	109 ± 10	41%	176 ± 18	116 ± 11	153	216	63	650	2.0%
Isorlersuup	P1 220 ± 11	156 ± 8	41%	257 ± 11	166 ± 9	134	209	75	516	2.2%
	P2 148 ± 17	119 ± 10	24%	169 ± 17	124 ± 11	143	212	69	612	1.6%
Ørkendalen	P1 246 ± 16	203 ± 22	21%	259 ± 16	212 ± 22	113	198	85	390	2.8%
	P2 163 ± 17	111 ± 9	47%	205 ± 17	118 ± 11	155	212	57	623	1.5%
Russell G.	P1 121 ± 13	87 ± 5	38%	139 ± 13	93 ± 7	137	211	74	559	2.2%
	P2 156 ± 18	113 ± 10	38%	177 ± 18	118 ± 11	160	215	55	692	1.9%
Isumnguata S.	P1 103 ± 9	93 ± 6	11%	112 ± 9	95 ± 7	136	201	64	615	2.1%
	P2 121 ± 21	79 ± 5	53%	145 ± 21	87 ± 7	178	250	71	802	1.5%
Sector	P1 175 ± 28	132 ± 26	32%	196 ± 28	140 ± 28	131	203	72	510	2.3%
	P2 148 ± 41	106 ± 20	40%	174 ± 41	113 ± 23	158	221	63	676	1.7%

m yr^{-1} at RG to 359 ± 18 m yr^{-1} at ØG. In general, the degree of speedup at each glacier is quite variable, in agreement with the findings of a previous survey based on TerraSAR-X measurements acquired in 2009 and 2010 in the same region (Fitzpatrick et al., 2013). Locally, we observe numerous regions where the seasonal speedup is greater than 100 m yr^{-1} , for instance reaching 150 m yr^{-1} ($\sim 75\%$) near to the glacier fronts of IG and RG (Figure 4.1c). Our results agree well with previous studies in the same region. For example, seasonal velocity changes of 50–100% between 2004 and 2007 have been reported (Joughin et al., 2008), and (Sundal et al., 2011) reported speedup in the range of 50–125% between 1993 and 1998. Not all glaciers, however, show such a large degree of speedup. The neighbouring glacier ØG, for example, exhibits a much lower seasonal speedup of ~ 30 m yr^{-1} (21%), and maintains relatively high rates of ice flow even during winter months near the ice margin.

We examined the geometrical configurations of each glacier to investigate the possible reasons for the heterogeneous speedup (Figure 4.2) using surface and bed elevations from GIMP-DEM (Howat et al., 2014) and IceBridge BedMachine Greenland, Version 3 (Morlighem et al., 2017), respectively. Although the surface slopes of the glaciers are relatively uniform (2.8% at ØG and 2% elsewhere), their average thicknesses are considerably more variable (from 390 m at ØG to 802 m at IS). The five glaciers also present different flow regimes and, in contrast to marine-terminating glaciers (Lucchitta et al., 1995; Goldstein et al., 1993), reach their peak speeds at distances between 8 and 18 km inland. At G1, IG and ØG, this location is approximately 650 m.a.s.l. The relative speedup is non-uniform and excluding IS where the velocity profile is incomplete, ranges from 21 to 49% (Table 4.1). Despite being the fastest glacier, ØG had the lowest seasonal variation of all the studied glaciers (Table 4.1), which suggests that its flow was predominantly driven either by gravity with a low sensitivity to transient increases in basal lubrication, or it had been influenced by non-uniform basal motion due to friction at the bed-ice interface (Ryser et al., 2014; Armstrong et al., 2016).

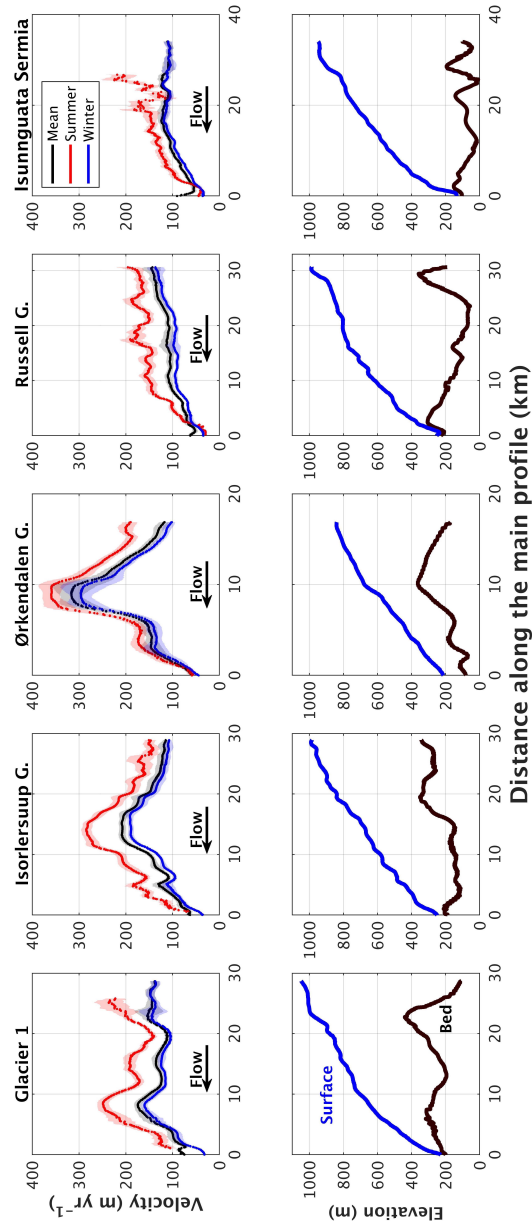


Figure 4.2: Mean summer and winter ice velocity (a–e) and geometry (f–j) along central profiles of five glaciers in west-central Greenland (see Figure 4.1 for glacier locations) in 2016 and 2017. Surface and bed elevations are from the Greenland Ice Mapping Project digital elevation model (GIMP-DEM) (Howat et al., 2014) and IceBridge BedMachine Greenland, Version 3 (Morlighem et al., 2017), respectively.

Our velocity maps have sufficient spatial coverage to provide continuous profiles of summer and winter ice speed across the central flow unit of each glacier (Figure 4.3). Speedup is primarily confined to the central, fast flowing parts of each glacier and at ~ 600 m.a.s.l., peaks in the range of 22% (\emptyset G) to 66% (RG). At this altitude all of the glaciers sit in distinct bedrock depressions where the ice is far thicker than in the slower flowing neighbouring regions. In general, speedup is largely confined to fast-flowing glaciers or their tributaries (e.g., at 25–30 km and 58–60 km along the transect). Local variations in the input and routing of surface melt water may be responsible for this heterogeneity in the degree of seasonal ice speedup. With the exception of RG, the regional glaciers do not show inter-annual variations in the degree of summer speedup. At RG, however, summer rates of ice flow were 32% faster in 2016 than in 2017. This indicates that changes in a single glacier system are not always indicative of wider patterns, highlighting the value of large-scale systematic satellite monitoring. The only other place of significant inter-annual difference in seasonal speedup is the slow flowing sector between RG and IS. Here, however, ice flowed faster in 2017 than in 2016.

A unique benefit of the S1 constellation is its systematic and high temporal sampling, which supports continuous, multi-year records of ice motion. For each of the glaciers in our study region, we explored this novel capability by charting their speed every 6 days across two full seasonal cycles (Figure 4.4). We then analysed the velocity time-series within two distinct elevation bands: 650–750 m.a.s.l. (P1) and above 820 m.a.s.l. (P2) to investigate differences in their seasonal flow at high and low altitudes (Table 4.1). There is clear heterogeneity in the seasonal flow of the five principal glaciers in this sector of the ice sheet (Figure 4.4). G1, IG and RG exhibited coherent speedup periods during summer time at both altitudes. \emptyset G showed a clear seasonal cycle at high elevations, but at lower elevations the seasonality was much less pronounced and is characterized by a longer duration speedup over the winter months, and at IS there was no apparent summer speedup at either location. However, the velocity data in these regions is generally of poorer quality than elsewhere due to the absence of clear persistent features in the SAR imagery, limiting our ability to draw firm conclusions about seasonal changes in ice flow in these glaciers. At the three glaciers where a coherent seasonal cycle is resolved, in all cases our data show that lower elevations (P1) speed up first, followed by the upper elevations (P2).

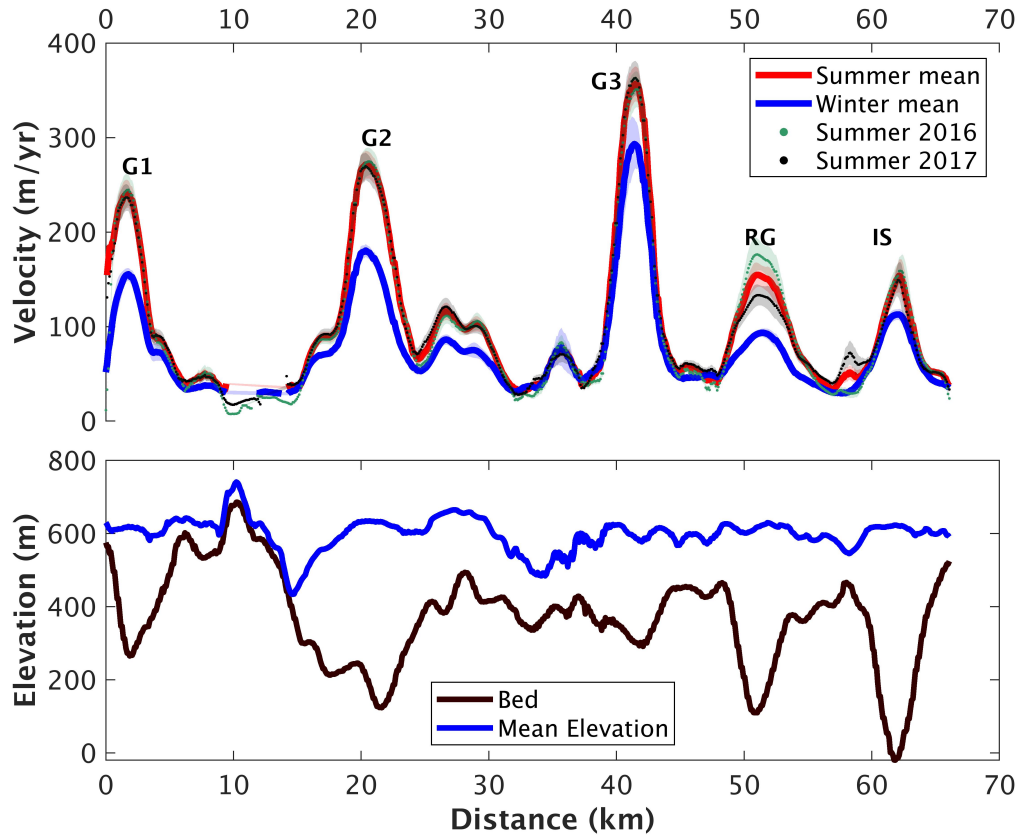


Figure 4.3: Ice velocity (Top), with uncertainty ranges represented by the light shading, and geometry (Bottom) along an across-flow profile of the study area (see Figure 4.1 for location) in 2016 to 2017.

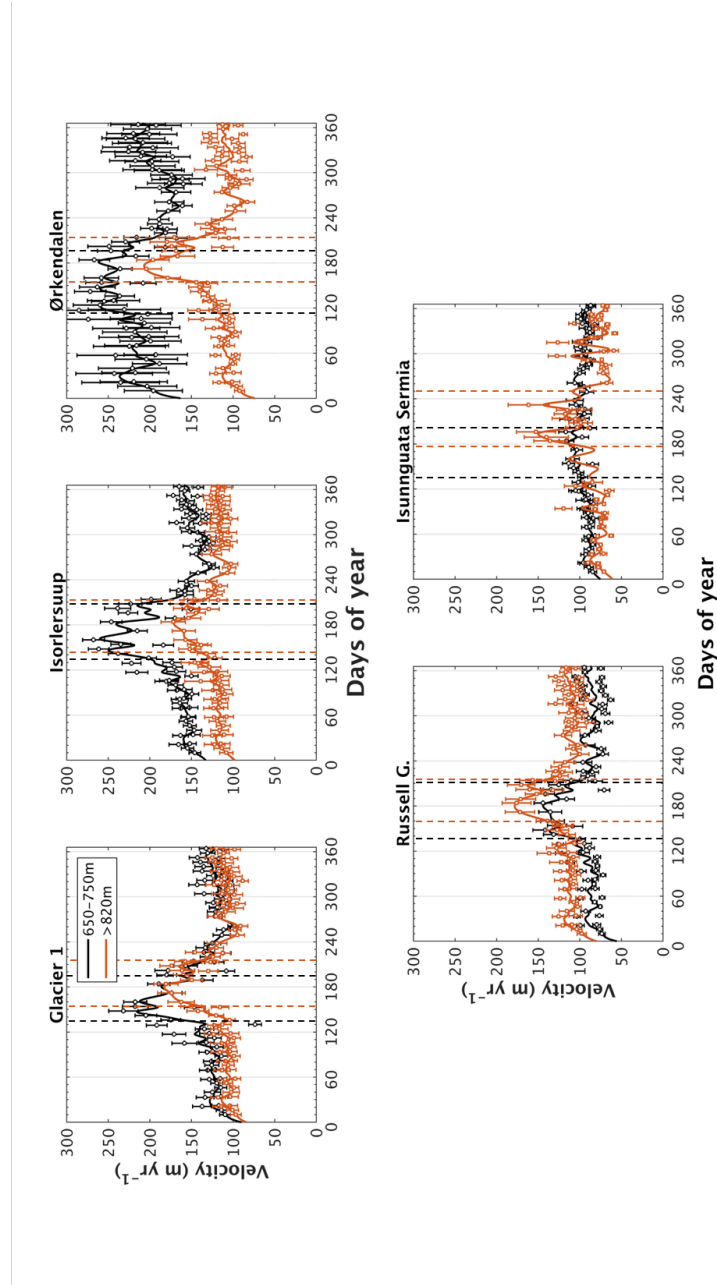


Figure 4.4: Seasonal changes in ice flow at two different elevations bands on each glacier. Actual measurements are represented by the dots, spline fits as continuous lines, and speedup periods the intervals between the consecutive coloured dotted lines.

We analysed the velocity data to determine the persistence of speedup, and the

start and end day of the summer season across the sector. To do this, we first applied a spline fit to each velocity time-series and identified local maxima using the precompiled MATLAB function ‘findpeaks’. We then identified the peak speedup, rejecting locations under a prominent peak threshold of 25 m yr^{-1} . After testing thresholds of 25, 50 and 70 m yr^{-1} we found that this threshold provided a reasonable balance between spatial coverage and consistent speedup persistence, even in slow-moving areas. We also found the number of prominent peaks per pixel which are on average between 1 and 3, as well as consistent speedup persistence results. The persistence of the summer season is defined by the duration of the width of the peak, shown as the time interval between the dotted lines in Figure 4.4. For time-series which exhibit multiple and consecutive prominent peaks, we calculate the speedup persistence as the sum of each peak width. However, when this occurs, we calculate the start and end dates of the summer season using the first and last prominent peaks, respectively (Figure 4.5b,c). We applied the method to spatially-averaged time-series within discrete elevation bands (P1 and P2, Figure 4.4) and also at individual locations to resolve the spatial pattern (Figure 4.5).

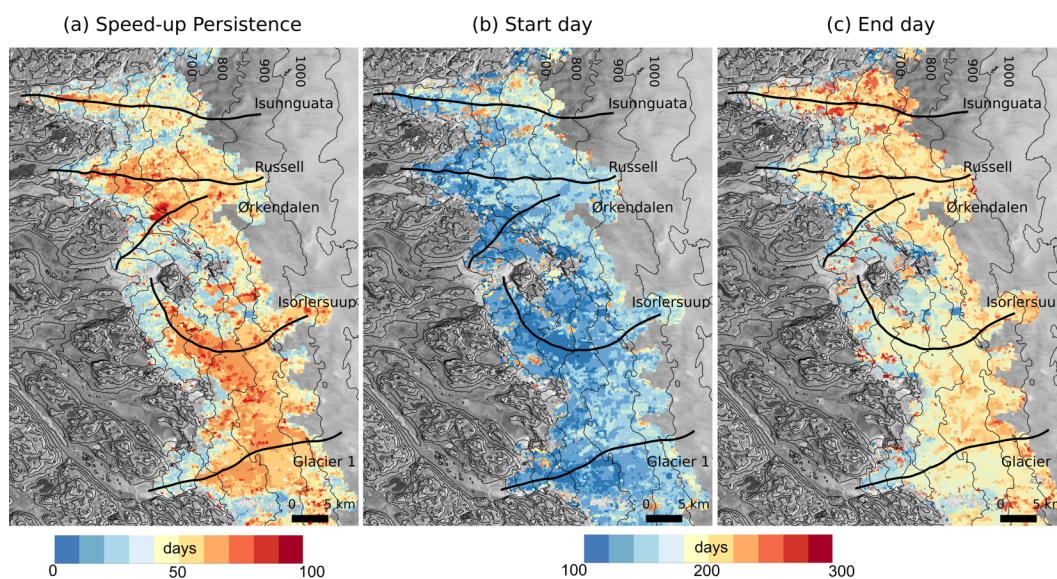


Figure 4.5: Persistence of ice speedup (a), the start (b) and end date (c) of the summer season.

Across all glaciers, the persistence of seasonal speedup ranges from 72 to 63 days

at P1 and P2, respectively (Table 4.1). The persistence of speedup is shorter at higher elevations on all glaciers except G1. At RG, our estimated persistence of 55 days at P2 is lower but similar to the 66 day estimate made by Palmer et al. (2011) for the period of 2004–2007 at the same location. For the first time we are able to map spatial variations in the pattern of summer speedup persistence (Figure 4.5). The persistence of summer speedup shows clear altitudinal variation at all glaciers, ranging from 60 to 90 days and from 50 to 70 days, respectively, at P1 and P2. At IG, speedup generally has a duration of around 75 days, but persists for 80 days at isolated locations in the fastest flowing section of the glaciers (around 700 m.a.s.l.). In general, at lower altitudes (< 500 m.a.s.l.), speedup persists for a significantly shorter period (~ 40 days). Lower regions are likely to have relatively high surface melting, potentially supplying more water to the subglacial drainage system, allowing channels to develop sooner and thereby shortening the speedup period (Schoof, 2010; Cowton et al., 2013). We estimated the start and end dates of the summer season using the date of peak speedup and the persistence, assuming the period is symmetrical. Near to the ice sheet margin (P1), summertime speedup begins around day 130 and lasts for around 90 days (Table 4.1 and Figure 4.5). The summer duration affects a wider section of the ice sheet up to 25 km inland, however the onset date is delayed by approximately 25 days on average at higher elevations (P2).

To investigate the relationship between seasonal velocity changes and environmental forcing in more detail, we compared the regional variation to a local estimate of surface melting. For this comparison, we computed the mean velocity of G1, IG and RG in 2017, when a continuous 6-day sampling was possible (Figure 4.6). OG and IS were excluded due to their unusual geometry (high slope) and relatively poor tracking coverage, respectively. We then computed positive degree days (PDDs) as a measure of the surface melting (Figure 4.6) using air temperatures recorded at the nearby KAN.L (670 m.a.s.l., Figure 4.1a) automatic weather station and distributed by the Programme for Monitoring of the Greenland Ice Sheet (PROMICE, <https://www.promice.dk/WeatherStations.html>). PDD's were integrated over six day periods to match the sampling of the satellite velocity measurements.

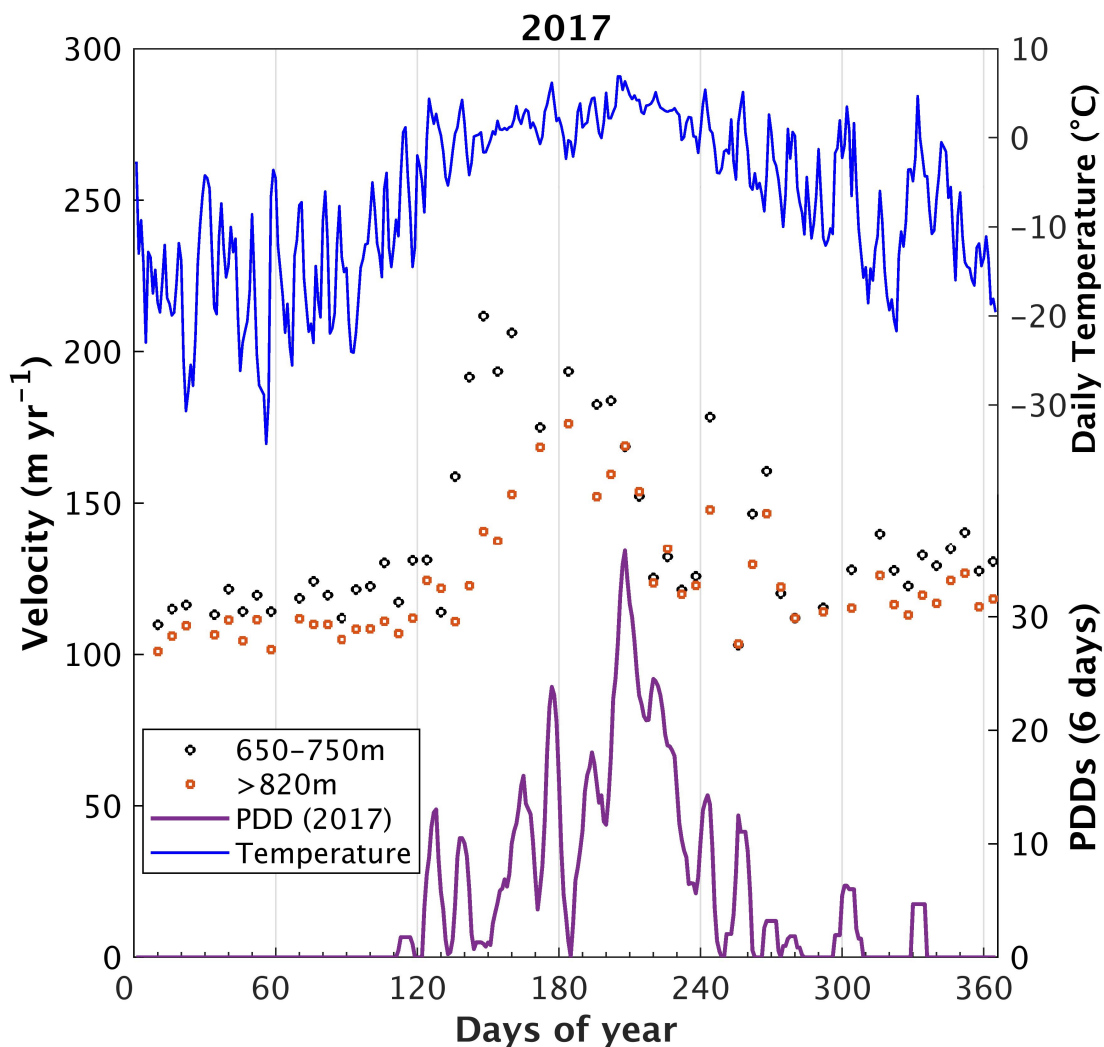


Figure 4.6: Averaged speed of three glaciers (G1, IG, and RG) with similar geometry and data sampling at two elevations bands during 2017. Also shown are daily temperature and positive degree days (PDDs) recorded at the nearby KAN.L automatic weather station (670 m.a.s.l.) and distributed by the Programme for Monitoring of the Greenland Ice Sheet.

The onset of speedup begins shortly after the first PDDs was recorded at KAN.L on day 125. Onset began on day 130 at P1 and on day 140 at P2. The high speeds were sustained for ~ 90 days at P1 and ~ 80 days at P2. The seasonal speedup, likely

caused by melt-induced acceleration (Zwally et al., 2002; Bartholomew et al., 2010; Hewitt, 2013), starts in P1 shortly after the melt onset possibly reaches the bed (e.g., through moulins or crevasses), followed by P2, located at higher elevation and then undergoing less melting (Joughin et al., 2008; Bartholomew et al., 2010; Chu, 2014; Moon et al., 2014). Future investigations using the SAR backscatter information will improve the characterization of the surface melt days. After the maximum PDDs were reached on day 207, the ice speed at P1 and P2 began to slow down rapidly at similar rates, returning to near winter levels by day 220. Two further speedup events then occur around days 244 and 268 and these coincide with isolated short-lived melt events evident within the PDD record. Later spikes in velocity, enhanced by short-term basal sliding, are likely to happen due to excess amount of water input combined with the time required for the drainage system to accommodate the extra melt-water, since the size of cavities adjusts progressively in time (Bartholomew et al., 2010; Schoof, 2010).

4.5 Conclusions

We have computed seasonal changes in the motion of five land-terminating glaciers in the central-west sector of the Greenland Ice Sheet using Sentinel-1a and-1b synthetic aperture radar imagery. The systematic acquisition schedule of Sentinel-1 provides a capacity to track ice motion with significantly greater spatial and temporal sampling than previous satellite missions. In our study, we were able to produce 96 unique ice velocity maps over a two-year period, which corresponds to approximately four times the sampling frequency of previous studies (Palmer et al., 2011; Sundal et al., 2011; Fitzpatrick et al., 2013). The high data volumes allow us to study spatial and temporal changes in ice flow across this sector of the Greenland ice sheet. Despite being located in the same sector and being exposed to similar environmental conditions, the five glaciers we have surveyed show different patterns of speedup; peak summer speedup for example ranges from 21% (Ørkendalen) to 49% (Glacier 1) relative to winter. Speedup is clearly concentrated along the central portions of each glacier, with only isolated instances elsewhere. For the first time we mapped spatial variations in the seasonal speedup persistence cycle. In this sector, the start date of the speedup period ranges from day 113 to 178, and the end date ranges from day 196 to 250, leading to a persistence

ranging from 55 to 85 days. Our study highlights the unique value of the Sentinel-1 mission for tracking short term changes in ice motion.

References

- L. C. Andrews, G. A. Catania, M. J. Hoffman, J. D. Gulley, M. P. Lüthi, C. Ryser, R. L. Hawley, and T. A. Neumann. Direct observations of evolving subglacial drainage beneath the Greenland Ice Sheet. *Nature*, 514(7520):80–83, 2015. ISSN 14764687. doi: 10.1038/nature13796. 84
- W. H. Armstrong, R. S. Anderson, J. Allen, and H. Rajaram. Modeling the WorldView-derived seasonal velocity evolution of Kennicott Glacier, Alaska. *Journal of Glaciology*, 62(234):763–777, 2016. ISSN 00221430. doi: 10.1017/jog.2016.66. 91
- W. H. Armstrong, R. S. Anderson, and M. A. Fahnestock. Spatial Patterns of Summer Speedup on South Central Alaska Glaciers. *Geophysical Research Letters*, 44(18):9379–9388, 2017. ISSN 19448007. doi: 10.1002/2017GL074370. 85
- I. D. Bartholomew, P. Nienow, D. Mair, A. Hubbard, M. a. King, and A. Sole. Seasonal evolution of subglacial drainage and acceleration in a Greenland outlet glacier. *Nature Geoscience*, 3(6):408–411, 2010. ISSN 1752-0894. doi: 10.1038/ngeo863. URL <http://www.nature.com/doi/10.1038/ngeo863>. 84, 85, 86, 99
- I. D. Bartholomew, P. Nienow, A. Sole, D. Mair, T. Cowton, M. King, and S. Palmer. Seasonal variations in Greenland Ice Sheet motion: Inland extent and behaviour at higher elevations. *Earth and Planetary Science Letters*, 307(3-4):271–278, 2011. ISSN 0012-821X. doi: 10.1016/j.epsl.2011.04.014. URL <http://www.sciencedirect.com/science/article/pii/S0012821X11002305>. 86
- I. D. Bartholomew, P. Nienow, A. Sole, D. Mair, T. Cowton, and M. a. King. Short-term variability in Greenland Ice Sheet motion forced by time-varying meltwater drainage: Implications for the relationship between subglacial drainage system behavior and ice velocity. *Journal of Geophysical Research: Earth Surface*, 117:1–17, 2012. ISSN 21699011. doi: 10.1029/2011JF002220,2012. 85, 86

- D. M. Chandler, J. L. Wadham, G. P. Lis, T. Cowton, A. Sole, I. D. Bartholomew, J. Telling, P. Nienow, E. B. Bagshaw, D. Mair, S. Vinen, and A. Hubbard. Evolution of the subglacial drainage system beneath the Greenland Ice Sheet revealed by tracers. *Nature Geoscience*, 6(3):195–198, 2013. ISSN 1752-0894. doi: 10.1038/ngeo1737. URL <http://www.nature.com/doifinder/10.1038/ngeo1737>. 86
- V. W. Chu. *Greenland ice sheet hydrology: A review*, volume 38. 2014. ISBN 0309133313507. doi: 10.1177/0309133313507075. URL <http://ppg.sagepub.com/cgi/doi/10.1177/0309133313507075>. 84, 99
- C. C. Clason, D. W. F. Mair, P. W. Nienow, I. D. Bartholomew, a. Sole, S. Palmer, and W. Schwanghart. Modelling the transfer of supraglacial meltwater to the bed of Leverett Glacier, Southwest Greenland. *The Cryosphere*, 9(1):123–138, 2015. ISSN 1994-0424. doi: 10.5194/tc-9-123-2015. URL <http://www.the-cryosphere.net/9/123/2015/>. 86
- T. Cowton, P. Nienow, A. Sole, J. Wadham, G. Lis, I. D. Bartholomew, D. Mair, and D. Chandler. Evolution of drainage system morphology at a land-terminating Greenlandic outlet glacier. *Journal of Geophysical Research: Earth Surface*, 118(1):29–41, 2013. ISSN 21699011. doi: 10.1029/2012JF002540. 84, 97
- J. Crozier, L. Karlstrom, and K. Yang. Basal control of supraglacial meltwater catchments on the Greenland Ice Sheet. *The Cryosphere*, 12:3383–3407, 2018. ISSN 1994-0440. doi: doi.org/10.5194/tc-12-3383-2018. 84, 85
- R. de Lange, A. Luckman, and T. Murray. Improvement of satellite radar feature tracking for ice velocity derivation by spatial frequency filtering. *IEEE Transactions on Geoscience and Remote Sensing*, 45(7):2309–2318, 2007. ISSN 01962892. doi: 10.1109/TGRS.2007.896615. 89
- A. Dehecq, N. Gourmelen, and E. Trouve. Deriving large-scale glacier velocities from a complete satellite archive: Application to the Pamir-Karakoram-Himalaya. *Remote Sensing of Environment*, 162:55–66, 2015. ISSN 00344257. doi: 10.1016/j.rse.2015.01.031. URL <http://dx.doi.org/10.1016/j.rse.2015.01.031>. 85

REFERENCES

- E. M. Enderlin, I. M. Howat, S. Jeong, M.-J. Noh, J. H. van Angelen, and M. R. van den Broeke. An improved mass budget for the Greenland ice sheet. *Geophys. Res. Lett.*, 41:1–7, 2014. doi: 10.1002/2013GL059010. Received. 84
- M. Fahnestock, T. Scambos, T. Moon, A. Gardner, T. Haran, and M. Klinger. Rapid large-area mapping of ice flow using Landsat 8. *Remote Sensing of Environment*, 185:84–94, 2016. ISSN 00344257. doi: 10.1016/j.rse.2015.11.023. URL <http://dx.doi.org/10.1016/j.rse.2015.11.023>. 85
- A. A. Fitzpatrick, A. Hubbard, I. Joughin, D. J. Quincey, D. Van As, A. P. Mikkelsen, S. H. Doyle, B. Hasholt, and G. A. Jones. Ice flow dynamics and surface meltwater flux at a land-terminating sector of the Greenland ice sheet. *Journal of Glaciology*, 59(216):687–696, 2013. ISSN 00221430. doi: 10.3189/2013JoG12J143. 85, 86, 91, 99
- GAMMA REMOTE SENSING. Interferometric SAR Processor - ISP. Volume 1.9. Technical Report December, 2015. 88
- A. S. Gardner, G. Moholdt, T. Scambos, M. Fahnestock, S. Ligtenberg, and M. V. D. Broeke. Increased West Antarctic ice discharge and East Antarctic stability over the last seven years. *The Cryosphere*, 12:521–547, 2018. doi: <https://doi.org/10.5194/tc-12-521-2018>. 85
- R. M. Goldstein, H. Engelhardt, B. Kamb, and R. M. Frolich. Satellite Radar Interferometry for Monitoring Ice Sheet Motion: Application to an Antarctic Ice Stream. *Science*, 262(3 December):1525–1530, 1993. 85, 91
- E. Hanna, S. H. Mernild, J. Cappelen, and K. Steffen. Recent warming in Greenland in a long-term instrumental (1881-2012) climatic context: I. Evaluation of surface air temperature records. *Environmental Research Letters*, 7(4), 2012. ISSN 17489326. doi: 10.1088/1748-9326/7/4/045404. 84
- E. Hanna, X. Fettweis, S. H. Mernild, J. Cappelen, M. H. Ribergaard, C. a. Shuman, K. Steffen, L. Wood, and T. L. Mote. Atmospheric and oceanic climate forcing of the exceptional Greenland ice sheet surface melt in summer 2012. *International Journal of Climatology*, 34(4):1022–1037, 2014. ISSN 08998418. doi: 10.1002/joc.3743. 84

REFERENCES

- J. T. Harper, N. F. Humphrey, W. T. Pfeffer, T. Fudge, and S. O'Neel. Evolution of subglacial water pressure along a glacier's length. *Annals of Glaciology*, 40(1981): 31–36, 2005. ISSN 02603055. doi: 10.3189/172756405781813573. 84, 85
- I. J. Hewitt. Seasonal changes in ice sheet motion due to melt water lubrication. *Earth and Planetary Science Letters*, 371-372:16–25, 2013. ISSN 0012821X. doi: 10.1016/j.epsl.2013.04.022. 99
- M. J. Hoffman, G. A. Catania, T. A. Neumann, L. C. Andrews, and J. A. Rumrill. Links between acceleration, melting, and supraglacial lake drainage of the western Greenland Ice Sheet. *Journal of Geophysical Research: Earth Surface*, 116(4):1–16, 2011. ISSN 21699011. doi: 10.1029/2010JF001934. 84
- A. E. Hogg, A. Shepherd, S. L. Cornford, K. Briggs, N. Gourmelen, J. Graham, I. Joughin, J. Mouginot, T. Nagler, A. J. Payne, E. Rignot, and J. Wuite. Increased ice flow in Western Palmer Land linked to ocean melting. *Geophys. Res. Lett.*, 44: 1–9, 2017. doi: 10.1002/2016GL072110. 89
- I. M. Howat, S. de la Peña, J. H. van Angelen, J. T. M. Lenaerts, and M. R. van den Broeke. Brief Communication: "Expansion of meltwater lakes on the Greenland Ice Sheet". *The Cryosphere*, 7(1):201–204, 2013. ISSN 1994-0424. doi: 10.5194/tc-7-201-2013. URL <http://www.the-cryosphere.net/7/201/2013/>. 86
- I. M. Howat, a. Negrete, and B. E. Smith. The Greenland Ice Mapping Project (GIMP) land classification and surface elevation data sets. *The Cryosphere*, 8(4):1509–1518, 2014. ISSN 1994-0424. doi: 10.5194/tc-8-1509-2014. URL <http://www.the-cryosphere.net/8/1509/2014/tc-8-1509-2014.html>. xiii, 88, 91, 92
- I. Joughin, D. P. Winebrenner, and M. A. Fahnestock. Observations of ice-sheet motion in Greenland using satellite radar interferometry. *Geophysical Research Letters*, 22(5):571–574, 1995. ISSN 0094-8276. doi: 10.1029/95GL00264. 85
- I. Joughin, S. B. Das, M. a. King, B. E. Smith, I. M. Howat, and T. Moon. Seasonal Speedup Along the Western Flank of the Greenland Ice Sheet - Supplementary. *Science*, 320(April), 2008. ISSN 1095-9203. doi: 10.1126/science.1153288. URL <http://www.ncbi.nlm.nih.gov/pubmed/18420901>. 85, 86, 91, 99

- I. Joughin, B. E. Smith, I. M. Howat, T. Scambos, and T. Moon. Greenland flow variability from ice-sheet-wide velocity mapping. *Journal of Glaciology*, 56(197):415–430, aug 2010. ISSN 00221430. doi: 10.3189/002214310792447734. URL <http://openurl.ingenta.com/content/xref?genre=article&issn=0022-1430&volume=56&issue=197&spage=415>. 85
- I. Joughin, S. B. Das, G. E. Flowers, M. D. Behn, R. B. Alley, M. A. King, B. E. Smith, J. L. Bamber, M. R. Van Den Broeke, and J. H. Van Angelen. Influence of ice-sheet geometry and supraglacial lakes on seasonal ice-flow variability. *Cryosphere*, 7(4):1185–1192, 2013. ISSN 19940416. doi: 10.5194/tc-7-1185-2013. 85
- I. Joughin, B. E. Smith, and I. Howat. Greenland Ice Mapping Project: Ice Flow Velocity Variation at sub-monthly to decadal time scales. *The Cryosphere*, 12:2211–2227, 2018. doi: <https://doi.org/10.5194/tc-12-2211-2018>. 85, 88
- C. P. Koziol and N. Arnold. Modelling seasonal meltwater forcing of the velocity of land-terminating margins of the Greenland Ice Sheet. *The Cryosphere*, 12(3):971–991, 2018. ISSN 19940424. doi: 10.5194/tc-12-971-2018. 86
- A. Leeson, A. Shepherd, S. Palmer, A. Sundal, and X. Fettweis. Simulating the growth of supraglacial lakes at the western margin of the Greenland ice sheet. *Cryosphere*, 6(5):1077–1086, 2012. ISSN 19940416. doi: 10.5194/tc-6-1077-2012. 86
- A. Leeson, A. Shepherd, K. Briggs, and X. Fettweis. Supraglacial lakes on Greenland migrate inland under warming climate. *Nature Climate Change*, 16(January):51–55, 2015. ISSN 1758-678X. doi: 10.1038/NCLIMATE2463. 86
- A. A. Leeson, A. Shepherd, A. V. Sundal, A. M. Johansson, N. Selmes, K. Briggs, A. E. Hogg, and X. Fettweis. A comparison of supraglacial lake observations derived from MODIS imagery at the western margin of the Greenland ice sheet. *Journal of Glaciology*, 59(218):1179–1188, 2013. ISSN 00221430. doi: 10.3189/2013JoG13J064. 86
- A. Lemos, A. Shepherd, M. Mcmillan, A. E. Hogg, E. Hatton, and I. Joughin. Ice velocity of Jakobshavn Isbræ, Petermann Glacier, Nioghalvfjordsfjorden and Zachariæ Isstrøm, 2015-2017, from Sentinel 1-a/b SAR imagery. *The Cryosphere*, 12(June):2087–2097, 2018. doi: <https://doi.org/10.5194/tc-2017-251>. 85, 88, 89

- H. Liao, F. J. Meyer, B. Scheuchl, J. Mouginot, I. Joughin, and E. Rignot. Ionospheric correction of InSAR data for accurate ice velocity measurement at polar regions. *Remote Sensing of Environment*, 209(January):166–180, 2018. ISSN 00344257. doi: 10.1016/j.rse.2018.02.048. URL <https://doi.org/10.1016/j.rse.2018.02.048>. 89
- B. K. Lucchitta and H. M. Ferguson. Antarctica: measuring glacier velocity from satellite images. *Science (New York, N.Y.)*, 234(4780):1105–1108, 1986. ISSN 0036-8075. doi: 10.1126/science.234.4780.1105. 85
- B. K. Lucchitta, C. E. Rosanova, and K. F. Mullins. Velocities of Pine Island Glacier, West Antarctica, from ERS-1 SAR images. *Annals of Glaciology*, 21:277–283, 1995. ISSN 02603055. doi: 10.1017/S0260305500015949. 85, 91
- M. McMillan, A. Leeson, A. Shepherd, K. Briggs, T. W. K. Armitage, A. Hogg, P. K. Munneke, M. van den Broeke, B. Noël, W. J. van de Berg, S. Ligtenberg, M. Horwath, A. Groh, A. Muir, and L. Gilbert. A high resolution record of Greenland mass balance. *Geophysical Research Letters*, 43:1–9, 2016. doi: 10.1002/GRL.54619. 84
- T. Moon, I. Joughin, B. Smith, M. R. Broeke, W. J. Berg, B. Noël, and M. Usher. Distinct patterns of seasonal Greenland glacier velocity. *Geophysical Research Letters*, 41:7209–7216, 2014. doi: 10.1002/2014GL061836. 85, 99
- M. Morlighem, C. N. Williams, E. Rignot, L. An, J. E. Arndt, J. L. Bamber, G. Catania, N. Chauché, J. A. Dowdeswell, B. Dorschel, I. Fenty, K. Hogan, I. Howat, A. Hubbard, M. Jakobsson, T. M. Jordan, K. K. Kjeldsen, R. Millan, L. Mayer, J. Mouginot, B. P. Noël, C. O’Cofaigh, S. Palmer, S. Rysgaard, H. Seroussi, M. J. Siegert, P. Slabon, F. Straneo, M. R. van den Broeke, W. Weinrebe, M. Wood, and K. B. Zinglensen. BedMachine v3: Complete Bed Topography and Ocean Bathymetry Mapping of Greenland From Multibeam Echo Sounding Combined With Mass Conservation. *Geophysical Research Letters*, 44(21):11,051–11,061, 2017. ISSN 19448007. doi: 10.1002/2017GL074954. xiii, 91, 92
- T. Nagler, H. Rott, M. Hetzenecker, J. Wuite, and P. Potin. The Sentinel-1 Mission: New Opportunities for Ice Sheet Observations. *Remote Sensing*, 7(7):9371–9389,

REFERENCES

2015. ISSN 2072-4292. doi: 10.3390/rs70709371. URL <http://www.mdpi.com/2072-4292/7/7/9371/>. 85, 88, 89
- P. W. Nienow, A. L. Hubbard, B. P. Hubbard, D. M. Chandler, D. W. F. Mair, M. J. Sharp, and I. C. Willis. Hydrological controls on diurnal ice flow variability in valley glaciers. *Journal of Geophysical Research: Earth Surface*, 110(4):1–11, 2005. ISSN 21699011. doi: 10.1029/2003JF000112. 84, 85
- S. Palmer, A. Shepherd, P. Nienow, and I. Joughin. Seasonal speedup of the Greenland Ice Sheet linked to routing of surface water. *Earth and Planetary Science Letters*, 302(3-4):423–428, 2011. ISSN 0012821X. doi: 10.1016/j.epsl.2010.12.037. URL <http://dx.doi.org/10.1016/j.epsl.2010.12.037>. 85, 86, 97, 99
- F. Paul, T. Bolch, A. Kääb, T. Nagler, C. Nuth, K. Scharrer, A. Shepherd, T. Strozzi, F. Ticconi, R. Bhambri, E. Berthier, S. Bevan, N. Gourmelen, T. Heid, S. Jeong, M. Kunz, T. R. Lauknes, A. Luckman, J. Merryman, G. Moholdt, A. Muir, J. Neelmeijer, M. Rankl, J. VanLooy, and T. Van Niel. The glaciers climate change initiative: Methods for creating glacier area, elevation change and velocity products. *Remote Sensing of Environment*, 162:408–426, 2015. ISSN 00344257. doi: 10.1016/j.rse.2013.07.043. URL <http://dx.doi.org/10.1016/j.rse.2013.07.043>. 88, 89
- H. Pritchard, T. Murray, A. Luckman, T. Strozzi, and S. Barr. Glacier surge dynamics of Sortebrae, east Greenland, from synthetic aperture radar feature tracking. *Journal of Geophysical Research*, 110(F03005):1–13, 2005. ISSN 0148-0227. doi: 10.1029/2004JF000233. URL <http://doi.wiley.com/10.1029/2004JF000233>. 88
- E. Rignot and P. Kanagaratnam. Changes in the Velocity Structure of the Greenland Ice Sheet. *Science*, 311(February):986–990, 2006. doi: 10.1126/science.1121381. 85
- E. Rignot, I. Velicogna, M. R. Van Den Broeke, A. Monaghan, and J. T. M. Lenaerts. Acceleration of the contribution of the Greenland and Antarctic ice sheets to sea level rise. *Geophysical Research Letters*, 38(5):1–5, 2011. ISSN 00948276. doi: 10.1029/2011GL046583. 85
- C. Ryser, M. P. Lüthi, L. C. Andrews, M. J. Hoffman, G. A. Catania, R. L. Hawley, T. A. Neumann, and S. S. Kristensen. Sustained high basal motion of the Greenland

- ice sheet revealed by borehole deformation. *Journal of Glaciology*, 60(222):647–660, 2014. ISSN 00221430. doi: 10.3189/2014JoG13J196. 91
- C. Schoof. Ice-sheet acceleration driven by melt supply variability. *Nature*, 468(7325): 803–806, 2010. ISSN 0028-0836. doi: 10.1038/nature09618. URL <http://dx.doi.org/10.1038/nature09618>. 84, 97, 99
- A. Shepherd, A. Hubbard, P. Nienow, M. King, M. McMillan, and I. Joughin. Greenland ice sheet motion coupled with daily melting in late summer. *Geophysical Research Letters*, 36(L01501):1–4, 2009. ISSN 0094-8276. doi: 10.1029/2008GL035758. URL <http://doi.wiley.com/10.1029/2008GL035758>. 85, 86
- A. Shepherd, E. R. Ivins, G. A., V. R. Barletta, M. J. Bentley, S. Bettadpur, K. H. Briggs, D. H. Bromwich, R. Forsberg, N. Galin, M. Horwath, S. Jacobs, I. Joughin, M. A. King, J. T. M. Lenaerts, J. Li, S. R. M. Ligtenberg, A. Luckman, S. B. Luthcke, M. McMillan, R. Meister, G. Milne, J. Mouginot, A. Muir, J. P. Nicolas, J. Paden, A. J. Payne, H. Pritchard, E. Rignot, H. Rott, L. S. Sørensen, T. A. Scambos, B. Scheuchl, E. J. O. Schrama, B. Smith, A. V. Sundal, J. H. van Angelen, W. J. van de Berg, M. R. van den Broeke, D. G. Vaughan, I. Velicogna, J. Wahr, P. L. Whitehouse, D. J. Wingham, D. Yi, D. Young, and H. J. Zwally. A Reconciled Estimate of Ice-Sheet Mass Balance. *Science*, 338(November):1183–1189, 2012. doi: 10.1126/science.1228102. 84
- A. Sole, P. W. Nienow, I. D. Bartholomew, D. W. F. Mair, T. R. Cowton, A. J. Tedstone, and M. a. King. Winter motion mediates dynamic response of the Greenland Ice Sheet to warmer summers. *Geophysical Research Letters*, 40(15):3940–3944, 2013. ISSN 00948276. doi: 10.1002/grl.50764. 86
- A. J. Sole, D. W. F. Mair, P. W. Nienow, I. D. Bartholomew, M. A. King, M. J. Burke, and I. Joughin. Seasonal speedup of a Greenland marine-terminating outlet glacier forced by surface melt-induced changes in subglacial hydrology. *Journal of Geophysical Research: Earth Surface*, 116(3):1–11, 2011. ISSN 21699011. doi: 10.1029/2010JF001948. 85

- T. Strozzi, A. Luckman, T. Murray, U. Wegmuller, and C. L. Werner. Glacier motion estimation using SAR offset-tracking procedures. *IEEE Transactions on Geoscience and Remote Sensing*, 40(11):2384–2391, nov 2002. ISSN 0196-2892. doi: 10.1109/TGRS.2002.805079. URL <http://ieeexplore.ieee.org/lpdocs/epic03/wrapper.htm?arnumber=1166597>. 88, 89
- A. V. Sundal, A. Shepherd, P. Nienow, E. Hanna, S. Palmer, and P. Huybrechts. Melt-induced speed-up of Greenland ice sheet offset by efficient subglacial drainage. *Nature*, 469(7331):521–4, jan 2011. ISSN 1476-4687. doi: 10.1038/nature09740. URL <http://www.ncbi.nlm.nih.gov/pubmed/21270891>. 85, 86, 91, 99
- R. S. van de Wal, C. J. Smeets, W. Boot, M. Stoffelen, R. Van Kampen, S. H. Doyle, F. Wilhelms, M. R. Van Den Broeke, C. H. Reijmer, J. Oerlemans, and A. Hubbard. Self-regulation of ice flow varies across the ablation area in south-west Greenland. *The Cryosphere*, 9:603–611, 2015. ISSN 19940424. doi: 10.5194/tc-9-603-2015. 85, 86
- M. van den Broeke, E. Enderlin, I. Howat, P. Kuipers Munneke, B. Noël, W. J. van de Berg, E. van Meijgaard, and B. Wouters. On the recent contribution of the Greenland ice sheet to sea level change. *The Cryosphere*, 10:1933–1946, 2016. ISSN 1994-0440. doi: 10.5194/tc-2016-123. URL <http://www.the-cryosphere-discuss.net/tc-2016-123/>. 84
- H. J. Zwally, W. Abdalati, T. Herring, K. Larson, J. Saba, and K. Steffen. Surface Melt – Induced Acceleration of Greenland Ice-Sheet Flow. *Science*, 297(July):218–223, 2002. doi: 10.1126/science.1072708. 84, 85, 99

Chapter 5

The combined use of Sentinel-2 and Sentinel-1 imagery to track features in the Central-west sector of Greenland

Authors: **Adriano Lemos, Andrew Shepherd, Malcolm McMillan, Anna E. Hogg, Heather Selley**

Abstract

Increased discharge of ice from marine-terminating glaciers is responsible for approximately one half of the current mass loss from the Greenland ice sheet. Recently, the availability of systematic, short-repeat satellite acquisitions has improved the understanding of the timescales and mechanisms that control high frequency fluctuations in these glaciers' flow. However, the orbital configuration of single-sensor satellites – such as the Sentinel-1A/B constellation – limits acquisitions to, at best, weekly repeats, and under sub-optimal conditions the sampling frequency can be further degraded. Increasing the monitoring frequency beyond this limit is, however, theoretically possible, through the combination of data from different sensors, operating across different parts

of the electromagnetic spectrum. In this study, we investigate the glaciological application of near-coincident data acquired at optical (Sentinel-2) and microwave (Sentinel-1) frequencies, to assess the complementarity and consistency of these different satellite platforms. Specifically, we use co-located, contemporaneous Sentinel-1 and Sentinel-2 imagery of Jakobshavn Isbræ in west-central Greenland to monitor iceberg drift, the evolution of supraglacial lakes, marine glacier calving, ice front position and ice sheet motion. The fine spatial and temporal sampling of the data allowed us to track, during a 14 day interval, icebergs drifting at 250 m day^{-1} and glacier calving rates of 15 m day^{-1} . The sharpness of the Sentinel-2 images allowed us to estimate subtle changes in the area of two supraglacial lakes of 23 % and 24 % during the same period. The combined use of the two missions to track ice velocity allowed us to achieve unparalleled year-round spatial coverage ($> 97 \%$) and summertime temporal sampling (2-3 days), which, until now has been impossible from a single sensor alone. These results demonstrate that by combining results from multiple operational satellite sensors, unprecedented sampling of the polar regions can now be achieved.

5.1 Introduction

Rates of ice loss from Greenland have been higher in recent decades than at any time in the past 350 years (Trusel et al., 2018), due to increased surface melting and ice discharge (Shepherd et al., 2012; McMillan et al., 2016). At the western coast of Greenland, the speedup of marine-terminating glaciers has been triggered by ice front retreat and surface melting (Joughin et al., 2014; Moon et al., 2014, 2015), which are in turn associated with rises in the regional air and ocean temperatures (Holland et al., 2008; Hanna et al., 2012). Meltwater that forms at the ice surface can either accumulate in topographic depressions, forming supraglacial lakes (Leeson et al., 2013) that often drain (McMillan et al., 2007), or it can flow directly into the ice sheet through moulins or crevasses (Chu, 2014). Once it has entered the ice sheet, meltwater can feed the englacial drainage system and, after reaching the interface ice-bedrock, can enhance ice flow via basal lubrication (Hoffman et al., 2011; Chu, 2014). Marine-terminating glacier flow is also highly-influenced by seasonal changes in the position of their calving front, which periodically alters lateral and basal resistive stresses at the terminus (Joughin et al., 2014; Moon et al., 2014, 2015; Lemos et al., 2018b). Calving front

retreat can also occur over longer timescales through episodic creation of ice-bergs, and their melting contributes to up 50 % of the total fresh-water mass loss in Greenland (Enderlin et al., 2014). Our understanding of the timescales and mechanisms underpinning these and other processes that control fluctuations in the Greenland ice sheet flow has been dramatically improved by the availability of continuous and systematic satellite observations (Joughin et al., 2014, 2018; Hill et al., 2018; Lemos et al., 2018b).

Images from spaceborne sensors have been widely used to identify and monitor glaciological features. Optical imagery has been used to observe the Earth’s surface since the launch of the Landsat constellation in 1972 (Wulder et al., 2012). Thanks to optical missions and glacier inventories (Rastner et al., 2012; Pfeffer et al., 2014), velocity changes have been systematically monitored (Joughin et al., 2010; Rignot et al., 2011; Nagler et al., 2015; Rosenau et al., 2015; Fahnestock et al., 2016). These records are now important indicators of how the cryosphere has been affected by climate change. Glacier velocities, in particular, have been routinely tracked in repeat optical (Rosenau et al., 2015; Fahnestock et al., 2016; Gardner et al., 2018) and synthetic aperture radar (SAR) imagery (Goldstein et al., 1993; Lucchitta et al., 1995; Joughin et al., 2010; Rignot et al., 2011; Nagler et al., 2015). Although both techniques can yield high-quality measurements of ice sheet flow, they are also affected by changing environmental conditions. In the case of optical imagery, clouds frequently interfere, and in the case of SAR imagery, surface melting can be especially problematic. A combination of the two methods is therefore likely the best approach for continuous and consistent monitoring. Here, we present an assessment and inter-comparison of ice sheet motion at Jakobshavn Isbræ (JI) in west-central Greenland tracked in optical and SAR imagery. To do this, we use near-coincident optical and SAR imagery acquired by the Sentinel-2 and Sentinel-1 constellations to monitor changes in the movement of ice-bergs, supraglacial lakes, the glacier calving ice front position and the wider pattern of ice sheet flow.

5.2 Study Area

Jakobshavn Isbræ is a marine terminating glacier located in the west-central sector of the Greenland Ice Sheet. Western Greenland is regarded as the major source of recent mass losses from the ice sheet, and was responsible, between 2011–2014, for 41 % of the total mass imbalance (McMillan et al., 2016). JI drains ~ 6.5 % of the ice sheet and

terminates in the Ilulissat Icefjord (Joughin et al., 2004). Since the 1990s it has been experiencing successive retreat (Joughin et al., 2008b), and observations show that, in response, the glacier has been thinning continuously since the early 2000's (McMillan et al., 2016; Sørensen et al., 2018). Although in the recent past JI maintained a floating ice tongue, this broke up in 2003, and as a result JI is now a tidewater that calves directly into the ocean (Joughin et al., 2004, 2014; Enderlin et al., 2014). In terms of the forcing mechanisms that have driven JI acceleration, enhanced basal-sliding triggered by surface meltwater has a small contribution to JI speedup in comparison to calving events (Joughin et al., 2008a). Although supraglacial lakes are observed to form seasonally within the JI catchment, their draining is more widely linked to transient increases in the velocity of land-terminating sectors (Joughin et al., 2008a). Nonetheless, the influence of lake drainage on freshwater discharge, upwelling and enhanced ocean melting at the calving front, is a process that is relatively poorly understood, and its influence on ice dynamics remains uncertain (Nick et al., 2013). Historically, JI has had a dynamic ice front that advances and retreats by ~ 3 km during each winter and summer, respectively, significantly contributing to the glaciers iceberg discharge (Joughin et al., 2004, 2012, 2014). In addition to these seasonal changes, there has also been several retreat events of the calving front since the 1950s before the complete disintegration in 2003 (Joughin et al., 2008b). Fluctuations in the calving front position have been identified as the main trigger for seasonal and inter-annual changes in JI's speed, as it leads to reduced basal and lateral resistive stresses (Joughin et al., 2012, 2014, 2018; Lemos et al., 2018b). Since 2012, however, JI has started to slow down (Lemos et al., 2018b), and systematic monitoring of the glaciers speed and geometry should help to identify the underlying cause.

5.3 Data and Methods

Sentinel-2 is the optical imaging component of the European Commission's (EC) Copernicus Earth Observation satellite program, built and launched in partnership with the European Space Agency (ESA). The first of the satellites, Sentinel-2a, was launched in June 2015, followed by Sentinel-2b, which was launched in March 2017. The main sensor on each Sentinel-2 satellite is the Multi-Spectral Instrument (MSI), which acquires images within 13 different spectral bands and with a spatial resolution that varies from

10 to 30 m. Sentinel-2 Level-1C (L1C) images are recorded as top-of-atmosphere reflectance, with ground footprints of 109 by 109 km. The L1C images are orthorectified using the PlanetDEM digital elevation model (DEM), posted in a 90 x 90 m grid. Although each satellite has a 10 day orbital repeat period, when combined they provide repeat sampling every 5 days because their orbits are offset. The actual frequency of repeat acquisitions however depends on the capacity of the entire system, which is defined in an image acquisition plan. At higher latitudes where the imaging swaths from neighbouring orbits overlap, the revisit time offered by the constellation is even shorter than 5 days (Kääb et al., 2016). Here we use six Sentinel-2 images to track the movement of Jakobshavn Isbræ using an automated software (GAMMA REMOTE SENSING, 2015), and we contrast the motion to estimates determined from Sentinel-1 SAR imagery (Lemos et al., 2018b).

Table 5.1: List of Sentinel-2 and Sentinel-1 used in this study

Satellite Platform Tracking	Product type	Time (UTC)	Velocity
Sentinel-2	Multi-Spectral L1C	12-09-2016 15:28:22	Autumn
		26-09-2016 15:09:52	
		04-05-2017 15:09:11	Spring
		27-05-2017 15:19:11	
		13-07-2017 15:09:11	Summer
		23-07-2017 15:11:15	
Sentinel-1	Single Look Complex	30-09-2016 20:46:48	Autumn
		06-10-2016 20:46:34	
		22-01-2017 20:46:31	Winter
		28-01-2017 20:47:13	
		04-05-2017 20:47:12	Spring
		04-05-2017 20:46:48	
		10-05-2017 20:46:33	
		15-07-2017 20:47:18	Summer
		27-07-2017 20:47:19	
		02-08-2017 20:46:37	

When applied to glacier surfaces, optical image feature tracking relies on the detection of coherent visible features such as crevasses, calving fronts and supraglacial lakes in consecutively acquired images to determine ice motion (Lucchitta and Ferguson, 1986; Scambos et al., 1992). Initially, this was done by visual comparison using individual pixels, and this limited the scope and precision of the resulting estimates of ice motion (Bindschadler and Scambos, 1991; Scambos et al., 1992). Nowadays, the feature-tracking technique commonly applies the cross-correlation method to automatically detect the motion of small areas (chips), and requires good visual contrast between the images used (Rosenau et al., 2015; Fahnestock et al., 2016). The major limitation when tracking ice motion using optical images is the availability of sunlight, which restricts their use during night or in winter. Furthermore, glaciers are usually located in relatively steep regions, and the presence of clouds and shadows created by the terrain topography are also a limit on the performance of optical feature tracking (Kääb et al., 2016; Paul et al., 2016, 2017). In this study, we estimate ice motion using a cross-correlation feature tracking algorithm (GAMMA REMOTE SENSING, 2015) applied to Sentinel-2 L1C Band 8 images (10 m resolution). First, the images are co-registered using a cross-correlation algorithm applied after masking out areas of known fast ice flow (Lemos et al., 2018b). The co-registration of two images from a repeat orbit reduces the final offset field containing geo-location noise and biases due to shifts and jitter Kääb et al. (2016). We track movement in patches of 75 x 75 pixels, corresponding to areas of 750 m by 750 m, and from these data we estimate ice velocity by assuming the ice flows parallel to the surface slope and at a constant pace between the image acquisition dates. Finally, we apply a median filter using a kernel of 100 m by 100 m to remove outliers. The major error source in ice velocity estimation using optical Landsat, and then Sentinel-2 images, is the inexact co-registration linked to the digital elevation model used to orthorectify the images (Jeong and Howat, 2015). In order to minimize mismatches due to orthorectification, we use pairs of Sentinel-2 images acquired from the same path (Kääb et al., 2016). We estimate individual velocity error maps based on the signal to noise ratio (SNR) of the cross-correlation algorithm (Lemos et al., 2018b,a). Here, SNR is the ratio of the cross-correlation function peak (C_p) and the average correlation level (C_l) within the used patch (de Lange et al., 2007).

5.4 Results

Optical images have two main limitations over the polar regions; the absence of light during winter at the time of the satellite overpass, and the presence of clouds (Kääb et al., 2016; Paul et al., 2016). A comparison of Sentinel-2 optical and Sentinel-1 SAR imagery acquired on the same day, separated by about five hours, illustrates the impact of clouds (Figure 5.1). In this example, a true-colour composite is generated by merging bands 2, 3 and 4 recorded by Sentinel-2 to provide sharper discrimination (Figure 5.1a), and the merger of Sentinel-1 SAR images acquired in neighbouring tracks and cropped to provide similar spatial coverage (Figure 5.1b). Clouds, and their shadows, obscure the northernmost portion of the Sentinel-2 scene. For simplicity, we classify the clouds in two main categories, dense and opaque Cumulus and thin and translucent Cirrus. Neither are easy to detect in optical imagery over JI as the scene contrast is relatively low, but on close inspection the Cumulus are most easily identified because they are highly reflective and because they obscure glacial features. Although an automatic cloud mask is included in all Sentinel-2 L1C imagery, based on a ratio of the reflectance recorded in different bands (European Space Agency (ESA), 2015), the algorithm is not designed for glaciated terrain and performs poorly in this example (Figure 5.1a). This is not surprising, as snow covered regions are known to be a challenge for cloud detection algorithms - especially for Cirrus clouds (Paul et al., 2016; Frantz et al., 2018). In contrast, clouds do not affect the SAR imagery at all (Figure 5.1b) as they present little interference to the radar signal.

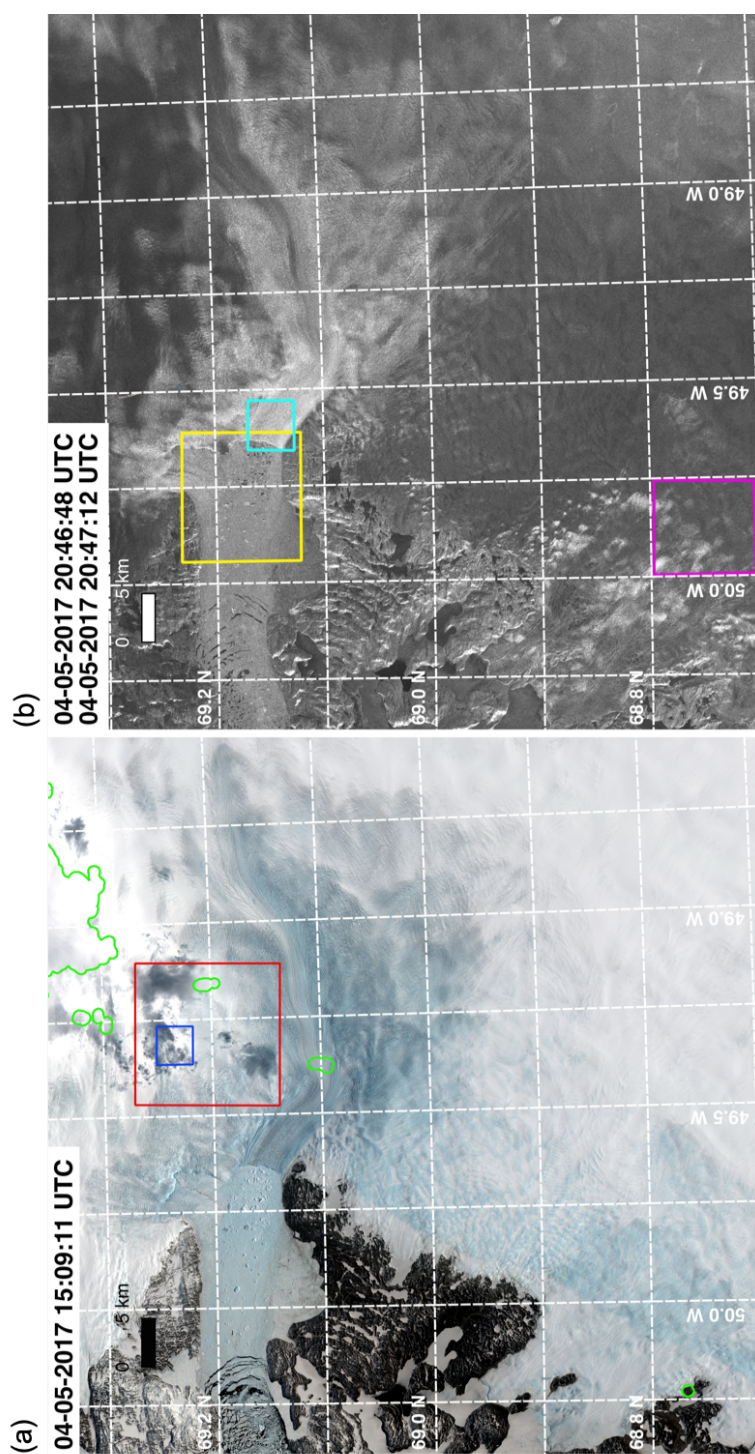


Figure 5.1: Optical true-color composite Sentinel-2 L1C (a) and SAR Sentinel-1 (b) same-day image comparison. The solid green contour represents cloud mask provided by ESA, and the coloured squares are insets of Figures 5.2–5.5.

In order to analyse the influence of clouds on the Sentinel-2 imagery in more detail, we extracted two areas of interest (see Figure 5.1a). At these locations, we compared a cloudy image (Figure 5.2a,b) acquired on 4th May 2017, with a cloud-free image (Figure 5.2c,d) from a different day (13th July 2017). The zoomed regions in Figures 5.2a and 2b show in more detail the combination of Cumulus and Cirrus clouds, and their shadows. We observe in Figure 5.2a that clouds can limit our ability to monitor the seasonal evolution of supraglacial lakes by, for instance, hiding a supraglacial lake (~ 1 km long) observed in Figure 5.2c, in the upper left region of the image, since supraglacial lakes are usually formed on the same area, due to the topography (Chu, 2014). Despite being an inconvenience for automated feature tracking processing to estimate ice velocity by obscuring stable features which are pre-requisite for the processing, the cloud-shadowed regions present less impact for visual analysis, if compared to Cumulus cloud regions. For instance, it is still possible to observe a sequence of crevasses on the shadowed region, located in the lower area of Figure 5.2a. The Cirrus clouds present in Figure 5.2b have similar visual impact as the shadowed areas (Figure 5.2d). Although the region is nebulous, features of the ice surface are still visible, but they are not as sharp as in a cloud-free image. Shadows and Cirrus clouds can cause cross-correlation mismatches if automated feature tracking algorithms are applied. Cumulus clouds, however, completely hide features in the ice surface and therefore have to be masked out.

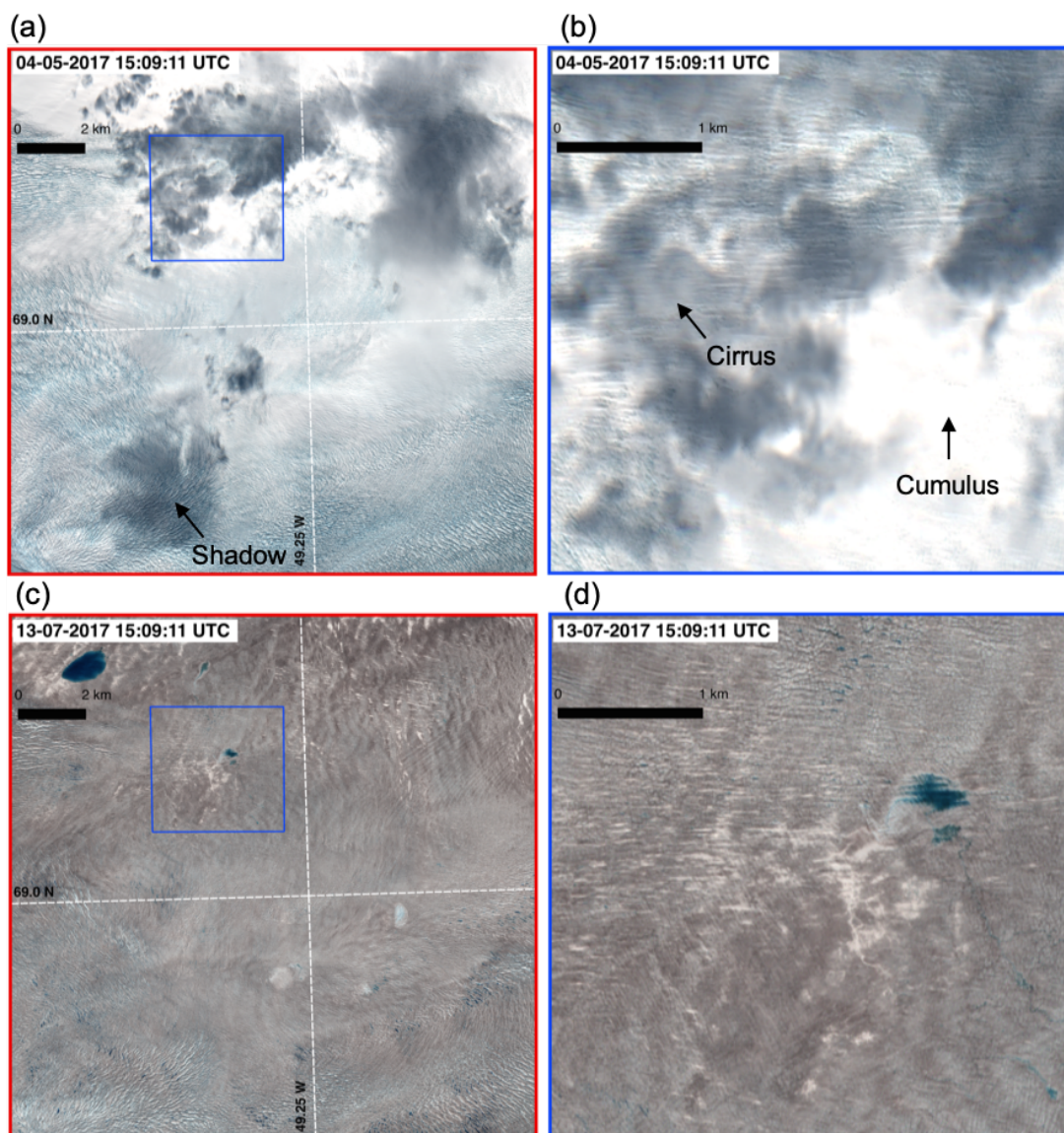


Figure 5.2: Zoom of cloud coverage (a-b) and cloud free areas (c-d) subsets extracted from Figure 5.1a inside the red and blue squares. The images are acquired in different days of the year as indicated in their upper left corner.

Next, we investigated the ability and the complementarity of the Sentinel-1 and Sentinel-2 missions for tracking, at high temporal frequency, the evolution of glaciological features, namely (1) iceberg drift, (2) marine glacier ice front migration, and (3) supraglacial lake evolution. Specifically, we focused on Sentinel-1/2 acquisitions

made during a two week period between 13th July 2017 and 27th July 2017 (Figures 5.3–5.5; Table 5.1). The image sequence shown in Figure 5.3 tracks the displacement of icebergs in the Ilulissat Icefjord. The icebergs in the mélange region flow at high rates (~ 250 m day^{-1}), induced by the Fjord’s ocean circulation and wind momentum transferred (Sundal et al., 2013). The icebergs are clear in the images acquired by both satellites, but the finer resolution (10 m) of Sentinel-2 resolves more clearly-defined edges in comparison to the SAR Sentinel-1 imagery (5 m in ground range and 20 m in azimuth). The calving front of JI is a very dynamic and complex region, which flows at speeds of ~ 12 km yr^{-1} and exhibits a very crevassed ice surface (Joughin et al., 2014; Lemos et al., 2018b). The sharpness of the optical true-colour composition helps us to identify, more easily, the ice front location (Figure 5.4). We can observe subtle changes in the Sentinel-2 sequence (Figures 5.4a,b) that is not clear between the Sentinel-1 images (Figure 5.4c,d). During the 14 days, the ice front advanced at an average rate of ~ 15 m day^{-1} . The use of high temporal and spatial resolution images are extremely important for monitoring calving dynamics over short time periods. For this reason, the combined use of Sentinel-1 and Sentinel-2 is valuable, because it allows us to identify systematically, and remotely, changes in calving front location every 2 days.

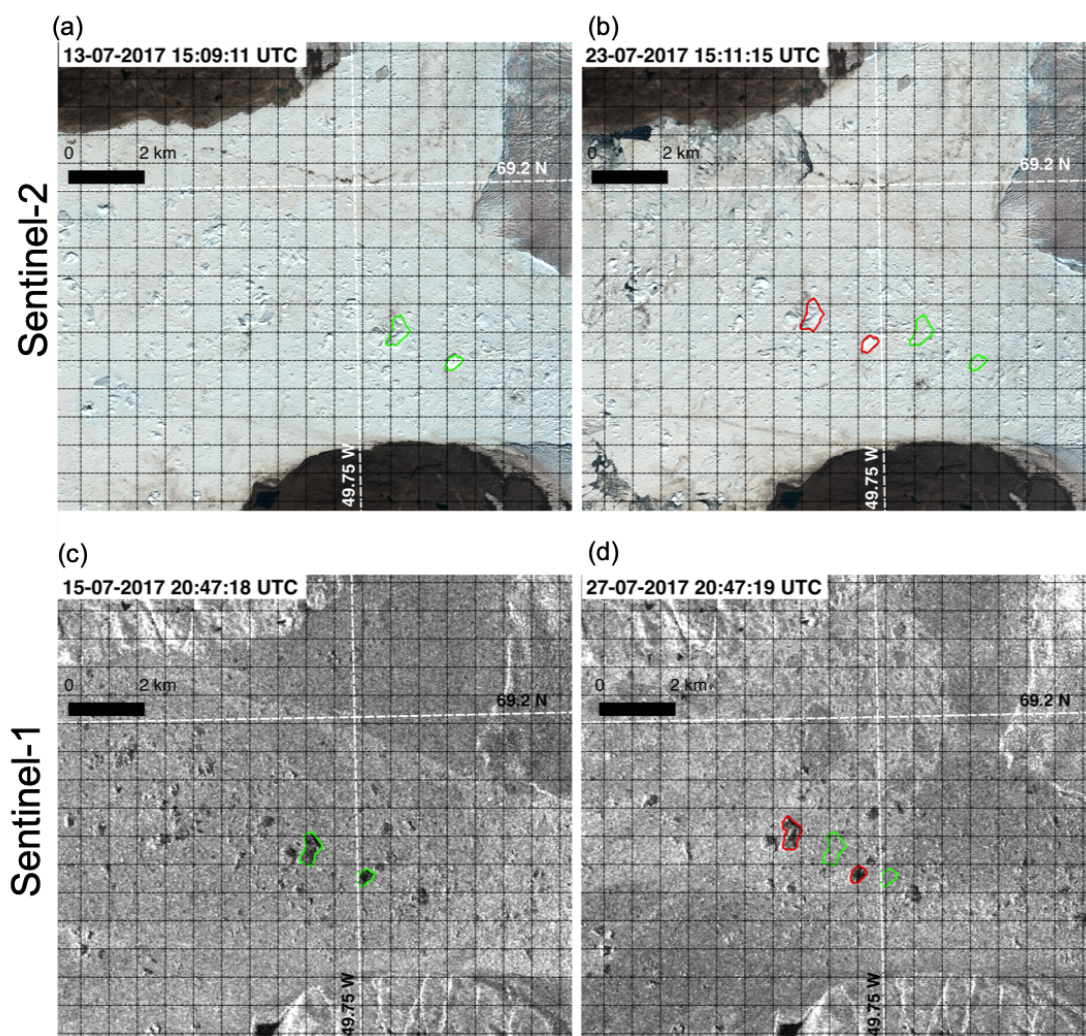


Figure 5.3: Tracked icebergs in the Ilulissat Fjord using true-colour composite Sentinel-2 (a-b) and SAR Sentinel-1 (c-d) images. The subsets were extracted in the yellow square from Figure 5.1b. The gridline is spaced by 750 m x 750 m. Solid green and red lines represent digitized features from the scenes a,c and b,d respectively.

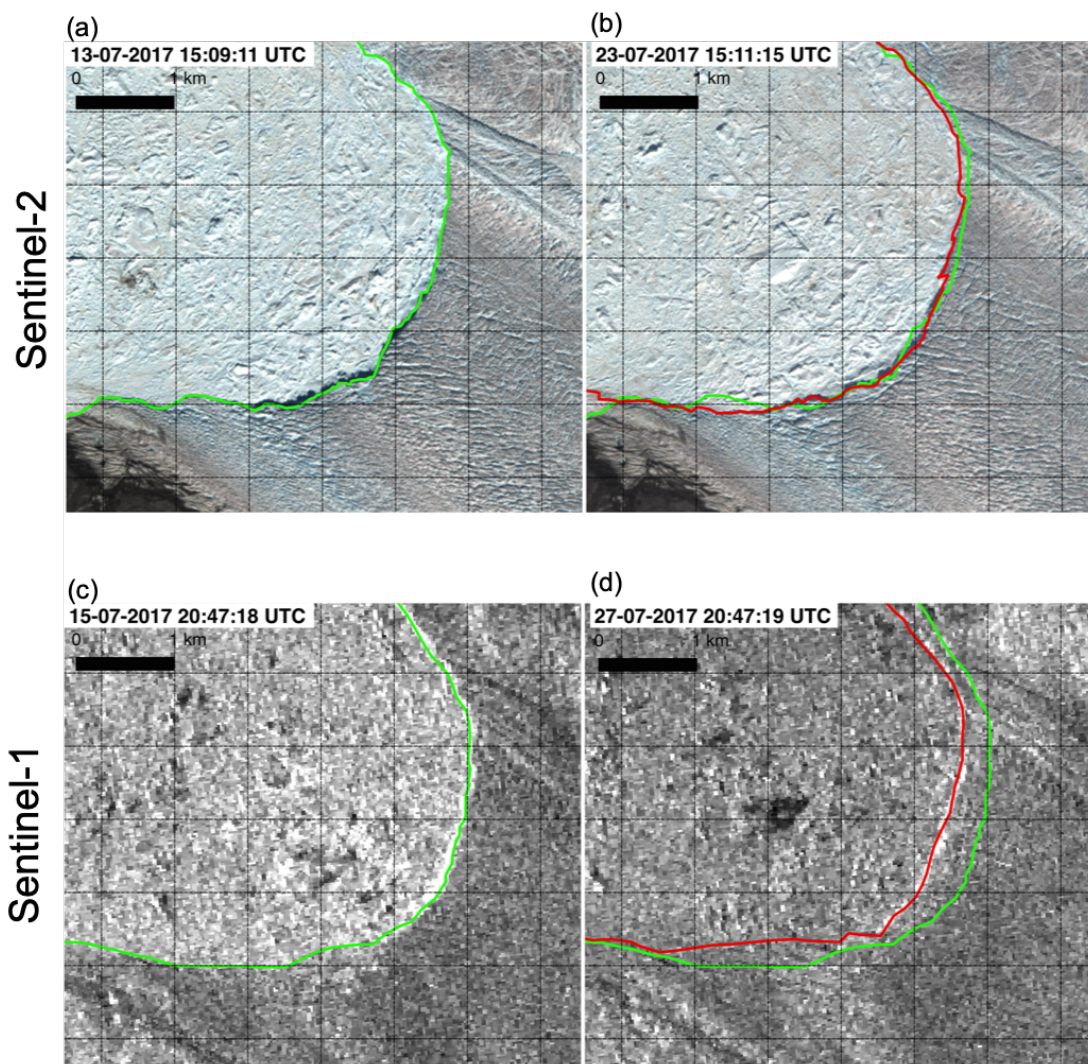


Figure 5.4: Calving front locations using true-colour composite Sentinel-2 (a-b) and SAR Sentinel-1 (c-d) images. The subsets were extracted in the cyan square from Figure 5.1b. The gridline is spaced by 750 m x 750 m. Solid green and red lines represent digitized features from the scenes a,c and b,d respectively.

Supraglacial lakes form in the ablation zone of the Greenland ice sheet when surface runoff accumulates in topographic depressions (Leeson et al., 2013; Chu, 2014). The location of supraglacial lakes is highly influenced by the subglacial topography, and they usually are formed over the same places every season (Chu, 2014). As summer

progresses, the area and volume of water stored in supraglacial lakes increases until either melting ceases or drainage occurs (McMillan et al., 2007; Leeson et al., 2013, 2015) - a process that has been linked to basal lubrication of ice flow (Hoffman et al., 2011; Chu, 2014). Several supraglacial lakes are present in our study area, and we focus on two - a northern and a southern lake (see Figure 5.5) - that are visible in both the Sentinel-1 and Sentinel-2 imagery. Both lakes have similar areas when traced manually in the optical and radar imagery acquired on similar dates (13th and 15th July, respectively). However, across the 14 day period of our satellite imagery, the northern and southern lakes increase in area by 24 % and 23 %, respectively (Table 5.2). The lakes are clearer in the Sentinel-2 imagery, and it is possible to observe supraglacial channels that are not present in the SAR scenes. Another potential use of the Sentinel-2 imagery is for estimating the depth of lakes due to their varying opacity, through a combination of different spectral bands (Pope et al., 2016). On the other hand, the SAR images have the potential to differentiate snow conditions through distinct backscatter values, such as the water content (Rau et al., 2001; Cuffey and Paterson, 2010), and the increases in intensity between the two images may be indicative of a change in the degree of surface melting.

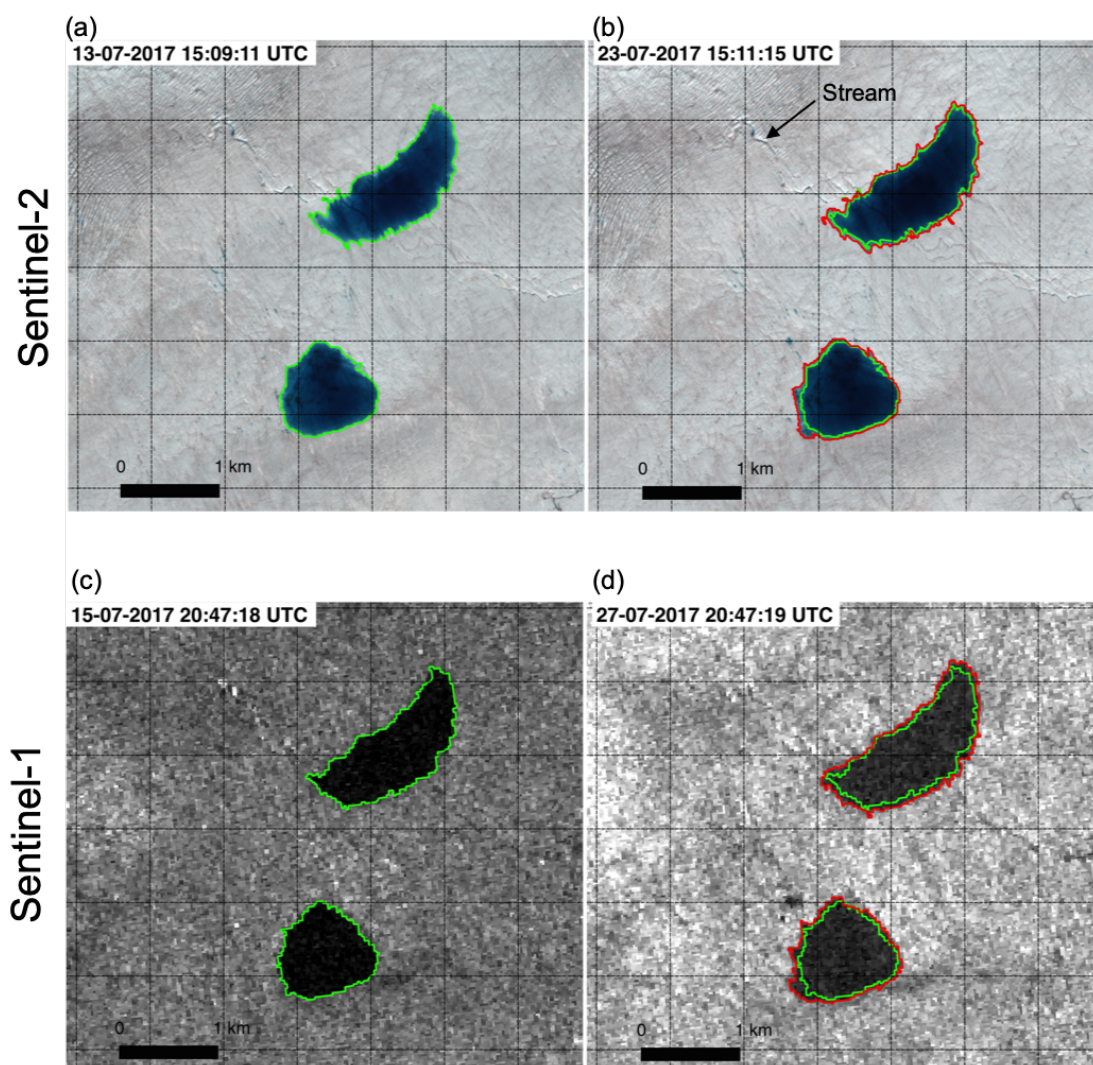


Figure 5.5: Supraglacial lakes observed in true-colour composite Sentinel-2 (a-b) and SAR Sentinel-1 (c-d) imagery (see magenta square in Figure 5.1b for location). The gridline is spaced by 750 m x 750 m. Solid green and red lines represent digitized features from the scenes a,c and b,d respectively.

Table 5.2: Changes in the area of supraglacial lakes records in Sentinel-1 and Sentinel-2 imagery (see Figure 5.5 for lake locations).

Date	Sensor	Northern lake Area (km^2)	Southern lake Area (km^2)
13-07-2017	Sentinel-2	0.95	0.68
15-07-2017	Sentinel-1	0.95	0.69
23-07-2017	Sentinel-2	1.09	0.79
27-07-2017	Sentinel-1	1.18	0.84

When applied to the Sentinel-2 imagery, the cross-correlation feature tracking technique produces a pattern of ice flow that is consistent with that determined from Sentinel-1 imagery (Lemos et al., 2018b), though with different spatial sampling (Figure 5.6). To compare the optical and radar estimates of ice motion in detail, we selected pairs of cloud-free Sentinel-2 images acquired during the seasons of complete or partial sunlight; i.e. spring, summer and autumn (Table 5.1). For comparison, we chose Sentinel-1 velocity maps (Lemos et al., 2018b) based on the proximity of the Sentinel-2 dates and, additionally, a map recorded during winter (Figure 5.6a). Although both satellite image classes have the ability to track ice motion on the fast and slow moving regions of JI and the surrounding ice sheet, there are marked differences in the quality of data recorded in each season (Figure 5.6). Sentinel-1 produces more extensive velocity maps in winter than in summer (Lemos et al., 2018b,a), because the near-stable scattering properties of the snowpack during winter allows the intensity-tracking algorithm to perform well (Strozzi et al., 2002; Paul et al., 2015), with poorer coverage in other seasons. In contrast, the Sentinel-2 velocity maps show near-complete coverage during the height of summer (Table 5.3) with deteriorating sampling at other times and none in winter due to darkness. The optical and radar imagery are therefore highly complementary for tracking ice motion, leading to improvements in both the coverage and frequency of observations.

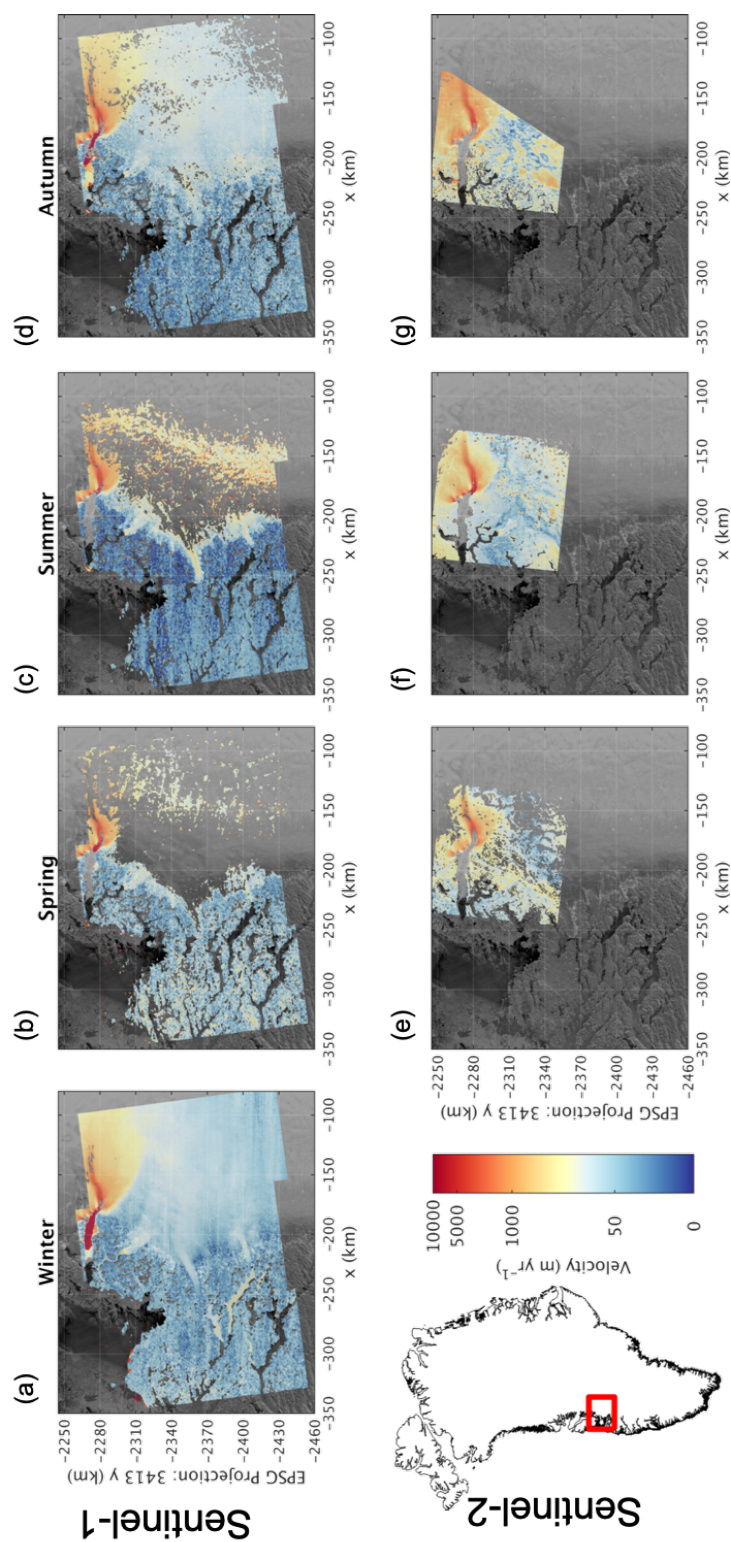


Figure 5.6: Seasonal variations in the speed of Jakobshavn Isbræ and the surrounding ice sheet estimated using Sentinel-1 (a-d) and Sentinel-2 (e-g) imagery.

Table 5.3: Common areas of the ice sheet covered by velocity tracking for each season.

Coverage	Winter	Spring	Summer	Autumn
Sentinel-1	98 %	30 %	47 %	88 %
Sentinel-2	0 %	60 %	93 %	59 %
S1 and S2 combined	98 %	67 %	97 %	93 %

We assess the ability of Sentinel-2 to track changes in ice flow by comparing the results with estimates determined from near-coincident Sentinel-1 imagery over the fast-flowing region of JI (Figure 5.7). In general, there is good agreement between the spatial and temporal variations in ice flow recorded in the two data sets, and the average difference in speed between near-coincident Sentinel-1 and Sentinel-2 data across the JI is $128 \pm 435 \text{ m yr}^{-1}$ (Table 5.4). The Sentinel-2 data perform best in summer, where the coverage exceeds by 46 % that afforded by Sentinel-1 (Table 5.3), and where the ice speeds are in close agreement ($224 \pm 136 \text{ m yr}^{-1}$ m/yr, on average) with those determined from Sentinel-1 (e.g. Figure 5.8). At other times, however, Sentinel-2 fails to track ice motion across the downstream 10 to 15 km section of the JI (Figures 5.7c,d and Figures 5.8c,d). Although Sentinel-2 fails to track the fastest section of ice flow in Spring, the remainder is also in close agreement ($100 \pm 72 \text{ m yr}^{-1}$, on average) with estimates determined from Sentinel-1. In Autumn, however, there is relatively poor agreement between the two datasets, and differences in excess of $293 \pm 309 \text{ m yr}^{-1}$ are common. Possible explanations for the poor agreement include the presence of translucent clouds in the Sentinel-2 imagery or errors in their initial co-registration (Paul et al., 2015). The ability of Sentinel-1 to track ice motion near the calving front of JI improved significantly after the launch of Sentinel-1b, because the revisit time reduced from 12 to 6 days which leads to improved coherence (Lemos et al., 2018b). Over the polar regions, Sentinel-2a/b themselves are able to track ice motion every three days, and in conjunction with Sentinel-1a/b images offers the potential to monitor ice flow every 2 days.

Table 5.4: Seasonal average speed separated by elevation bands estimated by near-coincident Sentinel-1 and Sentinel-2 imagery.

Elevation (m.a.s.l.)	Spring			Summer			Autumn		
	S1	S2	S2/S1	S1	S2	S2/S1	S1	S2	S2/S1
200-400	7116±666	-	-	8764±925	7586±818	13%	10689±1379	-	-
400-600	5018±1039	-	-	5140±337	5620±909	-9%	-	4785±70	-
600-800	3295±185	3121±182	5%	3465±391	3348±533	3%	3820±225	3603±635	6%
800-1000	2289±558	2135±455	7%	2067±388	1862±375	10%	2590±499	2194±440	15%
1000-1200	-	1367±90	-	1604±112	1243±124	22%	1763±138	1836±134	-4%

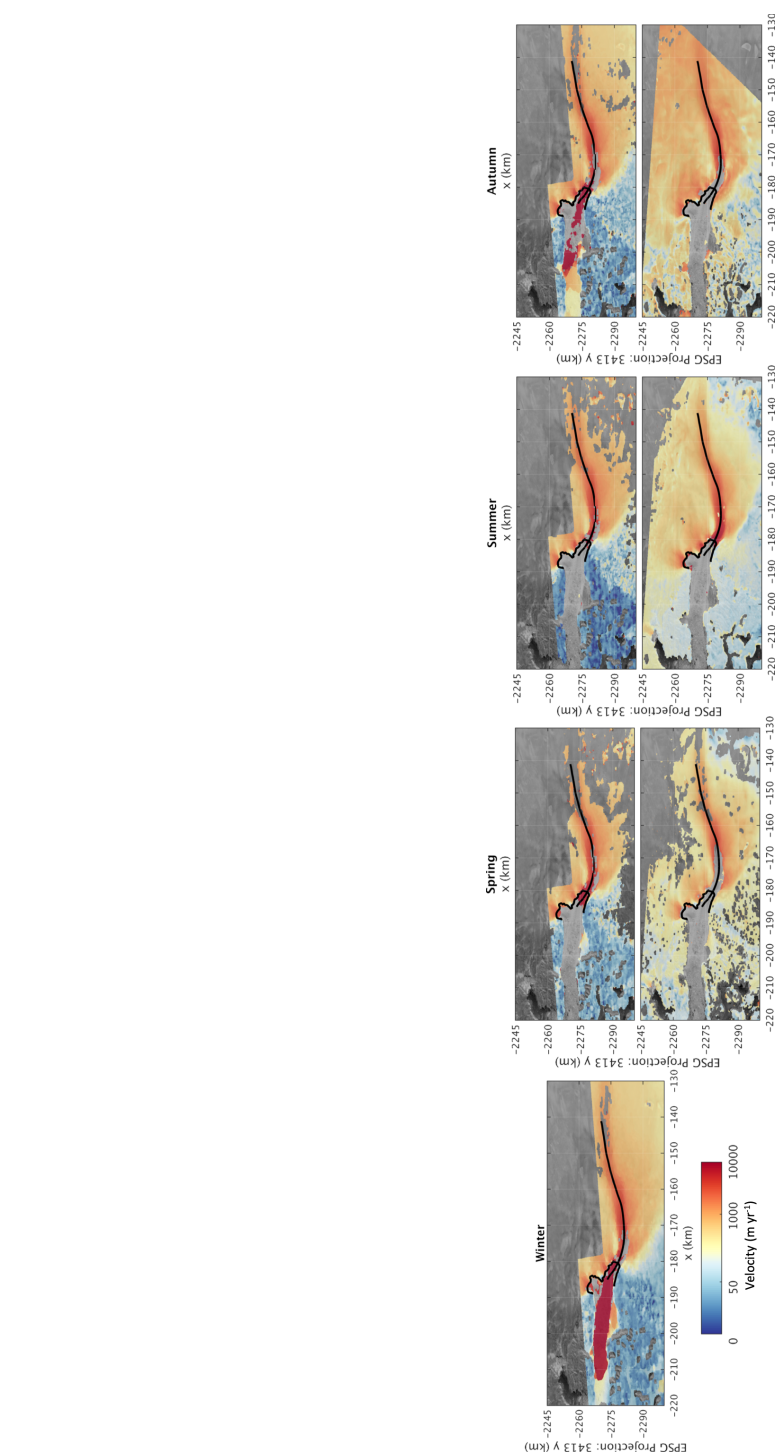


Figure 5.7: Ice velocity variation at the main trunk of Jakobshavn Isbræ in a logarithm colour scale. We present Sentinel-1 in winter, and Sentinel-2 (upper) and Sentinel-1 (lower) images in spring, summer and autumn. The solid black lines along and across the glacier represent the profile and ground line location, respectively, used in Figure 5.8.

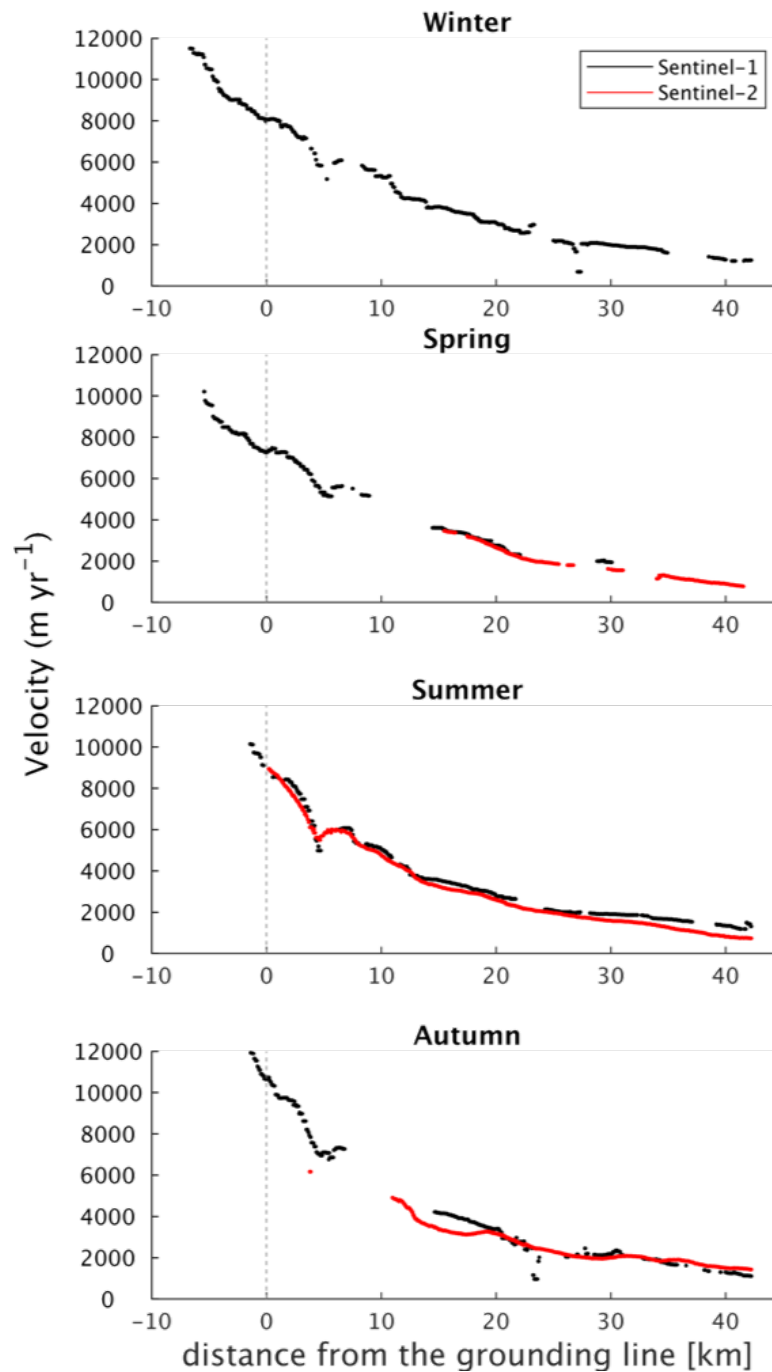


Figure 5.8: Velocity profiles extracted over the main trunk of Jakobshavn Isbræ. Black and red lines represent Sentinel-1 and Sentinel-2 profiles, respectively. The profile and ground line location are represented as solid black lines along and across the glacier, respectively, in Figure 5.7.

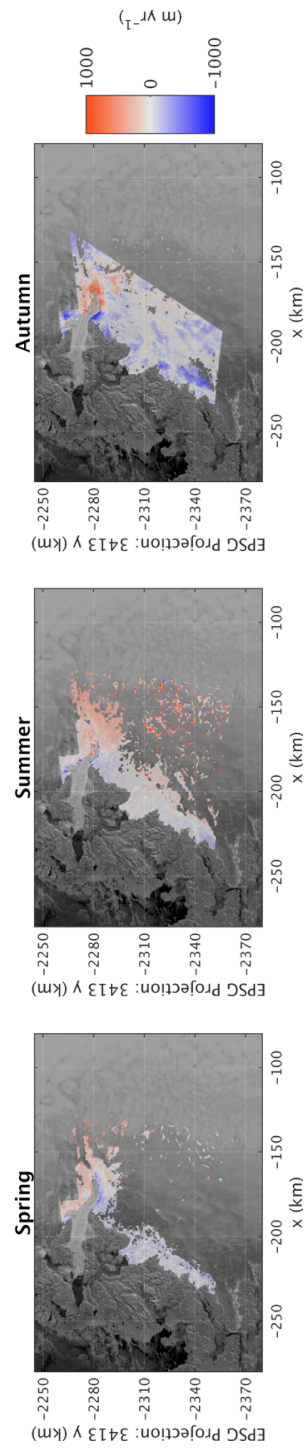


Figure 5.9: Differences in the velocities from Sentinel-2 and Sentinel-1 data in common areas of the ice sheet covered by velocity tracking for each season.

5.5 Discussions

In this study, we have presented the first analysis of the complementarity of near-coincident SAR and optical imagery, acquired by Sentinel-1 and Sentinel-2 satellites respectively, for a range of glaciological applications. Specifically, our assessment has focussed on tracking iceberg drift, marine glacier ice front migration, supraglacial lake evolution and ice surface flow at high temporal resolution.

Monitoring iceberg drift is important not only because it provides a direct measure of fjord circulation, but also because the melting of drifting ice provides a key freshwater input into the ocean. This information is required to inform the boundary conditions for fjord models, and also our understanding of the drivers of submarine melting at the grounded ice's calving front (Moon et al., 2018). Enderlin et al. (2016), for example, found that the total freshwater input into the Ilulissat Icefjord was dominated by mélange melting all year around. Although it is possible to monitor icebergs by installing time-lapse photography cameras to acquire images at high spatial-temporal resolution (Cassotto et al., 2015), such efforts are expensive and logistically arduous, which limits the routine, large-scale application of this method. Here we have demonstrated the potential of Sentinel-2, in conjunction with Sentinel-1, to monitor iceberg drift at rates of 250 m day^{-1} . The future automation of these techniques has the potential to provide systematic measurements of fjord circulation and meltwater input at the continental scale.

Similarly, although marine glacier front migration can also be monitored using field based surveys, it is again much more efficient to do this from space. For glaciers such as JI, which are highly dynamic in nature, it is important to be able to do this in a high temporal sampling frequency, in order to provide observational datasets that can be used to constrain and test calving laws and models (Benn et al., 2017). Here we find that the Sentinel-1/2 satellites combined can resolve calving rates during July 2017 of $\sim 15 \text{ m day}^{-1}$, which is consistent with the average rates of ~ 10 to 40 m day^{-1} resolved by Joughin et al. (2012). In a wider context, satellite-based studies have demonstrated that JI speedup has been triggered by calving events (Joughin et al., 2012, 2014), and can increase its speed by $\sim 1800 \text{ m yr}^{-1}$ in response to 1 km of retreat (Lemos et al., 2018b), thus highlighting the importance of continuous near-real-time monitoring of the calving front location.

The locations and dynamics of supraglacial lakes have been extensively monitored by optical imagery over Greenland (Sundal et al., 2009; Selmes et al., 2011; Leeson et al., 2013). These lakes have been observed to drain at different rates (McMillan et al., 2007; Selmes et al., 2011), varying from days (Selmes et al., 2011) to hours (Das et al., 2008) and via a range of mechanisms, including crevasse hydrofracture and overtopping into nearby moulins. In this study, we have demonstrated the value of Sentinel-2, working in conjunction with Sentinel-1, to increase the time sampling (up to 2 days) of supraglacial lakes at high spatial resolution (10 m). Specifically, we have mapped two filling lakes during a 14 day period, showing area changes of 24 % and 23 %. Expanding this type of mapping to the ice sheet scale holds the potential to greatly improve the observational datasets that are available for monitoring and understanding these lakes' seasonal evolution, and their corresponding impact upon ice dynamics.

Short-term environmental changes at marine-terminating glaciers are known to trigger responses in glacier dynamics, and associated ice mass loss and thinning (Joughin et al., 2012, 2014; Sundal et al., 2013). The highly variable patterns of seasonal and inter-annual speed changes of JI that have been observed over recent decades (Lemos et al., 2018b), highlight the importance of continuous monitoring with both high coverage and temporal resolution (Rosenau et al., 2015). Here, we have demonstrated the ability of Sentinel-2 to track ice motion in different seasons, and when combined with Sentinel-1, to improve the regularity with which ice speed estimates can be made to up to 2 days. Over common regions of JI, by combining velocity data from both Sentinel-1 and Sentinel-2, we have demonstrated that improved coverage of 97 % can be achieved in summer (Table 5.3). In winter, when the optical imagery has limited performance to track ice motion, Sentinel-1 is still able to provide 98 % of coverage (Table 5.3). This demonstrates that, through the combination of sensors, it is possible to achieve a high degree of year-round coverage, that is impossible from a single sensor alone. Furthermore, the new Sentinel-2 velocity products show good agreement with estimates from Sentinel-1 along the main flow profiles, as demonstrated in figure 5.8. Spatially, we observe velocities differencing by $224 \pm 136 \text{ m yr}^{-1}$ (29 %) in summer (Table 5.4), and up to 1000 m yr^{-1} near to the ice front in autumn (Figure 5.9). Despite the slight slow-down in speed that has been observed since 2012 (Lemos et al., 2018b), JI remains the single highest glacier contributor to Greenland mass imbalance (Joughin et al., 2012), requiring continuous and frequent monitoring.

5.6 Conclusions

This study has demonstrated the utility of new multi-spectral imaging satellites for building systematic records of glacier and ice sheet evolution. The use of high spatial resolution images, acquired with a high sampling frequency, are extremely important for monitoring iceberg drift, calving front location, supraglacial lakes and ice dynamics. We have shown here that the sharpness and fine spatial resolution of the Sentinel-2 true-colour composite images allows us to identify and track all of these features, and thus provide complementarity with other sensors, such as Sentinel-1. One of the main disadvantages of optical images is their sensitivity to the presence of clouds, which affect the capability to reliably track surface features, and are a source of errors during the co-registration procedure that is required to align images. Nonetheless, when clouds are absent, we find that Sentinel-2 offers several advantages relative to Sentinel-1. We observed subtle changes in the calving dynamics over a short period of time using Sentinel-2 images, that were not clear between the Sentinel-1 SAR images, especially during summer due to the high backscatter levels in the latter. The supraglacial lakes were also clearer in the optical imagery, and it was possible to observe more defined edges, thereby lending greater certainty to lake area estimates. The cross-correlation feature tracking applied to the Sentinel-2 imagery produced patterns of ice flow that were consistent with previous work in the same region (Lemos et al., 2018b). The optical velocity products presented near-complete coverage in summer, complementing the near-complete coverage achieved by SAR in winter, and improving both the year-round coverage and frequency of observations. Despite JI being a challenging region, the good agreement we find between Sentinel-2 and Sentinel-1 velocity estimates, indicates that Sentinel-2 can potentially extend the existing time series of ice velocity in conjunction with other sensors. The systematic acquisition cycle of Sentinel-2a/b is able to provide averaged velocity measurements every 3 days over the polar regions and, in conjunction with Sentinel-1a/b products, offers the potential to monitor average ice flow every 2 days, which is unprecedented during the satellite era. Going forward, the novel combination of operational satellite missions at the continental scale is essential for the systematic identification of short-term changes of numerous glaciological features, and for understanding the processes that drive ice velocity change.

References

- D. I. Benn, T. Cowton, J. Todd, and A. Luckman. Glacier Calving in Greenland. *Current Climate Change Reports*, 3(4):282–290, 2017. ISSN 21986061. doi: 10.1007/s40641-017-0070-1. 131
- R. A. Bindshadler and T. A. Scambos. Satellite-Image-Derived Velocity Antarctic Ice Stream. *Science*, 252:242–246, 1991. 114
- R. Cassotto, M. Fahnestock, J. M. Amundson, M. Truffer, and I. Joughin. Seasonal and interannual variations in ice melange and its impact on terminus stability, Jakobshavn Isbræ, Greenland. *Journal of Glaciology*, 61(225):76–88, 2015. ISSN 00221430. doi: 10.3189/2015JoG13J235. 131
- V. W. Chu. *Greenland ice sheet hydrology: A review*, volume 38. 2014. ISBN 0309133313507. doi: 10.1177/0309133313507075. URL <http://ppg.sagepub.com/cgi/doi/10.1177/0309133313507075>. 110, 117, 121, 122
- K. M. Cuffey and W. Paterson. *The Physics of Glaciers*. 4th ed. edition, 2010. ISBN 9780123694614. 122
- S. B. Das, I. Joughin, M. D. Behn, I. M. Howat, M. A. King, D. Lizarralde, and M. P. Bhatia. Fracture Propagation to the Base of the Greenland Ice Sheet During Supraglacial Lake Drainage. *Science*, 320(May):778–782, 2008. 132
- R. de Lange, A. Luckman, and T. Murray. Improvement of satellite radar feature tracking for ice velocity derivation by spatial frequency filtering. *IEEE Transactions on Geoscience and Remote Sensing*, 45(7):2309–2318, 2007. ISSN 01962892. doi: 10.1109/TGRS.2007.896615. 114
- E. M. Enderlin, I. M. Howat, S. Jeong, M.-J. Noh, J. H. van Angelen, and M. R. van den Broeke. An improved mass budget for the Greenland ice sheet. *Geophys. Res. Lett.*, 41:1–7, 2014. doi: 10.1002/2013GL059010.Received. 111, 112
- E. M. Enderlin, G. S. Hamilton, F. Straneo, and D. A. Sutherland. Iceberg meltwater fluxes dominate the freshwater budget in Greenland’s iceberg-congested glacial fjords. *Geophysical Research Letters*, 43(21):11,287–11,294, 2016. ISSN 19448007. doi: 10.1002/2016GL070718. 131

- European Space Agency (ESA). Sentinel-2 User Handbook. (1):1–64, 2015. 115
- M. Fahnestock, T. Scambos, T. Moon, A. Gardner, T. Haran, and M. Klinger. Rapid large-area mapping of ice flow using Landsat 8. *Remote Sensing of Environment*, 185:84–94, 2016. ISSN 00344257. doi: 10.1016/j.rse.2015.11.023. URL <http://dx.doi.org/10.1016/j.rse.2015.11.023>. 111, 114
- D. Frantz, E. Haß, A. Uhl, J. Stoffels, and J. Hill. Improvement of the Fmask algorithm for Sentinel-2 images: Separating clouds from bright surfaces based on parallax effects. *Remote Sensing of Environment*, 215(March):471–481, 2018. ISSN 00344257. doi: 10.1016/j.rse.2018.04.046. 115
- GAMMA REMOTE SENSING. Interferometric SAR Processor - ISP. Volume 1.9. Technical Report December, 2015. 113, 114
- A. S. Gardner, G. Moholdt, T. Scambos, M. Fahnestock, S. Ligtenberg, and M. V. D. Broeke. Increased West Antarctic ice discharge and East Antarctic stability over the last seven years. *The Cryosphere*, 12:521–547, 2018. doi: <https://doi.org/10.5194/tc-12-521-2018>. 111
- R. M. Goldstein, H. Engelhardt, B. Kamb, and R. M. Frolich. Satellite Radar Interferometry for Monitoring Ice Sheet Motion: Application to an Antarctic Ice Stream. *Science*, 262(3 December):1525–1530, 1993. 111
- E. Hanna, S. H. Mernild, J. Cappelen, and K. Steffen. Recent warming in Greenland in a long-term instrumental (1881-2012) climatic context: I. Evaluation of surface air temperature records. *Environmental Research Letters*, 7(4), 2012. ISSN 17489326. doi: 10.1088/1748-9326/7/4/045404. 110
- E. A. Hill, J. R. Carr, C. R. Stokes, and G. H. Gudmundsson. Dynamic changes in outlet glaciers in northern Greenland from 1948 to 2015. *The Cryosphere*, 12:3243–3263, 2018. ISSN 1994-0440. doi: 10.5194/tc-2018-17. URL <https://www.the-cryosphere-discuss.net/tc-2018-17/>. 111
- M. J. Hoffman, G. A. Catania, T. A. Neumann, L. C. Andrews, and J. A. Rumrill. Links between acceleration, melting, and supraglacial lake drainage of the western Greenland Ice Sheet. *Journal of Geophysical Research: Earth Surface*, 116(4):1–16, 2011. ISSN 21699011. doi: 10.1029/2010JF001934. 110, 122

REFERENCES

- D. M. Holland, R. H. Thomas, B. D. Young, M. H. Ribergaard, and B. Lyberth. Acceleration of Jakobshavn Isbræ triggered by warm subsurface ocean waters. *Nature Geoscience*, 1:1–6, 2008. doi: 10.1038/ngeo316. 110
- S. Jeong and I. M. Howat. Performance of Landsat 8 Operational Land Imager for mapping ice sheet velocity. *Remote Sensing of Environment*, 170(8):90–101, 2015. ISSN 00344257. doi: 10.1016/j.rse.2015.08.023. URL <http://dx.doi.org/10.1016/j.rse.2015.08.023>. 114
- I. Joughin, W. Abdalati, and M. Fahnestock. Large fluctuations in speed on Greenland’s Jakobshavn Isbrae glacier. *Nature*, 432(7017):608–10, dec 2004. ISSN 1476-4687. doi: 10.1038/nature03130. URL <http://www.ncbi.nlm.nih.gov/pubmed/15577906>. 112
- I. Joughin, S. B. Das, M. A. King, B. E. Smith, I. M. Howat, and T. Moon. Seasonal Speedup Along the Western Flank of the Greenland Ice Sheet. *Science*, 320(April):781–784, 2008a. doi: 10.1126/science.1153288. 112
- I. Joughin, I. M. Howat, M. Fahnestock, B. Smith, W. Krabill, R. B. Alley, H. Stern, and M. Truffer. Continued evolution of Jakobshavn Isbrae following its rapid speedup. *Journal of Geophysical Research: Earth Surface*, 113(4):1–14, 2008b. ISSN 21699011. doi: 10.1029/2008JF001023. 112
- I. Joughin, B. E. Smith, I. M. Howat, T. Scambos, and T. Moon. Greenland flow variability from ice-sheet-wide velocity mapping. *Journal of Glaciology*, 56(197):415–430, aug 2010. ISSN 00221430. doi: 10.3189/002214310792447734. URL <http://openurl.ingenta.com/content/xref?genre=article&issn=0022-1430&volume=56&issue=197&spage=415>. 111
- I. Joughin, B. E. Smith, I. M. Howat, D. Floricioiu, R. B. Alley, M. Truffer, and M. Fahnestock. Seasonal to decadal scale variations in the surface velocity of Jakobshavn Isbrae, Greenland: Observation and model-based analysis. *Journal of Geophysical Research: Earth Surface*, 117(2):1–20, 2012. ISSN 21699011. doi: 10.1029/2011JF002110. 112, 131, 132
- I. Joughin, B. E. Smith, D. E. Shean, and D. Floricioiu. Brief communication: Further summer speedup of Jakobshavn Isbræ. *The Cryosphere*, 8(1):209–214, 2014. ISSN 19940416. doi: 10.5194/tc-8-209-2014. 110, 111, 112, 119, 131, 132

- I. Joughin, B. E. Smith, and I. Howat. Greenland Ice Mapping Project: Ice Flow Velocity Variation at sub-monthly to decadal time scales. *The Cryosphere*, 12:2211–2227, 2018. doi: <https://doi.org/10.5194/tc-12-2211-2018>. 111, 112
- A. Kääb, S. H. Winsvold, B. Altena, C. Nuth, T. Nagler, and J. Wuite. Glacier remote sensing using sentinel-2. part I: Radiometric and geometric performance, and application to ice velocity. *Remote Sensing*, 8(7):1–24, 2016. ISSN 20724292. doi: [10.3390/rs8070598](https://doi.org/10.3390/rs8070598). 113, 114, 115
- A. Leeson, A. Shepherd, K. Briggs, and X. Fettweis. Supraglacial lakes on Greenland migrate inland under warming climate. *Nature Climate Change*, 16(January):51–55, 2015. ISSN 1758-678X. doi: [10.1038/NCLIMATE2463](https://doi.org/10.1038/NCLIMATE2463). 122
- A. A. Leeson, A. Shepherd, A. V. Sundal, A. M. Johansson, N. Selmes, K. Briggs, A. E. Hogg, and X. Fettweis. A comparison of supraglacial lake observations derived from MODIS imagery at the western margin of the Greenland ice sheet. *Journal of Glaciology*, 59(218):1179–1188, 2013. ISSN 00221430. doi: [10.3189/2013JoG13J064](https://doi.org/10.3189/2013JoG13J064). 110, 121, 122, 132
- A. Lemos, A. Shepherd, M. Mcmillan, and A. E. Hogg. Seasonal Variations in the Flow of Land-Terminating Glaciers in Central-West Greenland Using Sentinel-1 Imagery. *Remote Sensing*, 10:1–12, 2018a. doi: <https://doi.org/10.3390/rs10121878>. 114, 124
- A. Lemos, A. Shepherd, M. Mcmillan, A. E. Hogg, E. Hatton, and I. Joughin. Ice velocity of Jakobshavn Isbræ, Petermann Glacier, Nioghalvfjerdingsfjorden and Zachariæ Isstrøm, 2015-2017, from Sentinel 1-a/b SAR imagery. *The Cryosphere*, 12(June):2087–2097, 2018b. doi: <https://doi.org/10.5194/tc-2017-251>. 110, 111, 112, 113, 114, 119, 124, 126, 131, 132, 133
- B. K. Lucchitta and H. M. Ferguson. Antarctica: measuring glacier velocity from satellite images. *Science (New York, N.Y.)*, 234(4780):1105–1108, 1986. ISSN 0036-8075. doi: [10.1126/science.234.4780.1105](https://doi.org/10.1126/science.234.4780.1105). 114
- B. K. Lucchitta, C. E. Rosanova, and K. F. Mullins. Velocities of Pine Island Glacier, West Antarctica, from ERS-1 SAR images. *Annals of Glaciology*, 21:277–283, 1995. ISSN 02603055. doi: [10.1017/S0260305500015949](https://doi.org/10.1017/S0260305500015949). 111

REFERENCES

- M. McMillan, P. Nienow, A. Shepherd, T. Benham, and A. Sole. Seasonal evolution of supra-glacial lakes on the Greenland Ice Sheet. *Earth and Planetary Science Letters*, 262:484–492, 2007. ISSN 0012821X. doi: 10.1016/j.epsl.2007.08.002. 110, 122, 132
- M. McMillan, A. Leeson, A. Shepherd, K. Briggs, T. W. K. Armitage, A. Hogg, P. K. Munneke, M. van den Broeke, B. Noël, W. J. van de Berg, S. Ligtenberg, M. Horwath, A. Groh, A. Muir, and L. Gilbert. A high resolution record of Greenland mass balance. *Geophysical Research Letters*, 43:1–9, 2016. doi: 10.1002/GRL.54619. 110, 111, 112
- T. Moon, I. Joughin, B. Smith, M. R. Broeke, W. J. Berg, B. Noël, and M. Usher. Distinct patterns of seasonal Greenland glacier velocity. *Geophysical Research Letters*, 41:7209–7216, 2014. doi: 10.1002/2014GL061836. 110
- T. Moon, I. Joughin, and B. Smith. Seasonal to multiyear variability of glacier surface velocity, terminus position, and sea ice/ice mélange in northern Greenland. *Journal of Geophysical Research: Earth Surface*, 120:818–833, 2015. doi: 10.1002/2015JF003494.Received. 110
- T. Moon, D. A. Sutherland, D. Carroll, D. Felikson, L. Kehrl, and F. Straneo. Subsurface iceberg melt key to Greenland fjord freshwater budget. *Nature Geoscience*, 11(1):49–54, 2018. ISSN 17520908. doi: 10.1038/s41561-017-0018-z. URL <http://dx.doi.org/10.1038/s41561-017-0018-z>. 131
- T. Nagler, H. Rott, M. Hetzenecker, J. Wuite, and P. Potin. The Sentinel-1 Mission: New Opportunities for Ice Sheet Observations. *Remote Sensing*, 7(7):9371–9389, 2015. ISSN 2072-4292. doi: 10.3390/rs70709371. URL <http://www.mdpi.com/2072-4292/7/7/9371/>. 111
- F. M. Nick, A. Vieli, M. L. Andersen, I. Joughin, A. Payne, T. L. Edwards, F. Pattyn, and R. S. Van De Wal. Future sea-level rise from Greenland’s main outlet glaciers in a warming climate. *Nature*, 497(7448):235–238, 2013. ISSN 00280836. doi: 10.1038/nature12068. URL <http://dx.doi.org/10.1038/nature12068>. 112
- F. Paul, T. Bolch, A. Kääb, T. Nagler, C. Nuth, K. Scharrer, A. Shepherd, T. Strozzi, F. Ticconi, R. Bhambri, E. Berthier, S. Bevan, N. Gourmelen, T. Heid, S. Jeong, M. Kunz, T. R. Lauknes, A. Luckman, J. Merryman, G. Moholdt, A. Muir,

- J. Neelmeijer, M. Rankl, J. VanLooy, and T. Van Niel. The glaciers climate change initiative: Methods for creating glacier area, elevation change and velocity products. *Remote Sensing of Environment*, 162:408–426, 2015. ISSN 00344257. doi: 10.1016/j.rse.2013.07.043. URL <http://dx.doi.org/10.1016/j.rse.2013.07.043>. 124, 126
- F. Paul, S. Winsvold, A. Kääb, T. Nagler, and G. Schwaizer. Glacier Remote Sensing Using Sentinel-2. Part II: Mapping Glacier Extents and Surface Facies, and Comparison to Landsat 8. *Remote Sensing*, 8(7):575, 2016. ISSN 2072-4292. doi: 10.3390/rs8070575. URL <http://www.mdpi.com/2072-4292/8/7/575>. 114, 115
- F. Paul, T. Bolch, K. Briggs, A. Kääb, M. McMillan, R. McNabb, T. Nagler, C. Nuth, P. Rastner, T. Strozzi, and J. Wuite. Error sources and guidelines for quality assessment of glacier area, elevation change, and velocity products derived from satellite data in the Glaciers_cci project. *Remote Sensing of Environment*, 203 (November):256–275, 2017. ISSN 00344257. doi: 10.1016/j.rse.2017.08.038. URL <https://doi.org/10.1016/j.rse.2017.08.038>. 114
- W. T. Pfeffer, A. A. Arendt, A. Bliss, T. Bolch, J. G. Cogley, A. S. Gardner, J. O. Hagen, R. Hock, G. Kaser, C. Kienholz, E. S. Miles, G. Moholdt, N. Mölg, F. Paul, V. Radić, P. Rastner, B. H. Raup, J. Rich, M. J. Sharp, L. M. Andreassen, S. Bajracharya, N. E. Barrand, M. J. Beedle, E. Berthier, R. Bhambri, I. Brown, D. O. Burgess, E. W. Burgess, F. Cawkwell, T. Chinn, L. Copland, N. J. Cullen, B. Davies, H. De Angelis, A. G. Fountain, H. Frey, B. A. Giffen, N. F. Glasser, S. D. Gurney, W. Hagg, D. K. Hall, U. K. Haritashya, G. Hartmann, S. Herreid, I. Howat, H. Jiskoot, T. E. Khromova, A. Klein, J. Kohler, M. König, D. Kriegel, S. Kutuzov, I. Lavrentiev, R. Le Bris, X. Li, W. F. Manley, C. Mayer, B. Menounos, A. Mercer, P. Mool, A. Negrete, G. Nosenko, C. Nuth, A. Osmonov, R. Pettersson, A. Racoviteanu, R. Ranzi, M. A. Sarikaya, C. Schneider, O. Sigurdsson, P. Sirguey, C. R. Stokes, R. Wheate, G. J. Wolken, L. Z. Wu, and F. R. Wyatt. The randolph glacier inventory: A globally complete inventory of glaciers. *Journal of Glaciology*, 60(221):537–552, 2014. ISSN 00221430. doi: 10.3189/2014JoG13J176. 111
- A. Pope, T. A. Scambos, M. Moussavi, M. Tedesco, M. Willis, D. Shean, and S. Grigsby. Estimating supraglacial lake depth in West Greenland using Landsat 8 and com-

- parison with other multispectral methods. *Cryosphere*, 10(1):15–27, 2016. ISSN 19940424. doi: 10.5194/tc-10-15-2016. 122
- P. Rastner, T. Bolch, N. Mölg, H. MacHguth, R. Le Bris, and F. Paul. The first complete inventory of the local glaciers and ice caps on Greenland. *Cryosphere*, 6(6): 1483–1495, 2012. ISSN 19940416. doi: 10.5194/tc-6-1483-2012. 111
- F. Rau, M. Braun, M. Friedrich, F. Weber, and H. Gobmann. Radar glacier zones and their boundaries as indicators of glacier mass balance and climatic variability. *Earsel eProceedings*, (1):317–327, 2001. 122
- E. Rignot, I. Velicogna, M. R. Van Den Broeke, A. Monaghan, and J. T. M. Lenaerts. Acceleration of the contribution of the Greenland and Antarctic ice sheets to sea level rise. *Geophysical Research Letters*, 38(5):1–5, 2011. ISSN 00948276. doi: 10.1029/2011GL046583. 111
- R. Rosenau, M. Scheinert, and R. Dietrich. A processing system to monitor Greenland outlet glacier velocity variations at decadal and seasonal time scales utilizing the Landsat imagery. *Remote Sensing of Environment*, 169:1–19, 2015. ISSN 00344257. doi: 10.1016/j.rse.2015.07.012. URL <http://dx.doi.org/10.1016/j.rse.2015.07.012>. 111, 114, 132
- T. a. Scambos, M. J. Dutkiewicz, J. C. Wilson, and R. a. Bindshadler. Application of image cross-correlation to the measurement of glacier velocity using satellite image data. *Remote Sensing of Environment*, 42(3):177–186, 1992. ISSN 00344257. doi: 10.1016/0034-4257(92)90101-O. URL <http://linkinghub.elsevier.com/retrieve/pii/0034425792901010>. 114
- N. Selmes, T. Murray, and T. D. James. Fast draining lakes on the Greenland Ice Sheet. *Geophysical Research Letters*, 38(15):1–5, 2011. ISSN 00948276. doi: 10.1029/2011GL047872. 132
- A. Shepherd, E. R. Ivins, G. A., V. R. Barletta, M. J. Bentley, S. Bettadpur, K. H. Briggs, D. H. Bromwich, R. Forsberg, N. Galin, M. Horwath, S. Jacobs, I. Joughin, M. A. King, J. T. M. Lenaerts, J. Li, S. R. M. Ligtenberg, A. Luckman, S. B. Luthcke, M. McMillan, R. Meister, G. Milne, J. Mouginot, A. Muir, J. P. Nicolas, J. Paden, A. J. Payne, H. Pritchard, E. Rignot, H. Rott, L. S. Sørensen, T. A.

REFERENCES

- Scambos, B. Scheuchl, E. J. O. Schrama, B. Smith, A. V. Sundal, J. H. van Angelen, W. J. van de Berg, M. R. van den Broeke, D. G. Vaughan, I. Velicogna, J. Wahr, P. L. Whitehouse, D. J. Wingham, D. Yi, D. Young, and H. J. Zwally. A Reconciled Estimate of Ice-Sheet Mass Balance. *Science*, 338(November):1183–1189, 2012. doi: 10.1126/science.1228102. 110
- L. S. Sørensen, S. B. Simonsen, R. Forsberg, K. Khvorostovsky, R. Meister, and M. E. Engdahl. 25 years of elevation changes of the Greenland Ice Sheet from ERS, Envisat, and CryoSat-2 radar altimetry. *Earth and Planetary Science Letters*, 495:234–241, 2018. ISSN 0012821X. doi: 10.1016/j.epsl.2018.05.015. URL <https://doi.org/10.1016/j.epsl.2018.05.015>. 112
- T. Strozzi, A. Luckman, T. Murray, U. Wegmuller, and C. L. Werner. Glacier motion estimation using SAR offset-tracking procedures. *IEEE Transactions on Geoscience and Remote Sensing*, 40(11):2384–2391, nov 2002. ISSN 0196-2892. doi: 10.1109/TGRS.2002.805079. URL <http://ieeexplore.ieee.org/lpdocs/epic03/wrapper.htm?arnumber=1166597>. 124
- A. V. Sundal, A. Shepherd, P. Nienow, E. Hanna, S. Palmer, and P. Huybrechts. Evolution of supra-glacial lakes across the Greenland Ice Sheet. *Remote Sensing of Environment*, 113(10):2164–2171, 2009. ISSN 00344257. doi: 10.1016/j.rse.2009.05.018. URL <http://dx.doi.org/10.1016/j.rse.2009.05.018>. 132
- A. V. Sundal, A. Shepherd, M. Van Den Broeke, J. Van Angelen, N. Gourmelen, and J. Park. Controls on short-term variations in Greenland glacier dynamics. *Journal of Glaciology*, 59(217):883–892, 2013. ISSN 00221430. doi: 10.3189/2013JoG13J019. 119, 132
- L. D. Trusel, S. B. Das, M. B. Osman, M. J. Evans, B. E. Smith, X. Fettweis, J. R. McConnell, B. P. Y. Noël, and M. R. van den Broeke. Nonlinear rise in Greenland runoff in response to post-industrial Arctic warming. *Nature*, 564(7734):104–108, 2018. ISSN 0028-0836. doi: 10.1038/s41586-018-0752-4. URL <http://www.nature.com/articles/s41586-018-0752-4>. 110
- M. A. Wulder, J. G. Masek, W. B. Cohen, T. R. Loveland, and C. E. Woodcock. Opening the archive: How free data has enabled the science and monitoring promise

REFERENCES

of Landsat. *Remote Sensing of Environment*, 122:2–10, 2012. ISSN 00344257. doi: 10.1016/j.rse.2012.01.010. URL <http://dx.doi.org/10.1016/j.rse.2012.01.010>.
111

Chapter 6

Discussions, Conclusions, and Future work

The aim of my thesis was to develop satellite measurements of Greenland glacier ice velocity fluctuations with higher temporal frequency than has been previously possible, as an indicator of environmental change. In the preceding chapters I met this aim using imagery acquired by the new Sentinel-1 and Sentinel-2 satellite constellations. I first produced and analysed new seasonal and inter-annual changes in the velocity of four key marine-terminating glaciers across Greenland (Chapter 3). I then produced and analysed seasonal changes in the velocity of five land-terminating glaciers in Central-west sector of Greenland (Chapter 4). Finally, I combined measurements from both missions to evaluate their complementarity for tracking ice motion of Jakobshavn Isbræ (Chapter 5). In this final chapter I will describe how my thesis has met the original motivations for conducting the research, by providing first a summary and then a synthesis of the work completed and the principal science results presented in each chapter. I will also discuss promising areas for future research that have emerged as a result of my thesis work.

6.1 Summary of main results

Fluctuations in marine-terminating glacier flow using Sentinel-1

In Chapter 3, I demonstrated, for the first time, the ability of the Sentinel-1a/b synthetic aperture radar constellation to track changes in the velocity of four marine-

terminating glaciers in Greenland with high temporal resolution, marking the start of a new era of operational monitoring. These marine-terminating glaciers are large, fast-flowing, units responsible for a sizeable fraction of the ice sheet discharge (Enderlin et al., 2014), and are known to respond quickly to changes in the surrounding ocean (Holland et al., 2008; Carr et al., 2017). I presented both seasonal and inter-annual velocity fluctuations, and I computed the persistence of summertime speedup thanks to the frequent temporal sampling of the Sentinel-1 data with mean errors going from 7 % to 30 % in isolated areas. In order to confidently build on existing ice velocity datasets developed from other satellite sensors, I first evaluated the Sentinel-1 velocity measurements using contemporaneous estimates derived from TerraSAR-X, which has finer spatial resolution and therefore greater precision. In this comparison, there was good agreement between the two ice velocity datasets at Jakobshavn Isbræ, with mean differences of 40 m yr^{-1} and 76 m yr^{-1} at sites J1 and J2 respectively, which are situated ~ 12 and ~ 17 km inland. At a third site, Jif, the mean difference was much higher (489 m yr^{-1}); however, this location is close to the ice front where speeds exceed 15 km yr^{-1} in 2012-2013 and is an extremely challenge region to track ice flow (Figure 3.4). I then demonstrated the benefit of the Sentinel-1a/b constellation's short (6-day) revisit time, which improves the degree of correlation between consecutively acquired images, and the value of the resulting measurements for tracking flow near to the calving front of Jakobshavn Isbræ (Figure 6.1). Using the extended velocity dataset, I quantified inter-annual variations and the seasonal cycle of ice motion at all four marine-terminating glaciers. Through this analysis, revealed the deceleration of Jakobshavn Isbræ by 321 m yr^{-1} over the last 5 years, after a 15 years period of progressive speedup, and I demonstrated the that seasonal changes in the glaciers speed are correlated with seasonal changes in its calving front position (Figure 3.6). Moreover, I estimated seasonal changes of 25 % and 18 % in Petermann Glacier and Zachariæ Isstrøm, respectively.

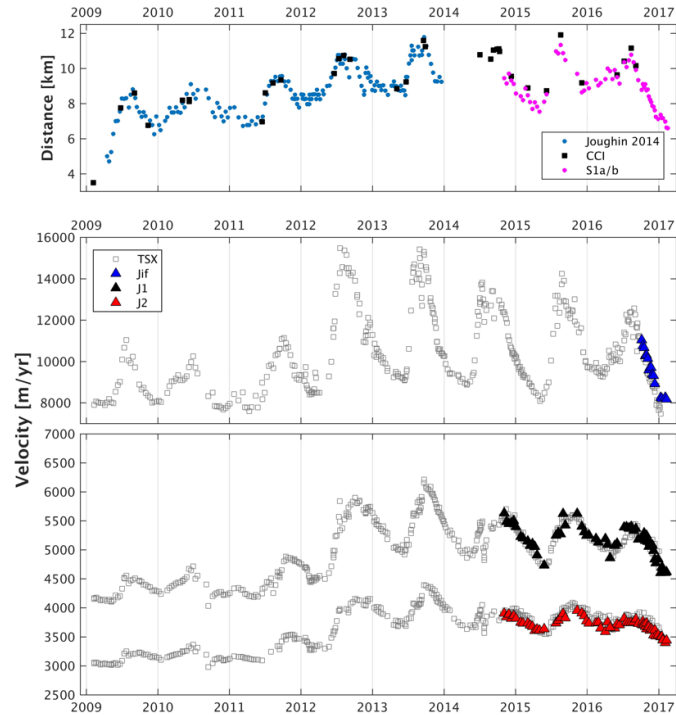


Figure 6.1: Copy of Figure 3.5. Temporal evolution of Jakobshavn Isbræ (a) ice front position extracted from Joughin et al. (2014), ESA Greenland Ice Sheet Climate Change Initiative (CCI) project (European Space Agency (ESA), 2017), and Sentinel-1a/b SAR images represented in blue, black and magenta dots respectively, where higher values correspond to ice front retreat. Changes in ice velocity through time is also shown (b, c), extracted at the locations indicated in Figure 3.1. The velocity data derived from TerraSAR-X (11 days - Joughin et al. (2016)) are shown as grey squares, and the data from Sentinel 1-a/b (6 to 12 days) as coloured triangles.

Fluctuations in land-terminating glacier flow using Sentinel-1

In Chapter 4, I extended my analysis of Sentinel-1a/b images to track the motion of five land-terminating glaciers in a $14,000 \text{ km}^2$ sector of central-west Greenland. Glaciers in this and other land-terminating sectors of the ice sheet are known to exhibit seasonal variations in flow that are related to the degree of surface melting through a process of basal ice lubrication (Bartholomew et al., 2010; Hoffman et al., 2011; Chu, 2014), and are therefore a sensitive indicator of changing atmospheric conditions (Sundal et al.,

2011; Bartholomew et al., 2012). Land-terminating glaciers flow, however, relatively slowly, and so tracking seasonal changes in their speed has proven to be a challenge with satellite data. I presented the capability of the new constellation, compared to previous missions, to track ice motion with significantly improved spatial and temporal resolution. I generated ice velocity maps for both summer and winter, with uncertainties around 10 % across the majority of the study area. These show different patterns of speedup between individual glaciers (Figure 4.1 and 4.2), and also differences in the spatial sampling that can be achieved in summer and winter due to the effects of surface melting. Despite being located in the same region, seasonal speedup at the five glaciers varies considerably, from 21 % and 49 % (Table 4.1). Russell Glacier, however, was the only glacier in the sector to present interannual variability in flow, amounting to a 32 % speedup between 2016 and 2017 (Figure 4.3). I also mapped, for the first time, the detailed spatial variation in speedup, revealing a marked altitudinal variation in the persistence of fast flow during summer (Figure 6.2). Altogether, my work on land-terminating glaciers has demonstrated the unique benefit of Sentinel-1’s high temporal sampling for track short-term changes in speed due to surface melting (Figure 4.6).

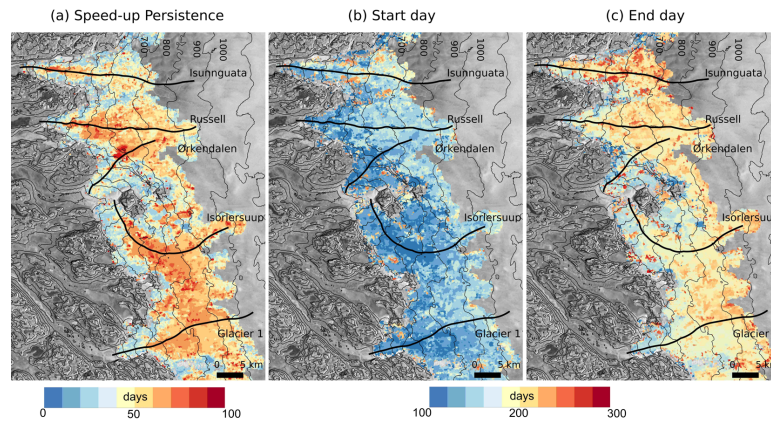


Figure 6.2: Copy of Figure 4.5. Persistence of ice speedup (a), the start (b) and end date (c) of the summer season.

Fluctuations in marine-terminating glacier flow using Sentinel-2

Chapter 4 demonstrated the potential of the Sentinel-2 constellation, a multi-spectral imager, to complement and continue systematic records of glacier and ice sheet motion

determined from other sensors. I showed the influence of clouds and shadows in the optical images (Figures 5.1 and 5.2), and how they impact on the capability to identify and track the movement of different glaciological features. The combined use of the Sentinel-2 constellation with Sentinel-1 not only shows how high spatiotemporal resolution of images is essential for tracking subtle changes in motion, but also the value in obtaining frequent observations of the polar regions all year-round. I first used the Sentinel-2 imagery to track the drift of icebergs in the ocean, drifting at 250 m day^{-1} (Figure 5.3), variations in the position of a marine-terminating glacier calving front (Figure 5.4), and changes of 0.23 km^2 in the extent of supraglacial lakes (Figure 6.3). The sharpness and fine spatial resolution of the Sentinel-2 true-colour composite images better define the ice front and lake edges when compared to Sentinel-1 SAR imagery. Furthermore, in order to assess Sentinel-2's performance for tracking ice motion, I generated surface ice velocity maps in spring, summer, and autumn, using cloud-free images and a cross-correlation feature tracking algorithm. Sentinel-2 performed very well at the Jakobshavn Isbræ when compared to measurements recorded by Sentinel-1 and presented in Chapter 2. The Sentinel-2 ice motion maps show near-complete coverage in summer (93 %), complementing the near-complete (98 %) coverage of Sentinel-1 in winter (Figures 5.6 and 5.7). Finally, I demonstrated the value of the combined use of Sentinel-1 and -2, which together offer - for the first time in the satellite era - the opportunity to map changes in glacier dynamics every 2 days.

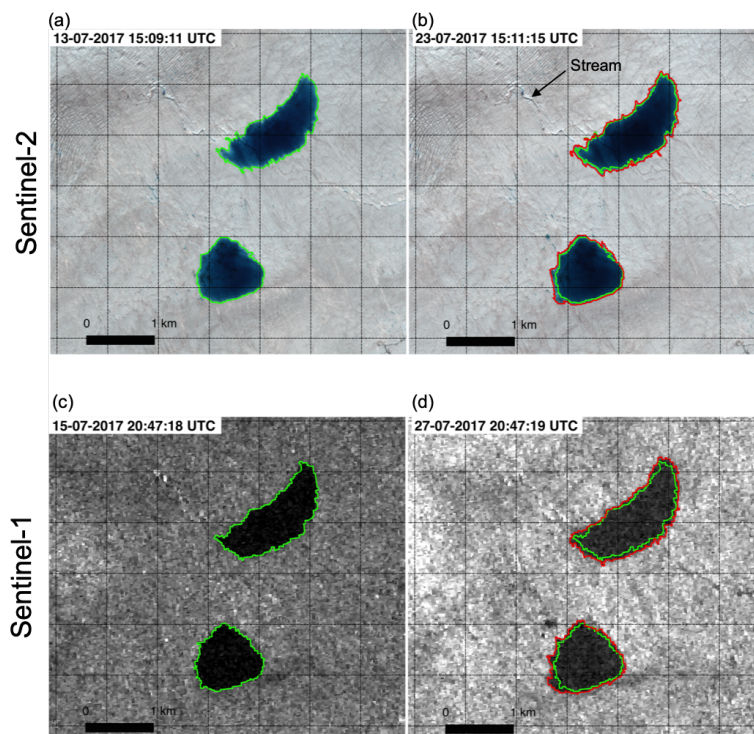


Figure 6.3: Copy of Figure 5.5. Supraglacial lakes observed in true-colour composite Sentinel-2 (a-b) and SAR Sentinel-1 (c-d) imagery (see magenta square in Figure 3.1b for location). The gridline is spaced by 750 m x 750 m. Solid green and red lines represent digitized features from the scenes a,c and b,d respectively.

6.2 Synthesis of the main conclusions

A core aim of this thesis was to explore the potential of Sentinel-1, a relatively new satellite mission, for tracking ice motion in the polar regions. In all three results chapters, I explored the unique characteristics of the mission and how it can help us to better monitor and analyse the flow of the Greenland ice sheet. The Sentinel-1 constellation offers, for the first time in the history of synthetic aperture radar missions, the opportunity for systematic sampling every 6-days across the entire ice sheet marginal zone. Different sectors of the ice sheet are known to respond differently to the environmental forcing they experience. In my thesis, I demonstrated the value of Sentinel-1 for tracking both seasonal and interannual changes in ice motion over marine- and

land-terminating sectors of the ice sheet. Moreover, I showed Sentinel-1's ability to determine changes in the speed of both slow- and fast-flowing glaciers, with velocities ranging from $\sim 200 \text{ m yr}^{-1}$ to $12,000 \text{ m yr}^{-1}$. The short-period acquisition also allowed me to track motion at the ice front of Jakobshavn Isbræ, which is exceptionally fast in glaciological terms. Furthermore, the availability of multiple acquisitions helped me to map, for the first time, the start and end dates of the summer speedup period in a land-terminating sector of central-west Greenland, highlighting marked differences among the regional glaciers. Overall, my thesis has demonstrated that the Sentinel-1 mission is capable of continuing the observational records that began with other sensors, identifying signals of dynamic imbalance, and helping us to understand the factors which drive short- and long-term changes in ice motion.

A second aim of this thesis, as well as the third objective, was to assess how variations in glacier flow relate to and reflect local environmental change over short (i.e. seasonal) and intermediate (multi-annual) timescales. In Chapter 3, I demonstrated the strong influence of calving events in triggering seasonal changes of ice motion over the last eight years in Jakobshavn Isbræ. Using Sentinel-1 data I showed, for example, that for every kilometre of calving front retreat the speed of Jakobshavn Isbræ increases by 1800 m yr^{-1} (Figure 6.4a). This forcing has both a seasonal cycle as the calving front advances and retreats in winter and summer, respectively, plus a longer-term signal associated with progressive collapse and retreat of the glaciers floating ice tongue (Joughin et al., 2008, 2012, 2014). However, since 2012, after consecutive years of retreat and speedup, I showed that Jakobshavn Isbræ has finally started to slow down, exhibiting a 321 m yr^{-2} decrease in speed. The underlying cause of this deceleration requires further investigation. However, Khazendar et al. (2019) linked the fact to the intrusion of cooled ocean current in Disko Bay. Although the land-terminating glaciers studied in Chapter 4 also showed seasonal changes in flow, this is due to changes in their inland hydrology. In west central Greenland, I showed that the seasonal speedup persisted for around 90 days, mirroring the seasonal cycle of melting at the ice sheet surface as estimated from air temperature measurements recorded at a nearby weather station (Figure 6.4b). On detailed inspection, the glaciers presented later spikes in velocities matching short-lived peaks of melting, further supporting my conclusion that the speedup is driven by the excess of meltwater input in the ice sheet bed. Finally, although changing oceanic

6.2 Synthesis of the main conclusions

conditions are generally assumed to control the flow of marine-terminating glaciers, Petermann Glacier exhibited unusual behaviour. The glacier presented the highest seasonal changes in speed among the marine-terminating glaciers included in my survey – a 25 % increased over a 25-day period, despite a ~ 1 km advance of its calving front. This suggests that, in contrast to other marine-terminating glaciers, changes in basal lubrication could be the dominant control on flow variability at Petermann Glacier.

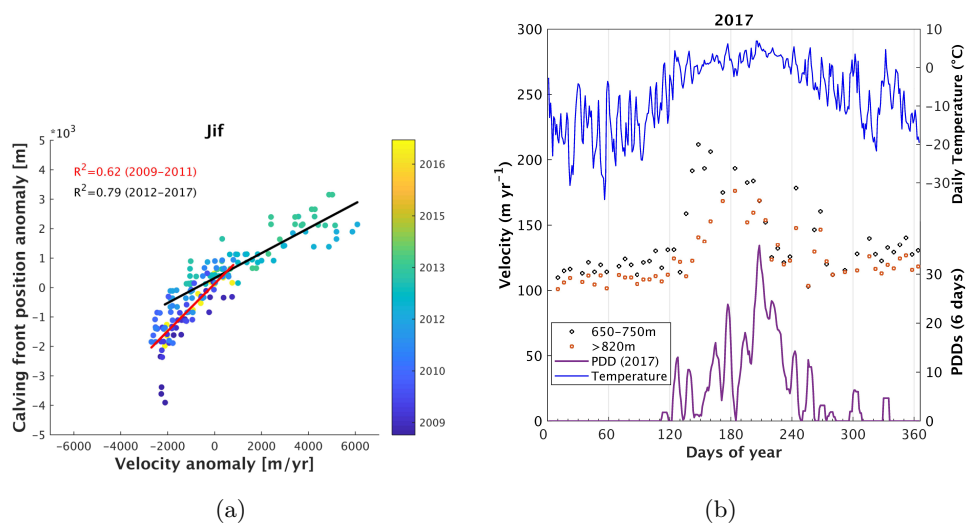


Figure 6.4: Copy of (a) Figure 3.6 and (b) Figure 4.6. In (a): Comparison between Jakobshavn Isbræ ice velocity and calving front position anomalies at the Jif site, 0.8 km upstream of the calving front, between 2009 and early 2017. Positive values correspond to ice front retreat and speed up respectively. The red and black lines represent the linear regression through the 2009-2011 and 2012-2017 periods, respectively, together with the correlation coefficients (R^2). In (b): Averaged speed of three glaciers (G1, IG, and RG) with similar geometry and data sampling at two elevations bands during 2017. Also shown are daily temperature and positive degree days (PDDs) recorded at the nearby KAN L automatic weather station (670 m.a.s.l.) and distributed by the Programme for Monitoring of the Greenland Ice Sheet.

The modern era of satellite-based earth observation is unique. Since the launch of the Sentinel-1 and Sentinel-2 constellations, the planet’s surface has been systematically and frequently monitored by multiple sensors. Because synthetic aperture radar and optical images have different strengths and weaknesses, the optimal approach to

monitoring glacier flow is to combine their measurements, to reduce the dependency on mission-specific limitations. In Chapter 3, I produced a three-year time series of Greenland glacier flow variations using Sentinel-1a/b and merged these with an eight-year time series produced from TerraSAR-X to create a single and consistent record of change. In Chapter 5, I illustrated the added value of Sentinel-2's multi-spectral sensor for tracking features in high spatial resolution, and in augmenting measurements developed from Sentinel-1 SAR imagery. Overall, there is good agreement between automated estimated of ice motion determined from repeat imagery acquired by each mission, and when combined they offer improved temporal sampling. The combined use of multiple missions increases the capability for monitoring subtle and short-term changes and movement of numerous glaciological features. Examples of this shown in Chapter 5 include the drift of icebergs, the movement of glacier calving fronts, and the growth in area of supraglacial lakes. Each of these features changes rapidly, and through combination can be surveyed every 2 days using both Sentinel-1 and Sentinel-2. Finally, I have shown that Sentinel-2 optical data prove to be a promising product for extending existing time-series of ice motion determined from Sentinel-1 SAR imagery, as the two image classes perform best in opposing seasons - thereby increasing the temporal sampling.

6.3 Recommendations for future work

In Chapters 3 and 4, I demonstrated Sentinel-1's capability to derive velocity on fast- and slow-moving glaciers in Greenland all year around. Because the constellation mission is a 20-year operational program, its measurements can be relied upon over the long-term. Because of this, operational services such as the Centre for Polar Observation and Modelling near-real-time ice velocity data portal (<http://www.cpom.ucl.ac.uk/csopr/iv/>) can reliably be extended to include slow moving sectors of Antarctica and Greenland, in addition to the principal outlet glaciers. Moreover, I would recommend the use of the extra-wide swath mode (EW) mode along the margins, which has similar as the interferometric wide swath mode. This will require only modest changes to processing systems to tailor the tracking procedure to detect slow movement. Frequent and long-term velocity measurements would then allow us to better understand seasonal and interannual variations in ice flow. For instance, the Austfonna ice cap in Svalbard

increased its discharge by 45-fold, and over the last twenty years, changed the velocity regime flow (McMillan et al., 2014). Furthermore, I would extend the systematic ice motion estimation to the northern region of the Antarctic Peninsula. This region has demonstrated, through a multi-mission analysis until late 2014, different responses in motion due to ice front variation (Seehaus et al., 2018), leading to a detailed and continuous monitoring in order to understand the main causes. The estimated errors can be improved by applying high-pass spatial-frequency filter prior to the main process chain, as suggested by de Lange et al. (2007). In Chapter 4, I produced example maps of documenting spatial variations in the persistence of summertime ice speedup; this is a promising area for future research given that systematic observations with high temporal frequency will continue to be routine. The new technique still needs improvement in order to be more robust and then can be applied to other polar regions. In the first instance, the technique could be extended to determine the persistence of speedup in other sectors of the ice sheet, such as the marine-terminating glaciers presented in Chapter 3, Petermann Glacier, Nioghalvfjerdingsfjorden and Zachariæ Isstrøm. Similarly, identifying the start and end dates on which speedup occurs at individual glaciers will inform on how they evolve in time. Such measurements will be of additional value both for identifying emerging signals of dynamic imbalance and for understanding processes driving velocity change.

Sentinel-2 is also a long-term mission with a systematic data acquisition strategy, and the complementarity of its images for tracking ice motion makes it a promising dataset for monitoring glacier change. The mission increased both the frequency and seasonality of temporal sampling, overcoming some weakness of tracking motion with synthetic aperture radar imagery. Sentinel-2's relatively fine spatial resolution is particularly suited to estimate ice motion in challenging regions, mainly due to irregular terrain, such as the Antarctic Peninsula and High Mountain glaciers in Asia, as has been demonstrated by Gardner et al. (2018) and Dehecq et al. (2019), using Landsat imagery. Moreover, mountainous glaciers in South America, such as Patagonia and the Andes, are also challenging regions to extract velocity data due to temporal decorrelation and high slope terrains (Mouginot and Rignot, 2015). The continuous monitoring of these regions would allow us to better understand not only the dynamics of these glaciers but also their seasonality, which is of wider importance because mountain communities rely

on glaciers as a water resource. I showed that optical images are, however, affected by the presence of clouds and shadows, which are extremely challenging to be identified over snowy regions (Paul et al., 2016). Thus, I would recommend further investigation, in order to improve the automated method to detect clouds and shadows, which will facilitate the use of the optical images during a processing chain to estimate ice velocity, or identify glaciological features. In addition to tracking ice motion, Sentinel-1 and Sentinel-2 images support the detection of other glacier features such as the formation of supraglacial and pro-glacial lakes; more frequent monitoring of these targets may help local communities and operators to avoid risk – for example from glacier lake outburst floods which are responsible for the sudden release of large volumes of water (Grabs and Hanisch, 1993; Carrivick and Tweed, 2016). I also recommend expanding the work presented in Chapters 5 to use Sentinel-1 and Sentinel-2 to monitor glacier change with high temporal sampling. For instance, frequent monitoring iceberg calving will inform on glacier boundary conditions and also on potential shipping hazards.

In this thesis I have shown that high temporal acquisition frequency provided by the new satellite missions are valuable tool for the large-scale analysis of the ice sheet surface, in order to understand how it responds to regional environmental changes. The new Sentinel-1 and Sentinel-2 data sets are extremely valuable resources that can and should be used to extend ice motion time series measurements back to the early 1990s, and provide an unprecedented opportunity to monitor ice discharge over several decades.

References

- I. D. Bartholomew, P. Nienow, D. Mair, A. Hubbard, M. a. King, and A. Sole. Seasonal evolution of subglacial drainage and acceleration in a Greenland outlet glacier. *Nature Geoscience*, 3(6):408–411, 2010. ISSN 1752-0894. doi: 10.1038/ngeo863. URL <http://www.nature.com/doifinder/10.1038/ngeo863>. 145
- I. D. Bartholomew, P. Nienow, A. Sole, D. Mair, T. Cowton, and M. a. King. Short-term variability in Greenland Ice Sheet motion forced by time-varying meltwater drainage: Implications for the relationship between subglacial drainage system behavior and

- ice velocity. *Journal of Geophysical Research: Earth Surface*, 117:1–17, 2012. ISSN 21699011. doi: 10.1029/2011JF002220,2012. 146
- J. R. Carr, C. R. Stokes, and A. Vieli. Threefold increase in marine-terminating outlet glacier retreat rates across the Atlantic Arctic: 1992–2010. *Annals of Glaciology*, 58(74):72–91, 2017. ISSN 02603055. doi: 10.1017/aog.2017.3. 144
- J. L. Carrivick and F. S. Tweed. A global assessment of the societal impacts of glacier outburst floods. *Global and Planetary Change*, 144:1–16, 2016. ISSN 09218181. doi: 10.1016/j.gloplacha.2016.07.001. URL <http://dx.doi.org/10.1016/j.gloplacha.2016.07.001>. 153
- V. W. Chu. *Greenland ice sheet hydrology: A review*, volume 38. 2014. ISBN 0309133313507. doi: 10.1177/0309133313507075. URL <http://ppg.sagepub.com/cgi/doi/10.1177/0309133313507075>. 145
- R. de Lange, A. Luckman, and T. Murray. Improvement of satellite radar feature tracking for ice velocity derivation by spatial frequency filtering. *IEEE Transactions on Geoscience and Remote Sensing*, 45(7):2309–2318, 2007. ISSN 01962892. doi: 10.1109/TGRS.2007.896615. 152
- A. Dehecq, N. Gourmelen, A. S. Gardner, F. Brun, D. Goldberg, P. W. Nienow, E. Berthier, C. Vincent, P. Wagnon, and E. Trouvé. Twenty-first century glacier slowdown driven by mass loss in High Mountain Asia. *Nature Geoscience*, 12(January), 2019. ISSN 1752-0894. doi: 10.1038/s41561-018-0271-9. URL https://www.nature.com/articles/s41561-018-0271-9?utm_source=researcher&utm_medium=referral&utm_campaign=MKEF_USG_Researcher_inbound. 152
- E. M. Enderlin, I. M. Howat, S. Jeong, M.-J. Noh, J. H. van Angelen, and M. R. van den Broeke. An improved mass budget for the Greenland ice sheet. *Geophys. Res. Lett.*, 41:1–7, 2014. doi: 10.1002/2013GL059010.Received. 144
- A. S. Gardner, G. Moholdt, T. Scambos, M. Fahnestock, S. Ligtenberg, and M. V. D. Broeke. Increased West Antarctic ice discharge and East Antarctic stability over the last seven years. *The Cryosphere*, 12:521–547, 2018. doi: <https://doi.org/10.5194/tc-12-521-2018>. 152

- W. E. Grabs and J. Hanisch. Objectives and Prevention Methods for Glacier Lake Outburst Moods (GLOFs). *Snow and Glacier Hydrology*, (218):341–352, 1993. URL <http://www.novacenturion.co.uk/>. 153
- M. J. Hoffman, G. A. Catania, T. A. Neumann, L. C. Andrews, and J. A. Rumrill. Links between acceleration, melting, and supraglacial lake drainage of the western Greenland Ice Sheet. *Journal of Geophysical Research: Earth Surface*, 116(4):1–16, 2011. ISSN 21699011. doi: 10.1029/2010JF001934. 145
- D. M. Holland, R. H. Thomas, B. D. Young, M. H. Ribergaard, and B. Lyberth. Acceleration of Jakobshavn Isbræ triggered by warm subsurface ocean waters. *Nature Geoscience*, 1:1–6, 2008. doi: 10.1038/ngeo316. 144
- I. Joughin, I. M. Howat, M. Fahnestock, B. Smith, W. Krabill, R. B. Alley, H. Stern, and M. Truffer. Continued evolution of Jakobshavn Isbrae following its rapid speedup. *Journal of Geophysical Research: Earth Surface*, 113(4):1–14, 2008. ISSN 21699011. doi: 10.1029/2008JF001023. 149
- I. Joughin, B. E. Smith, I. M. Howat, D. Floricioiu, R. B. Alley, M. Truffer, and M. Fahnestock. Seasonal to decadal scale variations in the surface velocity of Jakobshavn Isbrae, Greenland: Observation and model-based analysis. *Journal of Geophysical Research: Earth Surface*, 117(2):1–20, 2012. ISSN 21699011. doi: 10.1029/2011JF002110. 149
- I. Joughin, B. E. Smith, D. E. Shean, and D. Floricioiu. Brief communication: Further summer speedup of Jakobshavn Isbræ. *The Cryosphere*, 8(1):209–214, 2014. ISSN 19940416. doi: 10.5194/tc-8-209-2014. 149
- A. Khazendar, I. G. Fenty, D. Carroll, A. Gardner, C. M. Lee, I. Fukumori, O. Wang, H. Zhang, H. Seroussi, D. Moller, B. P. Y. Noël, M. R. van den Broeke, S. Dinardo, and J. Willis. Interruption of two decades of Jakobshavn Isbrae acceleration and thinning as regional ocean cools. *Nature Geoscience*, 2013, 2019. ISSN 1752-0894. doi: 10.1038/s41561-019-0329-3. URL <http://www.nature.com/articles/s41561-019-0329-3>. 149
- M. McMillan, A. Shepherd, N. Gourmelen, A. Dehecq, A. Leeson, A. Ridout, T. Flament, A. Hogg, L. Gilbert, T. Benham, M. D. Broeke, J. A. Dowdeswell, X. Fettweis,

REFERENCES

- B. Noël, and T. Strozzi. Rapid dynamic activation of a marine-based Arctic ice cap. *Geophysical Research Letters*, 41:8902–8909, 2014. doi: 10.1002/2014GL062255. 152
- J. Mouginot and E. Rignot. Ice motion of the Patagonian Icefields of South America : 1984 -2014. *Geophysical research letters*, 42:1441–1449, 2015. doi: 10.1002/2014GL062661.1. 152
- F. Paul, S. Winsvold, A. Kääb, T. Nagler, and G. Schwaizer. Glacier Remote Sensing Using Sentinel-2. Part II: Mapping Glacier Extents and Surface Facies, and Comparison to Landsat 8. *Remote Sensing*, 8(7):575, 2016. ISSN 2072-4292. doi: 10.3390/rs8070575. URL <http://www.mdpi.com/2072-4292/8/7/575>. 153
- T. Seehaus, A. J. Cook, A. B. Silva, and M. Braun. Changes in glacier dynamics in the northern Antarctic Peninsula since 1985. *Cryosphere*, 12(2):577–594, 2018. ISSN 19940424. doi: 10.5194/tc-12-577-2018. 152
- A. V. Sundal, A. Shepherd, P. Nienow, E. Hanna, S. Palmer, and P. Huybrechts. Melt-induced speed-up of Greenland ice sheet offset by efficient subglacial drainage. *Nature*, 469(7331):521–4, jan 2011. ISSN 1476-4687. doi: 10.1038/nature09740. URL <http://www.ncbi.nlm.nih.gov/pubmed/21270891>. 145

Appendix A

Appendix 1

A.1 Paper published in the journal *The Cryosphere*

The Cryosphere, 12, 2087–2097, 2018
 https://doi.org/10.5194/tc-12-2087-2018
 © Author(s) 2018. This work is distributed under
 the Creative Commons Attribution 4.0 License.



The Cryosphere  Open Access

Ice velocity of Jakobshavn Isbræ, Petermann Glacier, Nioghalvfjærdsfjorden, and Zachariæ Isstrøm, 2015–2017, from Sentinel 1-a/b SAR imagery

Adriano Lemos¹, Andrew Shepherd¹, Malcolm McMillan¹, Anna E. Hogg¹, Emma Hatton¹, and Ian Joughin²

¹Centre for Polar Observation and Modelling, University of Leeds, Leeds, UK

²Polar Science Center, Applied Physics Laboratory, University of Washington, Seattle, Washington, USA

Correspondence: Adriano Lemos (a.g.lemos14@leeds.ac.uk)

Received: 8 November 2017 – Discussion started: 12 February 2018

Revised: 12 May 2018 – Accepted: 30 May 2018 – Published: 18 June 2018

Abstract. Systematically monitoring Greenland’s outlet glaciers is central to understanding the timescales over which their flow and sea level contributions evolve. In this study we use data from the new Sentinel-1a/b satellite constellation to generate 187 velocity maps, covering four key outlet glaciers in Greenland: Jakobshavn Isbræ, Petermann Glacier, Nioghalvfjærdsfjorden, and Zachariæ Isstrøm. These data provide a new high temporal resolution record (6-day averaged solutions) of each glacier’s evolution since 2014, and resolve recent seasonal speedup periods and inter-annual changes in Greenland outlet glacier speed with an estimated certainty of 10 %. We find that since 2012, Jakobshavn Isbræ has been decelerating, and now flows approximately 1250 m yr^{-1} (10 %), slower than 5 years previously, thus reversing an increasing trend in ice velocity that has persisted during the last decade. Despite this, we show that seasonal variability in ice velocity remains significant: up to 750 m yr^{-1} (14 %) at a distance of 12 km inland of the terminus. We also use our new dataset to estimate the duration of speedup periods (80–95 days) and to demonstrate a strong relationship between ice front position and ice flow at Jakobshavn Isbræ, with increases in speed of $\sim 1800 \text{ m yr}^{-1}$ in response to 1 km of retreat. Elsewhere, we record significant seasonal changes in flow of up to 25 % (2015) and 18 % (2016) at Petermann Glacier and Zachariæ Isstrøm, respectively. This study provides a first demonstration of the capacity of a new era of operational radar satellites to provide frequent and timely monitoring of ice sheet flow, and to better resolve the timescales over which glacier dynamics evolve.

1 Introduction

Between 1992 and 2011, the Greenland Ice Sheet lost mass at an average rate of $142 \pm 49 \text{ Gt yr}^{-1}$ (Shepherd et al., 2012), increasing to $269 \pm 51 \text{ Gt yr}^{-1}$ between 2011 and 2014 (McMillan et al., 2016). Ice sheet mass balance is determined from the surface mass balance and ice discharge exported from the ice sheet (van den Broeke et al., 2009). In 2005, dynamic imbalance was responsible for roughly two-thirds of Greenland’s total mass balance, making an important contribution to freshwater input into the ocean and 0.34 mm yr^{-1} to the global sea level rise at that time (Rignot and Kanagaratnam, 2006). Despite the anomalous atmospheric warming events, especially in 2012 (Tedesco et al., 2013), presenting a more spatially extensive and longer lasting surface melt during this period, marine-terminating outlet glaciers in Greenland still contributed with roughly 30 % (2000–2012) of total mass loss (Enderlin et al., 2014). The observed acceleration of many marine-based glaciers in the western and northern regions of Greenland over the last decade may have been driven by rises in air and adjacent ocean temperatures, which enhanced the surface melting and terminus retreat (Holland et al., 2008; Moon et al., 2014, 2015). The associated increases in basal sliding and calving of their ice fronts in turn produce enhanced discharge, leading to dynamical imbalance and additional ice loss (Joughin et al., 2010, 2014). However, acceleration of marine-terminating glaciers is highly variable in space and time (Howat et al., 2010; Moon et al., 2012; Enderlin et al., 2014), due to the geometry of individual glaciers (Felixson et al., 2017), and the high spatial variability in the forcing mechanisms (Jensen et al.,

Published by Copernicus Publications on behalf of the European Geosciences Union.

2016; Carr et al., 2017). This complexity in glacier response challenges efforts to model their future evolution (Joughin et al., 2012; Bondzio et al., 2017) and, thus, frequent and systematic monitoring is essential to understand the processes governing their dynamic stability and contribution to future mean sea level rise (Joughin et al., 2010; Shepherd et al., 2012).

Ice motion measurements are essential for monitoring ice sheet dynamics and ice discharge, and for assessing an ice sheet's mass budget (Joughin et al., 1995). At present, the only way to monitor ice velocity at a continental scale is through satellite imagery. Glacier velocities were first measured using Landsat satellite data acquired during the 1970s through digital optical image comparison (Lucchitta and Ferguson, 1986). Currently, optical images are still largely used for mapping glaciers velocity at large scale (e.g. Dehecq et al., 2015; Fahnestock et al., 2016; Armstrong et al., 2017). However, due to the dependency upon daylight conditions and the limited acquisitions across the polar regions, the use of synthetic aperture radar (SAR) images has become common since the launch of ERS-1 in 1991. In the following decades, these data have been used to monitor dynamic processes occurring across remote areas such as the Greenland and Antarctic ice sheets (Joughin et al., 2010; Rignot and Mouginot, 2012; Nagler et al., 2015; Mouginot et al., 2017). More recently, after the launch by the European Space Agency (ESA) (2017) of the Sentinel 1-a and 1-b satellites, in April 2014 and April 2016, respectively, many key ice margin areas are systematically monitored every 6 to 12 days. This novel dataset provides the opportunity to systematically monitor the dynamical process driving glacier ice velocity over periodic and short temporal scales. Here we use the Sentinel SAR archive to investigate the temporal variation in ice flow since October 2014 at four large outlet glaciers of the Greenland Ice Sheet.

2 Study areas

In this study, we map ice velocity of the Jakobshavn Isbræ (JI), Petermann Glacier (PG), Nioghalvfjærdsfjorden (79-G) and Zachariæ Isstrøm (ZI), which are four of the largest marine-based ice streams in Greenland. Combined they contain ice equivalent to 1.8 m of global sea-level rise (Mouginot et al., 2015; Jensen et al., 2016) and drain $\sim 21.5\%$ of Greenland's ice (Rignot and Kanagaratnam, 2006; Rignot and Mouginot, 2012; Münchow et al., 2014).

Jakobshavn Isbræ terminates in the Ilulissat Icefjord in western Greenland (Fig. 1a) and is the fastest glacier draining the ice sheet (Enderlin et al., 2014; Joughin et al., 2014). During the late 1990s, the ice tongue experienced successive break-up events and the glacier began to speed up, exhibiting annual increases in speed of 7 % per year from 2004 and 2007 (Joughin et al., 2008a, 2012, 2014). Until 2012 and 2013, the speedup continued, reaching maximum velocities

in excess of 17 km yr^{-1} (Joughin et al., 2012, 2014). It has been suggested (van de Wal et al., 2015) that the speedup over this period in the southwest of Greenland might be enhanced by anomalously high melting across the ice sheet surface (Tedesco et al., 2013). Jakobshavn Isbræ is susceptible to changes in the adjacent ocean and Holland et al. (2008) have shown that warm water originating in the Irminger Sea likely enhanced basal melting and weakened the floating ice tongue, triggering its break up in 1997. Furthermore, Gladish et al. (2015) showed that the subsequent changes, which occurred between 2001 and 2014, were mainly triggered by changes in Ilulissat Icefjord water temperatures adjacent to the glacier. At present, JI is a tidewater glacier and has a bimodal behaviour, retreating by $\sim 3 \text{ km}$ during summer and advancing by a similar amount during winter seasons (Cassotto et al., 2015). Moreover, as showed by Jensen et al. (2016) through analysis of optical images from 1999 to 2013, it has not exhibited an unusually large change in area ($-10.3 \text{ km}^2 \text{ yr}^{-1}$).

Petermann Glacier flows into the Hall Basin in the Nares Strait in northwestern Greenland (Fig. 1b), and has a perennial floating ice tongue of 1280 km^2 in area (Hogg et al., 2016). PG is grounded on bedrock $\sim 300 \text{ m}$ below sea level and, thus, is also influenced by the adjacent ocean (Münchow et al., 2014; Hogg et al., 2016). The retreat of the ice stream calving front led to an area decrease of 352 km^2 from 1959 to 2008, 270 km^2 in 2010, and 130 km^2 in 2012 (Johannessen et al., 2013). It is considered a dynamically stable marine-terminating glacier despite several grounding line advancing and retreating events between 1992 and 2011, with a terminus retreat rate of 25.2 m a^{-1} (Hogg et al., 2016). PG has had an average velocity of $\sim 1100 \text{ m yr}^{-1}$ at its grounding line since the 1990s (Rignot, 1996; Rignot and Steffen, 2008) and a multi-annual trend (2006–2010) in flow speed of 30 m yr^{-2} (Nick et al., 2012). The ice shelf is thicker than 100 m and it is 15 km wide, with low resistive stresses along flow due to the limited attachment to the fjord walls, diminishing the velocity response after calving events (Nick et al., 2012).

Nioghalvfjærdsfjorden and Zachariæ Isstrøm are situated in the northeast of Greenland (Fig. 1c and d respectively). The two glaciers together drain more than 10 % of the Greenland Ice Sheet (Rignot and Mouginot, 2012), and their maximum velocities are found near the grounding line. They have exhibited different behaviour in recent years, although located in the same region. 79-G underwent a modest velocity increase of $\sim 150 \text{ m yr}^{-1}$ between 2001 and 2011 at the grounding line (Khan et al., 2014). In contrast, during the same period, ZI exhibited a much larger increase in speed greater than 600 m yr^{-1} (Khan et al., 2014). The ice thinning rates above the grounding line vary from 5.1 m yr^{-1} in ZI (2010–2014) to 1.4 m yr^{-1} in 79-G (2012–2014) (Mouginot et al., 2015). Between 1999 and 2013, ZI has undergone an average area change of $-26.0 \text{ km}^2 \text{ yr}^{-1}$, due to break off of the ice tongue and is now a tidewater glacier (Khan et al., 2014; Jensen et al., 2016). In contrast, 79-G had a

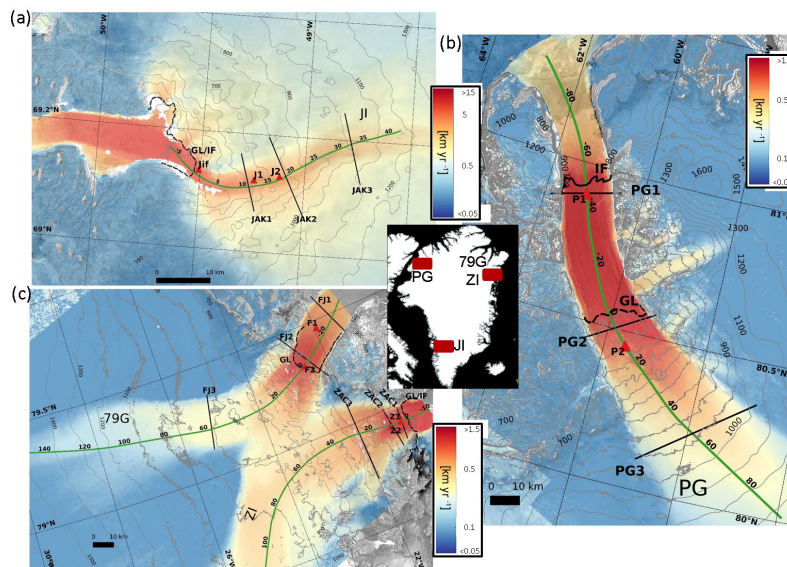


Figure 1. Time-averaged ice velocity magnitude maps for the period October 2014–February 2017: (a) Jakobshavn Isbræ (JI; 69° N, 50° W), (b) Petermann Glacier (PG; 81° N, 62° W), (c) Nioghalvfjærdssjorden (79G; 79° N, 20° W), and Zachariae Isstrøm (ZI; 78° N, 20° W) glaciers, derived from Sentinel-1 SAR images. Velocities are shown on a logarithmic scale and overlaid on a SAR backscatter intensity image and thin grey lines represent elevation. The along-flow profiles are indicated by solid green lines scaled in kilometres, the solid black lines show the across-flow transects, the red triangles represent the locations at which velocity time series are extracted, and the thick solid and dashed black lines represent the ice front locations (IF) and the grounding lines (GL), respectively. The inset figures show the location of each glacier.

much lower average area change during the same period of $-4.7 \text{ km}^2 \text{ yr}^{-1}$ and still retains a small ice shelf (Jensen et al., 2016), although recent ice shelf thinning (Mouginot et al., 2015) may increase vulnerability to break-up in the future.

3 Data and methodology

To map ice velocity, we used single look complex (SLC) synthetic aperture radar images acquired in the interferometric wide swath (IW) mode from the Sentinel-1a and Sentinel-1b satellites. Data used in this study were acquired in the period spanning from October 2014 to February 2017 and from October 2016 to February 2017, for Sentinel-1a and Sentinel-1b, respectively (Fig. S2 and Table S1 in the Supplement). Each satellite has a repeat cycle of 12 days and 180 degrees orbital phasing difference, resulting in a revisit time of 6 days over the same area after the Sentinel-1b launch. The Sentinel SAR instruments operate at c-band, with a centre frequency of 5.405 GHz, corresponding to a wavelength of 5.55 cm. The IW mode has a 250 km swath and spatial resolution of 5 m in ground range and 20 m in azimuth. It has burst synchronization for interferometry and acquires data in three

sub-swaths, each containing a series of bursts, which are acquired using the Terrain Observation with Progressive Scans SAR (TOPSAR) imaging technique (Yague-Martinez et al., 2016). We followed the workflow described below to derive 187 ice velocity maps from pairs of Sentinel-1a/b SAR images over Jakobshavn Isbræ, Petermann Glacier, Nioghalvfjærdssjorden and Zachariae Isstrøm, using the GAMMA-SAR software (Gamma Remote Sensing, 2015).

We used the SAR intensity tracking technique (Strozzi et al., 2002) to estimate surface ice velocities due to glacier flow, assuming that the ice flow occurs parallel to the surface. This method uses a cross-correlation algorithm applied to image patches (Strozzi et al., 2002; Pritchard et al., 2005; Paul et al., 2015) to estimate offsets between similar features, such as crevasses and radar speckle patterns, in two co-registered SAR images (Table S1). Images were co-registered using the precise orbit information, available 20 days after the image acquisition, establishing a co-registration accuracy of 5 cm 3-D $1-\sigma$ (Sentinels POD team, 2013). The elimination of the orbital offsets isolates displacement due to the glacier movement (Strozzi et al., 2002). To estimate ice flow, we then used windows sizes of 350 pixels in ground range ($\sim 1.7 \text{ km}$) and 75 pixels in azimuth ($\sim 1.5 \text{ km}$) for each glacier, to produce

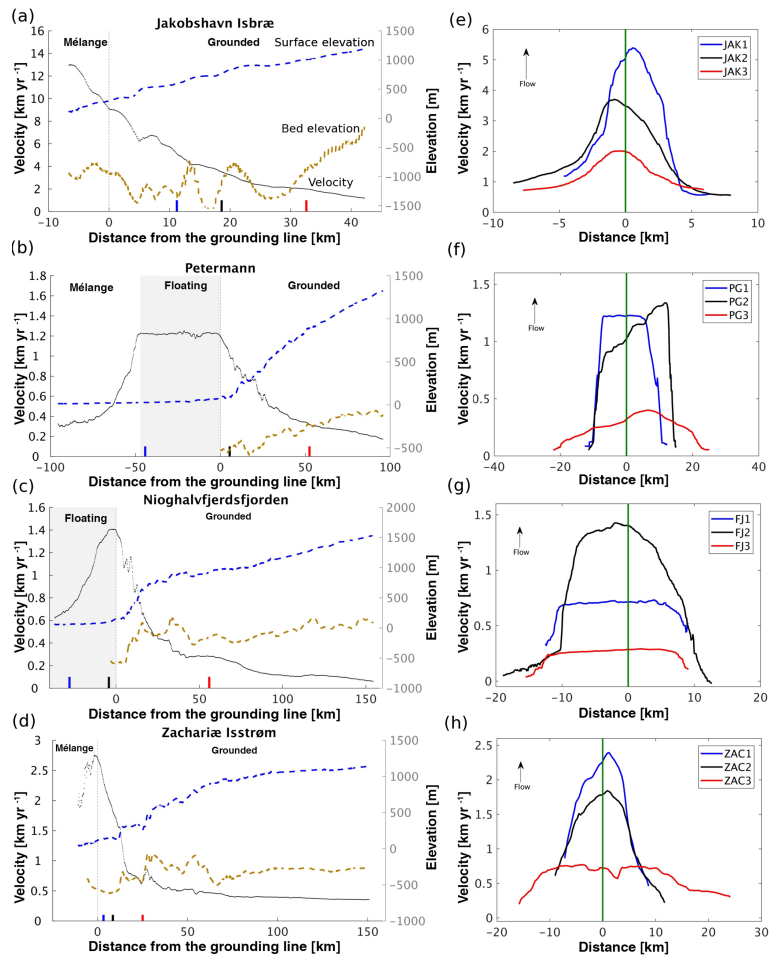


Figure 2. Average velocities (2014–2017) extracted from along- and across-flow profiles of Jakobshavn Isbræ, Petermann Glacier, Nioghalvfjærdsfjorden, and Zachariæ Isstrøm. Panels (a–d) present along-flow profiles of ice velocity (solid black lines), surface elevation from the GIMP DEM (Howat et al., 2014; dashed blue lines) and bed elevation from the IceBridge BedMachine Greenland V2 product (Morlighem et al., 2015; dashed yellow lines). The location of each profile is shown in Fig. 1 (green lines). The grey shaded area represents the floating regions, and the light grey dashed line the ice front positions. The blue, black, and red markers represent the locations of the across-flow profiles. (e–h) show the across-flow velocity profiles (solid white lines in Fig. 1), centred on the main profile (solid green line).

a series of velocity maps with spatial resolution of 388 m in ground range and 320 m in azimuth.

Image matches with low certainty, defined as returning a normalized cross-correlation of less than 5 % of its maximum peak, were rejected and the results were then converted into displacement in ground range coordinates using the Greenland Ice Mapping Project (GIMP) digital elevation model (DEM) posted on a 90 m grid (Howat et al., 2014). Along- and across-track displacement components were combined

to determine the displacement magnitude, which was then converted to an estimate of annual velocity using the temporal baseline of each image pair. Final velocity products were posted on 100 m by 100 m grids. Post-processing of ice velocity data reduces noise and removes outliers (Paul et al., 2015), so we applied a low-pass filter (moving mean) twice to the data, using a kernel of 1 km by 1 km, and we reject values where the deviation between the unfiltered and filtered velocity magnitude exceeds 30 %. We apply a labelling algo-

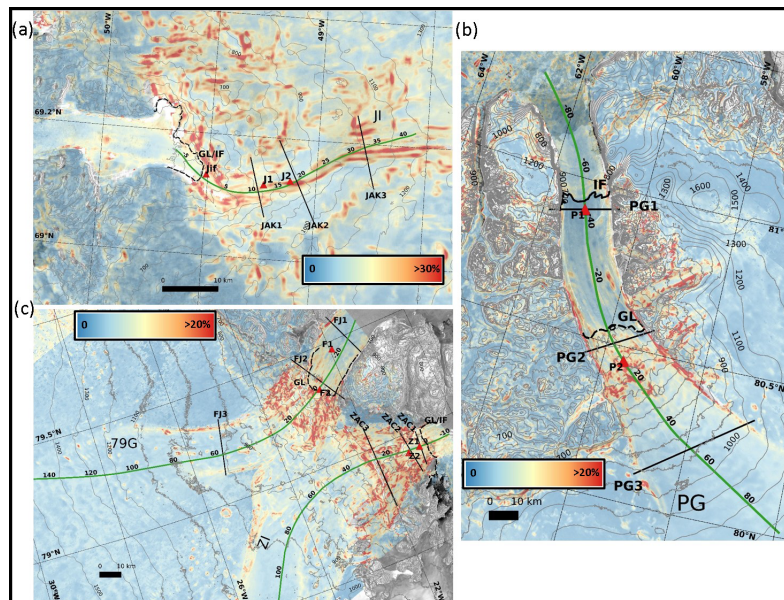


Figure 3. Time-averaged (2014–2017) uncertainty in ice velocity at each site expressed in percentage, based on the signal-to-noise ratio (SNR) for (a) JI, (b) PG, and (c) 79G and ZI.

rithm, based on the image histogram, to identify and classify regions with similar values, excluding isolated pixels with a non-coherent area of velocity values, or where the area of the classified region was smaller than 1/1000th of the processed image size.

Errors in our velocity estimates arise primarily through inexact co-registration of the SAR images, uncertainties in the digital elevation model used in the terrain correction, and fluctuations in ionospheric activity and tropospheric water vapour (Nagler et al., 2015; Hogg et al., 2017). To estimate the accuracy of our Sentinel-1 average velocity data (Figs. 1 and 3) we computed pixel-by-pixel errors based on the signal-to-noise ratio (SNR) of the cross-correlation function (Hogg et al., 2017). The SNR is the ratio between the cross-correlation function peak (C_p) and the average correlation level (C_l) on the tracking window used to estimate the velocities (de Lange et al., 2007). We then averaged these estimates across all images in our temporal stack to determine the percentage errors associated with our mean velocity maps (Fig. 3). Although in isolated areas the error exceeds 30 %, the mean error across the whole imaged area was approximately 10 % for JI, 7 % for PG, and 8 % for 79G and ZI. Due to the non-uniform flow, lack of stable features, and remaining geometry distortions, the four glaciers exhibit higher errors across their faster flowing and steeper areas, and along the shear margins. Where localized rates of surface elevation

change are high, the surface slope may have evolved away from that of the GIMP DEM used in our processing. To assess the sensitivity of our velocity estimates to this effect, we selected the JI site where thinning is most pronounced, and used airborne estimates of elevation change from IceBridge and Pre-Icebridge data acquired from the NASA Airborne Topographic Mapper (ATM) (Studinger, 2014) to update the DEM. We find that in this extreme case, the large thinning rates ($\sim 12 \text{ m yr}^{-1}$) may introduce an additional uncertainty of $200\text{--}300 \text{ m yr}^{-1}$ which may bias the velocity estimates in this region, albeit limited to the first 10 km upstream of the grounding line (Table S2). Over floating ice tongues, uncompensated vertical tidal displacement may also introduce additional uncertainty into our velocity fields. The sensitivity of our results to this effect was assessed based upon a net 50 cm tidal displacement over 6–12-day repeat period and a centre swath incidence angle of 35 degrees. We estimate that such a tidal signal would introduce $\sim 20\text{--}40 \text{ m yr}^{-1}$ additional uncertainty into the ground range component of our velocity fields. In the context of this study, this uncertainty does not affect the results at JI or ZI, and it is limited only to the floating sections of PG and 79G.

To provide an independent evaluation of our ice velocity dataset, we finally compared them (Table S1) to independent estimates derived from TerraSAR-X (TSX) SAR imagery through the speckle tracking technique (Joughin,

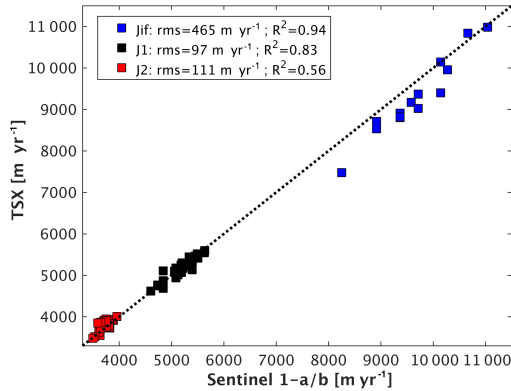


Figure 4. Comparison between co-located and contemporaneous Sentinel 1-a/b (6 to 12 days average) and TerraSAR-X (11 days average) Jakobshavn Isbræ velocity measurements at Jif, J1 and J2 locations (blue, black and red squares, respectively), together with root mean square (rms) and correlation coefficients (R^2).

2002), which has a repeat period acquisition of 11 days and spatial resolution up to 3 m (Joughin et al., 2016). The TSX data consist of 444 image pairs covering Jakobshavn Isbræ over the period January 2009 to January 2017, 18 pairs at Petermann Glacier over the period November 2010 to December 2016, and 17 pairs at Nioghalvfjærdsfjorden over the period March 2011 to December 2016. In general, the temporal evolution of the S1-a/b measurements matches very closely with the TSX estimates. At JI, we are able to compare S1 and TSX datasets at three different locations to assess their consistency (Fig. 4). Even though the flow speed at these sites is high, which typically proves more challenging for feature tracking techniques, we find good agreement between the two datasets, especially at the J1 and J2 sites, with mean differences of 40 and 76 m yr^{-1} respectively. However, nearer to the calving front (site Jif), the S1-a/b measurements tend to give significantly higher velocities than TSX with a mean difference of 489 m yr^{-1} (5% of the mean velocity) between the two datasets.

4 Results and discussion

We used our complete Sentinel-1a/b dataset (Table S1) to generate contemporary, time-averaged velocity fields at each of our study sites (Fig. 1). To investigate spatial and temporal variations in ice velocity, we then extracted profiles in the along- and across-flow directions, together with time series at fixed glacier locations (Fig. 1). Our velocity profiles in Jakobshavn Isbræ, Petermann Glacier, Nioghalvfjærdsfjorden, and Zachariæ Isstrøm reached maximum mean speeds, along the stacked dataset (averaged over the period 2014–2017), of approximately 9, 1.2, 1.4, and 2.7 km yr^{-1} , respec-

Table 1. Speedup persistence and seasonal percentage increase in speed relative to winter and annual background for each glacier for the Sentinel 1 dataset. Speedup persistence has an uncertainty of ± 12 days due to the image acquisition interval of Sentinel 1a.

	Speedup persistence	Summer speedup (%)	$V_{\text{annual}}/ V_{\text{winter}}$ (%)
JI (J1)	95 days (2015)	14 %	6 %
	80 days (2016)	9 %	4 %
PG (P1)	25 days (2015)	25 %	0 %
	55 days (2016)	17 %	6 %
79G (F2)	45 days (2016)	10 %	1 %
ZI (Z1)	45 days (2016)	18 %	3 %

tively. The location of the velocity maxima varied between glaciers, as a result of their differing geometries. For JI and ZI, neither of which have a significant floating tongue, we find a progressive increase in ice velocity towards the calving front (Fig. 2a and d). For PG, the maximum velocity is reached at the grounding line and remains steady along the ~ 46 km of ice tongue (Fig. 2b). In contrast, although 79G also reaches its maximum velocity close to the grounding line, its speed then diminishes by ~ 50 % (Fig. 2c) near the ice front location where the ice flow divides into two main portions before it reaches several islands and ice rises (Fig. S1b). Furthermore, it is interesting to note that, despite being located in the same region, the adjacent glacier ZI flows ~ 60 % faster in comparison. JI, PG, and ZI glaciers show velocity increases progressively downstream across the transverse profiles. The four glaciers, JI, PG, 79G and ZI respectively reduce their maximum velocity to half at distances of 12, 22, 18, and 12 km inland of their grounding lines, highlighting the importance of resolving glacier velocities within their near terminus regions.

Next, we used the Sentinel-1a/b and TerraSAR-X velocities to assess the seasonal and longer-term variations in Jakobshavn Isbræ ice velocity over the period 2009–2017. Our Sentinel-1a/b velocity estimates at JI resolve clear seasonal velocity fluctuations, superimposed upon longer term decadal-scale variability, which continues observations made by previous satellite instruments (Joughin et al., 2012, 2014). At site J1 we find an average seasonal change in speed of 750 m yr^{-1} , or 14 % between 2014 and 2015 and a speedup persistence of 80–95 days, twice as long than those for the other three glaciers (Table 1). Inland, the amplitude of seasonal variability diminishes, to an average of 300 m yr^{-1} (8 %) at J2. Our near-continuous, decadal-scale record clearly shows that the amplitude of the seasonal signal has evolved through time. At J1, for example, the average seasonal variability in ice speed was 400 m yr^{-1} during 2009–2011, increasing by more than a factor of 3, to

A. Lemos et al.: Sentinel 1-a/b SAR imagery

2093

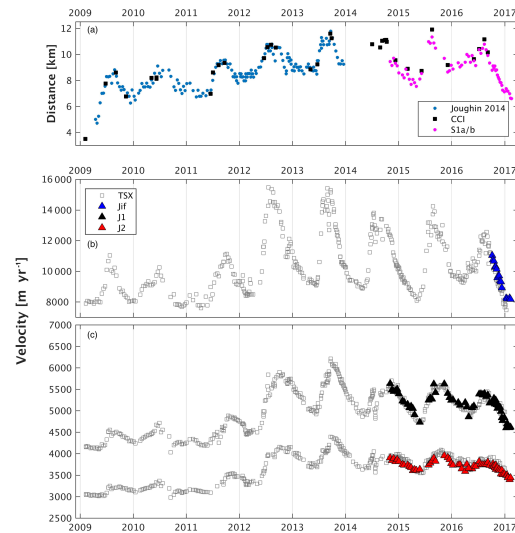


Figure 5. Temporal evolution of Jakobshavn Isbræ (a) ice front position extracted from Joughin et al. (2014), ESA Greenland Ice Sheet Climate Change Initiative (CCI) project (2017), and Sentinel-1a/b SAR images represented in blue, black, and magenta dots, respectively, where higher values correspond to ice front retreat. Changes in ice velocity through time is also shown (b, c), extracted at the locations indicated in Fig. 1. The velocity data derived from TerraSAR-X (11 days – Joughin et al., 2016) are shown as grey squares, and the data from Sentinel 1-a/b (6 to 12 days) as coloured triangles.

1400 m yr⁻¹ between 2012 and 2013 and then diminishing to 750 m yr⁻¹ between 2015 and 2017.

Turning to the longer term evolution of JI (Fig. 5; time series location shown in Fig. 1), fitting a linear trend to the data suggests an annual acceleration since 2009 of $\sim 218 \text{ m yr}^{-1}$ at Jif, diminishing inland to $\sim 128 \text{ m yr}^{-2}$ at J1, and $\sim 102 \text{ m yr}^{-2}$ at J2. Although this provides a simple characterization of the longer-term evolution in ice speed, it is clear from our time series that computing a linear trend does not capture the full decadal-scale variability in ice velocity. In particular, we note that much of the acceleration occurred between 2011 and 2013 (Fig. 5b and c), and since then there has been a notable absence of multi-annual acceleration as earlier records suggest (Joughin et al., 2014). Computing trends in ice velocity since 2012 near the glacier terminus (Jif), for example, shows a modest decline in speed of 321 m yr^{-2} over the 5-year period (Fig. 5b). The calving front position migration has been suggested as the trigger to the stresses regimes variations and consequently the main driver to the JI velocity fluctuations (Joughin et al., 2008a, b, 2012, 2014; Bondzio et al., 2017). After a successive and gradually increased rate of ice front retreat un-

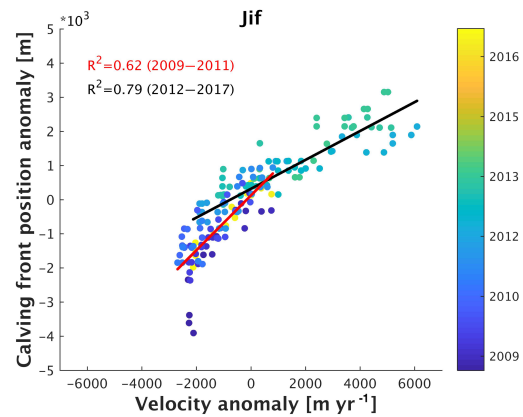


Figure 6. Comparison between Jakobshavn Isbræ ice velocity and calving front position anomalies at the Jif site, 0.8 km upstream of the calving front, between 2009 and early 2017. Positive values correspond to ice front retreat and speedup respectively. The red and black lines represent the linear regression through the 2009–2011 and 2012–2017 periods, respectively, together with the correlation coefficients (R^2).

til 2012 (Fig. 5a), the JI grounding line is now located on a higher bed location (Joughin et al., 2012; An et al., 2017). This may be acting to stabilize the grounding line, and in turn contribute to the glacier deceleration, although the main cause remains to be determined and further investigations is necessary. We used our observations of calving front position to assess the correlation between ice speed and calving front location, relative to their respective long-term means (Fig. 6). Based on the linear regression (Fig. 6), our dataset indicates correlation coefficients (R^2) of 0.62 (2009–2011) and 0.79 (2012–2017), and velocity changes by 1100 and 1600 m yr⁻¹ per kilometre of calving front retreat, respectively.

At Petermann Glacier we extracted two velocity time series at P1, located $\sim 45 \text{ km}$ downstream of the grounding line and close to the calving front of the ice tongue; and P2, $\sim 10 \text{ km}$ upstream of the grounding line. These locations were chosen to examine any differences in velocity evolution over the grounded and floating portions of the glacier. Our P1 time series starts in early 2015 because it is not covered by the TerraSAR-X dataset (Fig. 7a). We observe that, in general, ice at P1 flows $\sim 400 \text{ m yr}^{-1}$ faster than P2. Fitting a linear trend to the longer P2 dataset indicates no significant trend in ice velocity since 2011, although the precision of this trend is hampered by the sparse data coverage during the early part of this period. Continued monitoring by Sentinel-1 will improve our confidence in resolving any decadal-scale variability. The improvement in temporal sampling provided by Sentinel-1 at this site is clear (Fig. 7a) and allows us to resolve the seasonal cycle in velocity since 2015, and helps to

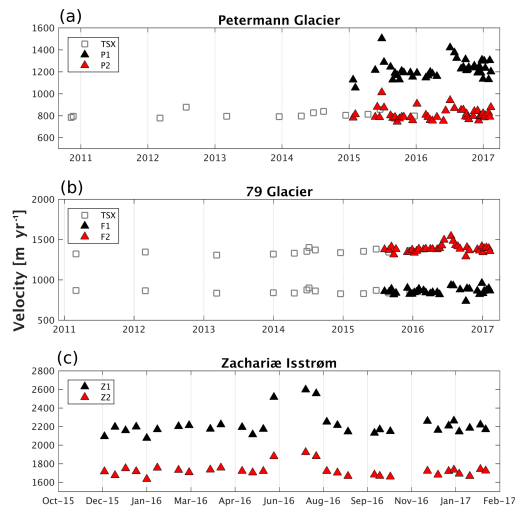


Figure 7. Temporal evolution of ice velocity at the locations indicated in Fig. 1 over (a) Petermann Glacier, (b) Nioghalvfjærdsfjorden and (c) Zachariae Isström. The data derived from TerraSAR-X (11 days – Joughin et al., 2016) and Sentinel 1-a/b (6 to 12 days) are represented as grey squares and coloured triangles, respectively.

delimit the duration of the speedup period. At P1, we detect a seasonal change in speed of $\sim 300 \text{ m yr}^{-1}$, equivalent to a 25 % increase relative to its winter velocity (Table 1). Despite the high seasonal change, the relation between P1’s annual mean and winter velocity is 0 %, likely due to the short speedup period (25 days – Table 1). This provides further evidence of a seasonal velocity cycle which has been observed at both Petermann and other glaciers in this region, and is understood to be predominantly controlled by changes in basal traction, and induced by penetration of surface melt water to the bed (Nick et al., 2012; Moon et al., 2014, 2015). This is further supported by our analysis of changes in calving front position (Fig. S1a), which shows that, in contrast to JI, seasonal acceleration does not coincide with ice front retreat. Specifically, we found that during the summers of 2015 and 2016, the calving front of PG advanced $\sim 1 \text{ km}$ during the speedup (Fig. S1a). These observations are consistent with previous modelling results, which did not find evidence of acceleration driven by large calving events in 2010 and 2012 (Nick et al., 2012; Münchow et al., 2014), suggesting that the ice shelf exerts low backstress on the glacier. More recently, we note that since September 2016 PG has developed a new crack near the ice front, which has continued to grow in length up to the present day.

At 79-G, we again extracted velocity time series over the ice shelf (F1, $\sim 20 \text{ km}$ downstream of the grounding line) and at the grounding line (F2). In contrast to PG and due to the steeper surface gradient upstream of the grounding line

(Fig. 2c), ice flow is slower on the floating tongue than at the grounding line location (Fig. 7b). We observe a seasonal speedup of $\sim 10 \%$ at F2 during summer 2016 (Table 1), although evidence of the same acceleration on the ice shelf is not clear given the magnitude of the signal and the precision of our data. Fitting a linear trend to our data returns an annual change in velocity of 15 m yr^{-2} since 2011, although assessing the significance of this result is difficult given the limited data sampling early in the period. Turning to Zachariae Isström, we extract time series at two locations slightly upstream of the grounding line in order to observe different temporal responses between them (Fig. 7c). At this glacier, no observations are available within the TSX dataset and so our time series is limited to the period December 2015 to January 2017. Nonetheless, like its neighbour ZI, we again find evidence of a summer speedup during 2016, equating to around 400 m yr^{-1} , or 18 % (Table 1). Given the short period of observations we do not attempt to derive a longer-term trend in ice velocity at this site.

We compared our estimates to the results of previous studies to assess the level of stability relative to past work. At Petermann, we have observed increases in ice velocity of $\sim 10 \%$ at P1 and $\sim 8 \%$ at P2 between the 2015/2016 and 2016/2017 winters, matching in percentage with the observations made by Münchow et al. (2016) between 2013/14 and 2015/16. Furthermore, the Sentinel-1a/b dataset indicates a multi-annual acceleration of $\sim 32 \text{ m yr}^{-2}$ between 2015–2017 at P1, which is similar to the $\sim 30 \text{ m yr}^{-2}$ reported by Nick et al. (2012) based upon observational measurements over a longer period, from 2006 to 2010. The same authors also show seasonal variations of $\sim 20\text{--}25 \%$ over the same location, similar to the $\sim 22 \%$ shown by the Sentinel-1 dataset. At 79-G, Mouginit et al. (2015) showed a speedup of 8 % from 1976 to 2014 with the main changes occurring after 2006, similar to our estimates which also suggest a slight multi-year trend of $\sim 16 \text{ m yr}^{-2}$ ($\sim 8 \%$) for F2 between 2015 and 2017. Zachariae Isström shows seasonal variation up to 15 % between 2015 and 2017 in the Sentinel-1 dataset, agreeing with seasonal variation up to 20 % estimated by Mouginit et al. (2017) using Landsat-8 optical images during 2014–2016. Overall, our Sentinel 1 results shows a close agreement with previous studies using different techniques and demonstrated to be a powerful tool for monitoring the cryosphere.

5 Conclusions

We have presented a new, high temporal resolution record of ice velocity evolution for four important, high discharge marine-based glaciers in Greenland, updated to the present day (October 2014 to February 2017). Using SAR data acquired by the Sentinel-1a/b constellation, with its 250 km wide swath and frequent revisit time, we have produced 187 velocity maps, which, in combination with 479 maps from

the TerraSAR-X satellite, provide detailed spatial and temporal coverage of these key sites. Importantly, the systematic acquisition cycle of Sentinel-1a/b, which now provides averaged measurements of all of these sites every 6 days and allows for detailed monitoring of both seasonal and multi-annual velocity fluctuations, and allow us to demonstrate the speedup persistence in a higher resolution. The short revisit time of 6 days, made possible since the launch of Sentinel-1b in April 2016, particularly benefits the retrieval of velocity signals across fast-flowing regions close to the ice front, due to a reduction in the decorrelation occurring between image pairs. Using this new dataset, we confirm evidence of intra-annual variations in ice velocity and clear seasonal cycles occurring over the past few years at JI, PG, 79G, and ZI. Of the sites studied here, JI exhibits the largest velocity variations, as demonstrated in other studies, which we show are strongly correlated with the evolution of the position of its calving front. However, it is notable that in the last 5 years the longer-term ice speed has started to decrease (321 m yr^{-2}). This study demonstrates the utility of a new era of operational SAR imaging satellites for building systematic records of ice sheet outlet glacier velocity and its good agreement with TerraSAR-X products, which indicates Sentinel-1 can confidently extend the times series that began with other sensors. Looking to the future, these datasets are key for the timely identification of emerging signals of dynamic imbalance, and for understanding the processes driving ice velocity change.

Data availability. Centre for Polar Observation and Modelling: Sentinel-1 Near Real Time Ice Velocity, available at: <http://www.cpom.ucl.ac.uk/csopr/iv/>, last access: 11 June 2018.

The Supplement related to this article is available online at <https://doi.org/10.5194/tc-12-2087-2018-supplement>.

Competing interests. The authors declare that they have no conflict of interest.

Acknowledgements. This work was led by the NERC Centre for Polar Observation and Modelling, supported by the Natural Environment Research Council (cpom300001), with the support of a grant (4000107503/13/I-BG), and the European Space Agency. Anna E. Hogg is funded by the European Space Agency's support of Science Element program and an independent research fellowship (4000112797/15/I-SBo). Adriano Lemos was supported by CAPES-Brazil PhD scholarship. The NASA MEASUREs program (NASA grants NNX08AL98A and NNX13AI21A) supported Ian Joughin's contribution. All data are freely available for download at <http://www.cpom.ucl.ac.uk/csopr/iv/> (last access: 11 June 2018). We thank the editor Andreas Vieli, and the two reviewers, Rachel

Carr and an anonymous referee, for their comments, which helped to improve the manuscript.

Edited by: Andreas Vieli

Reviewed by: Rachel Carr and one anonymous referee

References

- An, L., Rignot, E., Elieff, S., Morlighem, M., Millan, R., Mougnot, J., and Paden, J.: Bed elevation of Jakobshavn Isbræ, West Greenland, from high-resolution airborne gravity and other data, *Geophys. Res. Lett.*, 44, 3728–3736, <https://doi.org/10.1002/2017GL073245>, 2017.
- Armstrong, W. H., Anderson, R. S., and Fahnestock, M. A.: Spatial Patterns of Summer Speedup on South Central Alaska Glaciers, *Geophys. Res. Lett.*, 44, 9379–9388, <https://doi.org/10.1002/2017GL074370>, 2017.
- Bondzio, J. H., Morlighem, M., Seroussi, H., Kleiner, T., Rückamp, M., Mougnot, J., and Humbert, A.: The mechanisms behind Jakobshavn Isbræ's acceleration and mass loss: a 3D thermomechanical model study, *Geophys. Res. Lett.*, 44, 6252–6260, <https://doi.org/10.1002/2017GL073309>, 2017.
- Carr, J. R., Stokes, C. R., and Vieli, A.: Threefold increase in marine-terminating outlet glacier retreat rates across the Atlantic Arctic: 1992–2010, *Ann. Glaciol.*, 58, 72–91, <https://doi.org/10.1017/aog.2017.3>, 2017.
- Cassotto, R., Fahnestock, M., Amundson, J. M., Truffer, M., and Joughin, I.: Seasonal and interannual variations in ice melange and its impact on terminus stability, Jakobshavn Isbræ, Greenland, *J. Glaciol.*, 61, 76–88, <https://doi.org/10.3189/2015JG13J235>, 2015.
- Dehecq, A., Gourmelen, N., and Trouve, E.: Deriving large-scale glacier velocities from a complete satellite archive: Application to the Pamir-Karakoram-Himalaya, *Remote Sens. Environ.*, 162, 55–66, <https://doi.org/10.1016/j.rse.2015.01.031>, 2015.
- de Lange, R., Luckman, A., and Murray, T.: Improvement of satellite radar feature tracking for ice velocity derivation by spatial frequency filtering, *IEEE Trans. Geosci. Remote Sens.*, 45, 2309–2318, <https://doi.org/10.1109/TGRS.2007.896615>, 2007.
- Enderlin, E. M., Howat, I. M., Jeong, S., Noh, M.-J., Angelen, J. H. van, and van den Broeke, M. R.: An improved mass budget for the Greenland ice sheet, *Geophys. Res. Lett.*, 41, 1–7, <https://doi.org/10.1002/2013GL059010>, 2014.
- European Space Agency (ESA): Greenland Ice Sheet Climate Change Initiative (CCI) project: Greenland calving front locations v.3.0, available at: http://products.esa-icesheets-cci.org/products/details/greenland_calving_front_locations_v3_0.zip/ (last access: 11 June 2018), 2017.
- Fahnestock, M., Scambos, T., Moon, T., Gardner, A., Haran, T., and Klinger, M.: Rapid large-area mapping of ice flow using Landsat 8, *Remote Sens. Environ.*, 185, 84–94, <https://doi.org/10.1016/j.rse.2015.11.023>, 2016.
- Felikson, D., Bartholomäus, T. C., Catania, G. A., Korsgaard, N. J., Kjær, K. H., Morlighem, M., and Nash, J. D.: Inland thinning on the Greenland ice sheet controlled by outlet glacier geometry, *Nat. Geosci.*, 10, 366–369, <https://doi.org/10.1038/ngeo2934>, 2017.

- GAMMA Remote Sensing: Sentinel-1 processing with GAMMA software, Version 1.2, 2015.
- Gladish, C. V., Holland, D. M., Rosing-Asvid, A., Behrens, J. W., and Boje, J.: Oceanic Boundary Conditions for Jakobshavn Glacier. Part II: Provenance and Sources of Variability of Disko Bay and Ilulissat Icefjord Waters, 1990–2011, *J. Phys. Oceanogr.*, 45, 33–63, <https://doi.org/10.1175/JPO-D-14-0045.1>, 2015.
- Hogg, A., Shepherd, A., and Gourmelen, N.: A first look at the performance of Sentinel-1 over the West Antarctic Ice Sheet, *FRINGE 2015*, Frascati, Italy, 23–27 March, 2015.
- Hogg, A. E., Shepherd, A., Gourmelen, N., and Engdahl, M.: Grounding line migration from 1992 to 2011 on Petermann Glacier, North-West Greenland, *J. Glaciol.*, 62, 1–11, <https://doi.org/10.1017/jog.2016.83>, 2016.
- Hogg, A. E., Shepherd, A., Cornford, S. L., Briggs, K. H., Gourmelen, N., Graham, J., and Witte, J.: Increased ice flow in Western Palmer Land linked to ocean melting, *Geophys. Res. Lett.*, 44, 1–9, <https://doi.org/10.1002/2016GL072110>, 2017.
- Holland, D. M., Thomas, R. H., Young, B. De, Ribergaard, M. H., and Lyberth, B.: Acceleration of Jakobshavn Isbræ triggered by warm subsurface ocean waters, *Nat. Geosci.*, 1, 1–6, <https://doi.org/10.1038/ngeo316>, 2008.
- Howat, I. M., Box, J. E., Ahn, Y., Herrington, A., and McFadden, E. M.: Seasonal variability in the dynamics of marine-terminating outlet glaciers in Greenland, *J. Glaciol.*, 56, 601–613, <https://doi.org/10.3189/002214310793146232>, 2010.
- Howat, I. M., Negrete, A., and Smith, B. E.: The Greenland Ice Mapping Project (GIMP) land classification and surface elevation data sets, *The Cryosphere*, 8, 1509–1518, <https://doi.org/10.5194/tc-8-1509-2014>, 2014.
- Jensen, T. S., Box, J. E., and Hvidberg, C. S.: A sensitivity study of annual area change for Greenland ice sheet marine terminating outlet glaciers: 1999–2013, *J. Glaciol.*, 62, 1–10, <https://doi.org/10.1017/jog.2016.12>, 2016.
- Johannessen, O. M., Babiker, M., and Miles, M. W.: Unprecedented Retreat in a 50-Year Observational Record for Petermann, *Atmos. Ocean. Sci. Lett.*, 6, 259–265, <https://doi.org/10.3878/j.issn.1674-2834.13.0021.1>, 2013.
- Joughin, I.: Ice-sheet velocity mapping: a combined interferometric and speckle-tracking approach, *Ann. Glaciol.*, 34, 195–201, <https://doi.org/10.3189/172756402781817978>, 2002.
- Joughin, I., Winebrenner, D. P., and Fahnestock, M. A.: Observations of ice-sheet motion in Greenland using satellite radar interferometry, *Geophys. Res. Lett.*, 22, 571–574, <https://doi.org/10.1029/95GL00264>, 1995.
- Joughin, I., Howat, I. M., Fahnestock, M., Smith, B., Krabill, W., Alley, R. B., and Truffer, M.: Continued evolution of Jakobshavn Isbræ following its rapid speedup, *J. Geophys. Res.-Earth Surf.*, 113, 1–14, <https://doi.org/10.1029/2008JF001023>, 2008a.
- Joughin, I., Das, S. B., King, M. A., Smith, B. E., Howat, I. M., and Moon, T.: Seasonal Speedup Along the Western Flank of the Greenland Ice Sheet, *Science*, 320, 781–784, <https://doi.org/10.1126/science.1153288>, 2008b.
- Joughin, I., Smith, B. E., Howat, I. M., Scambos, T., and Moon, T.: Greenland flow variability from ice-sheet-wide velocity mapping, *J. Glaciol.*, 56, 415–430, <https://doi.org/10.3189/002214310792447734>, 2010.
- Joughin, I., Smith, B. E., Howat, I. M., Floricioiu, D., Alley, R. B., Truffer, M., and Fahnestock, M.: Seasonal to decadal scale variations in the surface velocity of Jakobshavn Isbræ, Greenland: Observation and model-based analysis, *J. Geophys. Res.-Earth Surf.*, 117, 1–20, <https://doi.org/10.1029/2011JF002110>, 2012.
- Joughin, I., Smith, B. E., Shean, D. E., and Floricioiu, D.: Brief Communication: Further summer speedup of Jakobshavn Isbræ, *The Cryosphere*, 8, 209–214, <https://doi.org/10.5194/tc-8-209-2014>, 2014.
- Joughin, I., Smith, B., Howat, I., and Scambos, T.: MEASURES Multi-year Greenland Ice Sheet Velocity Mosaic, Version 1. Boulder, Colorado USA, NASA National Snow and Ice Data Center Distributed Active Archive Center, <https://doi.org/10.5067/QUA5Q9SVMSJG>, 2016.
- Khan, S. A., Aschwanden, A., Bjørk, A. A., Wahr, J., Kjeldsen, K. K., and Kjær, K. H.: Greenland ice sheet mass balance: a review, *Reports on Prog. Phys.*, IOP Publishing, 4, 292–299, <https://doi.org/10.1088/0034-4885/78/4/046801>, 2014.
- Lucchitta, B. K. and Ferguson, H. M.: Antarctica: measuring glacier velocity from satellite images, *Science (New York, N.Y.)*, 234, 1105–1108, <https://doi.org/10.1126/science.234.4780.1105>, 1986.
- McMillan, M., Leeson, A., Shepherd, A., Briggs, K., Armitage, T. W. K., Hogg, A., and Gilbert, L.: A high resolution record of Greenland mass balance, *Geophys. Res. Lett.*, 43, 1–9, <https://doi.org/10.1002/GRL.54619>, 2016.
- Moon, T., Joughin, I., Smith, B., and Howat, I.: 21st-century evolution of Greenland outlet glacier velocities, *Science*, 336, 576–578, <https://doi.org/10.1126/science.1219985>, 2012.
- Moon, T., Joughin, I., Smith, B., Broeke, M. R., Berg, W. J., Noël, B., and Usher, M.: Distinct patterns of seasonal Greenland glacier velocity, *Geophys. Res. Lett.*, 41, 7209–7216, <https://doi.org/10.1002/2014GL061836>, 2014.
- Moon, T., Joughin, I., and Smith, B.: Seasonal to multiyear variability of glacier surface velocity, terminus position, and sea ice/ice mélange in northern Greenland, *J. Geophys. Res.-Earth Surf.*, 120, 818–833, <https://doi.org/10.1002/2015JF003494>, 2015.
- Morlighem, M., Rignot, E., Mouginot, J., Seroussi, H., and Larour, E.: IceBridge BedMachine Greenland, Version 2. Boulder, Colorado USA, NASA National Snow and Ice Data Center Distributed Active Archive Center, (09/08/2017) <https://doi.org/10.5067/AD7B0HQNSJ29>, 2015.
- Mouginot, J., Rignot, E., Scheuchl, B., Fenty, I., Khazendar, A., Morlighem, M., and Paden, J.: Fast retreat of Zachariæ Isstrøm, northeast Greenland, *Science Express*, 10.1126 (November), <https://doi.org/10.1126/science.aac7111>, 2015.
- Mouginot, J., Rignot, E., Scheuchl, B., and Millan, R.: Comprehensive Annual Ice Sheet Velocity Mapping Using Landsat-8, Sentinel-1, and RADARSAT-2 Data, *Remote Sens.*, 9, 1–20, <https://doi.org/10.3390/rs9040364>, 2017.
- Münchow, A., Padman, L., and Fricker, H. A.: Interannual changes of the floating ice shelf of Petermann Gletscher, North Greenland, from 2000 to 2012, *J. Glaciol.*, 60, 489–499, <https://doi.org/10.3189/2014JoG13J135>, 2014.
- Münchow, A., Padman, L., Washam, P., and Nicholls, K. W.: The ice shelf of Petermann Gletscher, North Greenland, and its connection to the Arctic and Atlantic Oceans, *Oceanography*, 29, 84–95, <https://doi.org/10.5670/oceanog.2016.101>, 2016.

- Nagler, T., Rott, H., Hetzenecker, M., Wuite, J., and Potin, P.: The Sentinel-1 Mission: New Opportunities for Ice Sheet Observations, *Remote Sens.*, 7, 9371–9389, <https://doi.org/10.3390/rs70709371>, 2015.
- Nick, F. M., Luckman, A., Viel, A., Van Der Veen, C. J., Van As, D., Van De Wal, R. S. W., and Floricioiu, D.: The response of Petermann Glacier, Greenland, to large calving events, and its future stability in the context of atmospheric and oceanic warming, *J. Glaciol.*, 58, 229–239, <https://doi.org/10.3189/2012JG11J242>, 2012.
- Paul, F., Bolch, T., Kääb, A., Nagler, T., Nuth, C., Scharer, K., and Van Niel, T.: The glaciers climate change initiative: Methods for creating glacier area, elevation change and velocity products, *Remote Sens. Environ.*, 162, 408–426, <https://doi.org/10.1016/j.rse.2013.07.043>, 2015.
- Pritchard, H., Murray, T., Luckman, A., Strozzi, T., and Barr, S.: Glacier surge dynamics of Sortebrae, east Greenland, from synthetic aperture radar feature tracking, *J. Geophys. Res.*, 110, 1–13, <https://doi.org/10.1029/2004JF000233>, 2005.
- Rignot, E.: Tidal motion, ice velocity and melt rate of Petermann Gletscher, Greenland, measured from radar interferometry, *J. Glaciol.*, 42, 476–485, 1996.
- Rignot, E. and Kanagaratnam, P.: Changes in the Velocity Structure of the Greenland Ice Sheet, *Science*, 311, 986–990, <https://doi.org/10.1126/science.1121381>, 2006.
- Rignot, E. and Mouginot, J.: Ice flow in Greenland for the International Polar Year 2008–2009, *Geophys. Res. Lett.*, 39, 1–7, <https://doi.org/10.1029/2012GL051634>, 2012.
- Rignot, E. and Steffen, K.: Channelized bottom melting and stability of floating ice shelves, *Geophys. Res. Lett.*, 35, 1–5, <https://doi.org/10.1029/2007GL031765>, 2008.
- Sentinels POD Team: Sentinels POD Service File Format Specifications, European Space Agency, Paris, France, 2013.
- Shepherd, A., Ivins, E. R., Geruo, A., Barletta, V. R., Bentley, M. J., Bettadpur, S., and Zwally, H. J.: A Reconciled Estimate of Ice-Sheet Mass Balance, *Science*, 338, 1183–1189, <https://doi.org/10.1126/science.1228102>, 2012.
- Strozzi, T., Luckman, A., Murray, T., Wegmuller, U., and Werner, C. L.: Glacier motion estimation using SAR offset-tracking procedures, *IEEE T. Geosci. Remote Sens.*, 40, 2384–2391, <https://doi.org/10.1109/TGRS.2002.805079>, 2002.
- Studinger, M. S.: IceBridge ATM L4 Surface Elevation Rate of Change, Version 1, Greenland subset. Boulder, Colorado USA, NASA National Snow and Ice Data Center Distributed Active Archive Center, <https://doi.org/10.5067/BCW6CI3TXOCY>, 2014.
- Tedesco, M., Fettweis, X., Mote, T., Wahr, J., Alexander, P., Box, J. E., and Wouters, B.: Evidence and analysis of 2012 Greenland records from spaceborne observations, a regional climate model and reanalysis data, *The Cryosphere*, 7, 615–630, <https://doi.org/10.5194/tc-7-615-2013>, 2013.
- van den Broeke, M., Bamber, J. L., Ettema, J., Rignot, E., Schrama, E., van de Berg, W. J., and Wouters, B.: Partitioning recent Greenland mass loss, *Science*, 326, 984–986, <https://doi.org/10.1126/science.1178176>, 2009.
- van de Wal, R. S. W., Smeets, C. J. P. P., Boot, W., Stoffelen, M., van Kampen, R., Doyle, S. H., Wilhelms, F., van den Broeke, M. R., Reijmer, C. H., Oerlemans, J., and Hubbard, A.: Self-regulation of ice flow varies across the ablation area in south-west Greenland, *The Cryosphere*, 9, 603–611, <https://doi.org/10.5194/tc-9-603-2015>, 2015.
- Yague-Martinez, N., Prats-Iraola, P., Gonzalez, F. R., Brcic, R., Shau, R., Geudtner, D., and Bamler, R.: Interferometric Processing of Sentinel-1 TOPS data, *IEEE T. Geosci. Remote Sens.*, 54, 2220–2234, <https://doi.org/10.1109/TGRS.2015.2497902>, 2016.

Supplement of *The Cryosphere*, 12, 2087–2097, 2018
<https://doi.org/10.5194/tc-12-2087-2018-supplement>
© Author(s) 2018. This work is distributed under
the Creative Commons Attribution 4.0 License.



Supplement of

Ice velocity of Jakobshavn Isbræ, Petermann Glacier, Nioghalvfjærdsfjorden, and Zachariæ Isstrøm, 2015–2017, from Sentinel 1-a/b SAR imagery

Adriano Lemos et al.

Correspondence to: Adriano Lemos (a.g.lemos14@leeds.ac.uk)

The copyright of individual parts of the supplement might differ from the CC BY 4.0 License.

Supplementary Material

Figure S1: Ice front location extracted from Sentinel-1 images on (a) Petermann Glacier and (b) Nioghalvfjærdsfjorden.

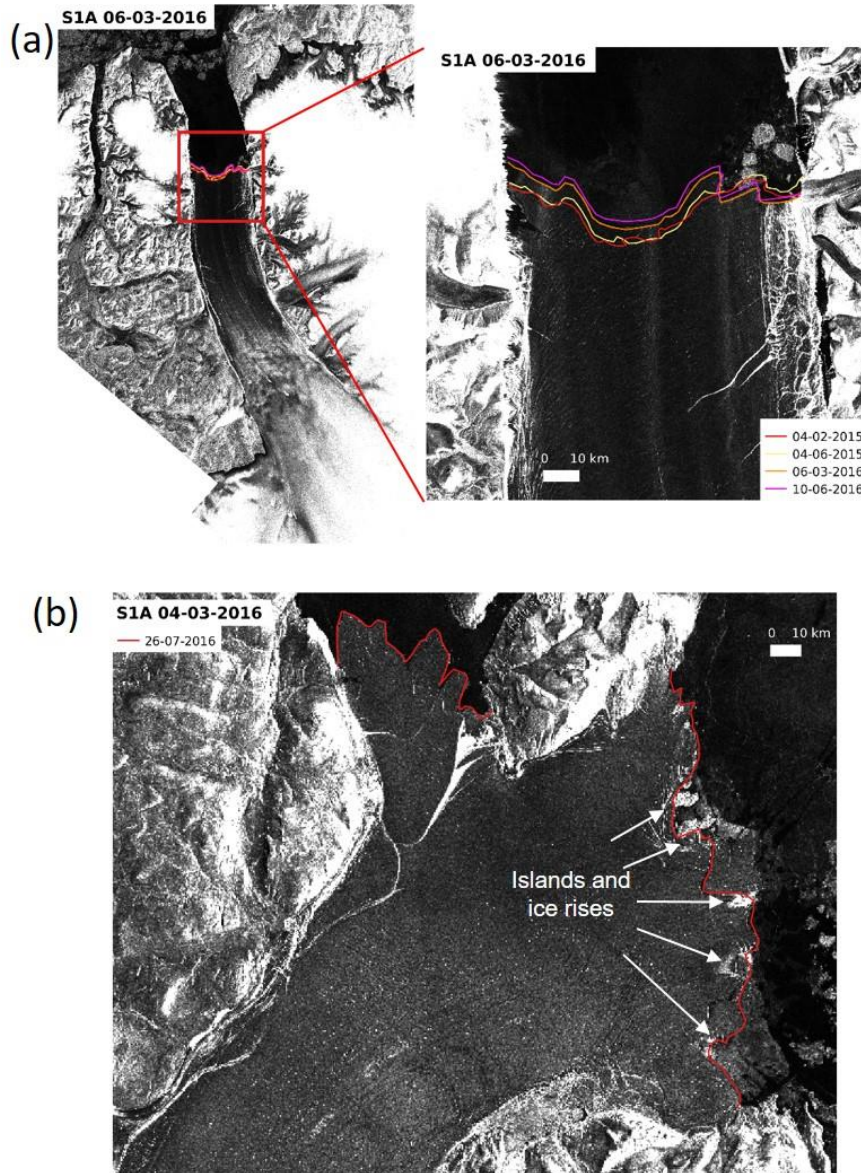


Figure S2: Number of images used separated per month.

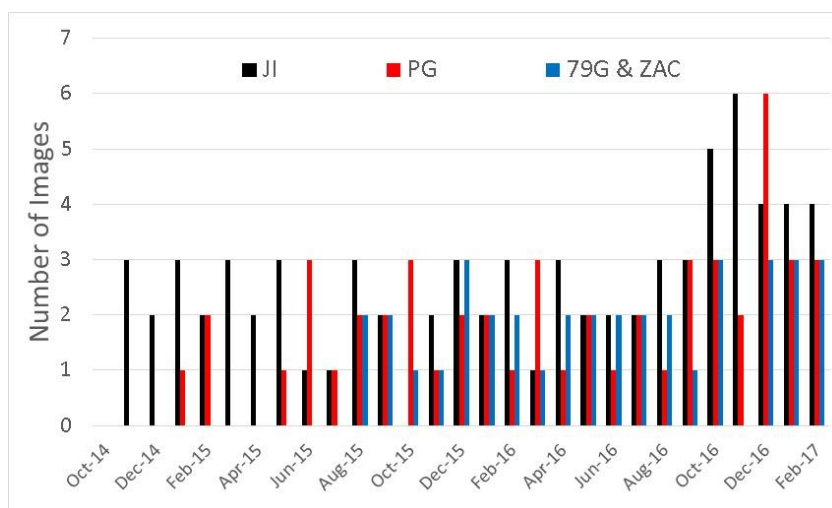


Table S1: List of Sentinel-1 images used.

Glacier	Scene 1				Scene 2			
	Satellite	day	month	year	Satellite	day	month	year
JI	S1A	4	Nov	14	S1A	16	Nov	14
	S1A	16	Nov	14	S1A	28	Nov	14
	S1A	28	Nov	14	S1A	10	Dec	14
	S1A	10	Dec	14	S1A	22	Dec	14
	S1A	22	Dec	14	S1A	3	Jan	15
	S1A	3	Jan	15	S1A	15	Jan	15
	S1A	27	Jan	15	S1A	8	Feb	15
	S1A	8	Feb	15	S1A	20	Feb	15
	S1A	20	Feb	15	S1A	4	Mar	15
	S1A	4	Mar	15	S1A	16	Mar	15
	S1A	16	Mar	15	S1A	28	Mar	15
	S1A	28	Mar	15	S1A	9	Apr	15
	S1A	9	Apr	15	S1A	21	Apr	15
	S1A	21	Apr	15	S1A	3	May	15
	S1A	3	May	15	S1A	15	May	15
	S1A	27	May	15	S1A	8	Jun	15
	S1A	8	Jun	15	S1A	26	Jul	15
	S1A	26	Jul	15	S1A	7	Aug	15
	S1A	7	Aug	15	S1A	19	Aug	15
	S1A	19	Aug	15	S1A	31	Aug	15
S1A	31	Aug	15	S1A	12	Sep	15	
S1A	12	Sep	15	S1A	24	Sep	15	

A.1 Paper published in the journal The Cryosphere

	S1A	11	Nov	15	S1A	23	Nov	15
	S1A	5	Dec	15	S1A	17	Dec	15
	S1A	17	Dec	15	S1A	29	Dec	15
	S1A	29	Dec	15	S1A	10	Jan	16
	S1A	10	Jan	16	S1A	22	Jan	16
	S1A	22	Jan	16	S1A	3	Feb	16
	S1A	3	Feb	16	S1A	27	Feb	16
	S1A	15	Feb	16	S1A	27	Feb	16
	S1A	27	Feb	16	S1A	10	Mar	16
	S1A	10	Mar	16	S1A	3	Apr	16
	S1A	3	Apr	16	S1A	15	Apr	16
	S1A	15	Apr	16	S1A	27	Apr	16
	S1A	27	Apr	16	S1A	9	May	16
	S1A	27	Apr	16	S1A	21	May	16
	S1A	9	May	16	S1A	21	May	16
	S1A	21	May	16	S1A	2	Jun	16
	S1A	2	Jun	16	S1A	14	Jun	16
	S1A	14	Jun	16	S1A	8	Jul	16
	S1A	14	Jun	16	S1A	1	Aug	16
	S1A	20	Jul	16	S1A	1	Aug	16
	S1A	1	Aug	16	S1A	13	Aug	16
	S1A	13	Aug	16	S1A	25	Aug	16
	S1A	25	Aug	16	S1A	6	Sep	16
	S1A	6	Sep	16	S1A	18	Sep	16
	S1A	18	Sep	16	S1A	30	Sep	16
	S1A	30	Sep	16	S1B	6	Oct	16
	S1B	6	Oct	16	S1A	12	Oct	16
	S1A	12	Oct	16	S1B	18	Oct	16
	S1B	18	Oct	16	S1A	24	Oct	16
	S1A	12	Oct	16	S1B	30	Oct	16
	S1A	24	Oct	16	S1B	30	Oct	16
	S1B	30	Oct	16	S1A	5	Nov	16
	S1B	30	Oct	16	S1B	23	Nov	16
	S1A	5	Nov	16	S1B	11	Nov	16
	S1B	11	Nov	16	S1A	17	Nov	16
	S1A	17	Nov	16	S1B	23	Nov	16
	S1B	23	Nov	16	S1A	29	Nov	16
	S1A	29	Nov	16	S1B	5	Dec	16
	S1B	5	Dec	16	S1A	11	Dec	16
	S1A	11	Dec	16	S1B	17	Dec	16
	S1B	17	Dec	16	S1A	23	Dec	16
	S1B	10	Jan	17	S1A	16	Jan	17
	S1A	16	Jan	17	S1B	22	Jan	17
	S1B	22	Jan	17	S1A	28	Jan	17
	S1A	28	Jan	17	S1B	3	Feb	17
	S1B	3	Feb	17	S1A	9	Feb	17
	S1A	9	Feb	17	S1B	15	Feb	17
	S1B	15	Feb	17	S1A	21	Feb	17
	S1A	23	Jan	15	S1A	4	Feb	15
	S1A	4	Feb	15	S1A	16	Feb	15
PG	S1A	23	May	15	S1A	4	Jun	15
	S1A	4	Jun	15	S1A	16	Jun	15
	S1A	16	Jun	15	S1A	28	Jun	15
	S1A	28	Jun	15	S1A	10	Jul	15

A.1 Paper published in the journal The Cryosphere

	S1A	10	Jul	15	S1A	15	Aug	15
	S1A	15	Aug	15	S1A	27	Aug	15
	S1A	27	Aug	15	S1A	8	Sep	15
	S1A	8	Sep	15	S1A	20	Sep	15
	S1A	20	Sep	15	S1A	2	Oct	15
	S1A	2	Oct	15	S1A	14	Oct	15
	S1A	14	Oct	15	S1A	26	Oct	15
	S1A	26	Oct	15	S1A	7	Nov	15
	S1A	1	Dec	15	S1A	13	Dec	15
	S1A	13	Dec	15	S1A	6	Jan	16
	S1A	6	Jan	16	S1A	18	Jan	16
	S1A	23	Feb	16	S1A	6	Mar	16
	S1A	6	Mar	16	S1A	18	Mar	16
	S1A	18	Mar	16	S1A	30	Mar	16
	S1A	30	Mar	16	S1A	23	Apr	16
	S1A	23	Apr	16	S1A	5	May	16
	S1A	29	May	16	S1A	10	Jun	16
	S1A	10	Jun	16	S1A	4	Jul	16
	S1A	4	Jul	16	S1A	28	Jul	16
	S1A	28	Jul	16	S1A	9	Aug	16
	S1A	9	Aug	16	S1A	2	Sep	16
	S1A	2	Sep	16	S1A	14	Sep	16
	S1A	14	Sep	16	S1A	26	Sep	16
	S1A	26	Sep	16	S1B	2	Oct	16
	S1B	2	Oct	16	S1A	8	Oct	16
	S1A	8	Oct	16	S1B	14	Oct	16
	S1B	14	Oct	16	S1B	7	Nov	16
	S1B	7	Nov	16	S1A	13	Nov	16
	S1A	13	Nov	16	S1B	1	Dec	16
	S1B	1	Dec	16	S1A	7	Dec	16
	S1A	7	Dec	16	S1B	13	Dec	16
	S1B	13	Dec	16	S1A	19	Dec	16
	S1A	19	Dec	16	S1B	25	Dec	16
	S1B	25	Dec	16	S1A	31	Dec	16
	S1A	31	Dec	16	S1B	6	Jan	17
	S1B	6	Jan	17	S1A	12	Jan	17
	S1A	12	Jan	17	S1B	30	Jan	17
	S1B	30	Jan	17	S1A	5	Feb	17
	S1A	5	Feb	17	S1B	11	Feb	17
	S1B	11	Feb	17	S1A	17	Feb	17
	S1A	6	Aug	15	S1A	30	Aug	15
	S1A	30	Aug	15	S1A	11	Sep	15
	S1A	11	Sep	15	S1A	23	Sep	15
	S1A	23	Sep	15	S1A	5	Oct	15
	S1A	5	Oct	15	S1A	10	Nov	15
	S1A	4	Dec	15	S1A	16	Dec	15
	S1A	16	Dec	15	S1A	28	Dec	15
	S1A	28	Dec	15	S1A	9	Jan	16
	S1A	9	Jan	16	S1A	21	Jan	16
	S1A	21	Jan	16	S1A	2	Feb	16
	S1A	2	Feb	16	S1A	26	Feb	16
	S1A	26	Feb	16	S1A	9	Mar	16
	S1A	9	Mar	16	S1A	2	Apr	16
	S1A	2	Apr	16	S1A	14	Apr	16

79-G and
ZI

A.1 Paper published in the journal The Cryosphere

S1A	14	Apr	16	S1A	8	May	16
S1A	8	May	16	S1A	20	May	16
S1A	20	May	16	S1A	1	Jun	16
S1A	1	Jun	16	S1A	13	Jun	16
S1A	13	Jun	16	S1A	19	Jul	16
S1A	19	Jul	16	S1A	31	Jul	16
S1A	31	Jul	16	S1A	12	Aug	16
S1A	12	Aug	16	S1A	24	Aug	16
S1A	24	Aug	16	S1A	5	Sep	16
S1A	5	Sep	16	S1B	5	Oct	16
S1B	5	Oct	16	S1A	11	Oct	16
S1A	11	Oct	16	S1A	23	Oct	16
S1A	23	Oct	16	S1B	4	Dec	16
S1B	4	Dec	16	S1B	16	Dec	16
S1B	16	Dec	16	S1B	28	Dec	16
S1B	28	Dec	16	S1A	3	Jan	17
S1A	3	Jan	17	S1B	9	Jan	17
S1B	9	Jan	17	S1B	21	Jan	17
S1B	21	Jan	17	S1B	2	Feb	17
S1B	2	Feb	17	S1A	8	Feb	17
S1A	8	Feb	17	S1B	14	Feb	17

- Table S2: Velocity magnitude differences of JI using surface elevation rate of change information derived from IceBridge and Pre-Icebridge data acquired from the NASA Airborne Topographic Mapper (ATM) [Studinger, 2014] for terrain correction, and velocity magnitude without using thinning correction.

Difference [m/yr]	Distance along the profile from the grounding line [km]								
	0 - 5	5 - 10	10 - 15	15 - 20	20 - 25	25 - 30	30 - 35	35 - 40	40 - 45
Mean	-65.7	-18.1	-12.4	-2.9	3.0	-3.8	0.9	1.9	1.9
Max	55.8	58.6	33.2	9.9	37.6	36.9	13.1	16.0	20.2
Min	-277.3	-160.4	-75.3	-17.2	-32.8	-39.3	-11.8	-6.0	-6.6

A.2 Paper published in the journal Remote Sensing



Article

Seasonal Variations in the Flow of Land-Terminating Glaciers in Central-West Greenland Using Sentinel-1 Imagery

Adriano Lemos , Andrew Shepherd, Malcolm McMillan and Anna E. Hogg

Centre for Polar Observation and Modelling, University of Leeds, Leeds LS2 9JT, UK;

A.Shepherd@leeds.ac.uk (A.S.); M.McMillan@leeds.ac.uk (M.M.); A.E.Hogg@leeds.ac.uk (A.E.H.)

* Correspondence: A.G.Lemos14@leeds.ac.uk

Received: 6 October 2018; Accepted: 21 November 2018; Published: 24 November 2018



Abstract: Land-terminating sectors of the Greenland ice sheet flow faster in summer after surface meltwater reaches the subglacial drainage system. Speedup occurs when the subglacial drainage system becomes saturated, leading to a reduction in the effective pressure which promotes sliding of the overlying ice. Here, we use observations acquired by the Sentinel-1a and b synthetic aperture radar to track changes in the speed of land-terminating glaciers across a 14,000 km² sector of west-central Greenland on a weekly basis in 2016 and 2017. The fine spatial and temporal sampling of the satellite data allows us to map the speed of summer and winter across the entire sector and to resolve the weekly evolution of ice flow across the downstream portions of five glaciers. Near to the ice sheet margin (at 650 m.a.s.l.), glacier speedup begins around day 130, persisting for around 90 days, and then peaks around day 150. At four of the five glaciers included in our survey the peak speedup is similar in both years, in Russell Glacier there is marked interannual variability of 32% between 2016 and 2017. We present, for the first time, seasonal and altitudinal variation in speedup persistence. Our study demonstrates the value of Sentinel-1's systematic and frequent acquisition plan for studying seasonal changes in ice sheet flow.

Keywords: Sentinel-1; ice velocity; land-terminating glacier; Synthetic Aperture Radar; Greenland

1. Introduction

In recent decades the Greenland Ice Sheet has lost ice at an increasing rate, rising by 89% between 2011–2014 relative to 1992–2011 [1,2]. The majority (60%) of this ice loss has been due to surface melting and runoff [3,4], which have risen as summers have warmed [5,6]. Between 2011 and 2014, 41% of all ice loss from Greenland (269 ± 51 GT yr⁻¹; [2]) was from the south-western sector alone, where changes in the degree of surface melting have been pronounced [7].

In addition to the direct impact on runoff, increased surface melting has also been linked to increases in the speed of ice flow through basal lubrication [8–10]. Rising air temperatures lead to increased surface melting, which can in turn lead to an increase in the amount of water feeding into the subglacial drainage system [10] after supraglacial lakes drain or moulins open [9,10]. As a consequence of this excess meltwater, subglacial water pressure rises, which reduces the effective pressure between the ice-bedrock interface and leads to enhanced basal sliding [11–13]. During the melting season, frictional heating caused by water flow enlarges the conduits of the subglacial hydrologic system, allowing a greater volume of water to be accommodated [14,15]. As a consequence, from mid-season to the end of the melt season, the drainage system transmission capacity exceeds the meltwater input, draining water efficiently through low-pressure channels [15,16].

Seasonal changes in ice flow have been observed in both fast-moving and slow-moving glaciers [17–23]. In south-west Greenland, the summertime speedup of land-terminating glaciers

is widespread and is widely interpreted as being driven by seasonal changes in the degree of basal lubrication [8,20,24]. At low elevations (under 1000 m), seasonal changes in the movement of Greenland's glaciers are thought to be dominated by short-term events, typically lasting between 1 day to 1 week during the summer [25,26], with ice speeds increasing by 100% to 150% relative to winter [20,27]. Resolving such changes has been a challenge, because observations of ice sheet flow have historically been made using episodically acquired satellite imagery [7,11,12] and GPS sensors installed at point locations on the ice sheet [14,19,25]. Systematically monitoring seasonal variations in ice flow is therefore an important task as it will improve our understanding of the present and likely future response of the Greenland Ice Sheet to a changing climate.

Since the 1970s, the speed of glacier flow in the polar regions has been measured with repeat optical satellite imagery [28]. However, despite their ongoing use [29–32], optical images are daylight dependent which limits their utility outside of the summer season. Unfortunately, satellite imagery may also be obscured by clouds. Synthetic aperture radar (SAR) images do not suffer from either limitation and have also been extensively used to measure ice speed since the launch of the European Remote Sensing Satellite 1 (ERS-1) in 1991 [33–37]. A persistent obstacle to the use of both optical and SAR satellite imagery for tracking ice motion has been the episodic nature of acquisitions. Since the launch of the Sentinel-1a (S1a) and Sentinel-1b (S1b) SAR constellation in April 2014 and April 2016, respectively, it has become possible to systematically measure changes in ice speed every 6 days [38–40]. Here, we use a sequence of Sentinel-1a and 1b SAR images to track seasonal changes in ice sheet flow across a land-terminating sector of the Greenland Ice Sheet between 2014 and 2017.

2. Study Area

Our study focusses on a 14,000 km² sector of central-west Greenland between 66.6°N–67.4°N (Figure 1). The study area includes five glaciers; Isorlersuup Glacier (IG), Ørkendalen Glacier (ØG), Russell Glacier (RG) and Isunnguata Sermia (IS), and an unnamed outlet glacier which we refer to as Glacier 1 (G1). The area has received a relatively high amount attention due to the propensity of its glaciers to exhibit seasonal speedup. In-situ GPS observations have shown that seasonal velocity variations are strongly linked to changes in surface melting [14,19,25,26,41–43]. Satellite measurements have provided a large-scale perspective of changes in ice flow [18,20,21,27] and in the extent of supraglacial lakes [44–47]. Together, these measurements, in conjunction with numerical ice flow modelling have led to an improved understanding of the link between regional hydrology and changes in ice flow, for example the role of supra-glacial lake drainage [48,49].

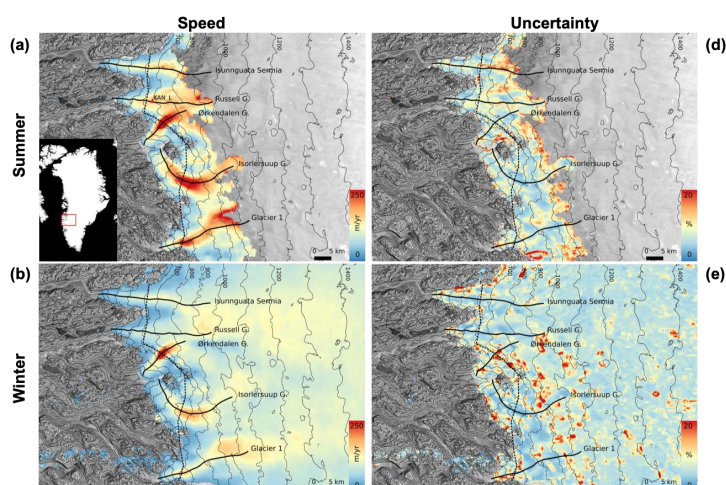


Figure 1. Cont.

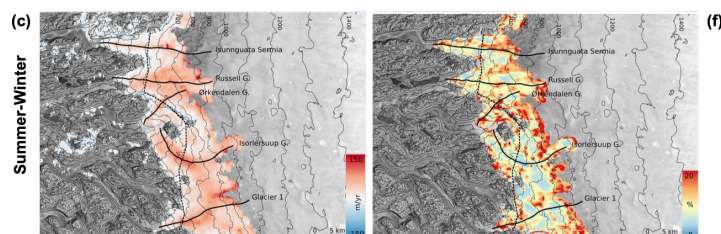


Figure 1. Average ice velocity in (a) summer (May–Jul), (b) winter (Aug–Apr), and (c) the difference between summer and winter, derived from Sentinel-1 (S1) synthetic aperture radar (SAR) imagery. The uncertainties in the maps associated with the summer, winter, and difference between the summer and winter ice speeds are also shown (d–f, respectively). Velocities and the uncertainties are overlaid on a SAR backscatter intensity image. Also shown are elevation contours (thin grey lines), profiles along (solid black lines) and across (dotted black lines) the centre of five glaciers. The location of the KAN_L weather station is also mapped (red dot, a).

3. Data and Methods

Previous studies have demonstrated the capability of Sentinel-1 (S1) for mapping ice sheet flow [38–40]. Here, we use single-look complex (SLC) synthetic aperture radar (SAR) images acquired in the interferometric wide (IW) mode to investigate the detailed patterns of seasonal glacier velocity change. The images used were acquired between January 2016 and December 2017, with a revisit time of 6 or 12 days due to the repeat cycle of 12 days and the 180 degree orbital phase difference between the two satellites. We used the GAMMA-SAR software [50] to generate 96 individual ice velocity maps from different pairs of Sentinel-1a (S1a) and Sentinel-1b (S1b) SAR images.

Ice velocities were computed using a feature tracking technique applied to SAR backscatter intensity images [51], assuming that the ice flow occurs parallel to the surface and at a constant rate during the image acquisition period. This is a well-established technique, measuring the displacement of similar SAR image features (e.g., crevasses and speckle patterns) based on a cross correlation algorithm applied to image segments (windows) in two co-registered SAR images [40,51–53]. The window and step size used was based on sensitivity testing of a range of values, where a trade-off between the spatial resolution, spatial coverage and measurement accuracy of the output result were considered. For an individual pair, the end results depend on the change in snow surface properties between the processed images, the correlation of the speckle pattern, and the scale of the local features observed. For the present study, ice motion was estimated using window sizes of 350×75 pixels in ground range and azimuth, respectively, corresponding to dimensions of approximately 1.7 and 1.5 km. We used the Greenland Ice Mapping Project (GIMP) digital elevation model (DEM) [54] to geocode the displacements, and the final velocity measurements were posted on to a regular 100 m grid. The post-processing to remove poor quality data followed the methodology of Lemos et al. [40]. We applied a low-pass filter twice, using a kernel of 1 km by 1 km, rejecting values where the deviation between the unfiltered and filtered speed magnitude exceeded 30%. Finally, we apply a labelling algorithm based on the image histogram, identifying regions with similar values and rejecting non-coherent velocity magnitudes and isolated measurements with an area smaller than 1/1000th of the processed image size.

Errors in ice velocity measurements derived from repeat satellite imagery can be caused by inaccurate image co-registration, mis-modelled terrain correction [38,55] and atmospheric interference, including changes in ionospheric properties and in tropospheric water vapour [56]. To estimate velocity errors, we scale each individual velocity map by the time-averaged signal to noise ratio (SNR) of the cross-correlation function [40]. The SNR is determined as the ratio between the cross-correlation function peak (C_p) and the average correlation level (C_l) on the tracking window used to estimate the

velocities [57]. Typically, the estimated velocity error is $\sim 10\%$ across the majority of the study area, rising to 20% in regions lacking stable features (Figure 1d–f).

4. Results and Discussion

First, we generated average summer and winter regional velocity maps (Figure 1a,b, respectively) in each calendar year using images that fell within the average periods of the start and end days of speedup in the sector (Table 1). The velocity coverage is better in winter than summer, especially over the slow-moving inland ice, due to the absence of melting. During winter, the scattering properties of the snowpack are relatively stable and this allows radar speckle to be tracked over the otherwise featureless terrain [51,53]. In contrast, the retrieval of summer velocities is limited to within ~ 30 km of the ice sheet margin where there is a sufficient amount of persistent physical features to be able to track motion. Nevertheless, because of the relatively large number of individual velocity maps, we were able to resolve the seasonal pattern of speedup with unprecedented detail and show, for example, that speedup is clearly concentrated towards the centre of each glacier (Figure 1c).

Table 1. Seasonal velocity, speedup, speedup persistence, ice thickness and surface slope of the five glaciers averaged in two elevations bands (P1, between 650 and 750 m.a.s.l.; P2, over 820 m.a.s.l.).

Location		Summer Speed (m yr ⁻¹)	Winter Speed (m yr ⁻¹)	Speedup Relative to Winter (%)	Summer Velocity Peak (m yr ⁻¹)	Annual Mean Velocity (m yr ⁻¹)	Speedup Start Day	Speedup End Day	Speedup Persistence (days)	Mean Thickness (m)	Mean Slope (%)
Glacier 1	P1	187 ± 13	125 ± 9	49%	214 ± 13	133 ± 10	136	196	60	470	2.2%
	P2	154 ± 18	109 ± 10	41%	176 ± 18	116 ± 11	153	216	63	650	2.0%
Isorlersuup	P1	220 ± 11	156 ± 8	41%	257 ± 11	166 ± 9	134	209	75	516	2.2%
	P2	148 ± 17	119 ± 10	24%	169 ± 17	124 ± 11	143	212	69	612	1.6%
Ørkendalen	P1	246 ± 16	203 ± 22	21%	259 ± 16	212 ± 22	113	198	85	390	2.8%
	P2	163 ± 17	111 ± 9	47%	205 ± 17	118 ± 11	155	212	57	623	1.5%
Russell G.	P1	121 ± 13	87 ± 5	38%	139 ± 13	93 ± 7	137	211	74	559	2.2%
	P2	156 ± 18	113 ± 10	38%	177 ± 18	118 ± 11	160	215	55	692	1.9%
Isunnguata S.	P1	103 ± 9	93 ± 6	11%	112 ± 9	95 ± 7	136	201	64	615	2.1%
	P2	121 ± 21	79 ± 5	53%	145 ± 21	87 ± 7	178	250	71	802	1.5%
Sector	P1	175 ± 28	132 ± 26	32%	196 ± 28	140 ± 28	131	203	72	510	2.3%
	P2	148 ± 41	106 ± 20	40%	174 ± 41	113 ± 23	158	221	63	676	1.7%

The maximum recorded winter speed ranges from 121 ± 5 m yr⁻¹ at IS to 296 ± 22 m yr⁻¹ at ØG, and the maximum recorded summer speed ranges from 196 ± 18 m yr⁻¹ at RG to 359 ± 18 m yr⁻¹ at ØG. In general, the degree of speedup at each glacier is quite variable, in agreement with the findings of a previous survey based on TerraSAR-X measurements acquired in 2009 and 2010 in the same region [27]. Locally, we observe numerous regions where the seasonal speedup is greater than 100 m yr⁻¹, for instance reaching 150 m yr⁻¹ ($\sim 75\%$) near to the glacier fronts of IG and RG (Figure 1c). Our results agree well with previous studies in the same region. For example, seasonal velocity changes of 50 – 100% between 2004 and 2007 have been reported [18], and Sundal et al. [20] reported speedup in the range of 50 – 125% between 1993 and 1998. Not all glaciers, however, show such a large degree of speedup. The neighbouring glacier ØG, for example, exhibits a much lower seasonal speedup of ~ 30 m yr⁻¹ (21%), and maintains relatively high rates of ice flow even during winter months near the ice margin.

We examined the geometrical configurations of each glacier to investigate the possible reasons for the heterogeneous speedup (Figure 2) using surface and bed elevations from GIMP-DEM [54] and IceBridge BedMachine Greenland, Version 3 [58], respectively. Although the surface slopes of the glaciers are relatively uniform (2.8% at ØG and 2% elsewhere), their average thicknesses are considerably more variable (from 390 m at ØG to 802 m at IS). The five glaciers also present different flow regimes and, in contrast to marine-terminating glaciers [34,35], reach their peak speeds at distances between 8 and 18 km inland. At G1, IG and ØG, this location is approximately 650 m.a.s.l. The relative speedup is non-uniform and excluding IS where the velocity profile is incomplete, ranges from 21 to 49% (Table 1). Despite being the fastest glacier, ØG had the lowest seasonal variation of all the studied glaciers (Table 1), which suggests that its flow was predominantly driven either by gravity with a low

sensitivity to transient increases in basal lubrication, or it had been influenced by non-uniform basal motion due to friction at the bed-ice interface [59,60].

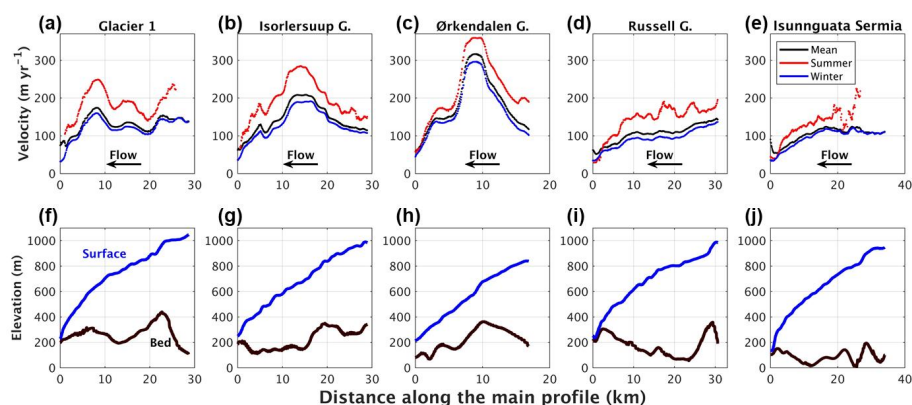


Figure 2. Mean summer and winter ice velocity (a–e) and geometry (f–j) along central profiles of five glaciers in west-central Greenland (see Figure 1 for glacier locations) in 2016 and 2017. Surface and bed elevations are from the Greenland Ice Mapping Project digital elevation model (GIMP-DEM) [54] and IceBridge BedMachine Greenland, Version 3 [58], respectively.

Our velocity maps have sufficient spatial coverage to provide continuous profiles of summer and winter ice speed across the central flow unit of each glacier (Figure 3). Speedup is primarily confined to the central, fast flowing parts of each glacier and at ~600 m.a.s.l., peaks in the range of 22% (ØG) to 66% (RG). At this altitude all of the glaciers sit in distinct bedrock depressions where the ice is far thicker than in the slower flowing neighbouring regions. In general, speedup is largely confined to fast-flowing glaciers or their tributaries (e.g., at 25–30 km and 58–60 km along the transect). Local variations in the input and routing of surface melt water may be responsible for this heterogeneity in the degree of seasonal ice speedup. With the exception of RG, the regional glaciers do not show inter-annual variations in the degree of summer speedup. At RG, however, summer rates of ice flow were 32% faster in 2016 than in 2017. This indicates that changes in a single glacier system are not always indicative of wider patterns, highlighting the value of large-scale systematic satellite monitoring. The only other place of significant inter-annual difference in seasonal speedup is the slow flowing sector between RG and IS. Here, however, ice flowed faster in 2017 than in 2016.

A unique benefit of the S1 constellation is its systematic and high temporal sampling, which supports continuous, multi-year records of ice motion. For each of the glaciers in our study region, we explored this novel capability by charting their speed every 6 days across two full seasonal cycles (Figure 4). We then analysed the velocity time-series within two distinct elevation bands: 650–750 m.a.s.l. (P1) and above 820 m.a.s.l. (P2) to investigate differences in their seasonal flow at high and low altitudes (Table 1). There is clear heterogeneity in the seasonal flow of the five principal glaciers in this sector of the ice sheet (Figure 4). G1, IG and RG exhibited coherent speedup periods during summer time at both altitudes. ØG showed a clear seasonal cycle at high elevations, but at lower elevations the seasonality was much less pronounced and is characterized by a longer duration speedup over the winter months, and at IS there was no apparent summer speedup at either location. However, the velocity data in these regions is generally of poorer quality than elsewhere due to the absence of clear persistent features in the SAR imagery, limiting our ability to draw firm conclusions about seasonal changes in ice flow in these glaciers. At the three glaciers where a coherent seasonal cycle is resolved, in all cases our data show that lower elevations (P1) speed up first, followed by the upper elevations (P2).

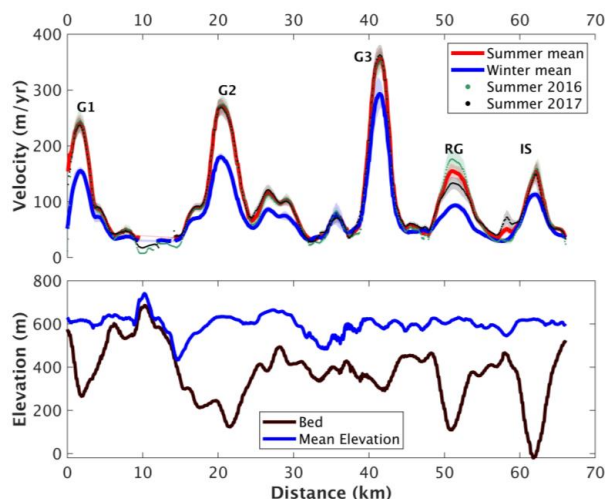


Figure 3. Ice velocity (Top), with uncertainty ranges represented by the light shading, and geometry (Bottom) along an across-flow profile of the study area (see Figure 1 for location) in 2016 to 2017.

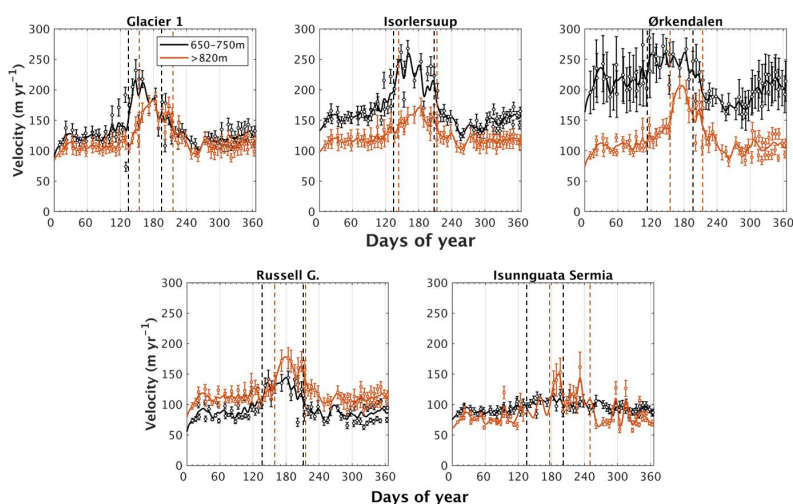


Figure 4. Seasonal changes in ice flow at two different elevations bands on each glacier. Actual measurements are represented by the dots, spline fits as continuous lines, and speedup periods the intervals between the consecutive coloured dotted lines.

We analysed the velocity data to determine the persistence of speedup, and the start and end day of the summer season across the sector. To do this, we first applied a spline fit to each velocity time-series and identified local maxima using the precompiled MATLAB function ‘findpeaks’. We then identified the peak speedup, rejecting locations under a prominent peak threshold of 25 m yr^{-1} . After testing thresholds of 25, 50 and 70 m yr^{-1} we found that this threshold provided a reasonable balance between spatial coverage and consistent speedup persistence, even in slow-moving areas. We also found the number of prominent peaks per pixel which are on average between 1 and 3, as well as consistent speedup persistence results. The persistence of the summer season is defined by the duration of the width of the peak, shown as the time interval between the dotted lines in Figure 4.

For time-series which exhibit multiple and consecutive prominent peaks, we calculate the speedup persistence as the sum of each peak width. However, when this occurs, we calculate the start and end dates of the summer season using the first and last prominent peaks, respectively (Figure 5b,c). We applied the method to spatially-averaged time-series within discrete elevation bands (P1 and P2, Figure 4) and also at individual locations to resolve the spatial pattern (Figure 5).

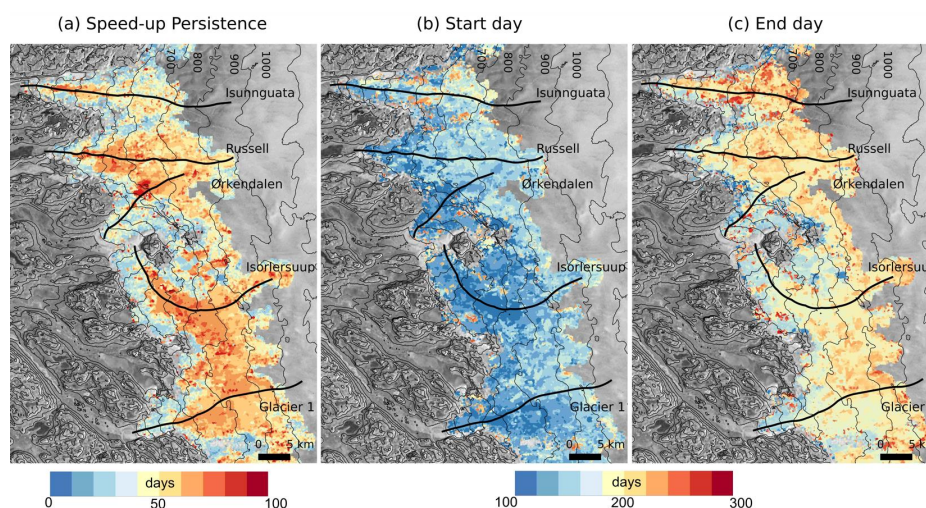


Figure 5. Persistence of ice speedup (a), the start (b) and end date (c) of the summer season.

Across all glaciers, the persistence of seasonal speedup ranges from 72 to 63 days at P1 and P2, respectively (Table 1). The persistence of speedup is shorter at higher elevations on all glaciers except G1. At RG, our estimated persistence of 55 days at P2 is lower but similar to the 66 day estimate made by Palmer et al. [21] for the period of 2004–2007 at the same location. For the first time we are able to map spatial variations in the pattern of summer speedup persistence (Figure 5). The persistence of summer speedup shows clear altitudinal variation at all glaciers, ranging from 60 to 90 days and from 50 to 70 days, respectively, at P1 and P2. At IG, speedup generally has a duration of around 75 days, but persists for 80 days at isolated locations in the fastest flowing section of the glaciers (around 700 m.a.s.l.). In general, at lower altitudes (<500 m.a.s.l.), speedup persists for a significantly shorter period (~40 days). Lower regions are likely to have relatively high surface melting, potentially supplying more water to the subglacial drainage system, allowing channels to develop sooner and thereby shortening the speedup period [15,16]. We estimated the start and end dates of the summer season using the date of peak speedup and the persistence, assuming the period is symmetrical. Near to the ice sheet margin (P1), summertime speedup begins around day 130 and lasts for around 90 days (Table 1 and Figure 5). The summer duration affects a wider section of the ice sheet up to 25 km inland, however the onset date is delayed by approximately 25 days on average at higher elevations (P2).

To investigate the relationship between seasonal velocity changes and environmental forcing in more detail, we compared the regional variation to a local estimate of surface melting. For this comparison, we computed the mean velocity of G1, IG and RG in 2017, when a continuous 6-day sampling was possible (Figure 6). ØG and IS were excluded due to their unusual geometry (high slope) and relatively poor tracking coverage, respectively. We then computed positive degree days (PDDs) as a measure of the surface melting (Figure 6) using air temperatures recorded at the nearby KAN_L (670 m.a.s.l., Figure 1a) automatic weather station and distributed by the Programme for Monitoring of the Greenland Ice Sheet (PROMICE, <https://www.promice.dk/WeatherStations.html>). PDD's were integrated over six day periods to match the sampling of the satellite velocity measurements.

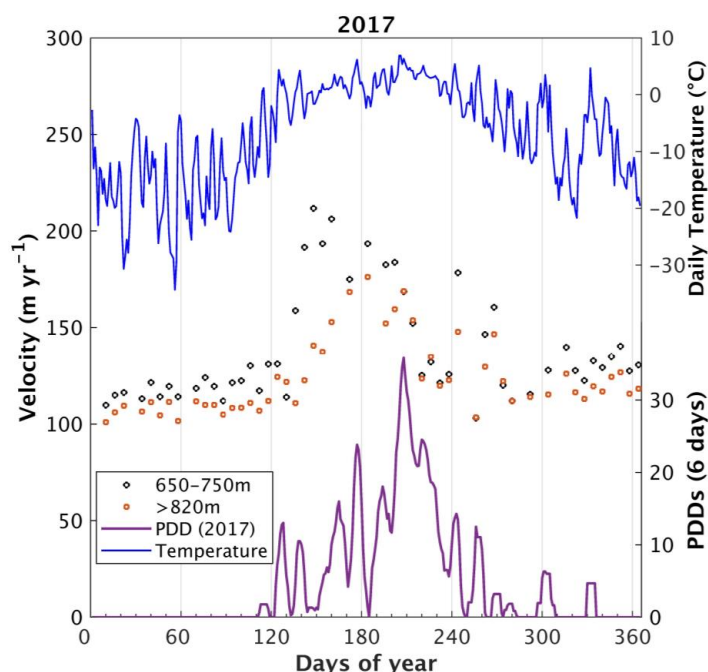


Figure 6. Averaged speed of three glaciers (G1, IG, and RG) with similar geometry and data sampling at two elevations bands during 2017. Also shown are daily temperature and positive degree days (PDDs) recorded at the nearby KAN_L automatic weather station (670 m.a.s.l.) and distributed by the Programme for Monitoring of the Greenland Ice Sheet.

The onset of speedup begins shortly after the first PDDs was recorded at KAN_L on day 125. Onset began on day 130 at P1 and on day 140 at P2. The high speeds were sustained for ~90 days at P1 and ~80 days at P2. The seasonal speedup, likely caused by melt-induced acceleration [8,14,61], starts in P1 shortly after the melt onset possibly reaches the bed (e.g., through moulines or crevasses), followed by P2, located at higher elevation and then undergoing less melting [10,14,18,23]. Future investigations using the SAR backscatter information will improve the characterization of the surface melt days. After the maximum PDDs were reached on day 207, the ice speed at P1 and P2 began to slow down rapidly at similar rates, returning to near winter levels by day 220. Two further speedup events then occur around days 244 and 268 and these coincide with isolated short-lived melt events evident within the PDD record. Later spikes in velocity, enhanced by short-term basal sliding, are likely to happen due to excess amount of water input combined with the time required for the drainage system to accommodate the extra melt-water, since the size of cavities adjusts progressively in time [14,16].

5. Conclusions

We have computed seasonal changes in the motion of five land-terminating glaciers in the central-west sector of the Greenland Ice Sheet using Sentinel-1a and-1b synthetic aperture radar imagery. The systematic acquisition schedule of Sentinel-1 provides a capacity to track ice motion with significantly greater spatial and temporal sampling than previous satellite missions. In our study, we were able to produce 96 unique ice velocity maps over a two-year period, which corresponds to approximately four times the sampling frequency of previous studies [20,21,27]. The high data volumes allow us to study spatial and temporal changes in ice flow across this sector of the Greenland ice sheet. Despite being located in the same sector and being exposed to similar environmental

conditions, the five glaciers we have surveyed show different patterns of speedup; peak summer speedup for example ranges from 21% (Ørkendalen) to 49% (Glacier 1) relative to winter. Speedup is clearly concentrated along the central portions of each glacier, with only isolated instances elsewhere. For the first time we mapped spatial variations in the seasonal speedup persistence cycle. In this sector, the start date of the speedup period ranges from day 113 to 178, and the end date ranges from day 196 to 250, leading to a persistence ranging from 55 to 85 days. Our study highlights the unique value of the Sentinel-1 mission for tracking short term changes in ice motion.

Author Contributions: A.L. led the project and wrote the paper, supervised by A.S., M.M. and A.E.H. A.L. and A.E.H. processed the data. All authors discussed the results and commented on the manuscript at all stages.

Funding: This work was led by the NERC Centre for Polar Observation and Modelling, supported by the Natural Environment Research Council (cpom300001), with the support of a grant (4000107503/13/I-BG), and the European Space Agency. Adriano Lemos was supported by the CAPES-Brazil PhD scholarship. Anna E. Hogg is funded by the European Space Agency's support of Science Element program and an independent research fellowship (4000112797/15/I-SBo).

Acknowledgments: The authors gratefully acknowledge the European Space Agency for the Copernicus Sentinel 1 data acquired from Data Hub, courtesy of the EU/ESA. The Sentinel-1 data are freely available at <https://scihub.copernicus.eu/> (last access: 18 September 2018). Data from the Programme for Monitoring of the Greenland Ice Sheet (PROMICE) and the Greenland Analogue Project (GAP) were provided by the Geological Survey of Denmark and Greenland (GEUS) at <http://www.promice.dk>. This work was led by the NERC Centre for Polar Observation and Modelling, supported by the Natural Environment Research Council (cpom300001), with the support of a grant (4000107503/13/I-BG), and the European Space Agency. Anna E. Hogg is funded by the European Space Agency's support of Science Element program and an independent research fellowship (4000112797/15/I-SBo). Adriano Lemos was supported by the CAPES-Brazil PhD scholarship. We thank the editor Suzanne Ji, and the four reviewers for their comments, which helped to improve the manuscript.

Conflicts of Interest: The authors declare no conflict of interest.

References

1. Shepherd, A.; Ivins, E.R.; Gero, A.; Barletta, V.R.; Bentley, M.J.; Bettadpur, S.; Briggs, K.H.; Bromwich, D.H.; Forsberg, R.; Galin, N.; et al. A Reconciled Estimate of Ice-Sheet Mass Balance. *Science* **2012**, *338*, 1183–1189. [[CrossRef](#)] [[PubMed](#)]
2. McMillan, M.; Leeson, A.; Shepherd, A.; Briggs, K.; Armitage, T.W.K.; Hogg, A.; Munneke, P.K.; van den Broeke, M.; Noël, B.; Berg, W.J.; et al. A high resolution record of Greenland mass balance. *Geophys. Res. Lett.* **2016**, *43*, 1–9. [[CrossRef](#)]
3. Enderlin, E.M.; Howat, I.M.; Jeong, S.; Noh, M.-J.; van Angelen, J.H.; van den Broeke, M.R. An improved mass budget for the Greenland ice sheet. *Geophys. Res. Lett.* **2014**, *41*, 1–7. [[CrossRef](#)]
4. Van den Broeke, M.; Enderlin, E.; Howat, I.; Kuipers Munneke, P.; Noël, B.; van de Berg, W.J.; van Meijgaard, E.; Wouters, B. On the recent contribution of the Greenland ice sheet to sea level change. *Cryosphere* **2016**, *10*, 1933–1946. [[CrossRef](#)]
5. Hanna, E.; Mernild, S.H.; Cappelen, J.; Steffen, K. Recent warming in Greenland in a long-term instrumental (1881–2012) climatic context: I. Evaluation of surface air temperature records. *Environ. Res. Lett.* **2012**, *7*. [[CrossRef](#)]
6. Hanna, E.; Fettweis, X.; Mernild, S.H.; Cappelen, J.; Ribergaard, M.H.; Shuman, C.A.; Steffen, K.; Wood, L.; Mote, T.L. Atmospheric and oceanic climate forcing of the exceptional Greenland ice sheet surface melt in summer 2012. *Int. J. Climatol.* **2014**, *34*, 1022–1037. [[CrossRef](#)]
7. Crozier, J.; Karlstrom, L.; Yang, K. Basal control of supraglacial meltwater catchments on the Greenland Ice Sheet. *Cryosphere* **2018**, *12*, 3383–3407. [[CrossRef](#)]
8. Zwally, H.J.; Abdalati, W.; Herring, T.; Larson, K.; Saba, J.; Steffen, K. Surface Melt—Induced Acceleration of Greenland Ice-Sheet Flow. *Science* **2002**, *297*, 218–223. [[CrossRef](#)] [[PubMed](#)]
9. Hoffman, M.J.; Catania, G.A.; Neumann, T.A.; Andrews, L.C.; Rumrill, J.A. Links between acceleration, melting, and supraglacial lake drainage of the western Greenland Ice Sheet. *J. Geophys. Res. Earth Surf.* **2011**, *116*, 1–16. [[CrossRef](#)]
10. Chu, V.W. Greenland ice sheet hydrology: A review. *Prog. Phys. Geogr.* **2014**, *38*, 19–54. [[CrossRef](#)]

A.2 Paper published in the journal Remote Sensing

Remote Sens. 2018, 10, 1878

10 of 12

11. Harper, J.T.; Humphrey, N.F.; Pfeffer, W.T.; Fudge, T.; O'Neel, S. Evolution of subglacial water pressure along a glacier's length. *Ann. Glaciol.* **2005**, *40*, 31–36. [[CrossRef](#)]
12. Nienow, P.W.; Hubbard, A.L.; Hubbard, B.P.; Chandler, D.M.; Mair, D.W.F.; Sharp, M.J.; Willis, I.C. Hydrological controls on diurnal ice flow variability in valley glaciers. *J. Geophys. Res. Earth Surf.* **2005**, *110*, 1–11. [[CrossRef](#)]
13. Andrews, L.C.; Catania, G.A.; Hoffman, M.J.; Gulley, J.D.; Lüthi, M.P.; Ryser, C.; Hawley, R.L.; Neumann, T.A. Direct observations of evolving subglacial drainage beneath the Greenland Ice Sheet. *Nature* **2015**, *514*, 80–83. [[CrossRef](#)] [[PubMed](#)]
14. Bartholomew, I.D.; Nienow, P.; Mair, D.; Hubbard, A.; King, M.A.; Sole, A. Seasonal evolution of subglacial drainage and acceleration in a Greenland outlet glacier. *Nat. Geosci.* **2010**, *3*, 408–411. [[CrossRef](#)]
15. Cowton, T.; Nienow, P.; Sole, A.; Wadham, J.; Lis, G.; Bartholomew, I.D.; Mair, D.; Chandler, D. Evolution of drainage system morphology at a land-terminating Greenlandic outlet glacier. *J. Geophys. Res. Earth Surf.* **2013**, *118*, 29–41. [[CrossRef](#)]
16. Schoof, C. Ice-sheet acceleration driven by melt supply variability. *Nature* **2010**, *468*, 803–806. [[CrossRef](#)] [[PubMed](#)]
17. Rignot, E.; Kanagaratnam, P. Changes in the Velocity Structure of the Greenland Ice Sheet. *Science* **2006**, *311*, 986–990. [[CrossRef](#)] [[PubMed](#)]
18. Joughin, I.; Das, S.B.; King, M.A.; Smith, B.E.; Howat, I.M.; Moon, T. Seasonal Speedup along the Western Flank of the Greenland Ice Sheet. *Science* **2008**, *320*, 781–784. [[CrossRef](#)] [[PubMed](#)]
19. Shepherd, A.; Hubbard, A.; Nienow, P.; King, M.; McMillan, M.; Joughin, I. Greenland ice sheet motion coupled with daily melting in late summer. *Geophys. Res. Lett.* **2009**, *36*, 1–4. [[CrossRef](#)]
20. Sundal, A.V.; Shepherd, A.; Nienow, P.; Hanna, E.; Palmer, S.; Huybrechts, P. Melt-induced speed-up of Greenland ice sheet offset by efficient subglacial drainage. *Nature* **2011**, *469*, 521–524. [[CrossRef](#)] [[PubMed](#)]
21. Palmer, S.; Shepherd, A.; Nienow, P.; Joughin, I. Seasonal speedup of the Greenland Ice Sheet linked to routing of surface water. *Earth Planet. Sci. Lett.* **2011**, *302*, 423–428. [[CrossRef](#)]
22. Joughin, I.; Das, S.B.; Flowers, G.E.; Behn, M.D.; Alley, R.B.; King, M.A.; Smith, B.E.; Bamber, J.L.; Van Den Broeke, M.R.; Van Angelen, J.H. Influence of ice-sheet geometry and supraglacial lakes on seasonal ice-flow variability. *Cryosphere* **2013**, *7*, 1185–1192. [[CrossRef](#)]
23. Moon, T.; Joughin, I.; Smith, B.; Broeke, M.R.; Berg, W.J.; Noël, B.; Usher, M. Distinct patterns of seasonal Greenland glacier velocity. *Geophys. Res. Lett.* **2014**, *41*, 7209–7216. [[CrossRef](#)] [[PubMed](#)]
24. Sole, A.J.; Mair, D.W.F.; Nienow, P.W.; Bartholomew, I.D.; King, M.A.; Burke, M.J.; Joughin, I. Seasonal speedup of a Greenland marine-terminating outlet glacier forced by surface melt-induced changes in subglacial hydrology. *J. Geophys. Res. Earth Surf.* **2011**, *116*, 1–11. [[CrossRef](#)]
25. Bartholomew, I.D.; Nienow, P.; Sole, A.; Mair, D.; Cowton, T.; King, M.A. Short-term variability in Greenland Ice Sheet motion forced by time-varying meltwater drainage: Implications for the relationship between subglacial drainage system behavior and ice velocity. *J. Geophys. Res. Earth Surf.* **2012**, *117*, 1–17. [[CrossRef](#)]
26. Van de Wal, R.S.W.; Smeets, C.J.P.P.; Boot, W.; Stoffelen, M.; Van Kampen, R.; Doyle, S.H.; Wilhelms, F.; Van Den Broeke, M.R.; Reijmer, C.H.; Oerlemans, J.; et al. Self-regulation of ice flow varies across the ablation area in south-west Greenland. *Cryosphere* **2015**, *9*, 603–611. [[CrossRef](#)]
27. Fitzpatrick, A.A.W.; Hubbard, A.; Joughin, I.; Quincey, D.J.; Van As, D.; Mikkelsen, A.P.B.; Doyle, S.H.; Hasholt, B.; Jones, G.A. Ice flow dynamics and surface meltwater flux at a land-terminating sector of the Greenland ice sheet. *J. Glaciol.* **2013**, *59*, 687–696. [[CrossRef](#)]
28. Lucchitta, B.K.; Ferguson, H.M. Antarctica: Measuring glacier velocity from satellite images. *Science* **1986**, *234*, 1105–1108. [[CrossRef](#)] [[PubMed](#)]
29. Dehecq, A.; Gourmelen, N.; Trouve, E. Deriving large-scale glacier velocities from a complete satellite archive: Application to the Pamir-Karakoram-Himalaya. *Remote Sens. Environ.* **2015**, *162*, 55–66. [[CrossRef](#)]
30. Fahnestock, M.; Scambos, T.; Moon, T.; Gardner, A.; Haran, T.; Klinger, M. Rapid large-area mapping of ice flow using Landsat 8. *Remote Sens. Environ.* **2016**, *185*, 84–94. [[CrossRef](#)]
31. Armstrong, W.H.; Anderson, R.S.; Fahnestock, M.A. Spatial Patterns of Summer Speedup on South Central Alaska Glaciers. *Geophys. Res. Lett.* **2017**, *44*, 9379–9388. [[CrossRef](#)]
32. Gardner, A.S.; Moholdt, G.; Scambos, T.; Fahnestock, M.; Ligtenberg, S.; Van Den Broeke, M.; Nilsson, J. Increased West Antarctic ice discharge and East Antarctic stability over the last seven years. *Cryosphere* **2018**, *12*, 521–547. [[CrossRef](#)]

A.2 Paper published in the journal Remote Sensing

Remote Sens. 2018, 10, 1878

11 of 12

33. Joughin, I.; Winebrenner, D.P.; Fahnestock, M.A. Observations of ice-sheet motion in Greenland using satellite radar interferometry. *Geophys. Res. Lett.* **1995**, *22*, 571–574. [[CrossRef](#)]
34. Lucchitta, B.K.; Rosanova, C.E.; Mullins, K.F. Velocities of Pine Island Glacier, West Antarctica, from ERS-1 SAR images. *Ann. Glaciol.* **1995**, *21*, 277–283. [[CrossRef](#)]
35. Goldstein, R.M.; Engelhardt, H.; Kamb, B.; Frolich, R.M. Satellite Radar Interferometry for Monitoring Ice Sheet Motion: Application to an Antarctic Ice Stream. *Science* **1993**, *262*, 1525–1530. [[CrossRef](#)] [[PubMed](#)]
36. Rignot, E.; Velicogna, I.; Van Den Broeke, M.R.; Monaghan, A.; Lenaerts, J.T.M. Acceleration of the contribution of the Greenland and Antarctic ice sheets to sea level rise. *Geophys. Res. Lett.* **2011**, *38*, 1–5. [[CrossRef](#)]
37. Joughin, I.; Smith, B.E.; Howat, I.M.; Scambos, T.; Moon, T. Greenland flow variability from ice-sheet-wide velocity mapping. *J. Glaciol.* **2010**, *56*, 415–430. [[CrossRef](#)]
38. Nagler, T.; Rott, H.; Hetzenecker, M.; Wuite, J.; Potin, P. The Sentinel-1 Mission: New Opportunities for Ice Sheet Observations. *Remote Sens.* **2015**, *7*, 9371–9389. [[CrossRef](#)]
39. Joughin, I.; Smith, B.E.; Howat, I. Greenland Ice Mapping Project: Ice Flow Velocity Variation at sub-monthly to decadal time scales. *Cryosphere* **2018**, *12*, 2211–2227. [[CrossRef](#)]
40. Lemos, A.; Shepherd, A.; Mcmillan, M.; Hogg, A.E.; Hatton, E.; Joughin, I. Ice velocity of Jakobshavn Isbræ, Petermann Glacier, Nioghalvfjærdssjøen and Zachariæ Isstrøm, 2015–2017, from Sentinel 1-a/b SAR imagery. *Cryosphere* **2018**, *12*, 2087–2097. [[CrossRef](#)]
41. Bartholomew, I.D.; Nienow, P.; Sole, A.; Mair, D.; Cowton, T.; King, M.A.; Palmer, S. Seasonal variations in Greenland Ice Sheet motion: Inland extent and behaviour at higher elevations. *Earth Planet. Sci. Lett.* **2011**, *307*, 271–278. [[CrossRef](#)]
42. Sole, A.; Nienow, P.W.; Bartholomew, I.D.; Mair, D.W.F.; Cowton, T.R.; Tedstone, A.J.; King, M.A. Winter motion mediates dynamic response of the Greenland Ice Sheet to warmer summers. *Geophys. Res. Lett.* **2013**, *40*, 3940–3944. [[CrossRef](#)]
43. Chandler, D.M.; Wadham, J.L.; Lis, G.P.; Cowton, T.; Sole, A.; Bartholomew, I.D.; Telling, J.; Nienow, P.; Bagshaw, E.B.; Mair, D.; et al. Evolution of the subglacial drainage system beneath the Greenland Ice Sheet revealed by tracers. *Nat. Geosci.* **2013**, *6*, 195–198. [[CrossRef](#)]
44. Howat, I.M.; de la Peña, S.; van Angelen, J.H.; Lenaerts, J.T.M.; van den Broeke, M.R. Brief Communication: “Expansion of meltwater lakes on the Greenland Ice Sheet”. *Cryosphere* **2013**, *7*, 201–204. [[CrossRef](#)]
45. Leeson, A.A.; Shepherd, A.; Palmer, S.; Sundal, A.; Fettweis, X. Simulating the growth of supraglacial lakes at the western margin of the Greenland ice sheet. *Cryosphere* **2012**, *6*, 1077–1086. [[CrossRef](#)]
46. Leeson, A.A.; Shepherd, A.; Sundal, A.V.; Johansson, A.M.; Selmes, N.; Briggs, K.; Hogg, A.E.; Fettweis, X. A comparison of supraglacial lake observations derived from MODIS imagery at the western margin of the Greenland ice sheet. *J. Glaciol.* **2013**, *59*, 1179–1188. [[CrossRef](#)]
47. Leeson, A.; Shepherd, A.; Briggs, K.; Fettweis, X. Supraglacial lakes on Greenland migrate inland under warming climate. *Nat. Clim. Chang.* **2015**, *16*, 51–55. [[CrossRef](#)]
48. Clason, C.C.; Mair, D.W.F.; Nienow, P.W.; Bartholomew, I.D.; Sole, A.; Palmer, S.; Schwanghart, W. Modelling the transfer of supraglacial meltwater to the bed of Leverett Glacier, Southwest Greenland. *Cryosphere* **2015**, *9*, 123–138. [[CrossRef](#)]
49. Koziol, C.P.; Arnold, N. Modelling seasonal meltwater forcing of the velocity of land-terminating margins of the Greenland Ice Sheet. *Cryosphere* **2018**, *12*, 971–991. [[CrossRef](#)]
50. GAMMA REMOTE SENSING. Sentinel-1 Processing with GAMMA Software. Version 1.2; GAMMA Remote Sensing AG: Gumligen, Switzerland, 2015.
51. Strozzi, T.; Luckman, A.; Murray, T.; Wegmuller, U.; Werner, C.L. Glacier motion estimation using SAR offset-tracking procedures. *IEEE Trans. Geosci. Remote Sens.* **2002**, *40*, 2384–2391. [[CrossRef](#)]
52. Pritchard, H.; Murray, T.; Luckman, A.; Strozzi, T.; Barr, S. Glacier surge dynamics of Sortebrae, east Greenland, from synthetic aperture radar feature tracking. *J. Geophys. Res.* **2005**, *110*, 1–13. [[CrossRef](#)]
53. Paul, F.; Bolch, T.; Kääb, A.; Nagler, T.; Nuth, C.; Scharer, K.; Shepherd, A.; Strozzi, T.; Ticconi, F.; Bhambri, R.; et al. The glaciers climate change initiative: Methods for creating glacier area, elevation change and velocity products. *Remote Sens. Environ.* **2015**, *162*, 408–426. [[CrossRef](#)]
54. Howat, I.M.; Negrete, A.; Smith, B.E. The Greenland Ice Mapping Project (GIMP) land classification and surface elevation data sets. *Cryosphere* **2014**, *8*, 1509–1518. [[CrossRef](#)]

A.2 Paper published in the journal Remote Sensing

Remote Sens. **2018**, *10*, 1878

12 of 12

55. Hogg, A.E.; Shepherd, A.; Cornford, S.L.; Briggs, K.H.; Gourmelen, N.; Graham, J.; Joughin, I.; Mouginot, J.; Nagler, T.; Payne, A.J.; et al. Increased ice flow in Western Palmer Land linked to ocean melting. *Geophys. Res. Lett.* **2017**, *1–9*. [[CrossRef](#)]
56. Liao, H.; Meyer, F.J.; Scheuchl, B.; Mouginot, J.; Joughin, I.; Rignot, E. Ionospheric correction of InSAR data for accurate ice velocity measurement at polar regions. *Remote Sens. Environ.* **2018**, *209*, 166–180. [[CrossRef](#)]
57. De Lange, R.; Luckman, A.; Murray, T. Improvement of satellite radar feature tracking for ice velocity derivation by spatial frequency filtering. *IEEE Trans. Geosci. Remote Sens.* **2007**, *45*, 2309–2318. [[CrossRef](#)]
58. Morlighem, M.; Williams, C.; Rignot, E.; An, L.; Arndt, J.E.; Bamber, J.; Catania, G.; Chauché, N.; Dowdeswell, J.A.; Dorschel, B.; et al. Zinglersen IceBridge BedMachine Greenland. NASA National Snow and Ice Data Center Distributed Active Archive Center; Version 3; Boulder, Colorado, USA, 2017. [[CrossRef](#)]
59. Rysler, C.; Lüthi, M.P.; Andrews, L.C.; Hoffman, M.J.; Catania, G.A.; Hawley, R.L.; Neumann, T.A.; Kristensen, S.S. Sustained high basal motion of the Greenland ice sheet revealed by borehole deformation. *J. Glaciol.* **2014**, *60*, 647–660. [[CrossRef](#)]
60. Armstrong, W.H.; Anderson, R.S.; Allen, J.; Rajaram, H. Modeling the WorldView-derived seasonal velocity evolution of Kennicott Glacier, Alaska. *J. Glaciol.* **2016**, *62*, 763–777. [[CrossRef](#)]
61. Hewitt, I.J. Seasonal changes in ice sheet motion due to melt water lubrication. *Earth Planet. Sci. Lett.* **2013**, *371–372*, 16–25. [[CrossRef](#)]



© 2018 by the authors. Licensee MDPI, Basel, Switzerland. This article is an open access article distributed under the terms and conditions of the Creative Commons Attribution (CC BY) license (<http://creativecommons.org/licenses/by/4.0/>).